A Vortex Panel Method for Potential Flows with Applications to Dynamics and Controls

by

Curtis Paul Mracek, Capt, USAF

Dissertation submitted to the Faculty of the
Virginia Polytechnic Institute and State University
in partial fulfillment of the requirements for the degree of
Doctor of Philosophy
in
Engineering Mechanics

APPROVED:

Dean T. Mook, Co-Chairman	Ali H. Nayfeh, Co-Chairman
Scott L. Hendricks	Eugene M. Cliff
Charles W. Smith	Daniel Frederick

August 1988

Blacksburg, Virginia

A Vortex Panel Method for Potential Flows

with Applications to Dynamics and Controls

by

Curtis Paul Mracek, Capt, USAF

Dean T. Mook, Co-Chairman

Ali H. Nayfeh, Co-Chairman

Engineering Mechanics

(ABSTRACT)

A general nonlinear, nonplanar unsteady vortex panel method for potential-flow is developed. The surface is modeled as a collection of triangular elements on which the vorticity vector is piecewise linearly varying. The wake emanates from the sides and trailing edges of the thin lifting surfaces and is modeled as a progressively formed collection of vortex filaments. This model provides a continuous pressure distribution on the surface while allowing the wake to roll up as tightly as needed. The wake position is determined as part of the solution and no prior knowledge of the position or strength is assumed. An adaptive grid technique is used to redistribute the circulation of the vortex filaments of the wake as the wake sheet spreads. The aerodynamic model is coupled with dynamic equations of motion. Forced oscillation tests are conducted on flat rectangular and delta wings. Dynamic tests are performed to predict wing rock of a slender delta wing restricted to one degree of freedom in roll. The aerodynamic/dynamic model is coupled with control laws that govern the motion of flaperons so that a prescribed pitch motion is executed and wing rock is suppressed. (300 pages, 107 figures)

Acknowledgements

The author expresses his gratitude and appreciation to:

Dr. Dean Mook for his advice, guidance, and understanding throughout this work, and also for his perseverance in editing the manuscript.

Dr. Ali Nayfeh and Dr. Eugene Cliff for their timely suggestions and also for reading this document.

Dr. William Smith, Dr. Scott Hendricks and Dr. Daniel Frederick for giving their valuable time in reading this manuscript.

I would also like to express my appreciation to the U.S. Air Force in general and Dr. Peter Torvik in particular for allowing me to persue this effort.

Special thanks and love to my family. To my sister and her husband,

for their help, encouragement and compainionship. To my brother and his wife,

, and my parents for their love and moral support. To my children, for thier patience and understanding. Finally, my deepest graditude is expressed to my wife, for all the love she has given through the years.

Table of Contents

Dynamic Model

Control Model

Conclusions and Recommendations

Appendix I: Velocity Induced by a Triangular Element

Appendix II: Velocity Induced by a Variable Vortex Filament

Appendix III: Total Velocity at a Point in the Flow Field

List of Illustrations

List of Tables

Chapter I

Introduction

1.1 Problem Statement

The goal of this research are two-fold. The first is to develop a numerical simulation of general unsteady, subsonic-aerodynamic flowfields applicable, but not limited, to low aspect ratios and high angles of attack. The second is to develop a method that predicts the flowfield, motion of the body, and the control surface configuration, as functions of time, simultaneously and interactively.

1.2 Scope of Development

Obviously the stated problem is too complex to be properly addressed in any single effort; therefore, the scope of this development is restricted to rigid, constant velocity aircraft of simple configuration. Included in this effort is a newly developed unsteady aerodynamic model that has a progressively developed deforming wake, a three degree of freedom, in angular orientation, dynamic simulation and control surface movement that includes solving for the control motion that results in a specified maneuver. Since this investigation is primarily concerned with surfaces influenced by leading edge separation and the simplest configuration of this type is a delta wing, delta wings are primarily used in this effort.

1.3 Motivation for Research

As testing of aircraft designs becomes more expensive, computers become more powerful and the need for more exacting designs continues, computational methods have and will continue to become more prominent. To facilitate the use of computational methods by designers, the tools need to be developed and demonstrated. The present work extends a previously developed method, so that a more general computer simulation can be accomplished. The unique areas presented in this work are (1) an aerodynamic model previously

restricted to steady or quasi-steady flows is extended to general unsteady motion and (2) a control law is developed and evaluated using control surface motion coupled with an aerodynamic-dynamic simulation. Both these improvements are steps in the direction of allowing aircraft designers to evaluate designs using computational methods.

Low-speed, high-angle-of-attack aerodynamic/dynamic interaction has not traditionally received much attention in the development of aircraft. For example Young [1984], in his summary of the AGARD conference on vortex flows, presented the breakdown of the hours of wind-tunnel tests on the F-16, showing that in approximately eleven thousand hours there were no tests conducted for subsonic dynamic tests. This was done even though there can be considerable variation in aerodynamic parameters in unsteady flight. To further emphasize the need for the present investigation let me quote Orlik-Ruckemann [1979] . He says, "Although the manifestations of high angle-angle-of-attack or asymmetrical flows in terms of their effects on dynamic stability parameters are slowly becoming known, the nature of these flows - especially in oscillatory or unsteady situations - is still largely undefined. ... More research into the basic fluid dynamics aspects of dynamic stability problems, especially high angles of attack, is therefore needed."

Presently there are several good methods for predicting steady aerodynamic loads on aircraft at low angles of attack for slow speeds. This work deals not only with low but also with high angles of attack. The motivation for investigating higher angles of attack with vortex dominated flow is that many modern aircraft routinely fly in this regime and recently efforts have been made to harness the vorticity-induced forces by the use of strakes, leading-edge blowing, and vortex channels. Most numerical methods have trouble predicting the forces and moments for these conditions, and most cannot be used for unsteady motion. One reason they have trouble at high angles of attack is the fact that the flow around the wing is heavily influenced by the vortex separation along the leading edge.

Hoeijmaker [1984] gave a comprehensive review of computational methods for determining aerodynamic characteristics of vortical type flows. He started by discussing different methods for modeling the wake. He reviewed the discrete-vortex approximation, "cloud in cell" methods, panel methods, and vortex layer with finite core methods. Hoeijmaker pointed

out that the biggest drawback to using a system of discrete vortex cores is that eventually this approximation leads to "chaotic motion". As demonstrated by Mook, Roy, Choksi and Alexander [1987] for two-dimensional cases, a discrete vortex system can accurately simulate the tight roll-up and double branching of the vortex sheet before any unrealistic vortex core positioning is encountered. Of the other methods only the vortex layer and finite core methods remain numerically stable. But, with these methods the details of the wake are lost in the accumulated vortex core. With the two-dimensional simulation as inspiration the discrete vortex system was chosen for the wake.

Hoeijmaker then reviewed methods for three-dimensional flows which include the leading-edge-suction analogy of Polhamus, the vortex-lattice method, panel methods, and Euler equation methods. He believes that panel methods have a decided advantage over the suction analogy and the vortex-lattice method. Thus a panel method is used for the body.

In conclusion Hoeijmaker stated, "The main limitation of the panel-method approach is that the topology of the vortex flow must be known in advance". In reviewing Euler equation methods he concluded "It appears that also in the case of Euler methods the topology of the vortex structure must be known in advance if the grid is to be constructed with sufficient resolution at the right location." This conclusion further emphasizes the need for developing an unsteady model because the topology of the wake is not known prior to starting the analysis; rather it is part of the solution. An unsteady model can be started impulsively and the wake will evolve with time. Thus for the present method the topology of the wake surface does not have to be known a priori. The present method also uses an adaptive grid technique for the wake surface as this surface develops with time.

To reiterate, the thrust of this research effort is in the development and validation of a computational unsteady aerodynamic-dynamic model for low speed, high-angle-of-attack, flight conditions. The method chosen for the aerodynamic model is a first-order panel method. The body is modeled as a collection of triangular elements over which the surface vorticity varies linearly. The wake is modeled as a collection of discrete vortex cores in a method similar to the vortex-lattice methods, with the added feature of adapting the grid for the wake surface. The dynamic equations are coupled to the aerodynamic model by a predictor-

corrector algorithm. Finally the control-surface motion is determined to produce a predescribed maneuver.

1.4 Method of Approach

The first task was to develop a general unsteady aerodynamic model for aircraft that is valid at low speeds over a wide range of angles of attack. This development was a slow evolution with validation of each new feature as it was completed. The development and validation was carried out in seven steps. First the model was developed for closed nonlifting bodies. This was then validated by comparison with analytical solutions for several bodies. The method was then extended to lifting surfaces with edge separation. In this phase there where two areas of validation. As mentioned, the wake was modeled as a lattice of constant strength vortex cores. This approximation was compared with the velocity field induced by the comparable vortex sheet. The second area was a comparison with limited experimental results, for aerodynamic forces, moments and pressure distributions. The unsteady aerodynamic results were then validated by comparing the results for forced oscillation tests with predicted results. The integration technique was validated by comparison with exact solutions for a second-order differential equation. The aerodynamic-dynamic coupling was tested by using free vibration tests. These results were compared with experimental results. The control surfaces were then incorporated. The control surface effectiveness was evaluated by holding the surfaces at a fixed deflection and calculating the steady aerodynamic loads. The entire integration was used to develop a control law associated with a prescribed pitch maneuver and to suppress wing rock.

The development and validation was not the only purpose in this effort. Within this development the method was tested to determine its convergence properties. Convergence was tested by increasing the number of elements during the steady analysis.

As can be seen in this approach every effort has been made to include a wide range of test cases and as many comparisons with experimental results as possible. This effort is not intended as a complete comparison with other computational methods. The only method compared is the general unsteady vortex-lattice method. This method was chosen for com-

parison because it is a widely used computational method for lifting surfaces with edge separation. A comparison is made between the vortex-lattice and present methods for total aerodynamic forces of low-aspect-ratio wings.

1.5 Assumptions

The assumptions used in any development directly influence the range of applicability and thus they must be spelled out explicitly. The first restriction is that a potential model is used. Therefore all the assumptions used to arrive at Laplac'es equation are also used in this development. Second the separation lines are known a priori. This restriction is required because there has not been any attempt, in this effort, to include the boundary-layer calculations. Finally it is assumed that vortex bursting does not significantly influence the wing surface. This assumption is used throughout this paper, even though it was shown by Nakamura, Leonard and Spalart [1984] that vortex bursting can be simulated using vortex filaments. Further assumptions will be made during the actual mathematical development, but these assumptions are non-restrictive in that they are handled within the program. These assumptions make the model valid for low speeds where the higher order separations (secondary, etc.) are not significant to the aerodynamic loads and at angles of attack or dynamic geometry where vortex bursting does not significantly affect the surface.

1.6 Review of The Literature

The literature is reviewed for all known vortex-panel methods. This review is followed by a brief discussion of the development of the vortex-lattice methods. Finally, a review of experimental testing that is used in the validation of the aerodynamic/dynamic model is presented.

The first attempt at using triangular panels of linearly varying vorticity was made by Yen [1982]. In his development, Yen modeled a series of delta and rectangular wings using triangular panels of linearly varying vorticity. He modeled the wake as a combination of triangular panels of vorticity, a semi-infinite vortex sheet and a concentrated vortex core. The

core was used when the wake vortex system rolled up tightly. The vorticity on the lifting surface and in the wake and the position of the wake were determined by an iterative procedure. First, for an assumed position of the wake, the strength of the vortex sheets, was determined by minimizing the sum of the square of the errors of the algebraic equations that represent the no-penetration and the conservation (the divergence of the vorticity vector on the sheets is zero) conditions. The Kutta condition was imposed by requiring the vorticity be perpendicular to the edge of the surface. Once the vorticity was known the wake position was adjusted. The vorticity of the sheets was then re-determined. The iteration continued until the shape of the wake converged. This method had several problems associated with it: the method could only be applied to steady flow, the Kutta condition was imposed by requiring the vorticity be perpendicular to the edge of the surface and the roll-up of the wake had to be restricted by employing a capturing vortex core, the strength of the wake sheet was not adjusted as the wake spread, and the method could be applied to only flat uncambered surfaces.

About the same time Kandil, Chu and Yates [1980] presented the development of what they called a "Nonlinear Hybrid Vortex" method. They used quadrilateral panels with linear vorticity distribution for the lifting surface and triangular panels for the wake. They developed an approximation for far-field calculations using concentrated vortex cores. They found that the core approximation could be used with accuracy at a distance of five times the local length of the triangular element. In this first paper only the setup for solving the problem was presented. Kandil, Chu and Tureaud [1984] extended the development to unsteady flow. However, results were presented for only steady motion of rectangular plates with no wing tip separation and no far field calculations were included. One problem with this approach could have been the method used to impose the Kutta condition.

Kim [1985] extended the method developed earlier by Yen through eliminating a couple of problem areas. He started with a two-dimensional model in which the surface was represented by a set of panels with linearly varying vorticity, and the wake was modeled as a system of discrete vortex cores emanating from the trailing edge. The strength of the trailing edge core was related to the change in circulation of the airfoil and the Kutta condition was applied by setting the vortex sheet strength to zero at the trailing edge. This method had all

the elements of the future three-dimensional model. This method, as refined by Mook et al [1987] gave very good agreement with experimental results for both steady and unsteady two-dimensional potential-flow problems. Using this two-dimensional method as a guide, Kim then developed a steady three-dimensional model. He used triangular panels of linearly varying vorticity for lifting and nonlifting bodies. For lifting bodies the wake was modeled as a set of discrete vortex filaments emanating from the sharp edge. This effectively eliminated two problems with Yen's approach: the wake vortex sheet could now roll up as tightly as needed, and the strength of the vortex sheet was automatically adjusted as the sheet spread. However, the Kutta condition was still imposed in the same way as that by Yen. In the solution of the steady problem the position of the wake, the wake strength and the vorticity strength of the lifting surface were determined iteratively until the strengths and positions converged. One undesirable feature of this method is the use of a leading-edge extension to move the wake filaments away from the actual separation point. This feature is eliminated in the present model.

To the best of my knowledge, since Kim's development, there has been no further contributions using the idea of vortex panels for the lifting surface.

To determine the applicability and usefulness of the present method, some results are compared with results of the vortex-lattice method. Therefore, this method is briefly reviewed.

The vortex-lattice method has been widely used for both steady and unsteady aerodynamics for a variety of bodies and lifting surfaces. There is some duplication of effort using this method but generally this is only for the simplest configurations. Belotserkovskii [1969] was apparently the first to present results using the vortex-lattice method. He obtained steady total force and moment about the leading edge for a unit-aspect-ratio rectangular flat plate wing tip separation. Kandil [1974] and Konstadinopoulos [1981] also presented results for this configuration. Konstadinopoulos compared his method with those of Belotserkovskii and Kandil: the normal force showed no difference in the three solutions, the moment showed a slight difference with Kandil's not comparing well with the other two. Konstadinopoulos also used this configuration to show convergence of the method as the number of elements is in-

creased but convergence was not outstanding and the normal force coefficient was the only aerodynamic quantity presented.

The second steady configuration, evaluated by several authors, is a unit-aspect-ratio delta wing. This configuration was analyzed by Maddox [1973], Kandil [1974], Kandil, Mook and Nayfeh [1974], Konstadinopoulos [1981] and Elzebda [1986]. The last two attempted to show how the normal force converges as the number of elements increases, but the convergence is not uniform for the two supposedly identical methods.

The potential-flow solutions for flow around closed non-lifting bodies obtained by the vortex-lattice method were presented by Asfar, Mook and Nayfeh [1978]. Four bodies were analyzed: a sphere, an ellipsoid of revolution, an ogive-cylinder and a cone-cylinder. For the sphere fifty equidistant ring elements were used. The results show, even for this large mesh, that the pressure distribution differs slightly from the analytical solution.

The unsteady analysis using the vortex-lattice method was presented by Thasher [1979] and Atta [1976]. Thasher presented time histories of the normal force and pitching-moment coefficients for a rectangular wing of a unit-aspect-ratio pitching about its leading and trailing edges. Thrasher also presented results for a yawing type motion of a rectangular wing. The rolling moment for an aspect ratio 0.71 delta wing was presented by Atta for both constant and varying roll rates.

The coupling of the aerodynamic and dynamic equations was first accomplished by Thrasher [1977] using a fourth-order predictor-corrector scheme. This motivated Konstadinopoulos, Mook and Nayfeh [1981] to attempt a numerical simulation of one degree of freedom wing rock of slender delta wings. Elzebda et al [1985] extended the investigation to two degree of freedom dynamic model. Thrasher [1979] also presented results for rectangular wings with flaps.

There has been much experimental work for wings dominated by vortex flows. Unfortunately it seems as if there is more on flow visualization than dynamic testing. Apparently the first static tests on slender delta wings were performed by Tosti [1947]. He determined the classical stability derivatives for delta wings with aspect ratios of 0.5, 1.0, 2.0, and 3.0. A test of flat or nearly flat plates with various planforms was conducted by Peckham [1958] .

Included in the various planforms are delta wings of aspect ratio 1.00, 1.33 and 1.67. Peckham also included pressure distributions as part of the results. Shanks [1963] investigated a series of six sharp, thin delta wings with leading-edge-sweep angles between 70 and 84 degrees. The wings used by Shank had a centerline protrusion on the upper surface that housed the sting balance. His results are not consistent with the other experiments. He also presented the pitching-moment data referenced to the center of gravity location instead of the mean aerodynamic chord, which is the location for the other experiments. Earnshaw and Lawford [1964] also studied a series of six delta wings; the range of leading edge sweep for this series was 45 to 76 degrees. The pitching-moment data showed significant scatter for this set of experiments. Wentz and Kolman [1968] also investigated a series of delta wings with varying leading-edge sweep angles in increments of 2.5 degrees. The pitching-moment results for these tests were presented for only higher angles of attack. Hummel [1979] thoroughly investigated the flow around a unit-aspect-ratio delta wing at 20.5 degrees angle of attack. For this angle of attack, he presented pressure distributions on the wing and pressure contour plots in series of planes down stream of the wing perpendicular to the flow. The wing used by Hummel was flat on the top but diamond shaped on the bottom. This was done so that the pressure probes could be included. He also presented force and moment data for a range of angles of attack. Because the wing was not flat the aerodynamic quantities are not zero at zero angle of attack. Steady pressure distributions were presented by Harvey [1958], and Fink and Taylor [1955] for an aspect-ratio 0.71 delta wing at varying yaw orientations. The pressure distribution was presented at only one chord location. The static-test results for sharp delta wings are not always in good agreement.

Forced-oscillation tests were conducted about all three axis of the wing. Woodgate and Pugh [1963] and Woodgate [1968]performed cyclic pitch oscillation tests of two sharp delta wings. These wings had aspect ratios of 0.654 and 1.484. Nguyen, Yip and Chambers [1981] conducted forced rolling oscillation and rotary yawing tests on an aspect ratio 0.71 delta wing. Schlottmann [1971] presented results for forced rolling motion of a unit-aspect-ratio delta wing showing the effect of roll rate on the rolling-moment coefficient. The present method will be compared with the results of Woodgate and Pugh.

The only free oscillation tests of delta wings were conducted by Nguyen et al [1981] and Levin and Katz [1982]. Both experiments were run to investigate one-dimensional wing rock. For a complete review of the investigation of wing rock see Elzebda [1985].

1.7 Method of Presentation

Chapter II contains the complete development of the aerodynamic model. The formulation for closed non-lifting bodies will be presented in its entirety before the lifting problem is discussed. Chapter III contains the development of the dynamic model and the method used to couple the aerodynamics and dynamics. Chapter IV contains the control surface analysis and the results of simulated wind-tunnel tests. Finally the conclusions and recommendations are presented in Chapter V.

Chapter II

Aerodynamic Model

2.1 Introduction

In this chapter the aerodynamic model is completely developed. As mentioned in Chapter I, a panel method is used to describe the potential-flow aerodynamics. The bound surface is modeled as a collection of triangular panels on which the surface vorticity vector is piecewise linearly varying. The free vortex sheet, or wake, is modeled as a lattice of discrete vortex cores which is a generalization of the procedure employed in the unsteady vortex-lattice method. This choice of modeling capitalizes on the best features of both panel methods and vortex-lattice methods in the sence that the pressure on the bound surface is continuous, and the wake is progressively formed in the force-free position.

In this chapter the mathematical formulation of the potential-flow problem is presented in several subsections. First, the problem for non-lifting bodies and the integral equation for the velocity induced by a region of vorticity are developed. Next the evaluation of the integrals is presented for a general triangular element. The method for joining the elements is developed. The solution technique and examples for non-lifting bodies are discussed. The equation for determining the pressure on the surface is derived. Next the problem for lifting surfaces is presented. This formulation includes the features unique to lifting surfaces, namely the induced velocity of a vortex core, edge compatibility conditions, the Kutta condition and the development of the wake. The method used for redistributing the vorticity in the wake as the lattice stretches is presented. This is followed by a discussion of the tests performed to determine how well the discretized wake simulates a continuous vortex sheet. The general matrix equations are then developed. The results of the convergence and accuracy tests for thin lifting surfaces are discussed. The results for the two basic wing planforms are presented and compared with experimental results and results obtained from the vortex-lattice method.

2.2 Formulation for Non-lifting Closed Bodies

The continuity equation for incompressible flow is

$$\text{div } \vec{V} = 0, \qquad (2.2-1)$$

where $\vec{V}$ is the total velocity of the fluid. The boundary conditions for non-lifting bodies are that there is no flow through the body (the no-penetration condition), which can be written as

$$(\vec{V}_b - \vec{V}) \cdot \vec{n} = 0 \quad \text{on } S \qquad (2.2-2)$$

where S is the surface of the body, $\vec{n}$ is the normal to the surface and $\vec{V}_b$ is the velocity of S; and that the disturbance velocity tends to zero as the distance from the body is increased.

The total velocity can be written as the sum of the disturbance velocity $\vec{V}_d$ and the free-stream velocity $\vec{V}_{fs}$ for the case where the fluid is moving past the body, that is a wind-tunnel experiment, or as the difference of the disturbance velocity and the velocity of the body V_b moving through the stationary fluid, free flight. The total velocity is then

$$\vec{V} = \vec{V}_d + \vec{V}_{fs}. \qquad (2.2-3)$$

Next we determine the disturbance velocity induced by the body. By definition

$$\vec{\Omega}(\vec{r}) = \text{curl } \vec{V}_d(\vec{r}) \qquad (2.2-4)$$

where $\vec{\Omega}(\vec{r})$ is the vorticity field. The derivation presented by Karamcheti [1980] is followed. It follows from Equation 2.2-1 that field is chosen,

$$\vec{V} = \text{curl } \vec{A} \qquad (2.2-5)$$

where $\vec{A}$ is a twice continuously differentiable vector field, the continuity equation gives

$$\text{div (curl } \vec{A}) = 0 \qquad (2.2-6)$$

which is satisfied for any $\vec{A}$. One can further stipulate that div $\vec{A} = 0$, Karamcheti [1980]. Therefore, the problem of finding the disturbance velocity reduces to one of finding the solution of the following equation:

$$\vec{\Omega} = -\nabla^2 \vec{A}. \tag{2.2-7}$$

Green's theorem can be used to show that

$$\vec{A}(\vec{r},t) = \frac{1}{4\pi} \iiint_T \frac{\vec{\Omega}(\vec{s},t)}{|\vec{r} - \vec{s}|} d\tau \tag{2.2-8}$$

where $\vec{\Omega}$ is the vorticity at point $\vec{s}$, $\vec{r}$ is the point of interest and T is the region of the flow field containing vorticity. In the present work, the vorticity is confined to a thin region between two surfaces S and S_1; S is on and S_1 is slightly outside the body (a boundary layer of vorticity). In the present model, we let the thickness of the vorticity-containing region approach zero. In the limiting process, two things happen: (1) $|\vec{\Omega}|$ approaches infinity while the product of $|\vec{\Omega}|$ and the thickness remains constant, and (2) $\vec{\Omega}$ becomes tangent to the surface S. We can write

$$\vec{\gamma}(\vec{s},t) = \lim_{|\vec{\Omega}| \to \infty,\ h \to 0} \vec{\Omega} h \tag{2.2-9}$$

where h is the distance across the vorticity containing region and $\vec{s}$ is the position of a point on S. Clearly $\vec{\gamma}$ is the discontinuity, or jump, in the surface velocity across S. Equation 2.2-8 can be written as

$$\vec{A}(\vec{r},t) = \frac{1}{4\pi} \iint_S \frac{\vec{\gamma}(\vec{s},t)}{|\vec{r} - \vec{s}|} d\sigma. \tag{2.2-10}$$

As a consequence, the entire disturbance velocity is generated by an integral over the surface of the body, S:

$$\vec{V}_d(\vec{r},t) = \text{curl}\,\vec{A} = \frac{1}{4\pi}\,\text{curl}\iint_S \frac{\vec{\gamma}(\vec{s},t)}{|\vec{r}-\vec{s}|}\,d\sigma. \qquad (2.2-11)$$

The constraint equation comes from the fact that, the divergence of the curl of a vector is always zero. Thus, any vector field that is a possible representation of the surface velocity must satisfy

$$\text{div}\,\vec{\gamma} = 0. \qquad (2.2-12)$$

The problem is to find the vector $\vec{\gamma}(\vec{r})$ that most nearly satisfies Equation 2.2-2 subject to 2.2-12.

2.3 Velocity Induced by a Triangular Element

The disturbance velocity given by Equation 2.2-11 is approximated by representing the surface of the body by a system of triangular elements, determining the velocity field induced by each element, and then summing the results. A local coordinate system is used to obtain the contribution from each element. The local coordinate frame always has the positive x direction along the longest side of the triangle. The positive y direction is in the plane of the triangle such that the vertex not on the x axis has positive x and y coordinates. The local z direction completes the right-hand system. A general triangular element is shown in Figure 1.

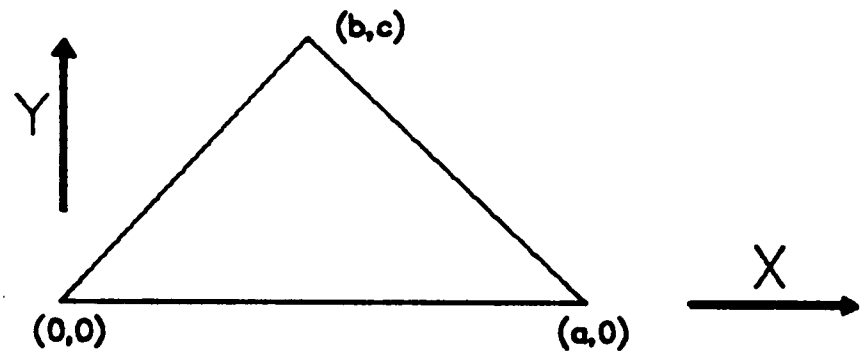

Figure 1. Triangular Element and Local Coordinate System

In the local coordinate frame the surface velocity vector is in the x and y directions. That is

$$\vec{\gamma} = \gamma_x \vec{i} + \gamma_y \vec{j}. \qquad (2.3-1)$$

The surface velocity vector of each element is approximated by a linearly varying function; thus, three basis functions are needed to express the linear variation of each component of this vector. The following are used:

$$f_1 = a_1 x + b_1 y + 1 \qquad (2.3-2)$$

$$f_2 = a_2 x + b_2 y \qquad (2.3-3)$$

$$f_3 = a_3 x + b_3 y \qquad (2.3-4)$$

where

$$a_1 = -\frac{1}{a}, \quad b_1 = \frac{b-a}{ac}, \quad a_2 = \frac{1}{a}, \quad b_2 = -\frac{b}{ac}, \quad a_3 = 0 \quad \text{and} \quad b_3 = \frac{1}{c} \qquad (2.3-5)$$

and a, b and c are the coordinates of the vertices in local coordinates as shown in Figure 1. Basis f_1 is unity at the origin and zero at the other vertices, basis f_2 is unity at the vertex (a,0) and zero at the other vertices, and f_3 is unity at vertex (b,c) and zero at the others.

The components of the vorticity vector can be written as

$$\gamma_x = \gamma_{x1} f_1 + \gamma_{x2} f_2 + \gamma_{x3} f_3 \qquad (2.3-6)$$

$$\gamma_y = \gamma_{y1} f_1 + \gamma_{y2} f_2 + \gamma_{y3} f_3 \qquad (2.3-7)$$

where the γ_{xi} and γ_{yi} are the six unknown magnitudes at the nodes. In this notation the divergence constraint, Equation 2.2-12, can easily be written as

$$\text{div}\vec{\gamma} = \frac{\partial \gamma_x}{\partial x} + \frac{\partial \gamma_y}{\partial y} = \sum_{i=1}^{3} a_i \gamma_{xi} + \sum_{i=1}^{3} b_i \gamma_{yi} = 0. \qquad (2.3-8)$$

The velocity induced by the vorticity on a triangular element can be expressed in terms of the γ_{xi} and γ_{yi}.

The following notation is used for the components of the disturbance velocity of an element in the local coordinate frame:

$$\vec{V}_d = V_x \vec{i} + V_y \vec{j} + V_z \vec{k}. \qquad (2.3-9)$$

Now let us consider a point in space where the disturbance velocity is to be calculated. In the local frame of the element, this point has the coordinates x_p, y_p and z_p. Then the contribution to the vector potential $\vec{A}$ from the vorticity on element i, $\vec{A}_i$, is given by

$$\vec{A}_i = A_{xi} \vec{i} + A_{yi} \vec{j} \qquad (2.3-10)$$

where

$$A_{xi} = \frac{1}{4\pi} \iint_{S_i} (\gamma_{x1} f_1 + \gamma_{x2} f_2 + \gamma_{x3} f_3) \frac{dxdy}{r} \qquad (2.3-11)$$

$$A_{yi} = \frac{1}{4\pi} \iint_{S_i} (\gamma_{y1} f_1 + \gamma_{y2} f_2 + \gamma_{y3} f_3) \frac{dxdy}{r} \qquad (2.3-12)$$

$$r = \left[(x - x_p)^2 + (y - y_p)^2 + z_p^2\right]^{1/2} \qquad (2.3-13)$$

and S_i is the area of element i. The contribution to the velocity field from the element is given by

$$\vec{V}_i = \text{curl } \vec{A}_i = -\frac{\partial A_{yi}}{\partial z_p}\vec{i} + \frac{\partial A_{xi}}{\partial z_p}\vec{j} + \left(\frac{\partial A_{yi}}{\partial x_p} - \frac{\partial A_{xi}}{\partial y_p}\right)\vec{k} \qquad (2.3-14)$$

The partial derivatives can be written in the following convenient forms:

$$-\frac{\partial A_y}{\partial z_p} = V_x = -\frac{1}{4\pi}\sum_{i=1}^{3}\gamma_{yi}\frac{\partial B_i}{\partial z_p} \qquad (2.3-15)$$

$$\frac{\partial A_x}{\partial z_p} = V_y = \frac{1}{4\pi}\sum_{i=1}^{3}\gamma_{xi}\frac{\partial B_i}{\partial z_p} \qquad (2.3-16)$$

$$\left(\frac{\partial A_y}{\partial x_p} - \frac{\partial A_x}{\partial y_p}\right) = V_z = \frac{1}{4\pi}\sum_{i=1}^{3}\left[\gamma_{yi}\frac{\partial B_i}{\partial x_p} - \gamma_{xi}\frac{\partial B_i}{\partial y_p}\right] \qquad (2.3-17)$$

where

$$B_i = = \iint_{S_i}\frac{1}{r} f_i \, d\sigma_i \qquad (2.3-18)$$

$$\frac{\partial B_i}{\partial x_p} = a_i I_1 + b_i I_4 + (a_i x_p + b_i y_p + \delta_{i1}) I_7 + a_i I_{10} \qquad (2.3-19)$$

$$\frac{\partial B_i}{\partial y_p} = a_i I_2 + b_i I_5 + (a_i x_p + b_i y_p + \delta_{i1}) I_8 + b_i I_{10} \qquad (2.3-20)$$

$$\frac{\partial B_i}{\partial z_p} = a_i I_3 + b_i I_6 + (a_i x_p + b_i y_p + \delta_{i1}) I_9 \qquad (2.3-21)$$

and where the a_i and b_i are defined by Equation 2.3-5 and δ_{ij} is the Kronecker delta. In closed form, for a general triangle as shown in Figure 1, the integrals I_i can be written as

$$I_1 = (x_p - a)\,H_1 + (\frac{a-b}{c})\,H_2 - x_p\,H_3 + \frac{b}{c}\,H_4\,, \quad I_2 = y_p\,H_1 - H_2 - y_p\,H_3 + H_4$$

$$I_3 = z_p\,H_1 - z_p\,H_3\,, \quad I_4 = x_p\,H_5 - H_6 + x_p\,H_7 - H_8 + r_3 - r_1$$

$$I_5 = y_p\,H_5 - \frac{b}{c}\,H_6 + (y_p + \frac{ac}{b-a})\,H_7 - \frac{c}{b-a}\,H_8 - y_p\,H_9$$

$$I_6 = z_p\,H_5 + z_p\,H_7 - z_p\,H_9\,, \quad I_7 = -H_1 + H_3\,, \quad I_8 = -H_5 - H_7 + H_9$$

$$I_9 = \mathrm{sgn}(z_p)[J_1 + J_2 + J_3 - \Delta\theta]$$

$$I_{10} = R_1\,Q_1 + R_2\,Q_2 + R_3\,Q_3 + |z_p|(J_1 + J_2 + J_3 - \Delta\theta), \qquad (2.3-22)$$

where the H_i are defined by

$$H_1 = \frac{Q_2}{\sqrt{\alpha_1}}\,, \quad H_2 = \frac{[r_2 - r_3]}{\alpha_1} - \frac{\alpha_2}{\alpha_1}\,H_1\,, \quad H_3 = \frac{Q_1}{\sqrt{\alpha_3}}$$

$$H_4 = \frac{[r_2 - r_1]}{\alpha_3} + \frac{\alpha_4}{\alpha_3}\,H_3\,, \quad H_5 = \frac{b}{c}\,H_3\,, \quad H_6 = \frac{[r_2 - r_1]}{\alpha_5} + \frac{\alpha_6}{\alpha_5}\,H_5$$

$$H_7 = \frac{a-b}{c}\,H_1\,, \quad H_8 = \frac{[r_3 - r_2]}{\alpha_7} + \frac{\alpha_8}{\alpha_7}\,H_7\,, \quad H_9 = Q_3. \qquad (2.3-23)$$

The α_i are defined by

$$\alpha_1 = \frac{(b-a)^2 + c^2}{c^2}\,, \quad \alpha_2 = \left(\frac{b-a}{c}\right)(a - x_p) - y_p\,, \quad \alpha_3 = \frac{b^2 + c^2}{c^2}$$

$$\alpha_4 = \frac{b}{c}\,x_p + y_p\,, \quad \alpha_5 = \frac{c^2 + b^2}{b^2}\,, \quad \alpha_6 = x_p + \frac{c}{b}\,y_p$$

$$\alpha_7 = \frac{(b-a)^2 + c^2}{(b-a)^2}, \qquad \alpha_8 = x_p + a\left(\frac{c}{b-a}\right)^2 + y_p \frac{c}{b-a}. \tag{2.3-24}$$

The r_i are defined as

$$r_1 = [x_p^2 + y_p^2 + z_p^2]^{1/2}, \qquad r_2 = [(b-x_p)^2 + (c-y_p)^2 + z_p^2]^{1/2}$$

$$r_3 = [(a-x_p)^2 + y_p^2 + z_p^2]^{1/2}. \tag{2.3-25}$$

The Q_i are defined by

$$Q_1 = \ln\left[\frac{r_1 + r_2 + d_1}{r_1 + r_2 - d_1}\right]$$

$$Q_2 = \ln\left[\frac{r_2 + r_3 + d_2}{r_2 + r_3 - d_2}\right]$$

$$Q_3 = \ln\left[\frac{r_3 + r_1 + d_3}{r_3 + r_1 - d_3}\right]. \tag{2.3-26}$$

and the J_i are defined by

$$J_1 = \mathrm{sgn}(R_1)\left[\tan^{-1}\left(\frac{|z_p|}{|R_1|}\,\frac{s_{12}}{r_2}\right) - \tan^{-1}\left(\frac{|z_p|}{|R_1|}\,\frac{s_{11}}{r_1}\right)\right]$$

$$J_2 = \mathrm{sgn}(R_2)\left[\tan^{-1}\left(\frac{|z_p|}{|R_2|}\,\frac{s_{22}}{r_3}\right) - \tan^{-1}\left(\frac{|z_p|}{|R_2|}\,\frac{s_{21}}{r_2}\right)\right]$$

$$J_3 = \mathrm{sgn}(R_3)\left[\tan^{-1}\left(\frac{|z_p|}{|R_3|}\,\frac{s_{32}}{r_1}\right) - \tan^{-1}\left(\frac{|z_p|}{|R_3|}\,\frac{s_{31}}{r_3}\right)\right]. \tag{2.3-27}$$

For integrals I_9 and I_{10}, $\Delta\theta = 2\pi$ if the projection of the point of interest onto the local x-y plane is inside the triangle, that is if R_1, R_2 and R_3 are all positive, and $\Delta\theta = 0$ elsewhere. The R_i are given by

$$R_1 = x_p S_1 - y_p C_1$$

$$R_2 = (x_p - b) S_2 - (y_p - c) C_2$$

$$R_3 = (x_p - a) S_3 - y_p C_3, \qquad (2.3-28)$$

the s_{ij} are specified by

$$s_{11} = -x_p C_1 - y_p S_1, \quad s_{12} = (b - x_p) C_1 + (c - y_p) S_1$$

$$s_{21} = (b - x_p) C_2 + (c - y_p) S_2, \quad s_{22} = (a - x_p) C_2 - y_p S_2$$

$$s_{31} = (a - x_p) C_3 - y_p S_3, \quad s_{32} = -x_p C_3 - y_p S_3, \qquad (2.3-29)$$

the C_i and S_i are given by

$$C_1 = \frac{b}{d_1}, \quad S_1 = \frac{c}{d_1}$$

$$C_2 = \frac{a-b}{d_2}, \quad S_2 = -\frac{c}{d_2}$$

$$C_3 = -1, \quad S_3 = 0. \qquad (2.3-30)$$

and finally the d_i are given by

$$d_1 = [b^2 + c^2]^{1/2}, \quad d_2 = [(a-b)^2 + c^2]^{1/2}, \quad d_3 = a. \qquad (2.3-31)$$

The integrals depend solely on the coordinates of the vertices of the triangular element and of the point where the velocity is to be found. Some of the closed-form integrals were obtained with the help of an article by Hess and Smith[1962]. The complete derivation of these equations is shown in Appendix I. The disturbance velocity clearly tends to zero as the distance from the singularity (i.e., element) increases. Thus, the "infinity condition" is satisfied.

The J_l are undefined on certain planes. This problem is resolved by evaluating the limits of J_l as these planes are approached and this limit is used as the value of the J_l on the plane. This resolution is appropriate because the J_l are continuous everywhere except along the edge of the triangular elements. Across the surface of the triangle the normal component of velocity is continuous, but the tangential components are not. All the limits needed to determine the disturbance velocity at any point in the field are also evaluated in Appendix I along with a listing of the subroutine that implements the above equations and limits. Now that the disturbance velocity at any point is expressed in terms of the vorticity on the surface, the problem of assembling the triangles can now be addressed

2.4 Assembly of the Elements

The contribution to the velocity field induced by one element has been derived, and now the contributions from all the elements need to be summed. As a preliminary step to describing this summation, this section describes the procedure used to maintain the direction and magnitude of the vorticity on the surface as it crosses the edge of adjoining elements.

Two adjoining elements are represented in Figure 2. The nodes (vertices) lie on the actual surface of the body. The unit vector normal to the actual surface at A is $\vec{N}$. The surface vorticity at A, $\vec{\Omega}$, lies in the plane tangent to the actual surface, that is in a plane perpendicular to $\vec{N}$. In the discretized approximation of the surface and the vorticity field, $\vec{\Omega}$ is rotated, with constant magnitude, in the plane defined by $\vec{\Omega}$ and $\vec{N}$ onto the planes of the triangular elements that have A as a common node. This rotation is an important feature of the present method. In Figure 2, $\vec{\gamma}_1$ and $\vec{\gamma}_2$ represent $\vec{\Omega}$ after $\vec{\Omega}$ has been rotated onto the planes of elements one and two, respectively. In the remainder of this discussion only one element is considered and $\vec{\gamma}$ is the vorticity vector at the node in the local element plane.

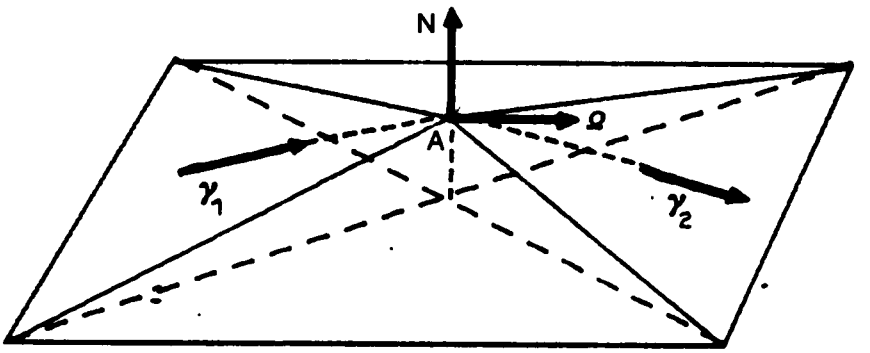

Figure 2. Rotation of the Vorticity Vector

The problem is posed in terms of the two independent components of $\vec{\Omega}$ in the body (global) reference frame. That is, the vorticity vector in the local reference frame of an element, $\vec{\gamma}$, is used only in the calculation of the influence coefficients. This vector is not used to find the solution to Equations 2.2-2 and 2.2-12. The formulas of Section 2.3, make it is necessary to express $\vec{\gamma}$ in terms of the components of $\vec{\Omega}$ consistent with the rotation described above. This choice of variables significantly reduces the number of equations and unknowns of the problem.

The relation between $\vec{\Omega}$ and $\vec{\gamma}$ is determined by defining a vector normal to the plane of $\vec{N}$ and $\vec{\Omega}$. By definition

$$\vec{P} = \vec{N} \times \vec{\Omega}. \qquad (2.4-1)$$

After $\vec{\Omega}$ is rotated onto the plane of an element (the rotated $\vec{\Omega}$ is denoted $\vec{\gamma}$), it is still in the original plane defined by $\vec{N}$ and $\vec{\Omega}$; thus,

$$c\vec{P} = \vec{N} \times \vec{\gamma} \qquad (2.4-2)$$

where the constant c has been introduced because the magnitudes of these cross products can be different. Eliminating $\vec{P}$ from Equations 2.4-1 and 2.4-2 leads to

$$c(\vec{N} \times \vec{\Omega}) = \vec{N} \times \vec{\gamma}. \qquad (2.4-3)$$

After $\vec{\Omega}$ has been rotated into the plane of an element, it still has the same magnitude. Setting the magnitude of the vorticity on the element equal to that at the node yields

$$\gamma_x^2 + \gamma_y^2 = \Omega_X^2 + \Omega_Y^2 + \Omega_Z^2. \qquad (2.4-4)$$

Note that γ_x and γ_y are components in the local frame and Ω_X, Ω_Y and Ω_Z are components in the body frame. Equations 2.4-3 and 2.4-4 are needed when the triangles are assembled; however, in their present form they are not useful. To obtain a more useful form of Equation 2.4-3, we first express both sides in the same coordinate frame. This requires the relationship between the local coordinate frame and the body frame. The body frame has unit vectors $\vec{I}$, $\vec{J}$ and $\vec{K}$ while the local frame has unit vectors $\vec{i}$, $\vec{j}$ and $\vec{k}$. The body frame will be the frame used to determine the vorticity components at the nodes. In other words, the unknowns of the problem are the components of the vorticity vector at the nodes in the body frame.

The body frame is related to the local frame of an element by a transformation (direction-cosine) matrix. There is one such matrix for each element. For element m, the direction-cosine matrix $[a]_m$ is defined by

$$\begin{Bmatrix} \vec{i} \\ \vec{j} \\ \vec{k} \end{Bmatrix} = [a]_m \begin{Bmatrix} \vec{I} \\ \vec{J} \\ \vec{K} \end{Bmatrix} \qquad (2.4-5)$$

The vector $\vec{N}$ is perpendicular to the actual surface of the body. The procedure to approximate this normal is to average the normals of all the elements sharing that node. This method assumes that there are no sharp edges on the closed bodies. (problem for thick wings?

The vectors of Equation 2.4-3 in their respective coordinate frames are

$$\vec{\Omega} = \Omega_X \vec{I} + \Omega_Y \vec{J} + \Omega_Z \vec{K} \qquad (2.4-6)$$

$$\vec{N} = N_X \vec{I} + N_Y \vec{J} + N_Z \vec{K} \qquad (2.4-7)$$

$$\vec{\gamma} = \gamma_x \vec{i} + \gamma_y \vec{j}. \qquad (2.4-8)$$

The body vectors written in the local frame of element m are

$$\vec{\omega} = [a]_m \vec{\Omega} = \omega_x \vec{i} + \omega_y \vec{j} + \omega_z \vec{k} \qquad (2.4-9)$$

$$\vec{n} = [a]_m \vec{N} = n_x \vec{i} + n_y \vec{j} + n_z \vec{k}. \qquad (2.4-10)$$

Because the surface vorticity at the node is perpendicular to the normal to the surface

$$\vec{\Omega} \cdot \vec{N} = 0. \qquad (2.4-11)$$

Or in the local frame of element "i"

$$\vec{\omega} \cdot \vec{n} = 0. \qquad (2.4-12)$$

Equation 2.4-12 leads to

$$\omega_z = -\frac{n_x}{n_z}\,\omega_x - \frac{n_y}{n_z}\,\omega_y. \qquad (2.4-13)$$

The component ω_z was chosen as the dependent component because n_z is not zero except under contrived cases. The vector $\vec{\omega}$ is used in this development because, even though the components of $\vec{\Omega}$ are related, there is no one equation such as 2.4-13 for this relationship for all orientations of the element in the body reference frame.

The vector $\vec{P}$ is then

$$\begin{aligned}\vec{P} = &-\left[\frac{n_x n_y}{n_z}\omega_x + \frac{n_y^2 + n_z^2}{n_z}\omega_y\right]\vec{i} \\ &+\left[\frac{n_x n_y}{n_z}\omega_y + \frac{n_x^2 + n_z^2}{n_z}\omega_x\right]\vec{j} \\ &+\left[n_x\omega_y - n_y\omega_x\right]\vec{k}\end{aligned} \qquad (2.4-14)$$

and

$$c\vec{P} = [-n_z\gamma_y]\vec{i} + [n_z\gamma_x]\vec{j} + [n_x\gamma_y - n_y\gamma_x]\vec{k}. \qquad (2.4-15)$$

Equating the components and determining the local vorticity yields

$$\gamma_x = c\left[\left(\frac{n_x^2 + n_z^2}{n_z^2}\right)\omega_x + \left(\frac{n_x n_y}{n_z^2}\right)\omega_y\right] \qquad (2.4-16)$$

$$\gamma_y = c\left[\left(\frac{n_x n_y}{n_z^2}\right)\omega_x + \left(\frac{n_y^2 + n_z^2}{n_z^2}\right)\omega_y\right]. \qquad (2.4-17)$$

Equating the third component results in a redundant equation. Solving for ω_x and ω_y yields

$$\omega_x = \frac{n_y^2 + n_z^2}{c(n_x^2 + n_y^2 + n_z^2)}\gamma_x - \frac{n_x n_y}{c(n_x^2 + n_y^2 + n_z^2)}\gamma_y \qquad (2.4-18)$$

$$\omega_y = -\frac{n_x n_y}{c(n_x^2 + n_y^2 + n_z^2)}\gamma_x + \frac{n_x^2 + n_z^2}{c(n_x^2 + n_y^2 + n_z^2)}\gamma_y. \qquad (2.4-19)$$

The factor c is determined by equating the magnitude of the vorticity at the node and the magnitude on the triangle at that same node. Putting Equations 2.4-16 and 2.4-17 into Equation 2.4-4 and determining c yields

$$c = \frac{[\omega_x^2 + \omega_y^2 + \omega_z^2]^{1/2}}{[\omega_x^2 + \omega_y^2 + \omega_z^2 + (\frac{\omega_z}{n_z})^2]^{1/2}}. \qquad (2.4-20)$$

In general for each element the factor c has a different value at each vertex.

The specific values of c are not known until the components of surface vorticity at the nodes are known, but the range of values can be determined. Because Equation 2.4-3 can be written as

$$c|\vec{\Omega}|\,|\vec{N}| = |\vec{\gamma}|\,|\vec{N}|\cos\theta \qquad (2.4-21)$$

where θ is the angle between the surface vorticity at the node and the surface vorticity on the triangle at the same node, and the magnitude of the surface vorticity vector is maintained, the relation between the direction of the vorticity vector and the factor c is

$$c = \cos\theta. \qquad (2.4-22)$$

The angle θ can have a range of values that depends on the direction of the vorticity vector. If the vorticity is oriented along the intersection of the elemental and tangential planes, θ is zero. The angle θ is greatest if the vorticity vector is in the plane containing the nodal and elemental normal vectors. Therefore, the maximum value of c is unity and the minimum is the cosine of the angle between the element and node normals. The variation of the angle θ and the orientation of the vorticity vector is shown in Figure 3. Thus if the elements are coplanar the factor c can only be unity. Because c is dependent on the vorticity, it is obtained by iteration to maintain the linearity of the equations. The actual procedure for obtaining the strength of the vorticity at a node is described in detail below.

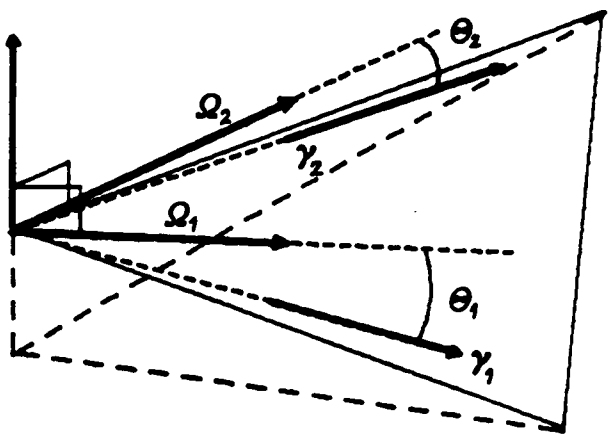

Figure 3. Limits on the Factor c.

The unknowns are the components of the vorticity vector in the body reference frame at the nodes; thus the two independent components of $\vec{\Omega}$ must be chosen and the relation between these unknowns and the components of $\vec{\omega}$ must be developed. For N_z different from zero, the dependent component is chosen to be Ω_z. Then

$$\Omega_Z = -\Omega_X \frac{N_x}{N_z} - \Omega_Y \frac{N_y}{N_z} \qquad (2.4-23)$$

and the unknowns are chosen to be Ω_x and Ω_y. The relationships between the components at the node and the components on the surface elements are

$$\omega_x = (a_{11} - a_{13}\frac{N_x}{N_z})\Omega_X + (a_{12} - a_{13}\frac{N_y}{N_z})\Omega_Y$$

$$\omega_y = (a_{21} - a_{23}\frac{N_x}{N_z})\Omega_X + (a_{22} - a_{23}\frac{N_y}{N_z})\Omega_Y. \qquad (2.4-24)$$

where the a_{ij} are the elements of the direction-cosine matrix defined in Equation 2.4-5. For N_z equal to zero and N_y not equal to zero, the dependent component is chosen to be Ω_Y, where

$$\Omega_Y = -\Omega_X \frac{N_x}{N_y}. \qquad (2.4-25)$$

For this condition, the unknowns are chosen to be Ω_X and Ω_Z. Then

$$\omega_x = (a_{11} - a_{12}\frac{N_x}{N_y})\Omega_X + a_{13}\Omega_Z$$

$$\omega_y = (a_{21} - a_{22}\frac{N_x}{N_y})\Omega_X + a_{23}\Omega_Z. \qquad (2.4-26)$$

For N_z and N_y both zero, Ω_X must be zero; therefore, the independent components are Ω_Y and Ω_Z, and the relationships are

$$\omega_x = a_{12}\Omega_Y + a_{13}\Omega_Z$$

$$\omega_y = a_{22}\Omega_Y + a_{23}\Omega_Z. \qquad (2.4-27)$$

2.5 Matrix Equations for Non-lifting Closed Bodies

There are two sets of equations to be solved simultaneously. The first set represents the no-penetration condition. The second set represents the divergenceless condition. The no-penetration condition requires the normal component of the relative velocity to vanish at all points on the surface. The method used to approximate this condition is to chose a point on each element where the normal component is set to zero. The point chosen is called the control point. The control point used for the entire analysis is the centroid of the nodes of the triangular element. The no-penetration condition at the control points can be made into a set of linear equations in the unknown strength of the components of the vorticity vector at the nodes. In general, for closed non-lifting bodies, the velocity at the control point on an element is the sum of the velocity induced by the surface disturbance and the velocity of the free stream. Summing the contributions one finds that the no-penetration condition for control point i is

$$\sum_{j=1}^{n} A_{ji}\,\Omega_{xj} + \sum_{j=1}^{n} A_{j+nl}\,\Omega_{yj} + \vec{V}_{fs}\cdot\vec{n}_i = 0 \qquad (2.5-1)$$

where the A_{ji} are the velocity components induced by unit vorticity in the body x or y directions at node j normal to element i at its control point and Ω_{xj} and Ω_{yj} are the independent components defined by Equations 2.4-23 through 2.4-27. The actual assembly is not difficult. The influence matrix is created by finding the velocity at a control point due to the six bases, two directions for each node and three nodes for each element. These influence coefficients are then added to the corresponding influence coefficients for all elements sharing a given node. Because the rotation is needed to assemble the influence matrix, a factor c must be chosen to start the process. The obvious choice is unity because this is the upper limit and it is the value when the elements are coplanar.

The matrix equation expressing the no-penetration condition can be written as

$$[A]\,\{\Omega\} = \{U\}. \qquad (2.5-2)$$

The divergenceless condition, Equation 2.3-8, can also be written in matrix form in terms of the same unknowns. This equation is

$$[B]\{\Omega\} = \{0\}. \qquad (2.5-3)$$

The matrix Equations 2.5-2 and 2.5-3 can be solved by a variety of techniques. The present method treats Equation 2.5-3 as weighted constraints. They are adjoined to Equation 2.5-2, and a weighting factor w is used. The weighting factor is a diagonal matrix with a constant factor along the diagonal. The combined equations can be written as

$$\begin{bmatrix} A \\ wB \end{bmatrix}\{\Omega\} - \begin{Bmatrix} U \\ 0 \end{Bmatrix} = \{e\}, \qquad (2.5-4)$$

where $\{e\}$ is the error. In general the number of equations is greater than the number of unknowns and thus $\{e\}$ is not identically zero. Because of this, the square of the error, $\{e\}^2$, is minimized. Using this principle, one can obtain the solution by solving the normal equation

$$\begin{bmatrix} A \\ wB \end{bmatrix}^T \begin{bmatrix} A \\ wB \end{bmatrix}\{\Omega\} = \begin{bmatrix} A \\ wB \end{bmatrix}^T \begin{Bmatrix} U \\ 0 \end{Bmatrix}. \qquad (2.5-5)$$

Equation 2.5-5 can easily be solved by any standard procedure. But since the matrix $[A]$ is dependent on the vorticity, because of the presence of c, the problem is solved by iteration. That is the initial guess for c is used to formulate $[A]$ and $[B]$ and then the unknowns at the nodes are obtained. Using these values, one can compute a new c, form new $[A]$ and $[B]$ matrices, and re-solve the problem. This procedure is repeated until there is no change, within small tolerances, in the unknowns at the nodes from one iteration to the next.

2.6 Results for Non-lifting Closed Bodies

Three test bodies were used to show the accuracy and convergence (robustness) of the method. The three bodies are a sphere, an oblate ellipsoid and a prolate ellipsoid. The ellipsoids are of thickness ratio 10 to 1. These shapes were chosen because the surface ve-

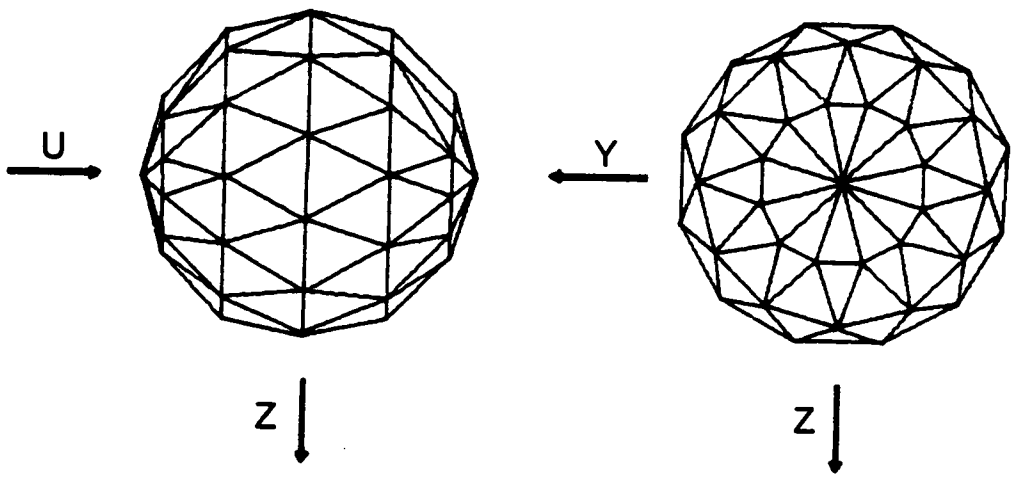

Figure 4. Discretizing the Body

locity is known analytically. Several runs were made with different numbers of elements to show how the numerical results converge to the analytical solution. The sphere, discretized into 120 elements, is shown in Figure 4. The other bodies were discretized in a similar manner. Table 1 shows the effect of the weighting *w* on the surface velocity of a sphere with 120 elements and a radius of one. The quantities presented are the magnitude of the surface velocity at angles of 0, 30, 60 and 90 degrees from the x axis. As seen there is no significant difference for the entire range of weights as long as the method converged. The higher weighting implies the divergence condition are satisfied more closely. There seems to be an upper bound where the divergence condition swamps the minimization process. This result suggests the divergence condition could be imposed exactly using a method of substitution or Lagrange multipliers. These were not implemented because the divergence conditions are not all independent and the method of weighted constraints is very easy to implement.

Table 1. Effect of Various Weights on the Divergenceless Condition

Weight	V(0)	V(30)	V(60)	V(90)
1.0E - 5	did not converge after 15 iterations			
1.0E - 4	0.000000	0.781943	1.309356	1.493643
1.0E - 3	0.000000	0.781948	1.309361	1.493649
1.0E+0	0.000000	0.781948	1.309361	1.493649
1.0E+3	0.000000	0.781948	1.309361	1.493649
1.0E+4	0.000001	0.781955	1.309353	1.493657
1.0E+5	0.000017	0.782052	1.309532	1.493054

The surface velocities at the nodes are compared to the analytical solution in Figure 5 through Figure 7for a weight of 1. The examples show good agreement with the analytical solutions. They also show convergence as the number of elements is increased. As shown in Figure 5, for a sphere the only configuration that does not approximate the analytical solution very closely is the sphere with 48 elements. This configuration is a very coarse mesh. The convergence is shown in Figure 6 and Figure 7. The convergence is most noticeable near the regions where the velocity is changing rapidly, that is, near the top of the oblate ellipsoid and near the front of the prolate ellipsoid. From these figures it is plain the larger meshes do better in approximating the surfaces then the small meshes.

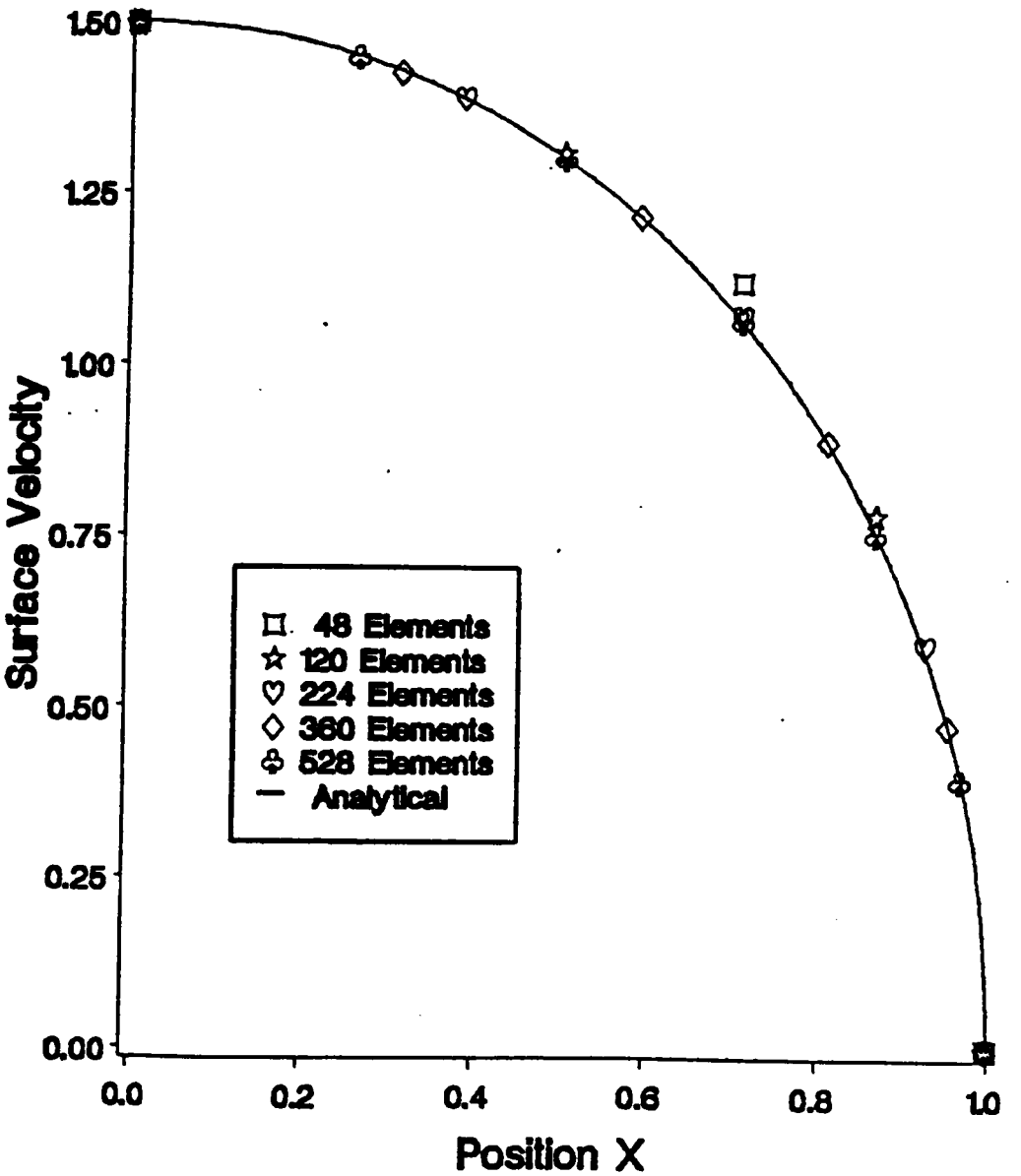

Figure 5. Surface Velocity on a Sphere

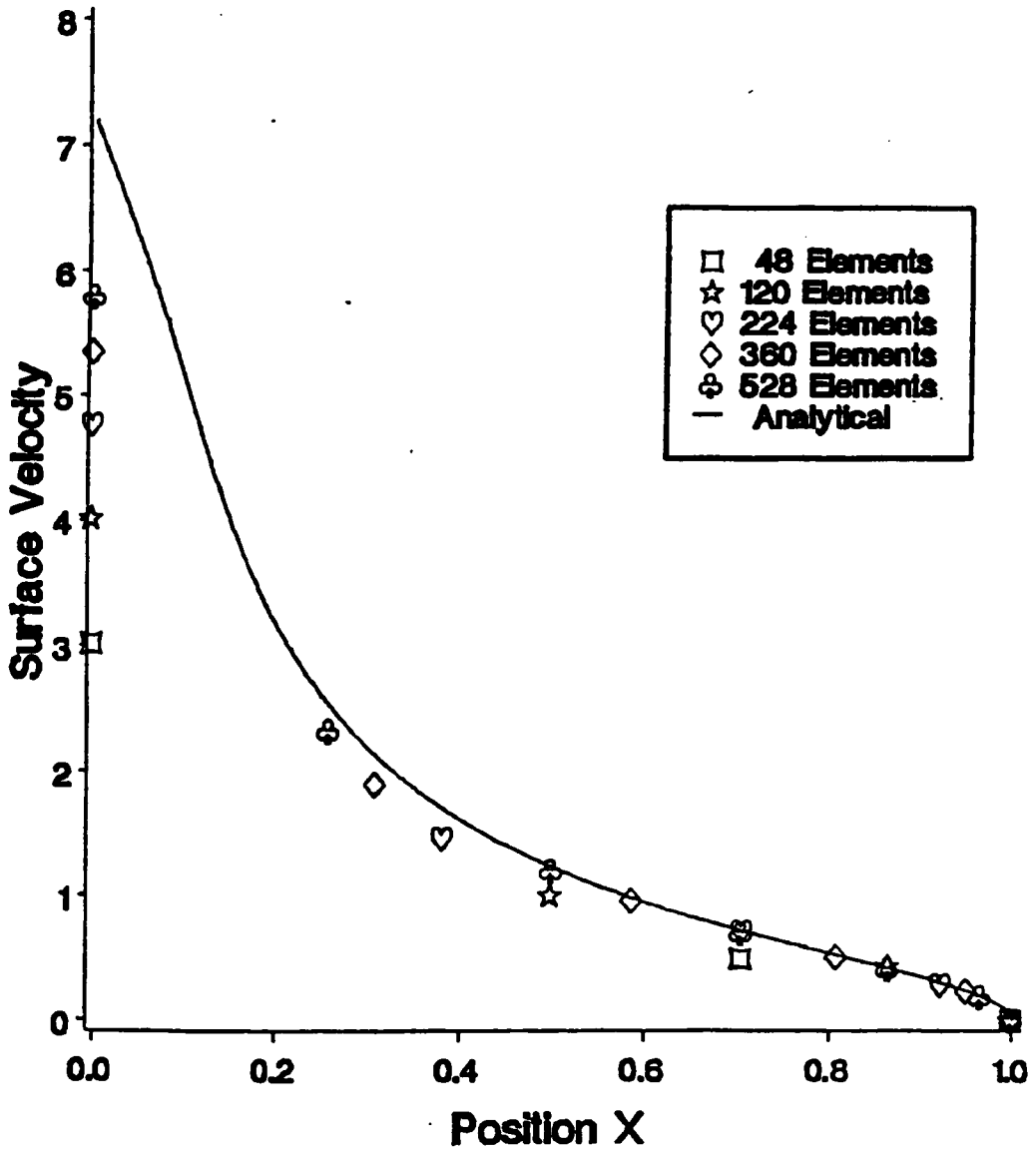

Figure 6. Surface Velocity on an Oblate Ellipsoid

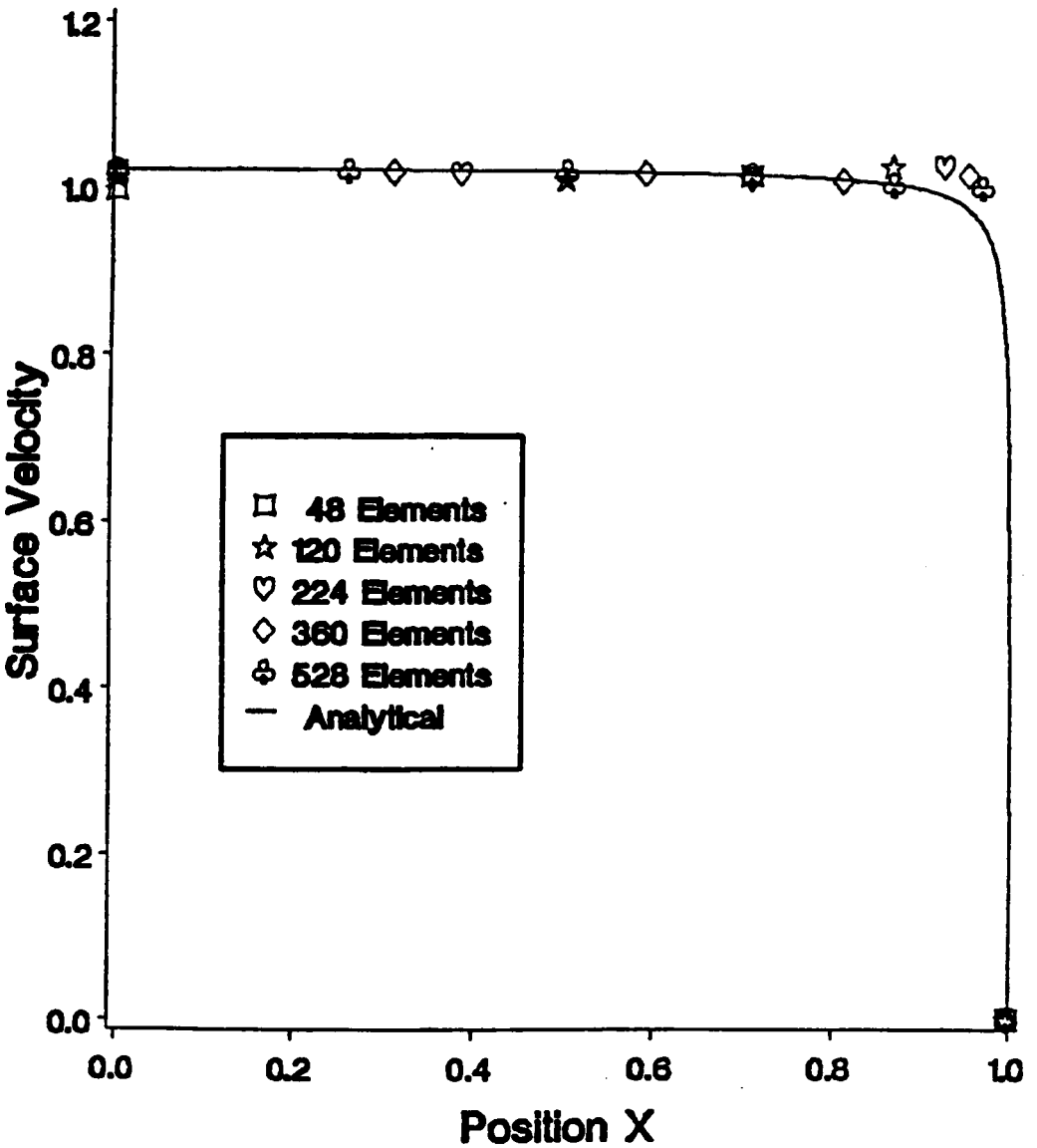

Figure 7. Surface Velocity on an Prolate Ellipsoid

The velocity field away from the body was also analyzed. The analytical solution for a sphere was used to generate the total velocity, at a grid of points. This set of velocities is shown in Figure 8. For this figure the velocity was artificially set to zero for all points inside the body. In Figure 9, the same grid points are also used to show the total velocity obtained from the present method with 120 elements to represent the sphere. The velocities inside the body for this figure were not set to zero, but as can be seen the total velocity inside the body is very nearly zero everywhere, as it should be. For the grid shown in Figure 8 and Figure 9, the maximum difference between the analytical solution and the numerical procedure was 0.087 at the point $(x_p, y_p, z_p) = (0.25, 1.00, 0.00)$. The difference is defined by

$$e = \frac{|\vec{V}_{ana} - \vec{V}|}{|\vec{V}_{fs}|} \qquad (2.6-1)$$

where $\vec{V}_{ana}$ is the velocity of the analytical solution. There is very good agreement between the predicted and analytical velocity throughout the flow field. For all the numerical results isosceles triangles were used for discretizing, and no attempt was made to analyze the effect of different element shapes.

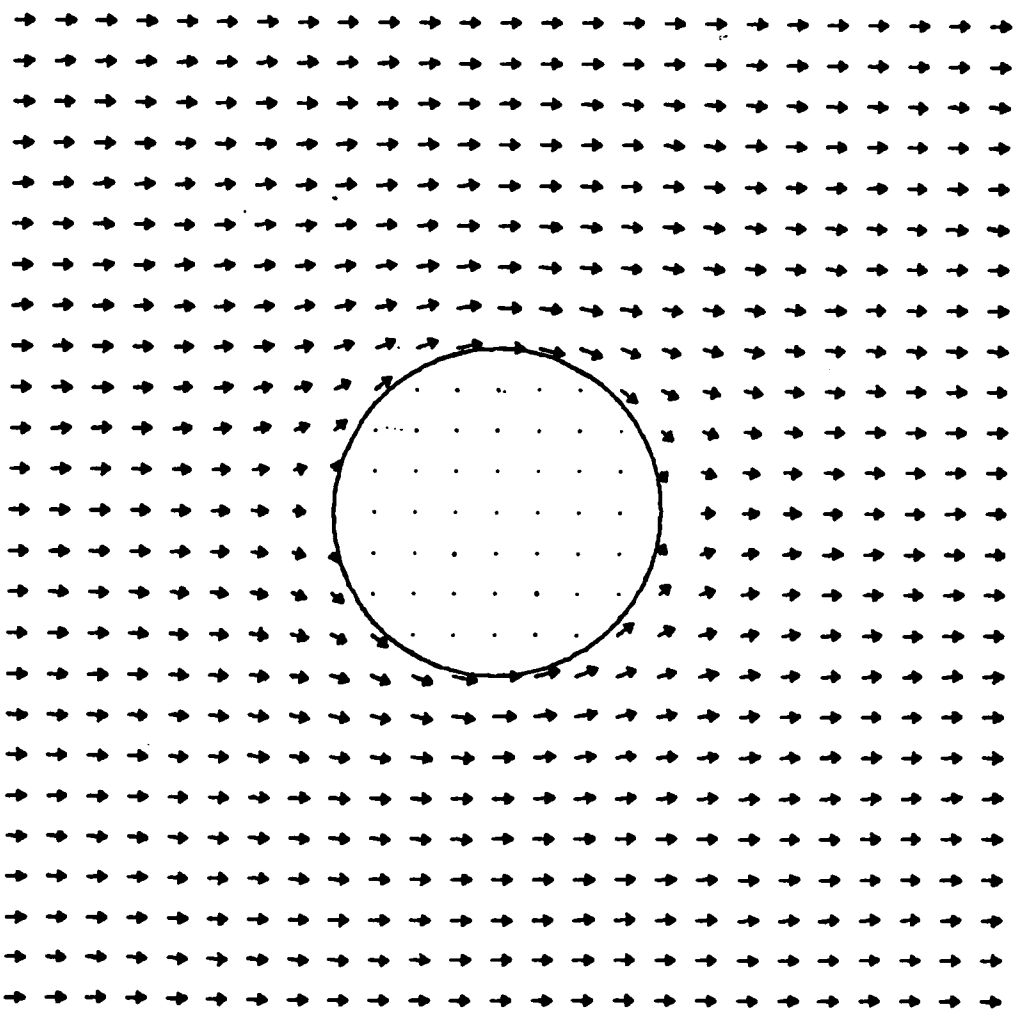

Figure 8. Velocity Around A Sphere Analytical Solution

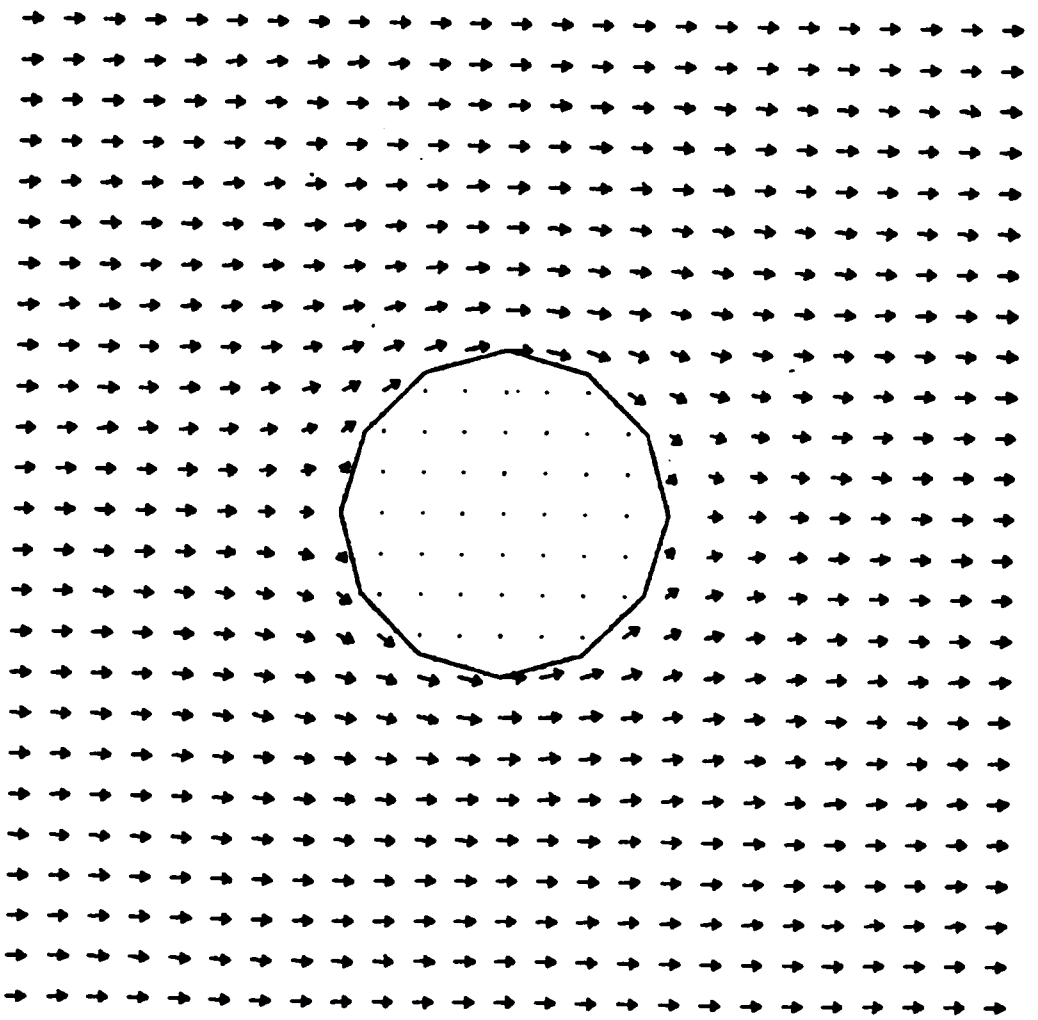

Figure 9. Velocity Around A Sphere Numerical Solution

2.7 Formulation for Thin Lifting Surfaces

The formulation is extended from closed nonlifting bodies to thin lifting surfaces. This extension involves including additional boundary conditions and compatibility equations. The additional boundary conditions are that the Kutta condition must be imposed along the edge where the wake is attached, the theorems of conservation of circulation apply and there cannot be a pressure jump across the surface of the wake. The compatibility equations are developed by requiring consistency between the order of smoothness of the singularity distributions for both closed bodies and thin surfaces. The complete formulation of the problem can be written as solving the continuity equation

$$\text{div}\,\vec{V} = 0 \qquad (2.7-1)$$

subject to

$$(\vec{V}_b - \vec{V})\cdot\vec{n} = 0 \quad \text{on } S \qquad (2.7-2)$$

$$\frac{D\Gamma}{Dt} = 0 \quad \text{on } W \qquad (2.7-3)$$

$$\Delta C_p = 0 \quad \text{along the edge where the wake joins the surface} \qquad (2.7-4)$$

and

$$\vec{V} \to 0 \quad \text{far from } S \text{ and } W \qquad (2.7-5)$$

where W is the wake surface. Equation 2.7-2 is the no-penetration condition on the surface of the body. Equation 2.7-3 is the Theorem of Kelvin and Helmholtz, 2.7-4 is the Kutta condition and Equation 2.7-5 is the infinity condition. Because there is no wake for nonlifting closed bodies, the above formulation reduces to that presented in Section 2.2.

The problem formulation points out the two differences between the two types of bodies. The first is, for thin lifting surfaces, there is an edge. The second is that there is a

wake emanating from that edge. These are important differences and each will be discussed in detail.

2.8 Edge Formulation and Compatibility Conditions

The surface of the body is represented by a vortex sheet. For there to be nonzero vorticity along the edge in the direction perpendicular to the edge there must be some mechanism for either generating or capturing the vortex sheet along the edge. This mechanism is a vortex core of variable strength. The circulation around a vortex core is related to the vortex sheet it adjoins by

$$\frac{d\Gamma}{dx} = -\gamma \qquad (2.8-1)$$

where Γ is the circulation at a point on the core, x is the position along the length of the core and γ is the strength of vortex sheet.

The functional form of the circulation along the edge can be obtained by applying the concept of spatial conservation of vorticity to an elemental piece along the edge. An infinitesimal element of the surface vortex sheet along the edge is shown in Figure 10.
For spatial conservation of vorticity

$$\gamma = \gamma_y. \qquad (2.8-2)$$

The component of vorticity perpendicular to the edge, γ_y , is a linear function on the triangular element. In Figure 11 the definitions of the local coordinate system and the vortex distribution along the edge of an element are shown.

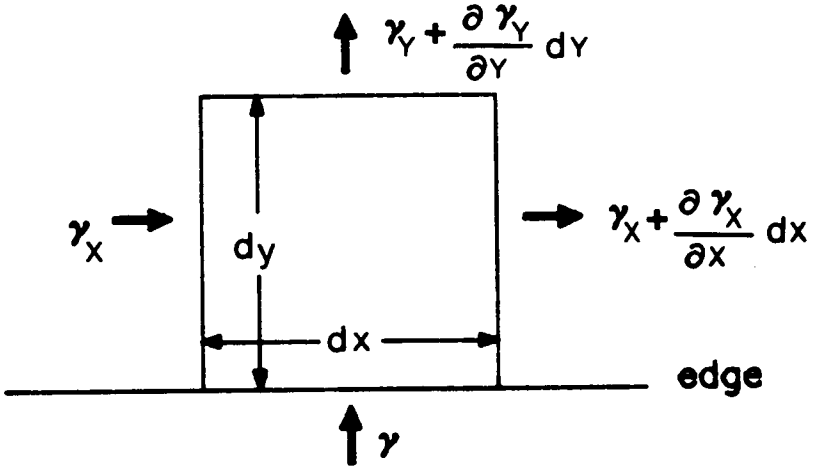

Figure 10. Vortex Sheet Strength Along an Edge

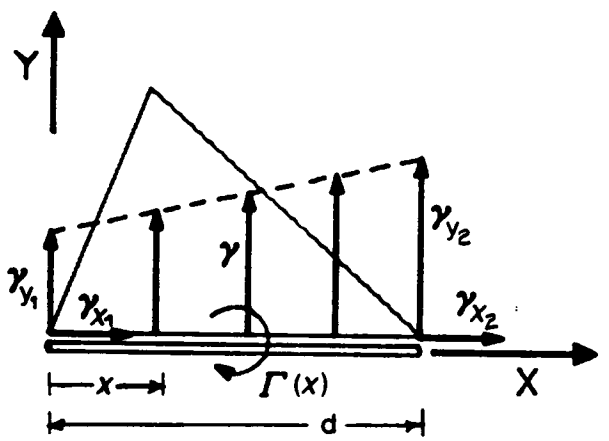

Figure 11. An Edge Core and an Edge Element

along the edge

$$\gamma_y = \frac{\gamma_{y2} - \gamma_{y1}}{d} x + \gamma_{y1}. \qquad (2.8-3)$$

Integrating equation 2.8-1 results in the circulation of the core being

$$\Gamma(x) = \left[\frac{\gamma_{y2} - \gamma_{y1}}{d} \right] \frac{x^2}{2} + \gamma_{y1} x + G \qquad (2.8-4)$$

where G is a constant of integration. Note that the γ_y of equation 2.8-4 is in the local coordinate frame of the variable vortex core, which is not necessarily the local coordinate frame of the adjoining element. Thus, a coordinate transformation may be needed to relate these variables to the unknown vorticity components at the nodes.

From Equation 2.8-4 it seems that unknowns have been added to the system of equations in the form of constants of integration. In reality, once the constraints on the continuity of the vortex core along the edge are introduced there are fewer new unknowns than new equations. Because the vortex sheet is modeled as a set of triangular elements with linearly varying vorticity, the magnitude of the vorticity is continuous but the first and higher derivatives are not necessarily continuous where the elements join. To remain consistent, the circulation around the vortex cores should be continuous through the first derivative because of the relation between the vortex core and the vortex sheet.

To make the circulation continuous in strength around the body, two adjoining edge segments must have the same circulation at the juncture. As an illustration, we suppose that there are two cores joined at a point, one segment be designated n and the other n+1. The circulation around n at the node is

$$\Gamma_n = \left[\frac{\gamma_{y2} - \gamma_{y1}}{d} \right] \frac{d^2}{2} + \gamma_{y1} d + G_n \qquad (2.8-5)$$

where d is the length of vortex core n (see Figure 11). Equation 2.8-5 can be reduced to

$$\Gamma_n = [\gamma_{y2} + \gamma_{y1}]\frac{d}{2} + G_n. \qquad (2.8-6)$$

The circulation around n+1 at the same node is

$$\Gamma_{n+1} = G_{n+1}. \qquad (2.8-7)$$

Then for continuous circulation strength

$$[\gamma_{y2} + \gamma_{y1}]\frac{d}{2} + G_n - G_{n+1} = 0. \qquad (2.8-8)$$

There is the same number of these equations as there are edge cores. Therefore, there is one new equation for each edge node.

For the circulation around the cores along the edges to be continuous through the first derivative, $\frac{d\Gamma}{dx}$ must be continuous. The only possible place the derivative would not be continuous is where two cores join. To illustrate, we suppose there are two cores, one designated n and the other n+1, that join at the point x_0. The smoothness requirement is

$$\left.\frac{d\Gamma_n}{dx}\right|_{x_0} = \left.\frac{d\Gamma_{n+1}}{dx}\right|_{x_0} \qquad (2.8-9)$$

or

$$\gamma_{y\,n}(x_0) = \gamma_{y\,n+1}(x_0) \qquad (2.8-10)$$

where $\gamma_{yn}(x_0)$ and $\gamma_{yn+1}(x_0)$ is the vorticity perpendicular to the cores at the joining node. These two vorticity components are in the coordinate frames of the cores n and n+1, respectively. Equation 2.8-10 is an added relation among the three components of vorticity $\vec{\Omega}$ at the joining nodes. These equations are only included in the system as constraints if adjoining cores are not collinear. If the cores are collinear Equation 2.8-10 is always satisfied provided only one vortex strength and direction is defined on the sheet where the edge cores join.

2.9 Velocity Induced by an Edge Vortex Core

As stated in Section 2.8, whenever there is an edge on a surface, there must be a variable-strength vortex core. For piecewise linearly varying vortex sheets, the circulation around the corresponding edge core is quadraticly varying. The model of the body now has two components, the linearly varying triangular vortex sheets on the surface and the variable strength vortex cores along the edges. The total disturbance velocity is simply the sum of the velocities induced by the components. That is

$$\vec{V}_{dis} = \vec{V}_d + \vec{V}_c \qquad (2.9-1)$$

where $\vec{V}_d$ is the disturbance velocity due to the elements and $\vec{V}_c$ is the velocity due to the edge cores. A general vortex core, its local coordinate frame and the definitions of the variables used to determine the disturbance velocity are shown in Figure 12.

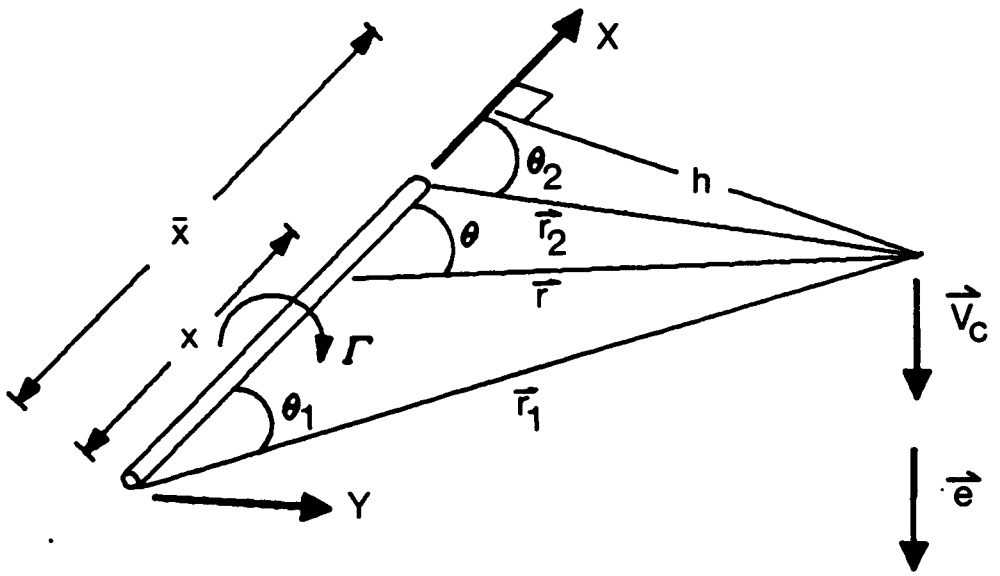

Figure 12. Vortex Core and Local Coordinate Frame

The velocity induced at a point by a variable strength vortex core can be written as

$$\vec{V}_c = V_x\vec{i} + V_y\vec{j} + V_z\vec{k} \qquad (2.9-2)$$

The velocity induced by the core can be obtained from the general formula

$$\vec{V}_c(\vec{r},t) = \frac{1}{4\pi} \text{ curl} \iiint_T \frac{\vec{\Omega}(\vec{s},t)}{|\vec{r}-\vec{s}|} d\tau \qquad (2.9-3)$$

where $\vec{\Omega}$ is the vorticity at point $\vec{s}$, $\vec{r}$ is the point of interest and T is the region of the flowfield containing vorticity (this is the same formulation as for a vortex sheet). The volume element of the core is the scalar product of a cross sectional surface area, in the direction normal to the surface, $\vec{n}dS$, and an element of length $\vec{dl}$ along the core. One can show that the disturbance velocity is

$$\vec{V}_c(\vec{r},t) = \frac{1}{4\pi} \int_L \Gamma(x,t) \frac{\vec{dl} \times (\vec{r}-\vec{s})}{|\vec{r}-\vec{s}|^3} \qquad (2.9-4)$$

where Γ is the circulation around the core. Equation 2.9-4 can be further simplified by changing variables. Then

$$\vec{V}_c = \frac{1}{4\pi} \int_{\theta_1}^{\theta_2} \frac{\Gamma(x,t) \sin\theta}{h} \, d\theta \vec{e}. \qquad (2.9-5)$$

where θ is the angle between the vector along the vortex core and the vector from the point along the core to the point of interest, h, is the perpendicular distance from the axis of the filament to the point and $\vec{e}$ is the unit vector in the direction of the induced velocity. This direction is

$$\vec{e} = \frac{\vec{i} \times \vec{r}}{|\vec{i} \times \vec{r}|} \qquad (2.9-6)$$

The strength of the vortex core can be written as the general quadratic expression

$$\Gamma(x,t) = G_1 \frac{x^2}{2} + G_2 x + G_3. \qquad (2.9-7)$$

In terms of the constants of the quadratic expression, the integral of Equation 2.9-5 can be evaluated. The closed-form expression for the induced velocity is

$$\vec{V}_c = \frac{\vec{e}}{4\pi h}\{G_1 I_1 + G_2 I_2 + G_3 I_3\} \qquad (2.9-8)$$

where

$$I_1 = \frac{1}{2} r^2 \sin^2\theta_1 \ln\left\{\frac{(1-\cos\theta_2)\sin\theta_1}{(1-\cos\theta_1)\sin\theta_2}\right\}$$
$$+\frac{1}{2} r^2 \cos 2\theta_1(\cos\theta_1 - \cos\theta_2) + \frac{1}{2} r^2 \sin 2\theta_1(\sin\theta_1 - \sin\theta_2)$$

$$I_2 = r(1-\cos(\theta_1 - \theta_2))$$

$$I_3 = \cos\theta_1 - \cos\theta_2 \qquad (2.9-9)$$

It should be noted that there are numerical difficulties in evaluating the velocity along the axis of the core. The limits as this region is approached are well behaved except on the core itself. The complete derivation, these limits and a listing of the subroutine used to determine the velocity induced by a variable-circulation vortex core is presented in Appendix II.

2.10 Determination of the Pressure and the Kutta Condition

Now the Kutta condition is developed. We must first determine the pressure coefficient. The pressure coefficient is defined as

$$C_p = \frac{P - P_\infty}{\frac{1}{2}\rho U^2} \qquad (2.10-1)$$

where P is the pressure at the point of interest, P_∞ is the pressure a large distance from the disturbance, ρ is the density and U is a reference velocity.

Bernoulli's equation for unsteady flow is

$$\frac{\partial \phi}{\partial t}\Big|_{\vec{R}} + \frac{V^2}{2} + \frac{P}{\rho} = H(t) \qquad (2.10-2)$$

where $\frac{\partial \phi}{\partial t}|_{\vec{R}}$ is the partial derivative of the velocity potential with respect to time for an inertially fixed point, V is the velocity at the point, P is the pressure, ρ is the density and $H(t)$ is a spatially uniform function of time. At a given instant

$$\frac{\partial \phi}{\partial t}\Big|_{\vec{R}} + \frac{V^2}{2} + \frac{P}{\rho} = \frac{\partial \phi_\infty}{\partial t}\Big|_{\vec{R}_\infty} + \frac{V_\infty^2}{2} + \frac{P_\infty}{\rho_\infty}. \qquad (2.10-3)$$

Far from the body the velocity is either constant, typically zero; therefore the velocity potential is not changing with time there and Equation 2.10-3 reduces to

$$\frac{P - P_\infty}{\rho} = \frac{V_\infty^2 - V^2}{2} - \frac{\partial \phi}{\partial t}\Big|_{\vec{R}} \qquad (2.10-4)$$

The pressure coefficient is then

$$C_p = \frac{1}{U^2}\left[V_\infty^2 - V^2 - 2\frac{\partial \phi}{\partial t}\Big|_{\vec{R}}\right]. \qquad (2.10-5)$$

The entire problem is posed in the body coordinate reference frame. The problem is the points, where the pressure is needed, are not fixed in an inertial reference frame. In fact, these points may not be fixed in the body reference frame. Therefore, Equation 2.10-5 cannot be used in its current form because of the presence of the last term. To find a more useful form, we look at a point on the surface. The point is defined by $\vec{R}$, which is the position vector from the origin of some inertially fixed point to the point on the body at a given instant, t. At some short time later, $t + \Delta t$, the point of interest has moved to a new inertial position, $\vec{R} + \Delta\vec{R}$. By definition

$$\frac{\partial \phi}{\partial t}\Big|_{\vec{R}} = \lim_{\Delta t \to 0} \frac{\phi(\vec{R}, t + \Delta t) - \phi(\vec{R}, t)}{\Delta t}. \qquad (2.10-6)$$

The problem is that the point on the surface is no longer at $\vec{R}$ when time is $t+\Delta t$, it is at $\vec{R}+\Delta\vec{R}$. Using a Taylor series expansion about $\vec{R}$ at time $t+\Delta t$, one can write

$$\phi(\vec{R}+\Delta\vec{R},t+\Delta t)=\phi(\vec{R},t+\Delta t)+\nabla\phi(\vec{R},t+\Delta t)\cdot\Delta\vec{R}+\text{H.O.T.} \qquad (2.10-7)$$

where H.O.T. are higher order terms. Equation 2.10-7 can be written as

$$\phi(\vec{R},t+\Delta t)\simeq\phi(\vec{R}+\Delta\vec{R},t+\Delta t)-\nabla\phi(\vec{R},t+\Delta t)\cdot\Delta\vec{R}+\text{H.O.T.} \qquad (2.10-8)$$

Substituting Equation 2.10-8 into Equation 2.10-6 leads to

$$\frac{\partial\phi}{\partial t}\Big|_{\vec{R}}=\lim_{\Delta t\to 0}\left[\frac{\phi(\vec{R}+\Delta\vec{R},t+\Delta t)-\phi(\vec{R},t)}{\Delta t}-\frac{\nabla\phi(\vec{R},t+\Delta t)\cdot\Delta\vec{R}}{\Delta t}\right] \qquad (2.10-9)$$

where the limit of the H.O.T. is zero. Equation 2.10-9 can be written as

$$\frac{\partial\phi}{\partial t}\Big|_{\vec{R}}=\frac{\partial\phi}{\partial t}\Big|_{\vec{r}}-\nabla\phi(\vec{R},t)\cdot\frac{d\vec{R}}{dt} \qquad (2.10-10)$$

where $\frac{\partial\phi}{\partial t}|_{\vec{r}}$ is the partial derivative of the velocity potential with respect to time for some point on the surface and $\frac{d\vec{R}}{dt}$ is the inertial (absolute) velocity of the point. The body frame is used as the reference frame, then one can write the velocity of any point on the surface as

$$\frac{d\vec{R}}{dt}=\vec{V}_p=\vec{V}_A+\omega\times\vec{r}+\vec{v} \qquad (2.10-11)$$

$\vec{V}_A$ is the inertial velocity of the origin of the body frame, $\vec{\omega}$ is the angular velocity of the body frame with respect to the inertial frame, $\vec{r}$ is the position vector of the point in the body frame and $\vec{v}$ is the velocity of this point with respect to the body frame. Because the gradient of the potential is the absolute velocity of the fluid, Equation 2.10-5 can be written as

$$C_p=\frac{1}{U^2}\left[V_\infty^2-V^2-2\frac{\partial\phi}{\partial t}\Big|_{\vec{r}}+2\vec{V}\cdot\vec{V}_p\right] \qquad (2.10-12)$$

Introducing the dimensionless variables

$$\vec{V}^* = \frac{\vec{V}}{U} \quad \phi^* = \frac{\phi}{UL} \quad \text{and } t^* = \frac{tU}{L} \tag{2.10 – 13}$$

L is a reference length and the superscript n denotes dimensionless quantities. Then Equation 2.10-12 can then be written as

$$C_p = V_\infty^{*2} - V^{*2} - 2\frac{\partial \phi^*}{\partial t^*}\Big|_{\vec{r}} + 2\vec{V}^n \cdot \vec{V}_p \tag{2.10 – 14}$$

Now that the pressure coefficient has been found, the Kutta condition can be formulated. The Kutta condition states.

$$\Delta C_p\Big|_{\text{edge}} = 0 \tag{2.10 – 15}$$

where edge refers to the edges where wakes join the lifting-surface and ΔC_p is defined as

$$\Delta C_p = C_{pl} - C_{pu} = \frac{P_l - P_u}{\frac{1}{2}\rho U^2} \tag{2.10 – 16}$$

The subscript l denotes the lower surface and u denotes the upper surface. The superscripts are dropped because all quantities are dimensionless. Equation 2.10-16 can also be written as

$$\Delta C_p = -V_l^2 - 2\frac{\partial \phi}{\partial t}\Big|_{\vec{r}_l} + 2\vec{V}_l \cdot \vec{V}_{pl} + V_u^2 + 2\frac{\partial \phi}{\partial t}\Big|_{\vec{r}_u} - 2\vec{V}_u \cdot \vec{V}_{pu} \tag{2.10 – 17}$$

Letting $\frac{\partial \phi}{\partial t}|_{\vec{r}_u} = \frac{\partial \phi_u}{\partial t}$ and $\frac{\partial \phi}{\partial t}|_{\vec{r}_l} = \frac{\partial \phi_l}{\partial t}$, using the fact that the scalar product of a vector with itself is the magnitude squared, and realizing that the upper and lower points are at the same location on the body, one can further simplify Equation 2.10-17 to

$$\Delta C_p = 2\frac{\partial(\phi_u - \phi_l)}{\partial t} - V_l \cdot (\vec{V}_l - 2\vec{V}_p) + V_u \cdot (\vec{V}_u - 2\vec{V}_p) \tag{2.10 – 18}$$

With the surface singularity, the velocity on both sides of the vortex sheet can be expressed as the sum of the mean velocity $\vec{V}_m$ and half the jump in velocity caused by the discontinuity, $\Delta\vec{V}$. The upper and lower surface velocities can be written as

$$\vec{V}_u = \vec{V}_m + \frac{1}{2}\Delta\vec{V}$$

$$\vec{V}_l = \vec{V}_m - \frac{1}{2}\Delta\vec{V}. \qquad (2.10-19)$$

Then

$$\Delta C_p = 2\vec{V}_m \cdot \Delta\vec{V} - 2\Delta\vec{V} \cdot \vec{V}_p + 2\frac{\partial(\phi_u - \phi_l)}{\partial t}\Big|_{\vec{r}}. \qquad (2.10-20)$$

Using a first order finite difference to approximate the partial derivative, one can write

$$\frac{\partial(\phi_u - \phi_l)\big|_{\vec{r}}}{\partial t} \simeq \frac{\left[(\phi_u - \phi_l)\big|_{t,\vec{r}} - (\phi_u - \phi_l)\big|_{t-\Delta t,\vec{r}}\right]}{\Delta t}. \qquad (2.10-21)$$

Imposing the Kutta condition along the edge requires

$$0 = 2\vec{V}_m \cdot \Delta\vec{V} - 2\Delta\vec{V} \cdot \vec{V}_p + 2\frac{\left[(\phi_u - \phi_l)\big|_{t,\vec{r}} - (\phi_u - \phi_l)\big|_{t-\Delta t,\vec{r}}\right]}{\Delta t}. \qquad (2.10-22)$$

Finally with the previous time step known the unsteady Kutta condition is

$$\frac{(\phi_u - \phi_l)}{\Delta t}\Big|_{t,\vec{r}} + \vec{V}_m \cdot \Delta\vec{V} - \Delta\vec{V} \cdot \vec{V}_p = \frac{(\phi_u - \phi_l)}{\Delta t}\Big|_{t-\Delta t,\vec{r}}. \qquad (2.10-23)$$

The jump in surface velocity ($\Delta\vec{V}$) is related to the vorticity on the sheet by

$$\Delta\vec{V} = \vec{\gamma} \times \vec{n} \qquad (2.10-24)$$

where $\vec{\gamma}$ is the vorticity at the point and $\vec{n}$ is the unit normal vector of the surface. The mean velocity, $\vec{V}_m$, is the velocity of the fluid between the upper and lower surface. The velocity $\vec{V}_p$

is the absolute velocity of the point on the body. The final term of the Kutta condition and the pressure equation is the unsteady term, that is the partial derivative of the difference in potential. Evaluation of this quantity is the topic of the next section.

To complete the formulation of the pressure coefficient, the change in pressure coefficient needs to be found for closed bodies. The change in pressure from on side of the surface to the other, for closed bodies, is

$$\begin{aligned}\Delta C_p = {} & V_\infty^2 - V_l^2 - 2\frac{\partial \phi_l}{\partial t}\Big|_{\vec{r}} + 2\vec{V}_l \cdot \vec{V}_p \\ & - V_\infty^2 + V_u^2 - 2\frac{\partial \phi_u}{\partial t}\Big|_{\vec{r}} + 2\vec{V}_u \cdot \vec{V}_p \quad .\end{aligned} \tag{2.10 - 25}$$

With the velocity on the interior of a closed body zero the mean velocity is one half the jump in velocity and thus the velocity on the surface is twice the mean velocity. Using these, one can write the change in pressure on the surface of a closed body as

$$\Delta C_p = 2\vec{V}_m \cdot \Delta\vec{V} - 2\Delta\vec{V} \cdot \vec{V}_p + 2\frac{\partial \phi}{\partial t}\Big|_{\vec{r}} \tag{2.10 - 26}$$

2.11 Evaluation of the Potential on the Surface

There are two regions that need to be discussed when evaluating the potential on the surface of a body. First there is the problem of getting onto the body. Second there is the problem of moving from one point to another when the potential at the first point is known.

There are two types of bodies investigated. They are closed nonlifting bodies and lifting surfaces. For closed bodies assuming there is a path from a point far from the body (where the disturbance velocity is nearly zero) to a point on the body on which the potential is always defined the potential on the surface can be found. The velocity potential is defined as

$$\text{grad}\phi = \vec{V} \tag{2.11-1}$$

or

$$\phi_b - \phi_\infty = \int_\infty^b \vec{V} \cdot d\vec{s}. \tag{2.11-2}$$

Letting ∞ being far from the body and b being the point on the surface. The integral of Equation 2.11-2 can be numerically evaluated at a given time step. The change in the potential at the point on the body, from one time to the next is

$$\Delta\phi_b = \int_\infty^b \vec{V}(t) \cdot d\vec{s} - \int_\infty^b \vec{V}(t - \Delta t) \cdot d\vec{s}. \tag{2.11-3}$$

The partial derivative required for the pressure calculations can then be approximated by the finite difference

$$\frac{\partial\phi}{\partial t}\Big|_{\vec{r}} \simeq \frac{\Delta\phi_b}{\Delta t} = \frac{1}{\Delta t}\left[\int_\infty^b \vec{V}(t) \cdot d\vec{s} - \int_\infty^b \vec{V}(t - \Delta t) \cdot d\vec{s}\right]. \tag{2.11-4}$$

We note that the potential far from the body does not have to be known to find the pressure since it is constant with time. That is, the potential far from the body can be changed arbitrarily by a constant without affecting the pressure on the body. The potential is evaluated at a point on the body by starting the line integral at a point far from the body and ending on the surface of the body. The potential at the starting point is assumed to be zero. We also use the same starting point far from the body for successive time steps.

The problem of thin lifting surfaces is different because the pressure coefficient is defined in terms of the change in potential from the upper to the lower surface.

$$\phi_u - \phi_l = \int_l^u \vec{V} \cdot d\vec{s}. \qquad (2.11-5)$$

In other words the difference in the potential across the thin surface at any point is defined as the line integral from the lower surface to the upper surface along any path on which the potential is defined. That is, the path cannot go through the surface or the wake. A typical path for the integral is shown in Figure 13.

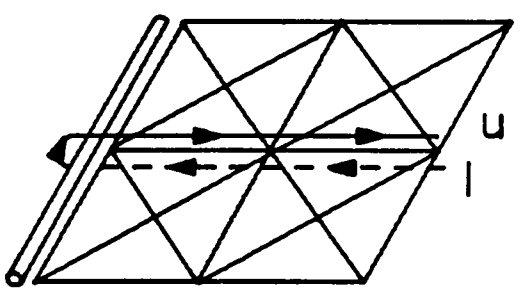

Figure 13. Typical Path for Evaluating the Difference in Potential

The difference in potential from the lower to the upper surface around a vortex core is simply the circulation around the core at the point where the path encircles the core. Another point is that the difference in the potential can only be evaluated by using the local edge circulation if the wake is not emanating from this edge core. If the wake is generated at the point along

the core, the difference in potential is not simply from one side of the core to the other because the potential does not exist on the wake. Therefore, to use the local circulation strength, the core must be along an edge that does not generate a wake. These cores are called nonconvecting. Assuming there is a nonconvecting core somewhere on the edge of the surface, one can choose a path such that a point on this core is crossed and the rest of the surface potentials can be found by skimming along the lower surface to that point, then returning to the starting point along the upper surface.

It remains to determine the sign of the difference of the potential. Before the sign can be determined the upper and lower surfaces need to be identified. The identification is done by examining the definitions already employed. By previous definition

$$\Delta\vec{V} = \vec{\gamma} \times \vec{n} \qquad (2.11-6)$$

$$\vec{V}_l = \vec{V}_m - \frac{1}{2}\Delta\vec{V}$$

$$\vec{V}_u = \vec{V}_m + \frac{1}{2}\Delta\vec{V}. \qquad (2.11-7)$$

In the local coordinates of the triangular element

$$\vec{\gamma} = \gamma_x\vec{i} + \gamma_y\vec{j} \qquad (2.11-8)$$

and

$$\vec{n} = \vec{k}. \qquad (2.11-9)$$

From these definitions it is obvious that positive vorticity in the x direction produces a negative velocity on the upper surface and a positive velocity on the lower surface. This means the lower surface is the side facing the negative local z direction and the upper surface is the side facing the positive z direction. The names upper and lower are only appropriate in a local sense. If the local z direction is downward (which is the standard orientation for aircraft), the lower surface is physically above the upper surface.

The sign is determined by the scalar product of the velocity induced by the edge core and the direction of the path from the lower to the upper surface. The upper and lower surfaces have been identified but the path has not. There is actually only one possible path because the velocity potential must be defined at all points on the path. A typical edge core and adjoining triangular surface element is presented in Figure 14.

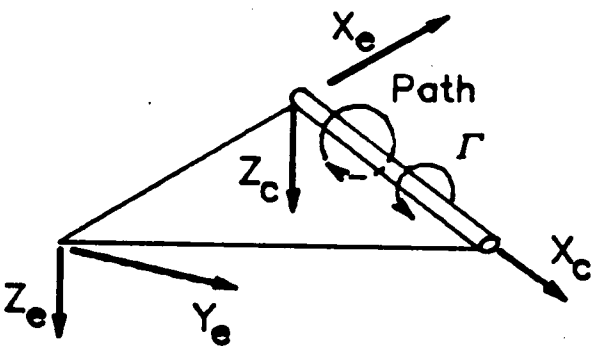

Figure 14. Evaluating the Potential on an Edge

The circulation Γ is defined as positive in the x direction around the core. The difference in the potential from upper to lower, for Figure 14, is negative because the path is in the opposite direction of the induced velocity. For any combination of edge cores and adjoining elements the difference in potential is written as

$$\phi_u - \phi_l = \pm\Gamma. \qquad (2.11-10)$$

Assuming the body is either closed or thin with at least one nonconvecting core along the edge, one must calculate the potential needed to calculate the pressure coefficient at one point on the body within a constant value. The problem now turns to evaluating the potential at every point on the surface when its value is known at some point.

The two types of bodies must be investigated separately. For closed bodies the potential on the outside surface is needed, letting *a* represent a point on the body where the potential is to be found, one can use the definition of the velocity potential to write

$$\phi_a = \int_b^a \vec{V} \cdot d\vec{s} + \phi_b \qquad (2.11-11)$$

Assuming all the local element normal vectors are outward pointing and knowing the velocity on the interior is zero, the mean velocity is

$$\vec{V}_m = \frac{1}{2}\Delta\vec{V}. \qquad (2.11-12)$$

It follows that the velocity on the surface is

$$\vec{V} = \Delta\vec{V} = \gamma \qquad (2.11-13)$$

where γ is the surface velocity. The potential at any point on the surface is then

$$\phi_a = \int_b^a \Delta\vec{V} \cdot d\vec{s} + \phi_b. \qquad (2.11-14)$$

For thin lifting surfaces the difference in potential from the upper to the lower surface is needed to determine the change in pressure coefficient. The difference in potential is defined as

$$(\phi_u - \phi_l)\Big|_a = \int_b^a \vec{V}_u \cdot d\vec{s} - \int_b^a \vec{V}_l \cdot d\vec{s} + (\phi_u - \phi_l)\Big|_b \qquad (2.11-15)$$

or

$$(\phi_u - \phi_l)\Big|_a = \int_b^a (\vec{V}_u - \vec{V}_l) \cdot d\vec{s} + (\phi_u - \phi_l)\Big|_b. \qquad (2.11-16)$$

Which is

$$(\phi_u - \phi_l)\Big|_a = \int_b^a \Delta\vec{V} \cdot d\vec{s} + (\phi_u - \phi_l)\Big|_b. \qquad (2.11-17)$$

As can be seen the quantity needed to determine the pressure coefficient for both types of bodies are actually the same expression. The integral expressions of Equations 2.11-14 and 2.11-17 can be expressed in terms of the local vorticity at the corners of a general triangular element as shown in Figure 15.

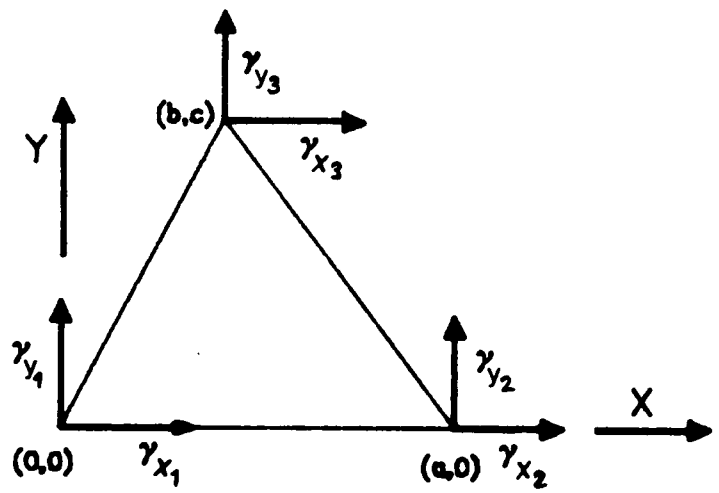

Figure 15. Triangular Element with Vorticity

Assuming the potential, for closed, or the difference in potential, for thin surfaces, is known at the vertex (0,0). The integral of the jump in velocity can be found at all other points on the triangle. Since the potential is independent of the path, the path chosen to get to the general point (x,y) is along y=0 until the desired x is reached and then holding x constant until the desired y is reached.

The jump in velocity is defined as

$$\Delta\vec{V} = \vec{\gamma} \times \vec{n}. \qquad (2.11-18)$$

Along the x axis $d\vec{s} = \vec{i}$, then

$$\int_{(0,0)}^{(x,0)} \Delta\vec{V} \cdot d\vec{s} = \int_{(0,0)}^{(x,0)} \gamma_y \, d\tilde{x}. \qquad (2.11-19)$$

The vorticity along the x axis is

$$\gamma_y = \gamma_{y1} + (\gamma_{y2} - \gamma_{y1}) \frac{\tilde{x}}{a}. \qquad (2.11-20)$$

Equation 2.11-19 is then

$$\int_{(0,0)}^{(x,0)} \Delta\vec{V} \cdot d\vec{s} = \gamma_{y1} x + (\gamma_{y2} - \gamma_{y1}) \frac{x^2}{2a}. \qquad (2.11-21)$$

In the y direction, $d\vec{s} = \vec{j}$. The integral is

$$\int_{(0,0)}^{(x,y)} \Delta\vec{V} \cdot d\vec{s} = \int_{(0,0)}^{(x,0)} \Delta\vec{V} \cdot d\vec{s} + \int_{(x,0)}^{(x,y)} -\gamma_x \, d\tilde{y}. \qquad (2.11-22)$$

On a triangular element

$$\gamma_x = \gamma_{x1} + (\gamma_{x2} - \gamma_{x1}) \frac{x}{a} + \left[\frac{\gamma_{x3} - \gamma_{x1}}{c} - \frac{b}{ac} (\gamma_{x2} - \gamma_{x1}) \right] y. \qquad (2.11-23)$$

Therefore,

$$\int_{(0,0)}^{(x,y)} \Delta\vec{V} \cdot d\vec{s} = \gamma_{y1} x + (\gamma_{y2} - \gamma_{y1}) \frac{x^2}{2a} - \gamma_{x1} y - (\gamma_{x2} - \gamma_{x1}) \frac{xy}{a} - \left[\frac{\gamma_{x3} - \gamma_{x1}}{c} - \frac{b}{ac} (\gamma_{x2} - \gamma_{x1}) \right] \frac{y^2}{2}. \qquad (2.11-24)$$

Equation 2.11-24 is valid for any point on a given triangle. Therefore, once one point on the mesh is known all the potentials of the triangle containing that point are known. These can in turn be used as starting points for evaluating the potential at the adjoining elements. In this way the potential needed to determine the pressure can be found for any point on the body. Two special cases of Equation 2.11-24 bear evaluating. These are the vertices in terms of the known vertex. These are

$$\int_{(0,0)}^{(a,0)} \Delta\vec{V} \cdot d\vec{s} = (\gamma_{y1} - \gamma_{y2}) \frac{a}{2} \qquad (2.11-25)$$

and

$$\int_{(0,0)}^{(a,0)} \Delta\vec{V} \cdot d\vec{s} = -\gamma_{x1} \frac{c(a-b)}{2a} - \gamma_{x2} \frac{cb}{2a} - \gamma_{x3} \frac{c}{2} + \gamma_{y1}(b - \frac{b^2}{2a}) + \gamma_{y2} \frac{b^2}{2a} \qquad (2.11-26)$$

To check the accuracy of the equations developed for determining the velocity potential on the body, the potential was determined analytically and numerically using a sphere with 120 elements. The potential far from the body was chosen such that the velocity potential at the front stagnation point is zero. The two methods are shown in Figure 16, as can be seen the potential compares very favorably.

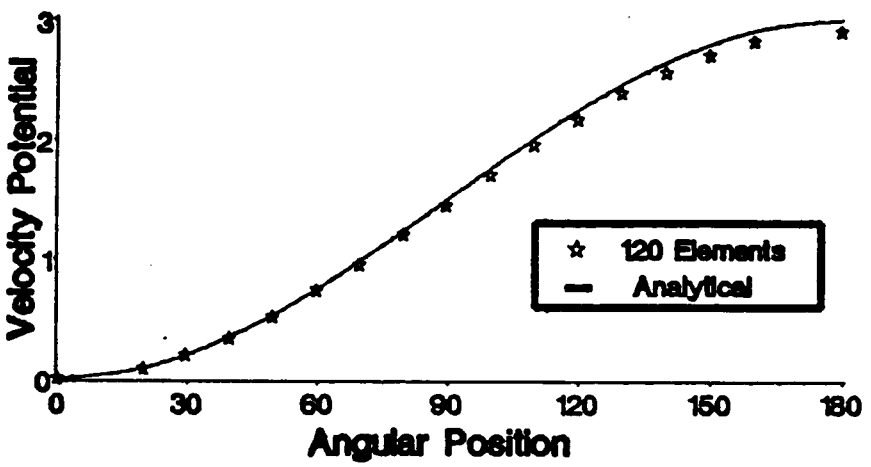

Figure 16. Comparison of Velocity Potentials on a Sphere

2.12 Aerodynamic Forces and Moments

In general the force can be written as

$$\vec{F} = F_x \vec{i} + F_y \vec{j} + F_z \vec{k} \qquad (2.12-1)$$

The force is the result of the pressure on a surface and of a vortex core in the moving fluid. The force due to a pressure distribution on a surface is given as

$$\vec{F} = \iint_S \Delta P \, \vec{n} \, dA \qquad (2.12-2)$$

where $\vec{F}$ is the force on the body, S is the surface of the body, ΔP is the difference in pressure from one side of the surface to the other and $\vec{n}$ is the local normal to the surface.

For a continuous vortex sheet the pressure distribution is continuous. The integral of Equation 2.12-2 is evaluated numerically. To simplify, the numerical integration scheme, we assume the pressure difference varies linearly on an element. This is not an unrealistic assumption since the vorticity on an element is linear and therefore if the velocity is constant the pressure distribution is also linear. A more accurate method of integration could be used to improve the accuracy but since only one point on the element is used for the no penetration condition a linear assumption seemed appropriate. Assuming the pressure difference is linear on an element Equation 2.12-2, for element i, reduces to

$$\vec{F}_i = \Delta P \Big|_{c_i} \vec{n}_i A_i \qquad (2.12-3)$$

where c_i is the centroid of the element. The total force due to the pressure difference is simply the sum of the forces on each element

$$\vec{F} = \sum_{i=1}^{n} \Delta P \Big|_{c_i} \vec{n}_i A_i. \qquad (2.12-4)$$

In terms of the pressure difference coefficient

$$\vec{F} = \frac{1}{2}\rho U^2 \sum_{i=1}^{n} \Delta C_p \Big|_{c_i} \vec{n}_i A_i \qquad (2.12-5)$$

where Equation 2.10-20 and Equation 2.10-26 define the change in pressure coefficient for the two types of bodies.

This is not the only force on the body. The thin surfaces also have nonconvecting edge cores with circulation. The force due to these cores is

$$\delta\vec{F} = \rho\vec{V}_R(x) \times \vec{\Gamma}(x)\, dx \qquad (2.12-6)$$

where $\delta\vec{F}$ is the force caused by a small segment of circulation, $\vec{V}_R$ is the relative velocity, $\vec{\Gamma}$ is the circulation and ρ is the density. To facilitate the evaluation of the force it is assumed that the relative velocity does not change appreciably over the length of the core. The force due to the circulation around an edge core is

$$\vec{F} = \rho\vec{V}_R \times \int_0^d \vec{\Gamma}(x)\, dx \qquad (2.12-7)$$

or

$$\vec{F} = \rho\vec{V}_R \times \vec{i}\,\Gamma_{ave} d \qquad (2.12-8)$$

where Γ_{ave} is the average circulation, d is the length of the core and $\vec{i}$ is a unit vector in the direction of the core. The relative velocity, $\vec{V}_R$, is the velocity of the fluid. This velocity was determined by evaluating the velocity at the point along the core where the circulation was the average value. The total force on a surface with n elements and m nonconvecting cores is

$$\vec{F}_{tot} = \sum_{i=1}^{m} \rho\vec{V}_{Ri} \times \vec{i}_i \Gamma_{avei} d_i + \sum_{i=1}^{n} \Delta P \Big|_{c_i} \vec{n}_i A_i \qquad (2.12-9)$$

The force coefficient is defined as

$$\vec{C}_f = C_{f_x}\vec{i} + C_{f_y}\vec{j} + C_{f_z}\vec{k} = \frac{\vec{F}_{tot}}{\frac{1}{2}\rho U^2 S} \qquad (2.12-10)$$

where S is the total surface area of the wing.

The moment is defined as

$$\vec{M} = \vec{r} \times \vec{F}. \qquad (2.12-11)$$

Again assuming the pressure difference is linearly varying on an element the moment calculations can be simplified. The total moment is the resultant of the moment caused by the pressure force being lumped at the centroid of each element, the moment due to the forces of each of the elements acting at the centroid and the moment of the nonconvecting cores.

The moment caused by the pressure acting at the centroid is

$$\vec{M}_{cl} = \vec{r}_l \times \Delta P\Big|_{c_l} \vec{n}_l A_l \qquad (2.12-12)$$

where $\vec{r}_l$ is the vector from the point where the moment is to be calculated to the centroid of element i . The moment caused by the pressure on the element about the centroid is defined as

$$\vec{M}_{pl} = \iint \vec{r}_l \times \Delta P_l \vec{n}_l \, dA_l. \qquad (2.12-13)$$

For a general triangular element (Figure 1) using the linear assumption of the pressure distribution, and that the centroid is at the point $(\frac{a+b}{3}, \frac{c}{3})$ Equation 2.12-13 can be integrated. The pressure distribution in general is the linear function

$$\Delta P = \Delta P_0 + \Delta P_1 x + \Delta P_2 y. \qquad (2.12-14)$$

The moment is then

$$\vec{M}_{pl} = \int_0^c \int_{\frac{b}{c}}^{\frac{b-a}{c}y+a} \left[\left(x - \frac{a+b}{3} \right) \vec{i} + \left(y - \frac{c}{3} \right) \vec{j} \right] \times \vec{k}\, \Delta P \, dxdy. \qquad (2.12-15)$$

The components of the moment are

$$M_{pxl} = \frac{ac^2}{72} [2\Delta P(b,c) - \Delta P(0,0) - \Delta P(a,0)]$$

$$M_{pyl} = \frac{ac}{72} [(a+b)\,\Delta P(0,0) - (2a-b)\,\Delta P(a,0) - (2b-a)\,\Delta P(b,c)] \qquad (2.12-16)$$

where $\Delta P(x,y)$ is the pressure difference at the point on the triangle (x,y)

The moment due to a nonconvecting core is

$$\vec{M}_{nl} = \int \vec{r} \times (\rho \vec{V}_R(x) \times \vec{\Gamma}(x)) \, dx \qquad (2.12-17)$$

Which, under the assumptions used to arrive at the force of a nonconvecting core, reduces to

$$\vec{M}_{nl} = \vec{r}_{ave} \times (\rho \vec{V}_{Rl} \times \vec{\Gamma}_{avel}) \, d_l \qquad (2.12-18)$$

where $\vec{r}_{ave}$ is the position vector from the point where the moment is to be found to the point on the vortex core where the circulation is the average value.

The total moment is then

$$\vec{M}_{tot} = \sum_{l=1}^{n} \vec{M}_{cl} + \sum_{l=1}^{n} \vec{M}_{pl} + \sum_{l=1}^{m} \vec{M}_{nl}. \qquad (2.12-19)$$

The dimensionless moment is defined as

$$\vec{C}_m = C_{m_x} \vec{i} + C_{m_y} \vec{j} + C_{m_z} \vec{k}. \qquad (2.12-20)$$

The aerodynamic moment coefficients are defined as

$$C_{m_x} = \frac{\vec{M}_{tot} \cdot \vec{i}}{\frac{1}{2}\rho U^2 S b}$$

$$C_{m_y} = \frac{\vec{M}_{tot} \cdot \vec{j}}{\frac{1}{2}\rho U^2 S \bar{c}}$$

$$C_{m_z} = \frac{\vec{M}_{tot} \cdot \vec{k}}{\frac{1}{2}\rho U^2 S b} \qquad (2.12-21)$$

where S is the surface area, b is the span and $\bar{c}$ is the mean aerodynamic chord. These definitions will be used whenever moment data are presented. A flow chart of the force and moment calculations is shown in Figure 17.

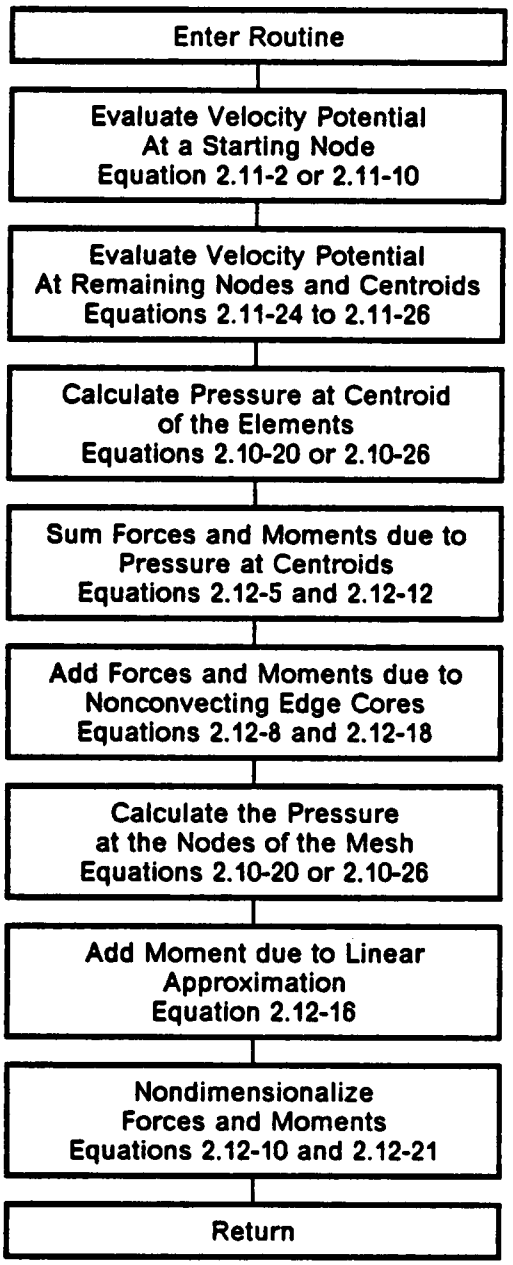

Figure 17. Flow Chart of the Force and Moment Calculations

2.13 The Formation of the Wake

The wake is a region of concentrated vorticity where the viscous effects have been neglected. Under the assumptions discussed in Chapter I the wake is considered a vortex sheet emanating from the edges of the lifting-surface. This vortex sheet must satisfy Equation 2.7-3 (conservation of circulation) and Equation 2.7-5 (infinity condition). Since the wake is a vortex sheet it must also satisfy Equation 2.2-10 (divergenceless condition). As stated the method used for forming the wake is the same procedure employed by the general unsteady vortex-lattice methods. The reason for this choice is that the wake is progressively formed and can roll up as tightly as needed to simulate the actual wake surface. Before proceeding into the details of the method used to form the wake, the approximations of the method will be explained.

One means of discussing, in detail, the development of the wake is to examine a wing starting impulsively. Before the motion there is no disturbance. At the instant the motion starts there is vorticity formed on the surface and a starting vortex core, with circulation, is developed along the edge, though not enough time has elapsed to allow this circulation to move into the fluid. As time progresses this circulation is swept downstream (what will be referred to as parallel to the flow) and the wake vortex sheet develops from the starting core to the edge of the surface. This vortex sheet satisfies all the equations mentioned earlier. As the starting vortex core and vortex sheet move, the flow field around the wing is altered. Thus the surface vorticity changes causing the wake to change continuously. Finally there is no change in the surface vorticity or the wake and a steady state is reached. As the strength of the sheet changes in the direction of the flow there is a corresponding change in the strength in the other direction so that the divergenceless condition is satisfied. This other direction is referred to as perpendicular to the flow. Therefore, before the steady state is reached the vorticity in the wake is in both directions.

Modeling this development requires a discrete formation of the wake. Actually the discrete formulation is easier to understand because the formation process can be frozen and examined at successive time steps. Again an impulsively started wing is examined. Before the motion starts there is no disturbance or wake. At the instant motion starts vorticity is formed

on the surface and the edge cores have circulation. The model of the surface, as developed in Sections 2.2 and 2.8, dictates the circulation of each edge core is quadraticly varying along the length of the core. This edge core is then swept a finite distance downstream. This is where the discretized model varies from the continuous. Since the variable strength core has moved there is a vortex sheet formed from the core to the edge of the surface. This sheet has linearly varying vorticity in the direction of the flow but no vorticity perpendicular to the flow. The strength of the sheet is exactly compatible with the with the vorticity on the edge of the surface since both originated from the same variable vortex core. This is the end of the first discrete time step. The surface developed vorticity and an edge core. This core was moved a finite distance and a vortex sheet was formed from the starting core to the surface edge that is compatible to both.

The problem with the discrete model is, as the starting vortex moved that finite distance, the starting vortex was changing the flow field around the surface. Therefore, by the time it got to its final position there was a new surface vorticity. This means the wake vortex sheet from the starting core to the surface is no longer compatible with the surface edge. There is a discontinuity. To make the two surfaces compatible again there must be another vortex core formed at the edge of the surface. The strength of this edge core is exactly the negative of the strength of the starting core added to the strength of the core needed to generate the surface vorticity assuming there is no wake.

At the start of the second time step a new vortex distribution is formed on the surface because the wake has caused some disturbance. The edge cores are again formed as in the first time step (no wake sheet entering the surface), and the negative of the starting vortex is placed on the edge to capture the wake sheet. The total edge strength is correct to account for the discontinuity of the two vortex sheets. The new wake, consisting of the starting vortex cores, the new edge cores and the sheet between them is moved a finite distance changing strength according to the conservation of circulation. The vortex sheet from the second edge core to the surface is formed. This is the end of the second time step. The same procedure could be used for all successive time steps.

In looking back at the development, the procedure outlined has actually approximated the vorticity perpendicular to the flow by a series of discrete vortex cores. To remain consistent and to simplify the conditions the wake sheet must satisfy, the vorticity of the wake sheet parallel to the flow is also approximated by a vortex core. For this approximation the strength of the edge vortex core swept into the wake must be replaced with constant strength cores, otherwise there would be a vortex sheet formed. The core circulation chosen is the average value of the variable vortex core. The conservation of circulation is imposed by using the same average circulation to approximate the vorticity connecting the ends of the cores and holding this circulation constant as the wake convects. The present method uses two successive approximations, first the vorticity perpendicular to the flow is lumped into discrete variable strength vortex cores and then the vorticity parallel to the flow is lumped into constant strength cores and the variable cores are averaged. In this way the procedure reduces to the general unsteady vortex-lattice method.

The method used can now be examined in detail. Again examining an impulsively started wing. First there is no disturbance. At the moment the motion starts vorticity is formed on the surface and the edge cores have circulation. This condition is shown in Figure 18 a. To make the figure clearer only the vortex cores along the trailing edge are convected and the collocated edge cores are shown slightly offset. The average circulation on each edge is calculated. This circulation is swept into the fluid. A closed four sided ring of circulation is then formed connecting the starting vortex core to the surface, and new vortex core is formed along the edge because of the changed caused by the presence of the wake. This condition is shown in Figure 18 b. The wake is then convected without changing the strength of the circulation around the rings formed by the mesh of the wake. The condition after one more time step is shown in Figure 18 c. The bookkeeping is extremely simple in that only the positions of the corners and the circulation around the closed loops need to be recorded to completely describe the wake.

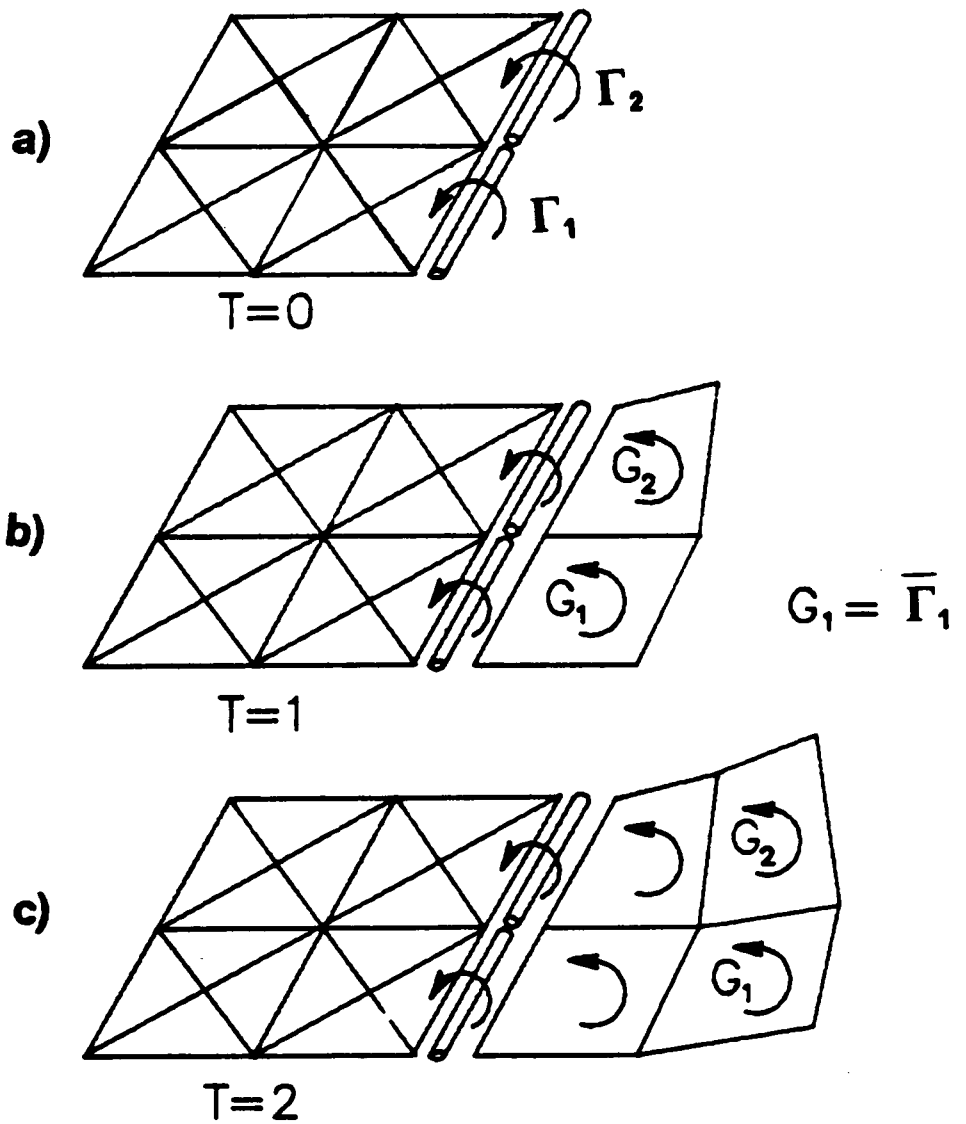

Figure 18. Development of the Wake Lattice

The average circulation Γ_{ave}, can easily be found knowing the strength of the edge core. With

$$\Gamma(x) = G_1 \frac{x^2}{2} + G_2 x + G_3 \qquad (2.13-1)$$

$$\Gamma_{ave} = \frac{\int_0^d G_1 \frac{x^2}{2} + G_2 x + G_3 \, dx}{d} = G_1 \frac{d^2}{6} + G_2 \frac{d}{2} + G_3 \qquad (2.13-2)$$

where

$$G_1 = \frac{\gamma_{y2} - \gamma_{y1}}{d} \qquad (2.13-3)$$

and

$$G_2 = \gamma_{y1}. \qquad (2.13-4)$$

The strength of the wake has been determined but the position has not. The placement of the wake is determined by the no pressure jump condition. To satisfy this condition the wake is convected at the local particle velocity. The position for the next time step is determined from the first order finite difference formula

$$\vec{r}(t + \Delta t) = \vec{r}(t) + \vec{V}(t)\Delta t. \qquad (2.13-5)$$

Where $\vec{r}(t + \Delta t)$ is the new position vector, $\vec{r}(t)$ is the old position vector and $\vec{V}(t)$ is the local particle velocity. This approximation was chosen because it does not require iteration. The local particle velocity is the sum of the velocity induced by the disturbance of the bound vorticity (the wing) the disturbance velocity of the wake and the velocity of the lifting surface,

$$\vec{V}(t) = \vec{V}_{Bound} + \vec{V}_{Wake} + V_{LS}. \qquad (2.13-6)$$

The subroutines used to calculate this total velocity are presented in Appendix III.

To complete the formulation of the wake the velocity induced by the collection of constant strength vortex cores can be determined by adding the velocity induced by each core. The velocity induced by a constant strength core is determined by the well known Biot-Savart Law. This velocity is a subset of the velocity of a variable strength vortex. The velocity is

$$\vec{V}_c = \frac{\vec{e}}{4\pi h} \Gamma_{ave}(\cos\theta_1 - \cos\theta_2). \qquad (2.13-7)$$

The approximation of using discrete vortex segments can be enhanced at the cost of more complex bookkeeping, by employing the experience obtained from using the vortex-lattice technique. The results of this experience says that rings with sides of nearly equal length give the best results. As the wake convects it deforms. Sometimes the rings get so deformed that the length of one side is significantly different from the other sides. One choice to correct this discrepancy is to redistribute the circulation in the spanwise direction so that the sides remain nearly equal in length. The size of the chordwise segments is dictated by the step size chosen. The redistribution of the circulation is an adaptive grid technique and is referred to as splitting the wake. The method employed is not the only alternative. The re-distribution chosen uses a linear interpolation between neighboring vortex cores. The assumptions used in determining a unique algorithm are that splitting only occurs in the spanwise direction, once a wake segment is split it never reforms and the wake is split from the starting location to the end of the wake.

One way to examine the method used to split the wake is to use an example. Figure 19 a shows a general section of the wake at some time. The G_{ij} is the circulation around the closed loop formed by the vortex cores. Figure 19 b shows the same wake at the next time step. The dashed vortex segment has lengthened past some specified amount and therefore splitting will be employed to return the stretched rings to rings with more nearly equal sides. The split wake mesh is shown in Figure 19 c.

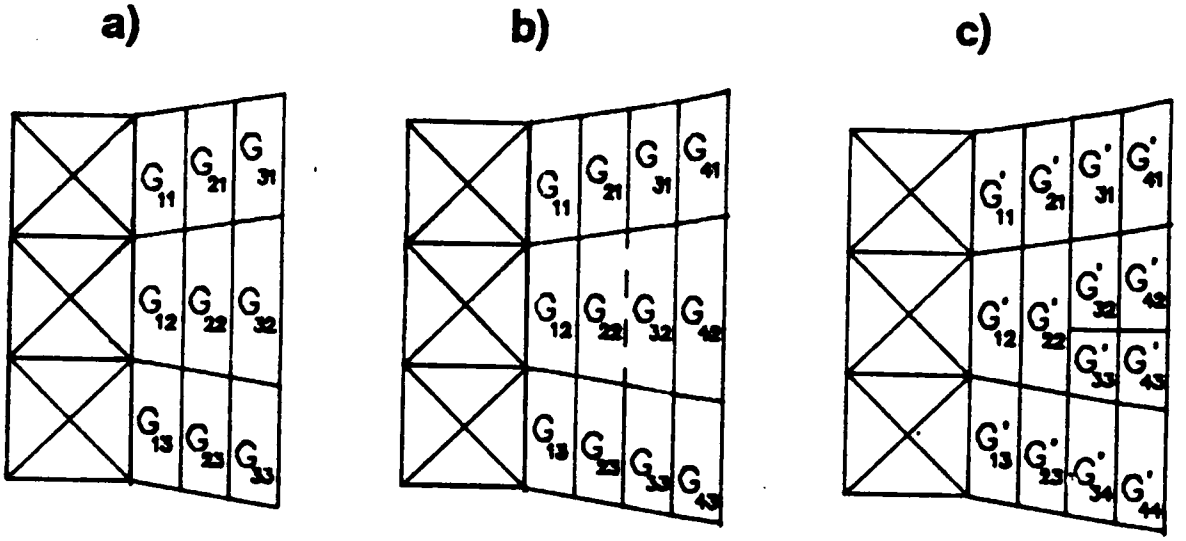

Figure 19. Splitting the Wake Lattice

The relations between the circulations of Figure 19 a and Figure 19 c are

$$G'_{21} = G_{11} \quad G'_{22} = G_{12} \quad G'_{23} = G_{13}$$

$$G'_{31} = G_{21} \quad G'_{32} = \frac{1}{3} G_{21} + \frac{2}{3} G_{22} \quad G'_{33} = \frac{2}{3} G_{22} + \frac{1}{3} G_{23} \quad G'_{34} = G_{23}$$

and

$$G'_{41} = G_{31} \quad G'_{42} = \frac{1}{3} G_{31} + \frac{2}{3} G_{32} \quad G'_{43} = \frac{2}{3} G_{32} + \frac{1}{3} G_{33} \quad G'_{44} = G_{33}. \quad (2.13-8)$$

In this way the circulation is conserved, the circulation has been redistributed linearly and the vortex rings remain nearly equal in length.

Finally the question needs to be addressed as to how well the wake of successive approximations (reducing the wake from a vortex sheet to a set of constant strength cores),

represents the actual surface. The first approximation, where the vorticity in the direction perpendicular to the flow is lumped into discrete variable strength vortex cores, is the result of using discrete time steps. This approximation does not have to be made but the procedure to establish a complete vortex sheet does not appear to be straight forward. The second approximation can be investigated readily since the velocity induced by a vortex sheet has been determined. The test case used to compare the two methods is a single row of the wake with four elements. The panel arrangement and the vortex distribution on the panels are shown in Figure 20.

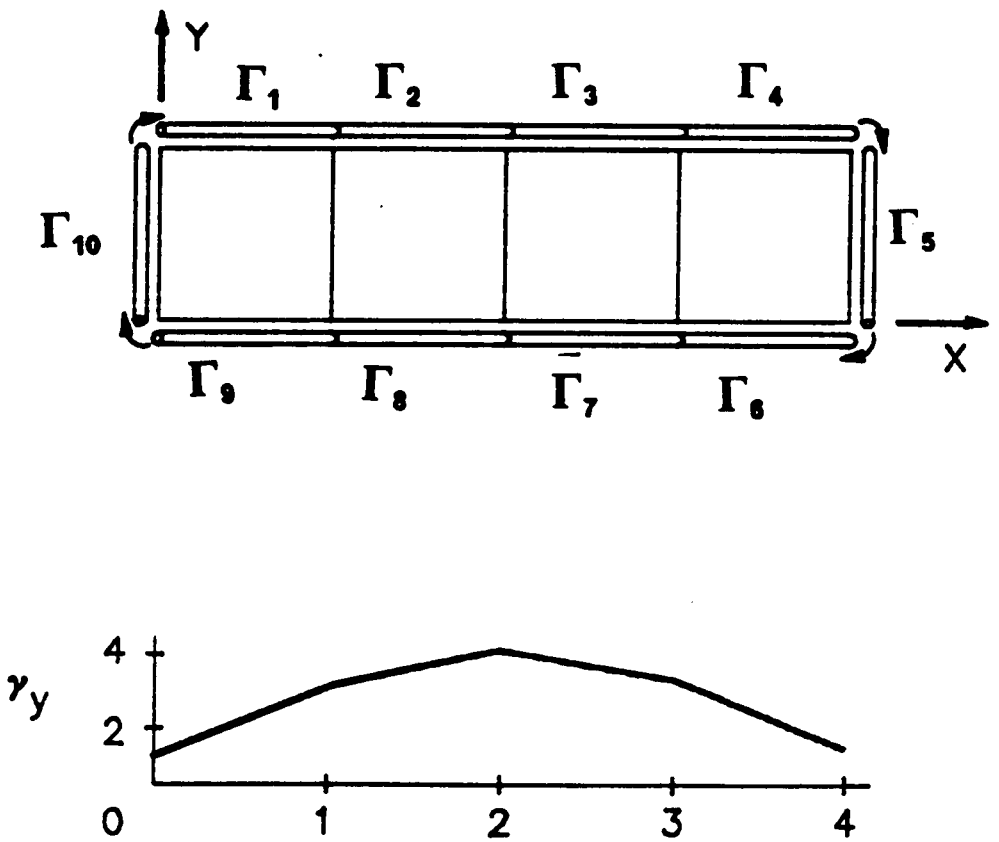

Figure 20. Test Configuration of A Vortex Sheet

Specifying $\Gamma_{10} = -\Gamma_5$ the equivalent arrangement of constant strength vortex cores can be found using Equation 2.13-3 and 2.13-4. This arrangement is shown in Figure 21.

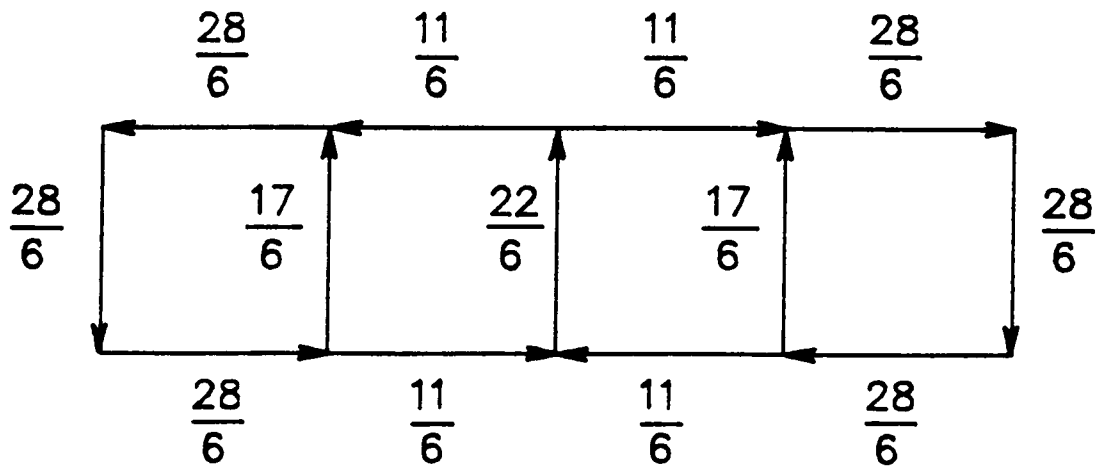

Figure 21. Equivalent Constant-Strength Vortex Core Arrangement

These two arrangements are compared by finding the total induced velocity at a grid of points around the two surfaces. The velocity distributions are shown in Figure 22 a for the vortex sheet and Figure 22 b for the vortex cores. Outside of a region around the discrete cores the velocity fields are nearly identical. Within the region there are differences as would be expected because one is an approximation of the other. The region where the difference is noticeable is inside a radius of approximately 0.25 around each discrete core where the distance between the cores is unity. The flow chart for the convection of the wake is presented in Figure 23.

a) Velocity Around Continuous Sheet

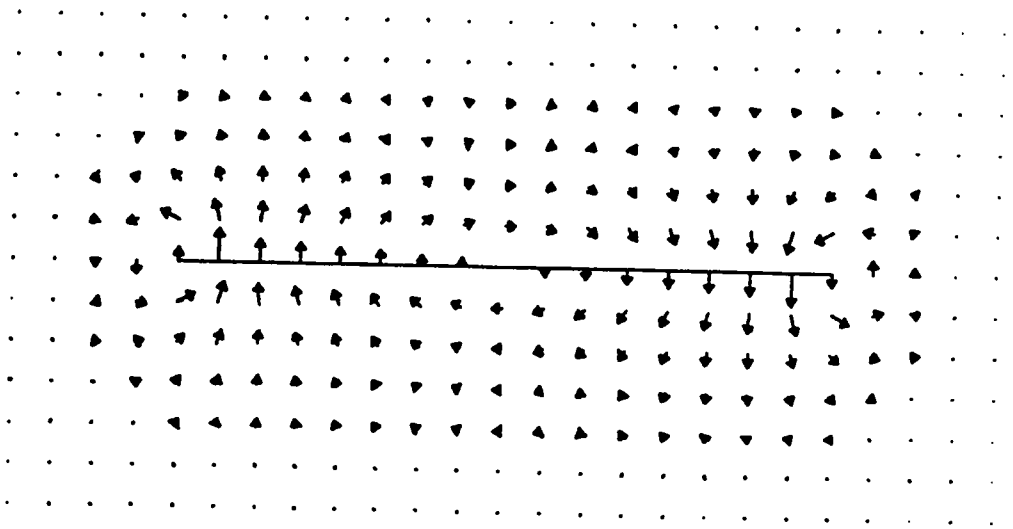

b) Velocity Around a Discrete Sheet

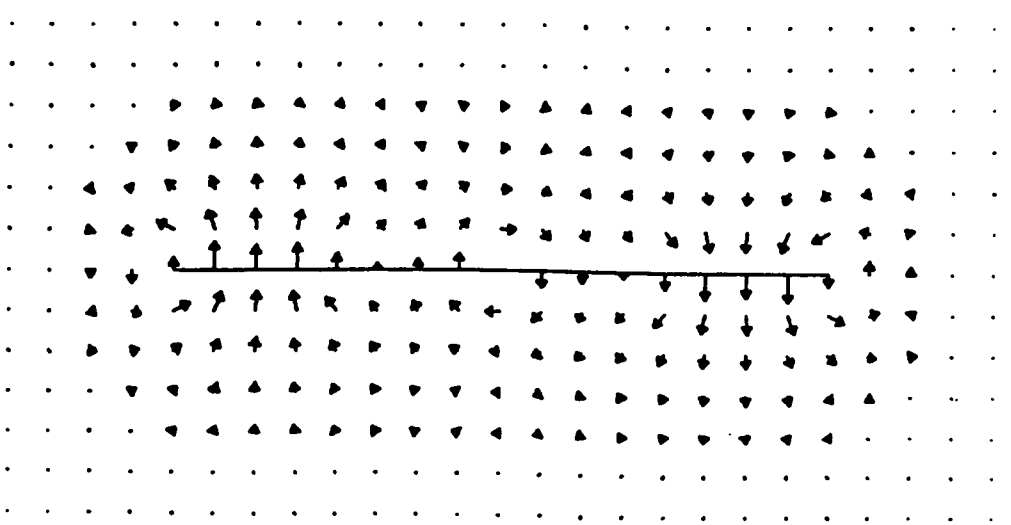

Figure 22. Velocity Field of the Test Wake Configuration

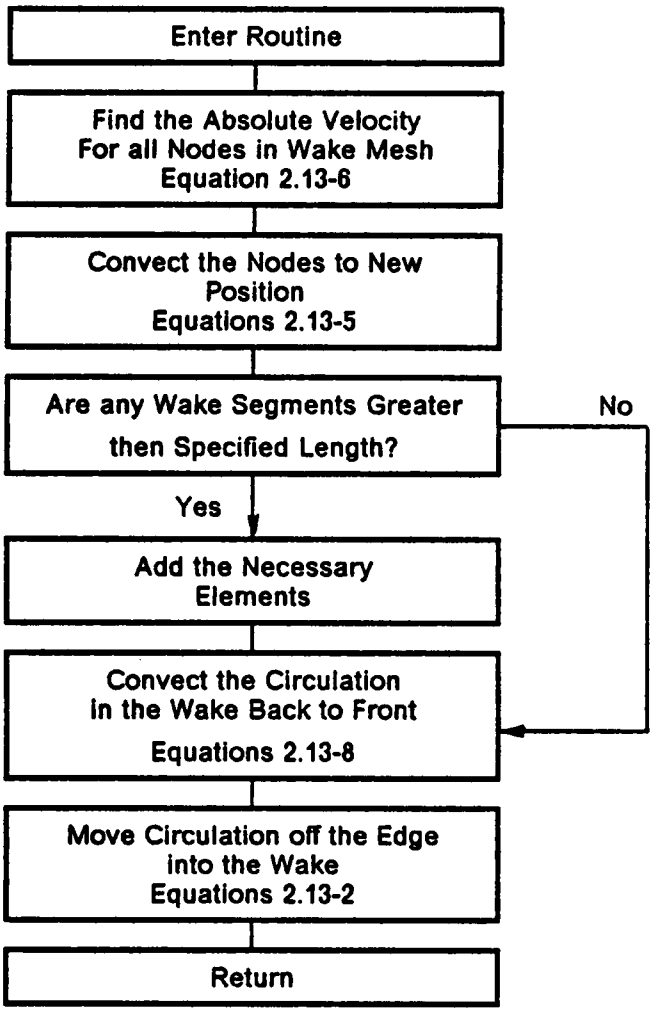

Figure 23. Flow Chart for Convecting the Wake

2.14 General Matrix Equation and Method of Solution

The complete unsteady aerodynamic model has been developed. The numerical procedure for solving the problem can now be discussed. The matrix equations developed for closed bodies include the no-penetration conditions at the control points on the surface

$$[A]\{\Omega\} = \{U\} \qquad (2.14-1)$$

For thin surfaces with edge separation, the velocity induced at the control points on the surface is also influenced by the edge cores, which in turn are dependent on the surface vorticity, and the velocity induced by the wake. The no-penetration condition can then be written as

$$[A+C \quad D]\begin{Bmatrix}\Omega\\ G\end{Bmatrix} = \{U-W\} \qquad (2.14-2)$$

where C_{ij} is the normal component of the velocity induced by node j caused by an edge core on control point i, D_{ik} is the normal velocity induced by the constants of integration on control point i, G_k is the constant core strength of edge segment k, U_i is the normal component of the freestream velocity and W_i is the velocity induced by the wake normal to the surface at control point i.

The divergenceless condition for the surface in terms of all the unknowns of the formulation is

$$[B \quad 0]\begin{Bmatrix}\Omega\\ G\end{Bmatrix} = \{0\} \qquad (2.14-3)$$

The compatibility conditions imposed on the edge cores, Equations 2.8-8 and 2.8-10, are linear in the unknown surface vorticity strength and the constant circulation of the edge cores and therefore they can be written as

$$\begin{bmatrix}E & F\\ J & 0\end{bmatrix}\begin{Bmatrix}\Omega\\ G\end{Bmatrix} = \{0\}. \qquad (2.14-4)$$

The final matrix equation is the Kutta condition, Equation 2.10-23. As seen, the difference in potential is a linear function of the problem variables. The only nonlinear term of equation 2.10-23 would be the second term on the left-hand side. For uncambered surfaces the mean velocity that is dependent on the surface vorticity is perpendicular to the surface. This means that for uncambered surfaces Equation 2.10-23 is linear in the unknowns of the problem. For cambered surfaces Equation 2.10-23 is nonlinear and thus an iteration at each time step is required. But for cambered surfaces the no-penetration conditions are also nonlinear, due to the factor c. Both these iterations can be accomplished simultaneously. The iteration method is initialized at the start of each time step by using values from the last time step for c and the

surface vorticity. One then uses these values to calculate the mean velocity at the point the Kutta condition is imposed. The problem is solved, the new vorticity distribution is found and the c factors are recalculated. The surface vorticity is then calculated again. This procedure continues until there is no change in the c factors and the surface vorticity.

It should be noted that for the first time step the Kutta condition cannot be imposed since the left-hand side of Equation 2.10-23 is not defined. The method used to circumvent this problem is simply to ignore the Kutta condition and not to calculate the loads on the first time step. The starting procedure for the iteration is the same as for closed bodies; that is, the initial guess of all the c factors is unity.

The linear Kutta equation can then be written as

$$[K \quad L]\begin{Bmatrix}\Omega\\ G\end{Bmatrix} = \{P\}. \qquad (2.14-5)$$

where P_l is the potential from the previous time step.

The placement of the Kutta condition is established next. The Kutta condition is imposed only at the nodes of the surface along the trailing edge. The condition is only imposed at these nodes because this makes the relation of Equation 2.10-23 involving $\Delta\vec{V}$ only contain the vorticity at one node instead of being a linear combination of two node strengths. Imposing the Kutta condition along the side edges of the surface would require the pressure jump to go to zero along that edge. Experimental data, however, show a large pressure gradient along the sides of wings. To capture this large gradient requires a large number of elements. Instead of requiring a large number of elements, the Kutta condition was not imposed along the sides of the wing.

Using the same procedure as used for closed bodies, (that is, the no-penetration condition is augmented by weighted constraints), one can write the entire matrix equation as

$$\begin{bmatrix} A+C & D \\ w_1 B & 0 \\ w_2 E & w_2 F \\ w_3 J & 0 \\ w_4 K & w_4 L \end{bmatrix} \begin{Bmatrix} \Omega \\ G \end{Bmatrix} = \begin{Bmatrix} U-W \\ 0 \\ 0 \\ 0 \\ w_4 P \end{Bmatrix} \qquad (2.14-6)$$

The weighting matrices are diagonal matrices with a constant weight for all nonzero elements. From the formulation for closed bodies the weighting of the divergenceless conditions, w_1 had no impact on the problem for a wide range of values. The weightings of the edge compatibility conditions, w_2 and w_3, need to be large because these conditions should be imposed exactly to be consistent with the formulation on the surface. The weighting of the Kutta condition at the nodes along the trailing edge, w_4, has not yet been investigated. The weighting of the divergence condition and the Kutta condition will be investigated for thin surfaces in Section 2.15

Letting

$$[S] = \begin{bmatrix} A+C & D \\ w_1 B & 0 \\ w_2 E & w_2 F \\ w_3 J & 0 \\ w_4 K & w_4 L \end{bmatrix} \qquad (2.14-7)$$

and

$$\{T\} = \begin{Bmatrix} U-W \\ 0 \\ 0 \\ 0 \\ w_4 P \end{Bmatrix} \qquad (2.14-8)$$

the entire problem can then be formulated as

$$[S]\begin{Bmatrix}\Omega\\ G\end{Bmatrix} = \{T\}. \qquad (2.14-9)$$

This set of linear algebraic equations can be solved by several techniques. Again the chosen method of solution was to minimize the sum of the squares of the errors (see Section 2.5 for details). This solution is the solution of the following linear equation

$$[S]^T[S]\begin{Bmatrix}\Omega\\ G\end{Bmatrix} = [S]^T\{T\}. \qquad (2.14-10)$$

This matrix equation can be solved by any standard routine.

Solving Equation 2.14-10 is just one step in the solution of the general unsteady problem. The overall method used to solve the unsteady problem is best understood by using a flow chart as shown in Figure 24. Initially, the only way to start the program is impulsively because the wake position and strength are not known. As mentioned above, for the first time step the Kutta condition is not used because the derivative of the velocity potential is not defined for an impulsive start. With the understanding that these equations are neglected for the first time step, the right-hand side of equation 2.14-9 is formed. On the first time step, the matrix T contains the component of the freestream velocity perpendicular to the surface at the control points augmented with a zero matrix. For subsequent time steps this matrix will include the velocity induced by the wake and the matrix will also contain the difference in the velocity potential from the previous time step at the nodes where the Kutta condition is applied. The influence matrix, the left hand side of Equation 2.14-9 is then formed. This matrix will change every time step for cambered surfaces and surfaces that are deforming. In fact, the influence matrix will have to be updated more then once every time step because of the nonlinearity of the equations. Equation 2.14-10 is then formed and solved. The vorticity on the surface and the circulation along the edge is now known. If an iteration is required, the influence matrix is redetermined and Equation 2.14-10 is recalculated. The procedure is repeated until some convergence criterion is met. The forces and moments can then be calculated. With the vorticity and circulation known, the amount of circulation being convected into the wake

is also known. The wake is then moved at the local particle velocity and thereby forms the lattice of the wake. Equation 2.14-9 is recalculated with the new information and the process is repeated until the final time is reached.

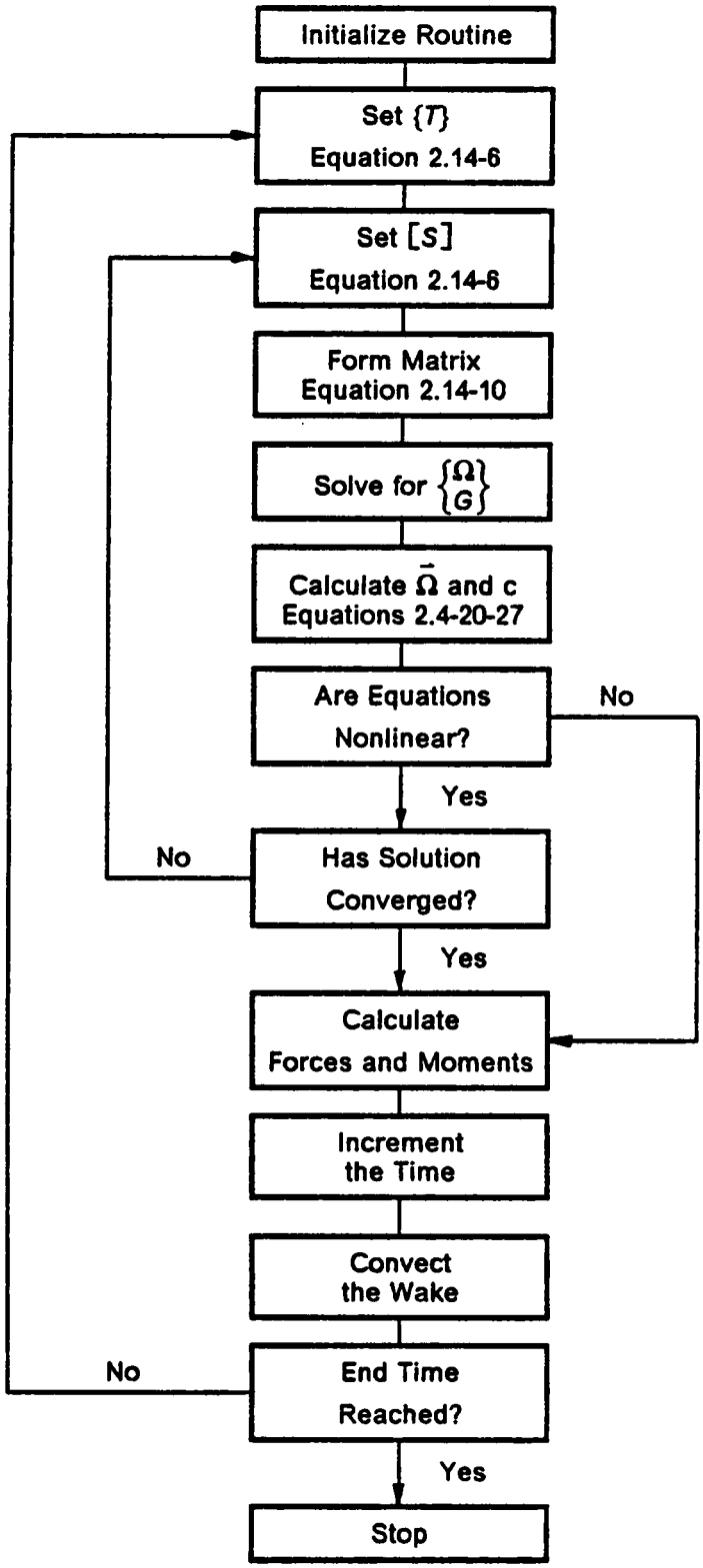

Figure 24. Flow Chart for the Aerodynamic Model

2.15 Determination of the Weighting Matrix and Other Parameters

The wake formation and surface vorticity distribution is dependent on the weight chosen for the constraints. In order to remain consistent between the surface and edge, the edge compatibility conditions should be weighted heavily. A weighting factor of 500 is chosen. To minimize the dependence on the other choices of the weights the method is run until the answer is insensitive for a range of weights. As an example a unit-aspect-ratio rectangular wing with 64 elements at 10 degrees angle of attack is examined. Since the closed bodies showed little variation due to a large range of weights on the divergenceless conditions, this weighting was chosen to be 10 and the weight on the Kutta condition was examined first. The steady state values for several weights is presented in Table 2.

Table 2. The Effects of Various Weights of the Kutta Condition

Weight	C_{f_z}	$C_{m_{y_{l.e.}}}$
1.0E - 3	-0.34525	-0.09301
1.0E - 2	-0.34524	-0.09300
1.0E - 1	-0.34436	-0.09230
1.0E+0	-0.33814	-0.08739
1.0E+1	-0.33771	-0.08702
1.0E+2	-0.33770	-0.08701
1.0E+3	-0.33770	-0.08701

As shown, the solution is insensitive for two ranges of weight, both low and high. The lighter weighting effectively ignores the Kutta condition while the heavier weighting imposes this condition more exactly. Since the Kutta condition is needed a weighting of 50 was chosen for all subsequent results. The weighting for the divergenceless condition is now considered. The results are presented in Table 3.

Table 3. The Effects of Various Weights of the Divergenceless Condition

Weight	C_{f_z}	$C_{m_{y_{l.e.}}}$
1.0E - 1	No steady state condition was reached	
1.0E+0	-0.33643	-0.08655
1.0E+1	-0.33770	-0.08701
1.0E+2	-0.33772	-0.08702
1.0E+3	-0.33772	-0.08702

Again there is a large range of weights for which the steady state forces and moments are nearly independent of the weight. A weighting of 50 is also chosen for the divergenceless conditions.

In arriving at the answers presented in Tables 2 and 3 other parameters had to be chosen. First is the distance inside which the vortex sheet, edge cores and wake cores do not induce a velocity. This is called the cutoff distance. As the wake forms the local particle velocity is needed. The velocity of the vortex discontinueties need to be calculated at the edge and the wake nodes. The actual velocity at these points would be infinite which is physically impossible. To eliminate this difficulty, as discussed in Appendix II, a distance is chosen inside of which the induced velocity was set to zero. This distance was chosen to be 0.00001, where the length of the edge cores are unity. This choice effectively eliminates the influence of the singularity on itself while the effect on the rest of the flow field is retained.

The second parameter is the length of the time step. As mentioned the dimensionless length of the convecting edge cores is unity, the dimensionless time step was chosen to be unity so that the wake mesh rings had sides of nearly equal length.

The final parameter was how much of the wake should be retained. The result presented in Tables 2 and 3 used a wake length equal to five chord lengths. This parameter is used to save computer time. As the wake moves down stream its influence on the surface decreases (the infinity condition). To find where the wake no longer has influence on the

surface several runs were made retaining different lengths of the wake. The results of these test are shown in Table 4.

Table 4. Variation due to Length of the Wake

Length	C_{f_z}	$C_{m_{y_{l.e.}}}$
2 chords	-0.33466	-0.08591
3 chords	-0.33645	-0.08658
4 chords	-0.33728	-0.08687
5 chords	-0.33772	-0.08702
6 chords	-0.33796	-0.08710

As shown there is little difference for wake lengths greater than about four chord lengths, for a unit-aspect-ratio rectangular wing.

2.16 Results for Thin Lifting Surfaces

Two wings where analyzed in detail. The first is a unit-aspect-ratio rectangular wing The second is a unit-aspect-ratio delta wing. Both wings are uncambered, but as pointed out throughout this work the method is valid for wings with camber. The method was tested for convergence as the number of elements is increased. The steady state results are compared with experimental data and the vortex-lattice method for a range of angles of attacks. The delta wing is also compared with the experimental results of Hummel [1979]

The wings are discretized as shown in Figure 25. The two meshes where chosen because the elements are nearly equilateral. The rectangular wing is shown with 64 elements and the delta wing is shown with 49 elements.

The evolution of the normal force coefficient for the rectangular wing started impulsively at 10 degrees angle of attack is shown in Figure 26. Figure 27 presents the evolution of the comparable moment coefficient about the leading edge. Table 5 lists steady state coefficeints of the unit-aspect-ratio rectangular wing at 10 and 20 degrees angle of attack. Figure 28 and Figure 29 present a comparison of the present method with experimental data

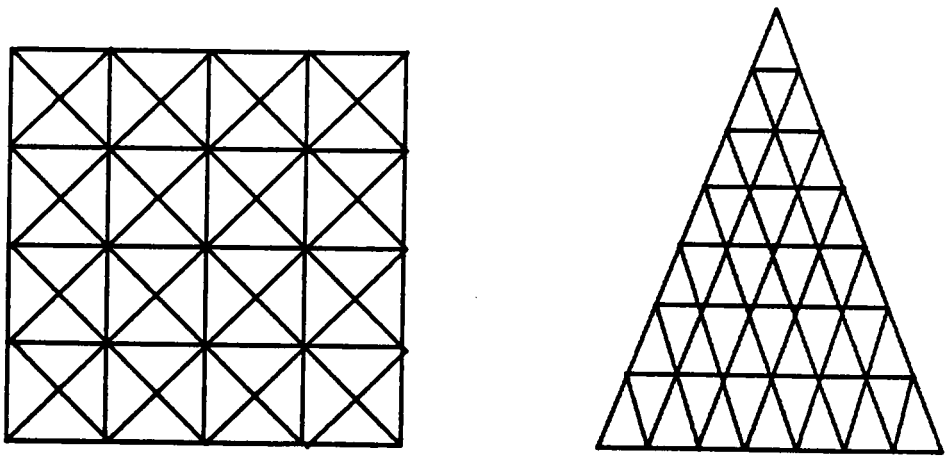

Figure 25. Discretizing the Wings

of Berlotserkovskii [1966] and Lamar [1974] and also with the vortex-lattice method over a range of angles of attack for 64 elements. The steady state pressure distributions using 256 elements at angles of attack of 10 and 20 degrees are shown in Figure 30 and Figure 31, respectively. The steady state wake mesh for 10 degrees angle of attack and 256 elements is shown in Figure 32.

Table 5. Convergence of a Unit-Aspect-Ratio Rectangular Wing

	$\alpha = 10°$		$\alpha = 20°$	
Number of Elements	C_{f_z}	$C_{m_{y_{l.e.}}}$	C_{f_z}	$C_{m_{y_{l.e.}}}$
64	-0.3372	-0.0870	-0.8472	-0.2250
100	-0.3477	-0.0906	-0.8504	-0.2272
144	-0.3531	-0.0927	-0.8507	-0.2281
196	-0.3568	-0.0938	-0.8509	-0.2291
256	-0.3592	-0.0944	-0.8510	-0.2298

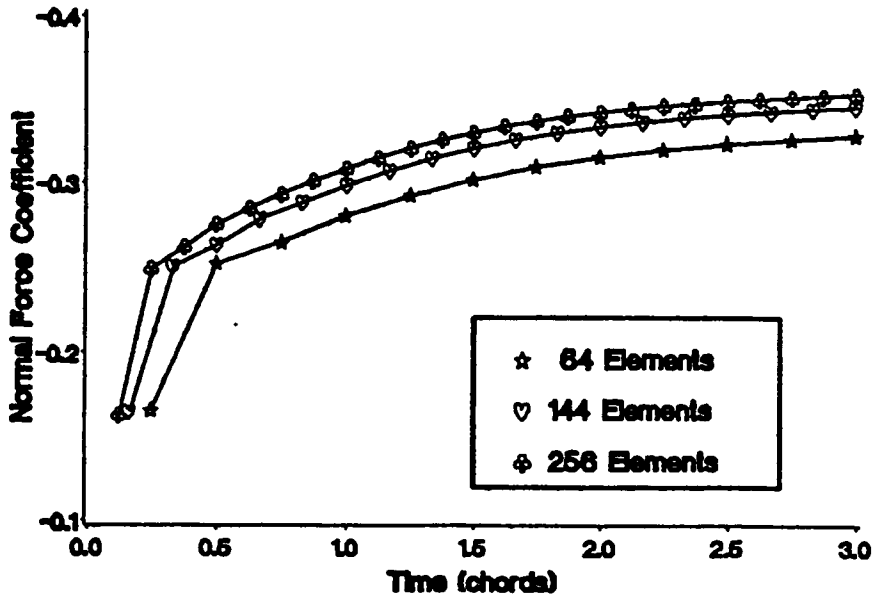

Figure 26. Normal Force Coefficient as Number of Elements is Increased

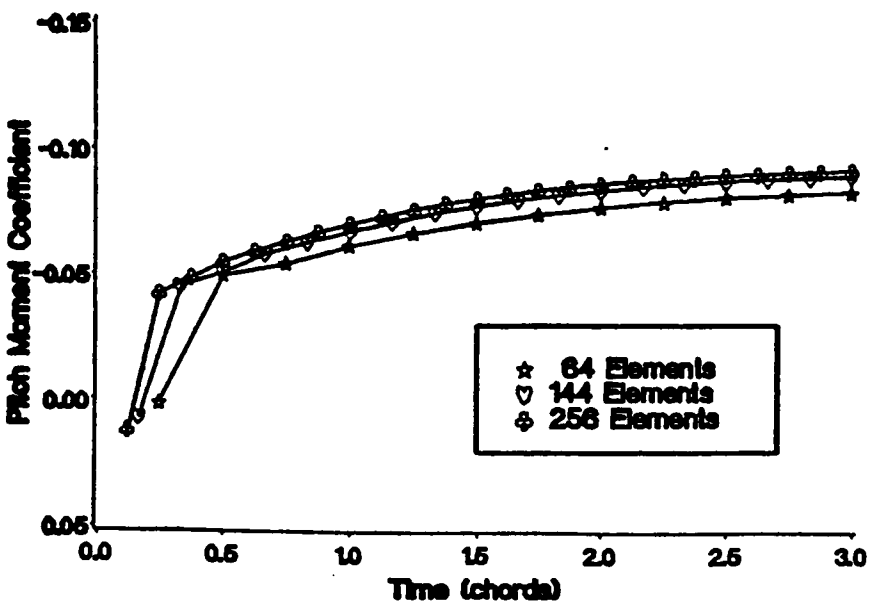

Figure 27. Pitch Moment Coefficient as Number of Elements is Increased

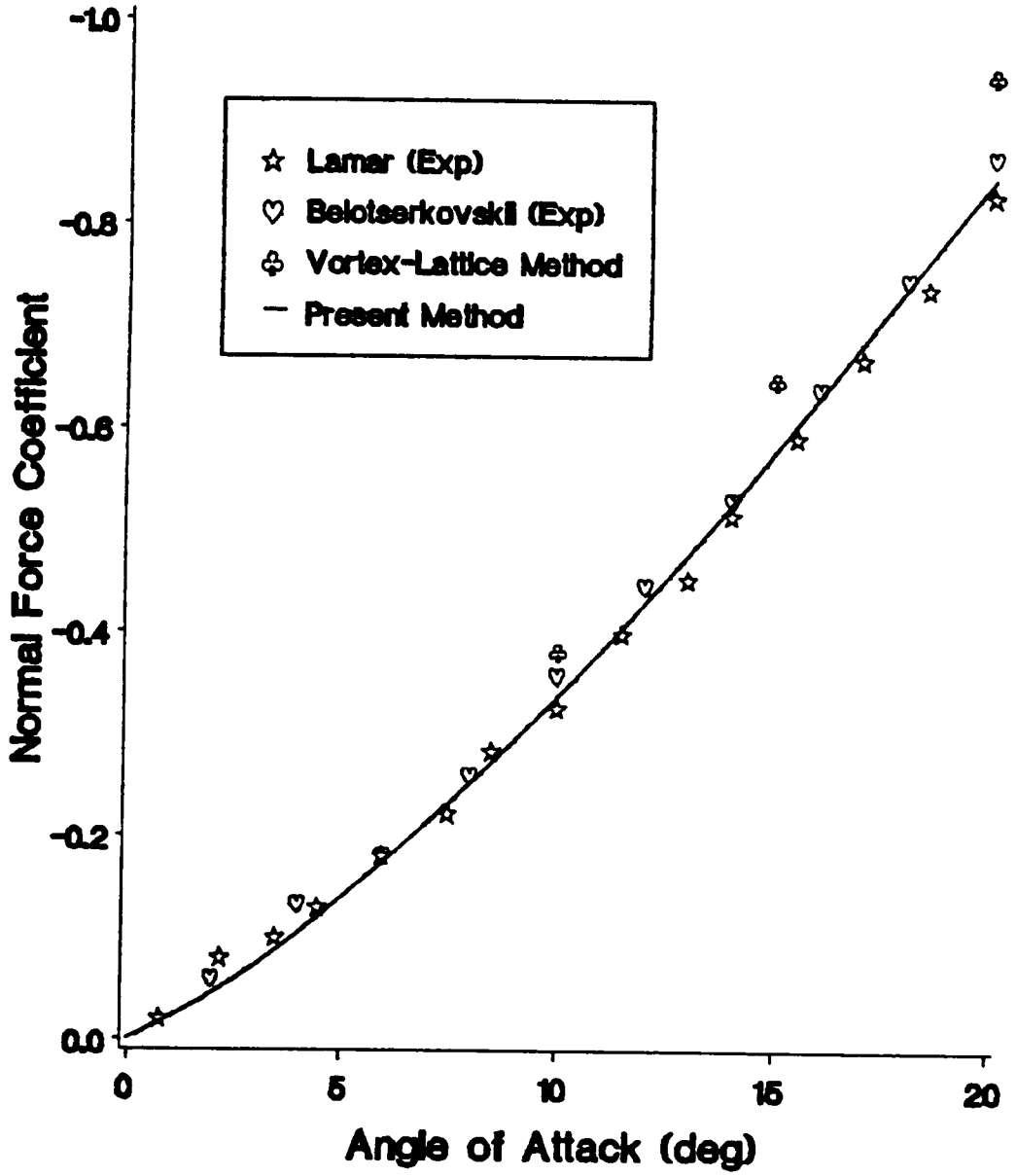

Figure 28. Normal Force Coefficient for a Range of Angles of Attack

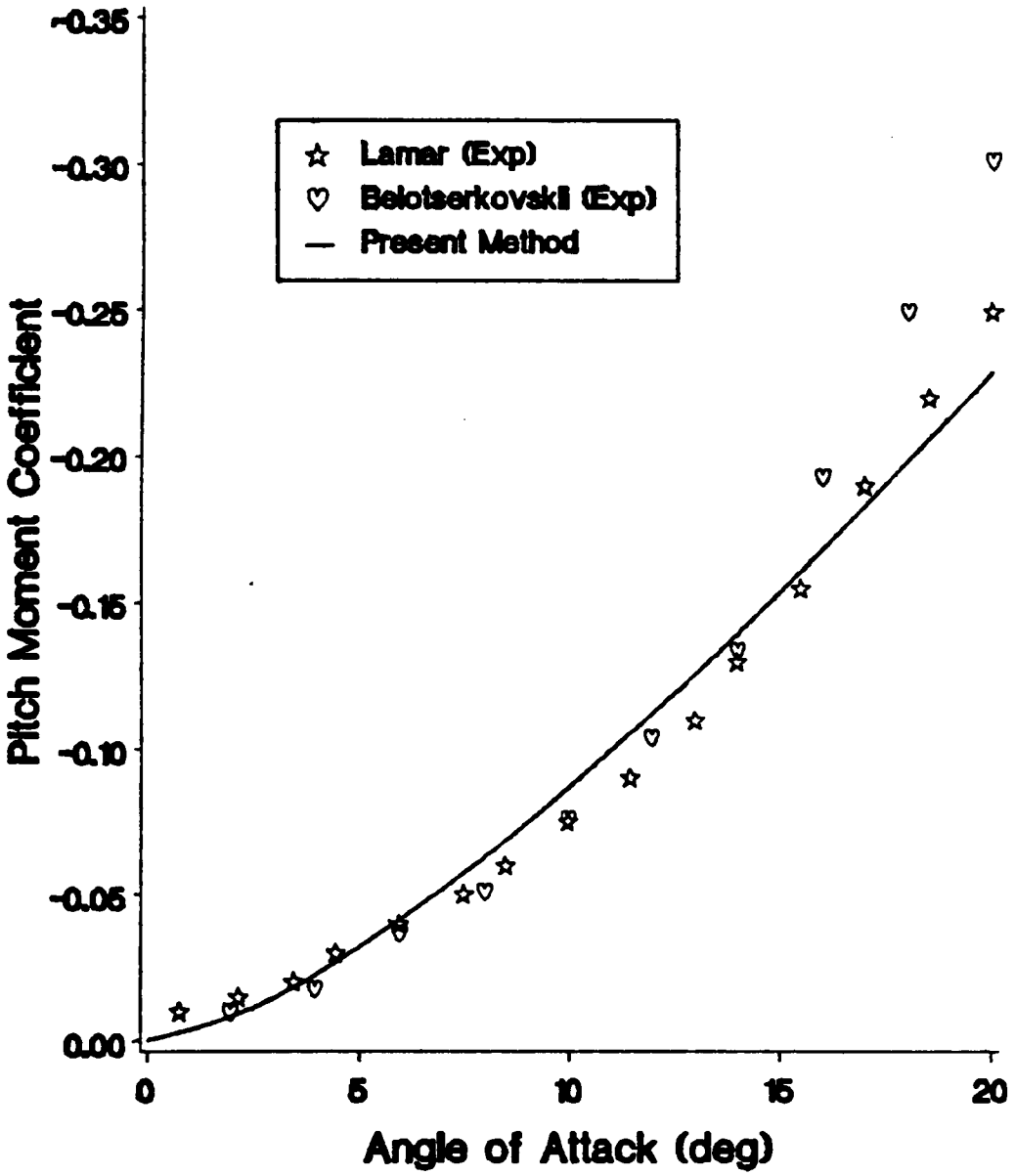

Figure 29. Pitch Moment Coefficient for a Range of Angles of Attack

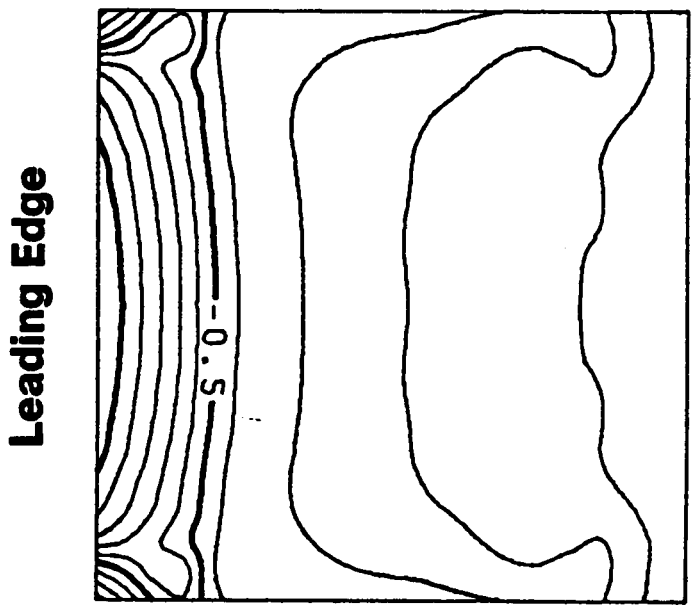

Figure 30. Steady State Pressure Distribution 10 Degrees Angle of Attack

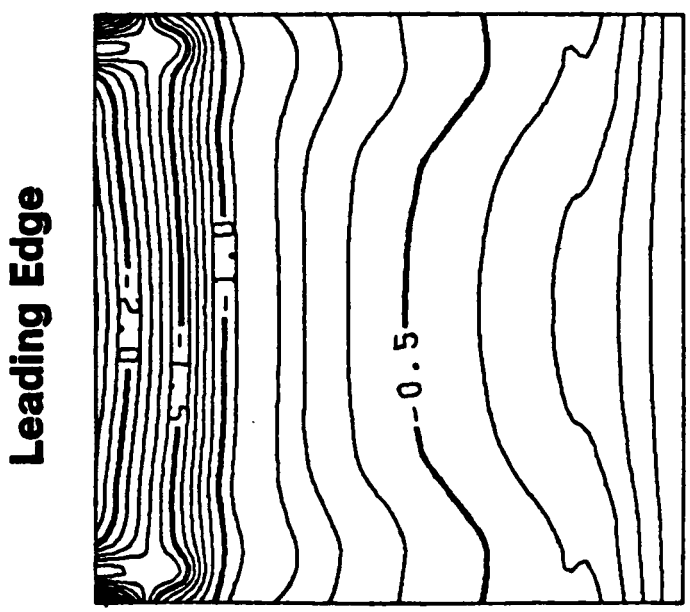

Figure 31. Steady State Pressure Distribution 20 Degrees Angle of Attack

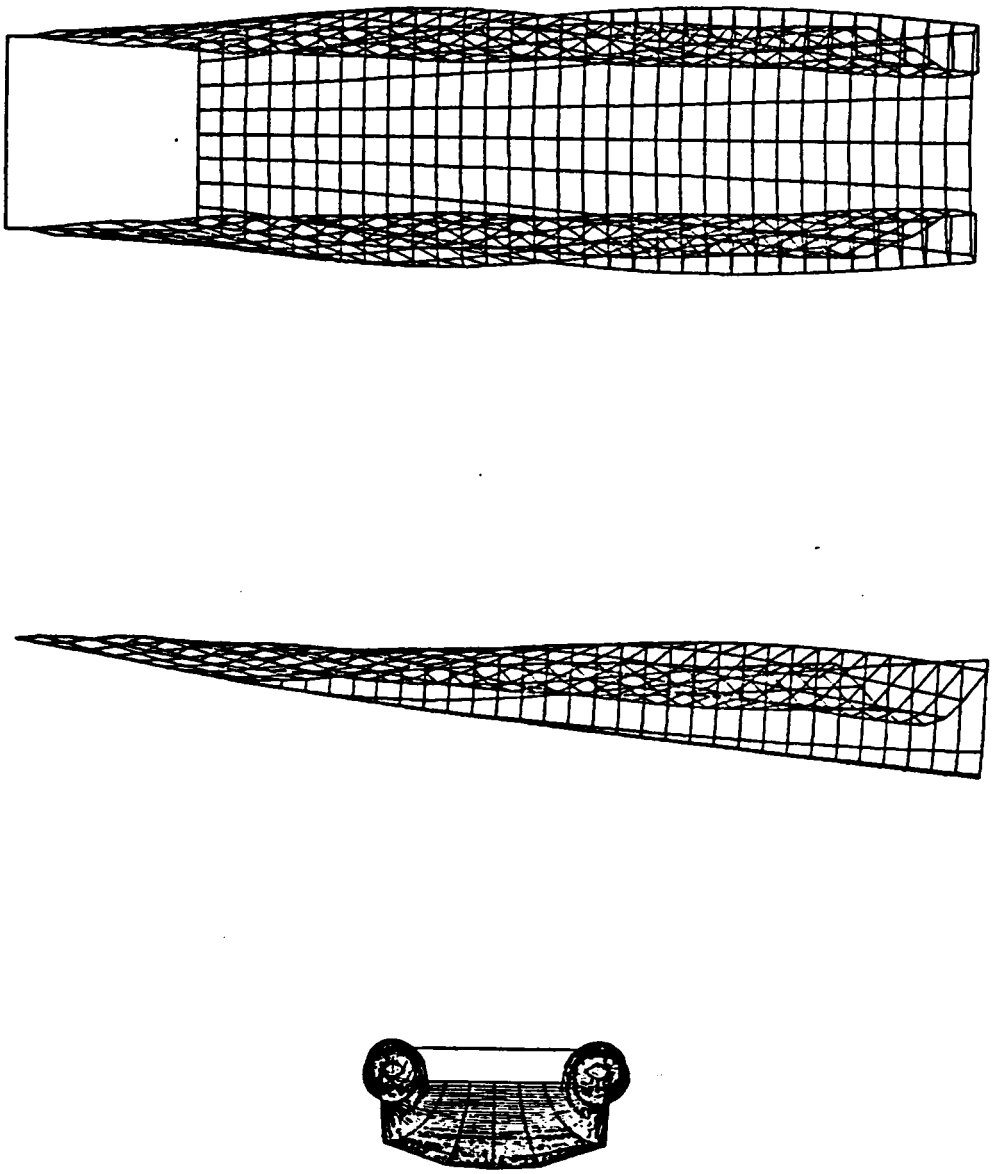

Figure 32. Steady State Wake Mesh

The unit-aspect-ratio delta wing is shown in Figure 33 through Figure 40. Figure 33 and Figure 34 and present the convergence of the normal force coefficient and moment coefficient, calculated about the one quarter mean aerodynamic chord, as the number of elements is increased, for the wing at 20.5 degrees angle of attack. Figure 35 and Figure 36 show the comparison of normal force and moment coefficients to experimental results over a range of angles of attack. The steady state listing of force and moment coefficients , for 20.5 degrees angle of attack is presented in Table 6. Figure 37 shows the steady state pressure distribution for the 169 element wing at four different chord positions. The steady state wake shape is shown in Figure 38 at six positions downstream of the wing. The steady state wake mesh is shown in Figure 39 and Figure 40. These last three figures are for a wing with 361 elements at 20.5 degrees angle of attack.

There are some difficulties with a delta wing compared with a rectangular wing. First the number of cores that should be convected off the wing is not as apparent. The number chosen depended on the size of the wing mesh. For a wing with less then 81 elements two cores on each side of the centerline were not convected. For wings with more than 80 elements three cores on each side of the centerline were not convected. The wake mesh shown in Figure 38, Figure 39 and Figure 40 has three nonconvecting cores on each side of the centerline of the wing. This particular choice gives a much more even wake mesh. Second the wake filaments tried to penetrate the wing, for larger wing meshes, as the wake rolled up over the wing. Because there is no mechanism for reattaching the wake to the wing, the wake was forced to remain a fixed distance above the wing. This distance also depended on the size of the wing mesh. The distance is chosen to be .03 chords. This choice provides a more consistent development of the normal force and pitching moment coefficient from an impulsive start.

Table 6. Convergence of a Unit-Aspect-Ratio Delta Wing

	$\alpha = 20.5°$	
Number Elements	C_{f_z}	$C_{m_{y_{\bar{c}}}}$
25	-0.7454	-0.1276
36	-0.7507	-0.1190
49	-0.7422	-0.1091
64	-0.7494	-0.1071
81	-0.7479	-0.1048
100	-0.7545	-0.1135
121	-0.7503	-0.1098
169	-0.7559	-0.1115

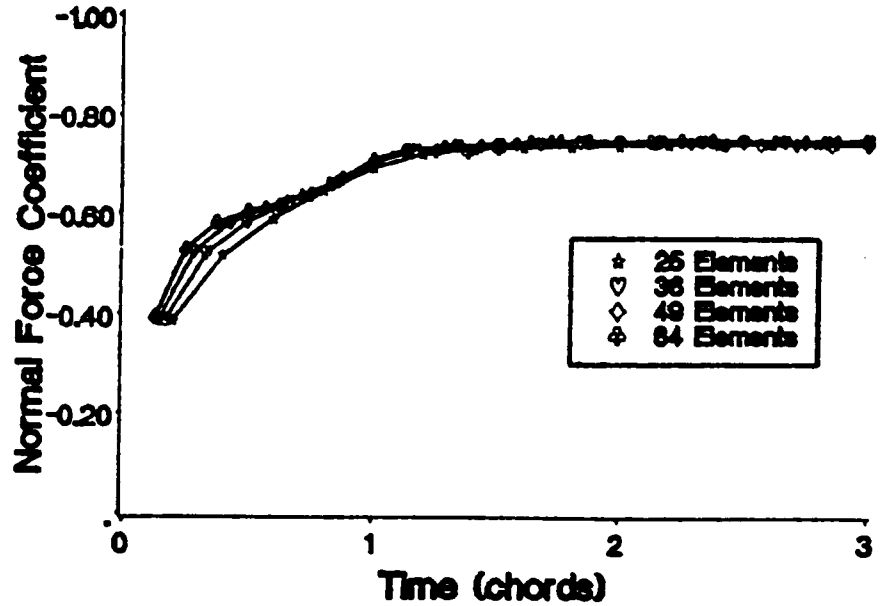

Figure 33. Normal Force Coefficient as Number of Elements is Increased

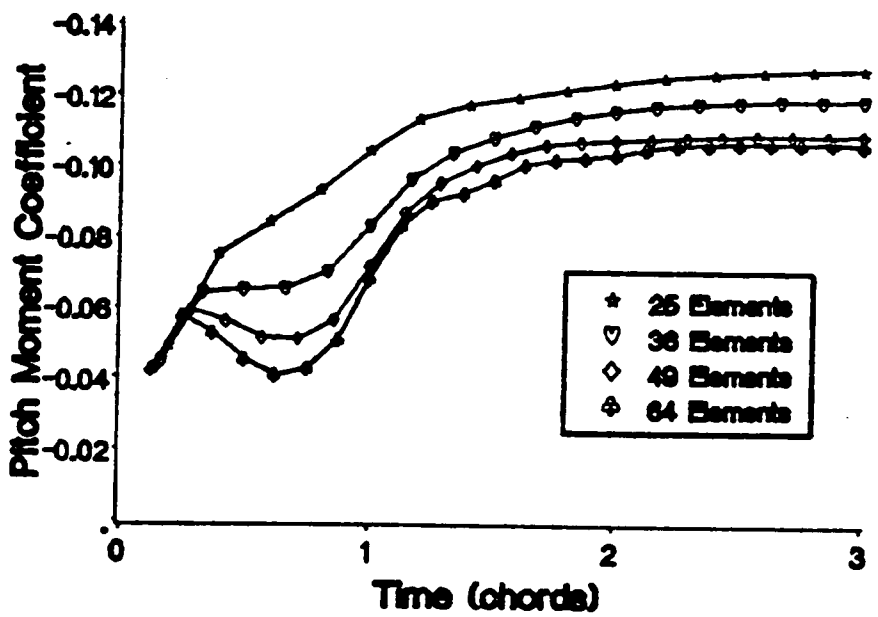

Figure 34. Pitch Moment Coefficient as Number of Elements is Increased

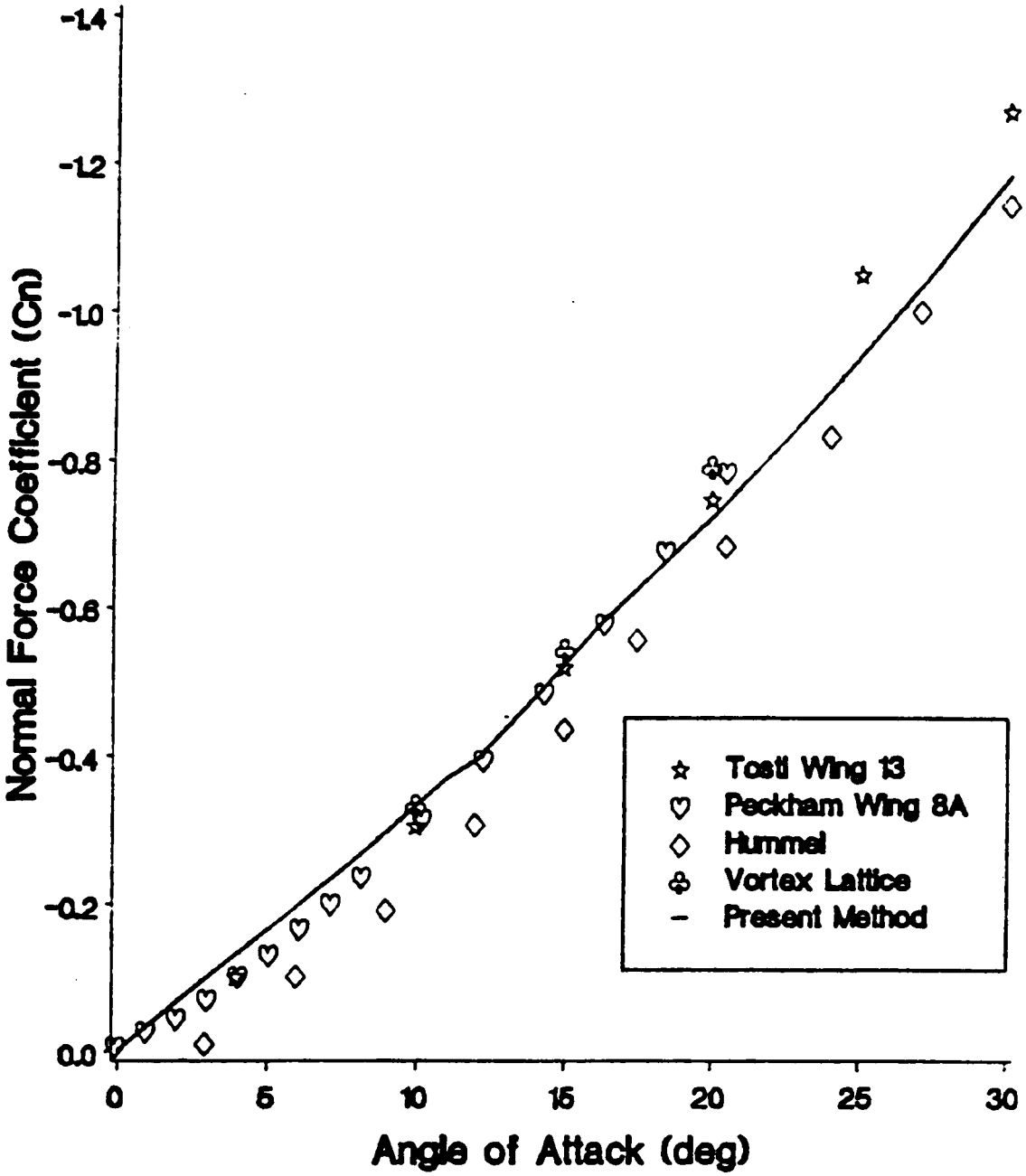

Figure 35. Normal Force Coefficient for a Range of Angles of Attack

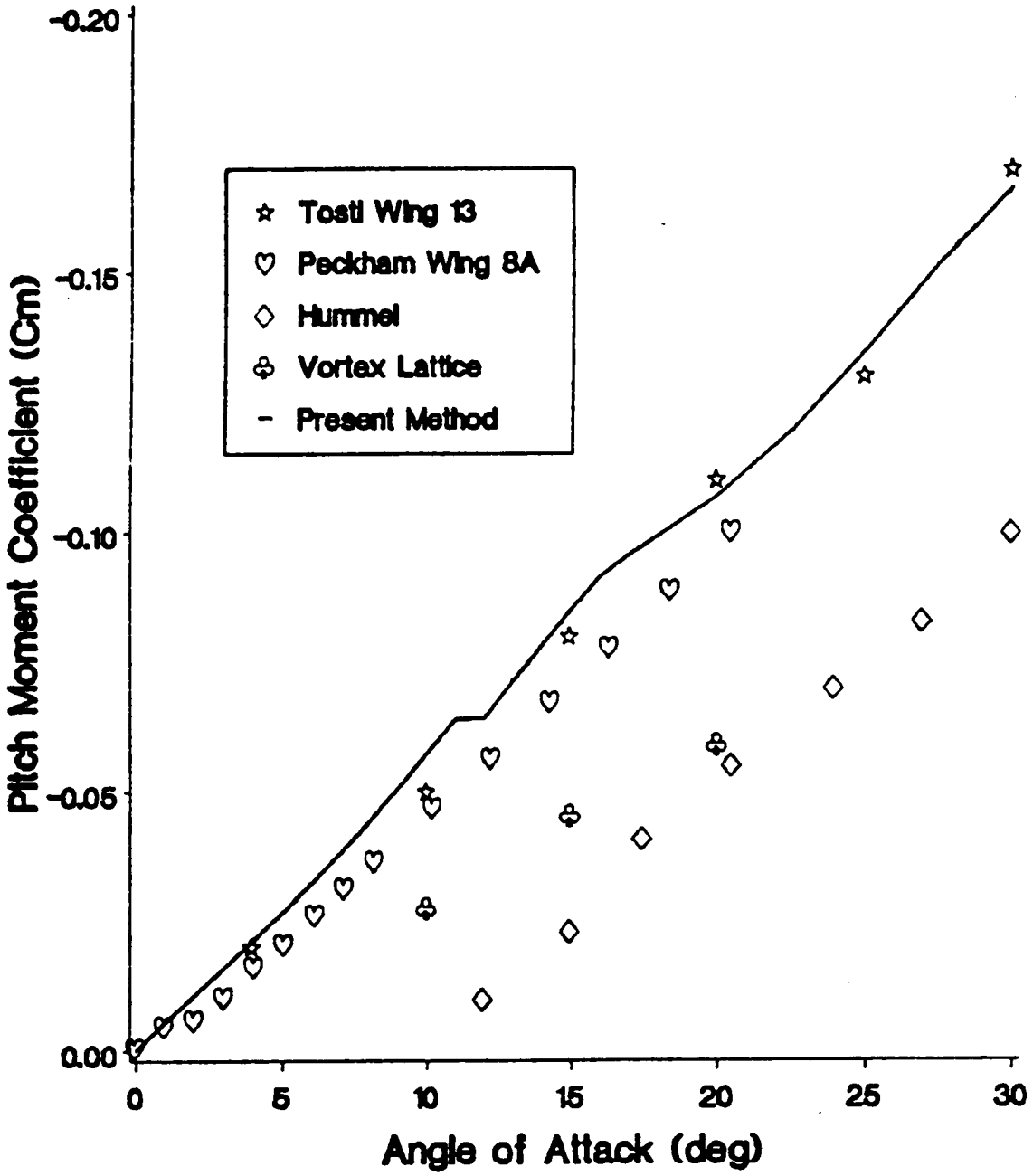

Figure 36. Pitch Moment Coefficient for a Range of Angles of Attack

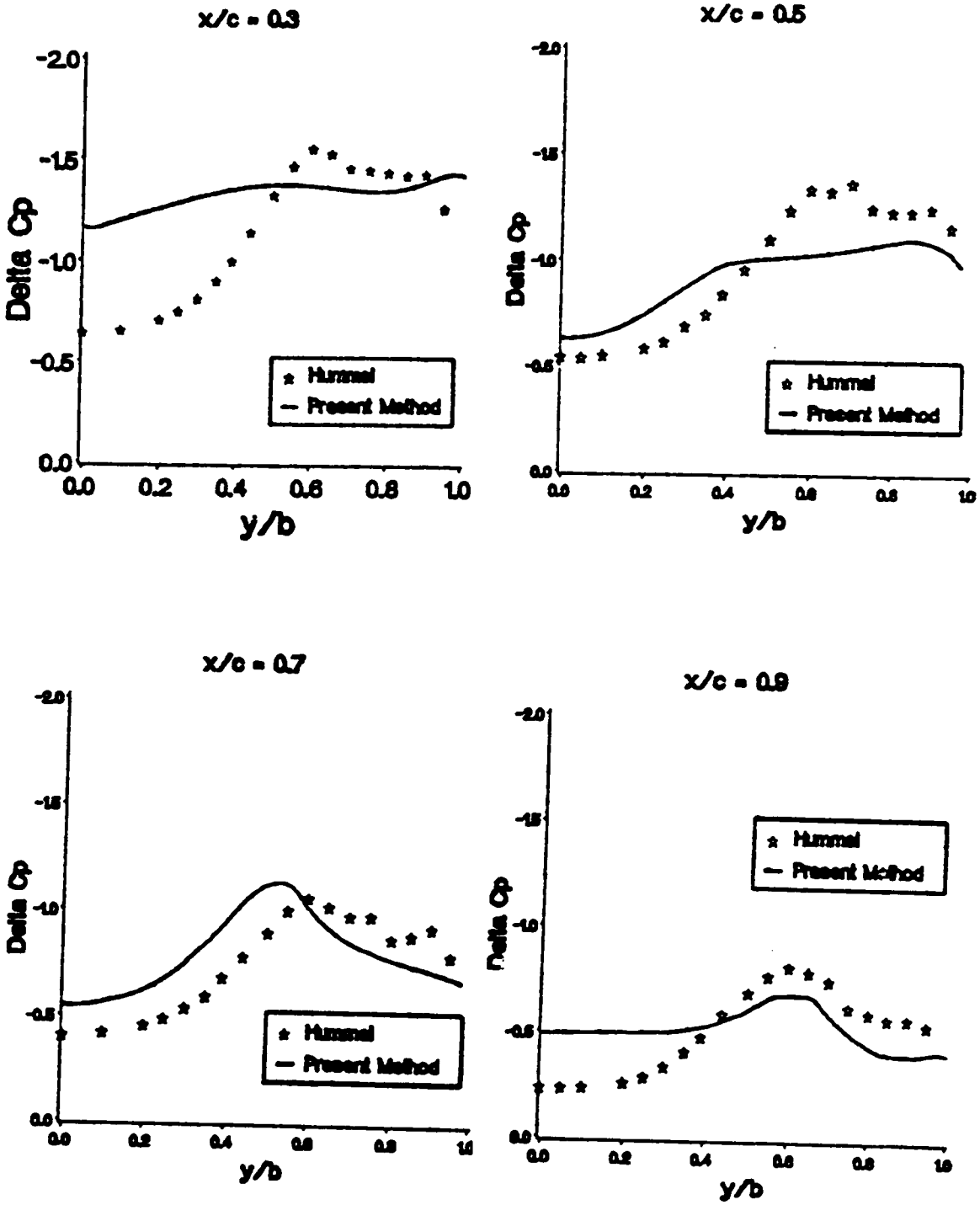

Figure 37. Steady State Pressure Distribution

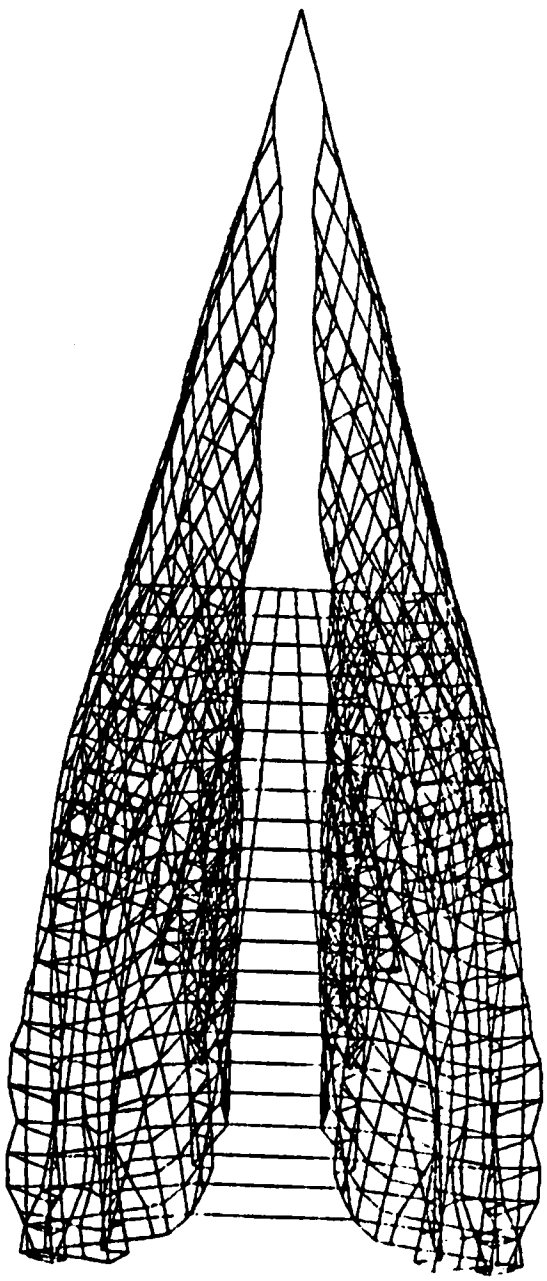

Figure 38. Steady State Wake Mesh

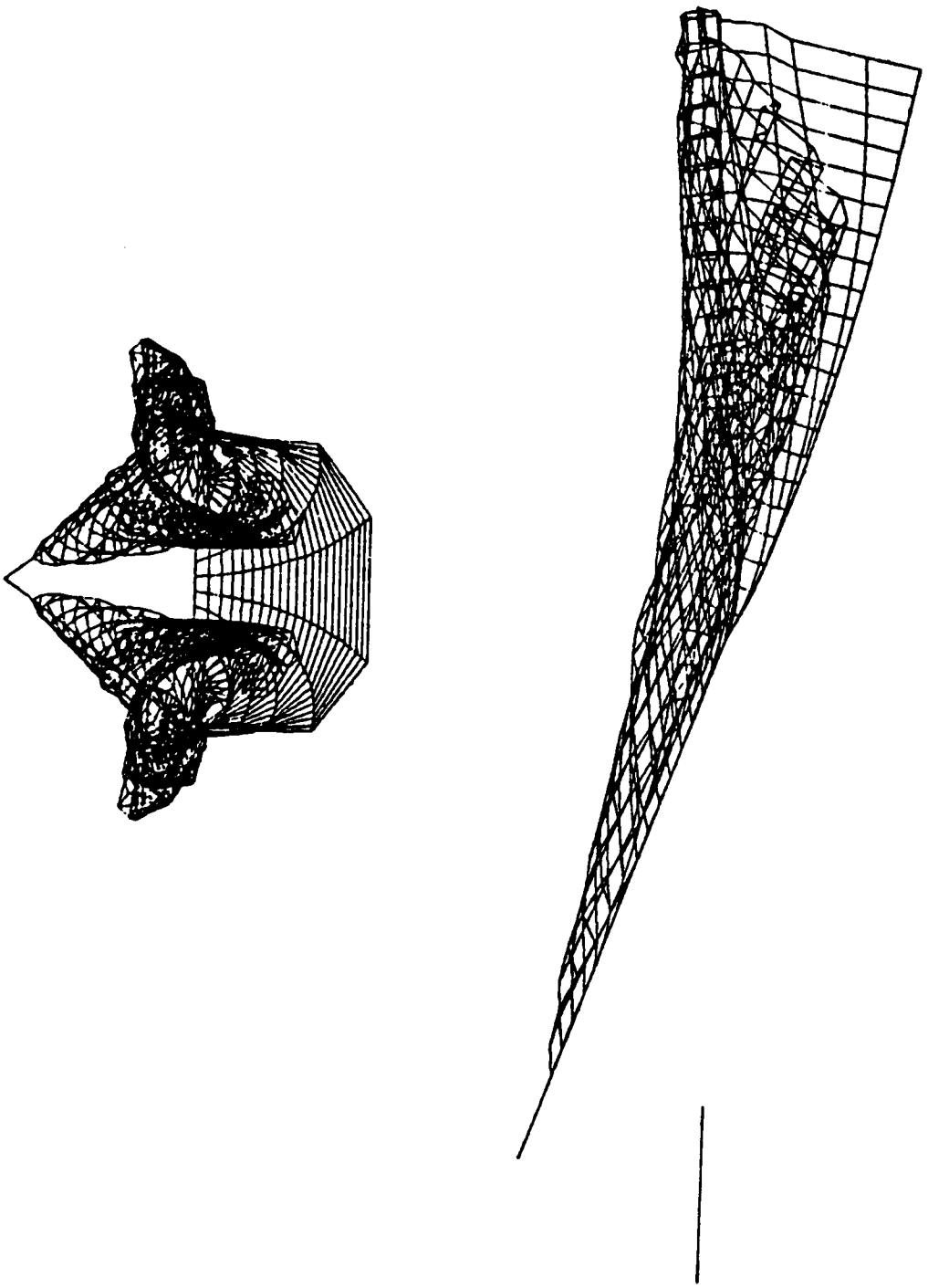

Figure 39. Steady State Wake Mesh (cont.)

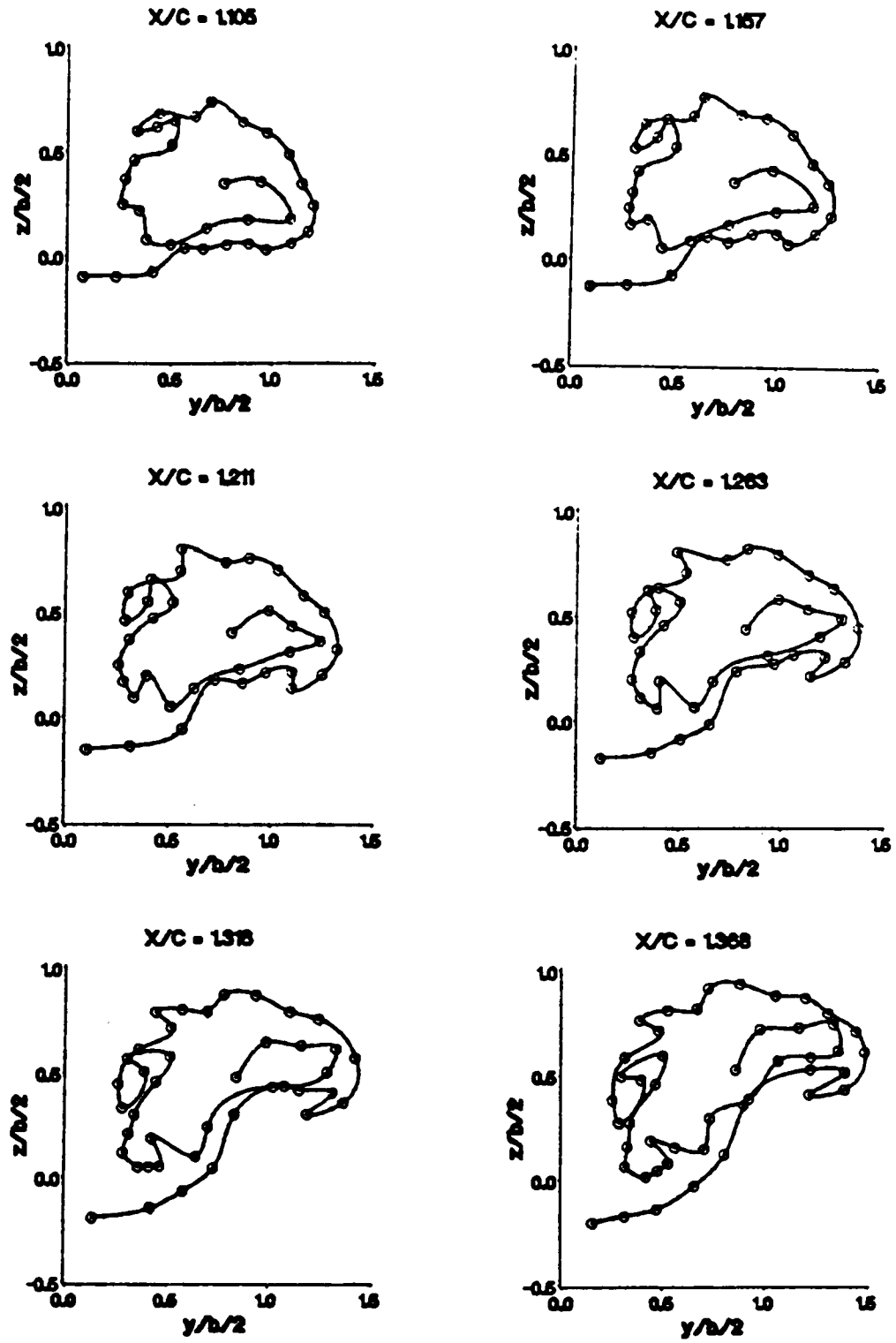

Figure 40. Vortex Sheet Location Downstream of the Wing

2.17 Conclusions for the Aerodynamic Model

This method represents an attractive procedure for predicting aerodynamic features of closed nonlifting bodies and thin wings. The method uses the concept of a continuous sheet of vorticity to represent the surface and a progressively developing lattice for the wake. The method presented provides advantages compared to both the vortex-lattice methods and other vortex panel methods.

The obvious advantage over the vortex-lattice method is the smooth pressure distribution on the surface. The method also removes the question of where the wing is located, the lattice method adjusts the position of the wing a certain amount so that the aerodynamic data is accurate. The present method has the wing in the same location as the mesh. The lattice method also uses an offset for the starting location of the wake mesh for a delta wing and no offset for a rectangular wing. This raises the question of the appropriate offset for wings of new planform. Because of the above questions the lattice method has been accused of providing accurate predictions only once the predictions are known. The method presented here does not have this problem because both the rectangular wing and delta wing were analyzed using the same method.

This method also has advantages to the other vortex panel methods. The main advantage is that the wake is progressively formed. Thus general unsteady motion can be analyzed. Another advantage is that the other models using vortex panels in the wake have a mechanism to capture the wake into a discrete core of vorticity. The present method does not require a capturing vortex core because the wake is already a set of discrete cores. The last, and perhaps the most subtle, advantage is this method employs the Kutta condition by Bernoulli's equation for unsteady motion.

Chapter III

Dynamic Model

3.1 Introduction

In Chapter II, a complete unsteady aerodynamic model was presented. This model is capable of predicting the aerodynamic forces and moments for bodies executing arbitrary maneuvers. As mentioned in Chapter I, the dynamic simulation will be restricted to surfaces with constant speed. That is, the model will be used to simulate wind tunnel experiments. The focus is on two types of motions that have been investigated in wind tunnels. These motions are forced and free oscillation tests. Both of these motions can be examined by coupling the aerodynamic model with equations of motion.

In this chapter will present the definition of the coordinate frames, the method of solution of the equations of motion, the procedure used in coupling the equations of motion with the aerodynamic model, the results for forced pitching oscillation tests, the development of the governing equations of motion for three degrees of freedom (in angular orientation) and finally the free oscillation tests for one degree of freedom, "wing rock" are presented.

3.2 Reference Coordinate Frames

Two coordinate systems are used to develop the equations of motion. One is an inertial reference frame, and the other is a moving reference frame attached to the body called the body-fixed frame. In general, the motion of a body has six degrees of freedom. These degrees are the three components of the position vector of the origin of the body-fixed reference frame and a set of three Euler angles. With the restriction that the speed is held constant, the degrees of freedom reduce to the three Euler angles. The body-fixed reference frame is oriented, as shown in Figure 41, with the positive x axis through the nose, the positive y axis through the right (starboard) wing tip, and the positive z axis downward. The three Euler angles chosen to relate the angular orientation of the body-fixed frame to the inertial frame

frame is the 3-2-1 set. That is, the following sequence moves the wing from the inertial frame to a given orientation:

1) A yaw-like rotation around the original z axis through an azimuth angle ψ, followed by

2) a pitch-like rotation around the new position of the y axis through an elevation angle θ, followed by

3) a roll-like rotation around the new position of the x axis through a bank angle ϕ.

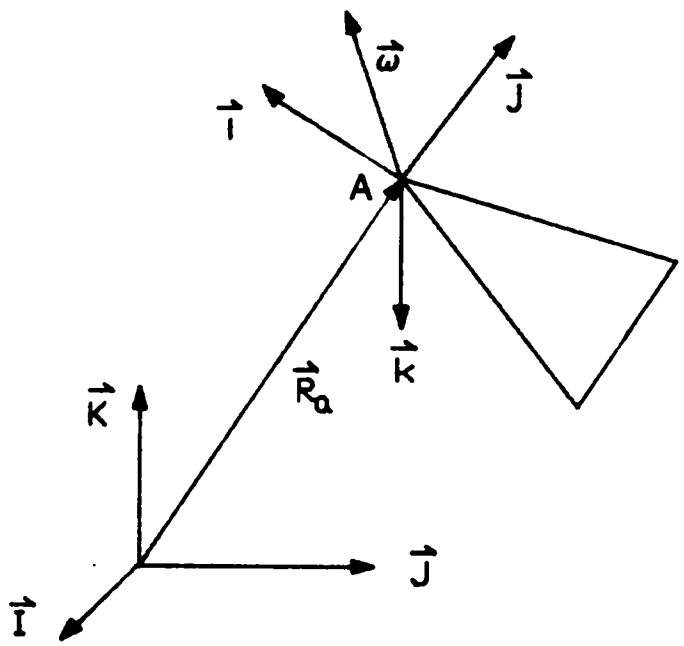

Figure 41. Coordinate Reference Frames

The unit vectors of the body-fixed frame $(\vec{i}, \vec{j}, \vec{k})$ are related to those of the inertial frame $(\vec{I}, \vec{J}, \vec{K})$ as follows:

$$\begin{Bmatrix} \vec{i} \\ \vec{j} \\ \vec{k} \end{Bmatrix} = [C] \begin{Bmatrix} \vec{I} \\ \vec{J} \\ \vec{K} \end{Bmatrix} \qquad (3.2-1)$$

where

$$[C] = \begin{bmatrix} \cos\theta\cos\psi & \cos\theta\sin\psi & -\sin\theta \\ \sin\phi\sin\theta\cos\psi - \cos\phi\sin\psi & \sin\phi\sin\theta\sin\psi + \cos\phi\cos\psi & \sin\phi\cos\theta \\ \cos\phi\sin\theta\cos\psi - \sin\phi\sin\psi & \cos\phi\sin\theta\sin\psi - \sin\phi\cos\psi & \cos\phi\cos\theta \end{bmatrix}. \qquad (3.2-2)$$

The components of the angular velocity of the wing written in the body-fixed reference frame are

$$\vec{\omega} = \omega_x \vec{i} + \omega_y \vec{j} + \omega_z \vec{k}. \qquad (3.2-3)$$

These components are related to the time derivatives of the Euler angles as follows.

$$\begin{Bmatrix} \omega_x \\ \omega_y \\ \omega_z \end{Bmatrix} = [B] \begin{Bmatrix} \dot{\phi} \\ \dot{\theta} \\ \dot{\psi} \end{Bmatrix} \qquad (3.2-4)$$

where

$$[B] = \begin{bmatrix} 1 & 0 & -\sin\theta \\ 0 & \cos\phi & \sin\phi\cos\theta \\ 0 & -\sin\phi & \cos\phi\cos\theta \end{bmatrix}. \qquad (3.2-5)$$

3.3 Equations of Motion and Method of Solution

In this presentation the forced oscillations of interest are simple harmonic motions. In general, the equations of motion can be written as

$$\begin{Bmatrix} \ddot{\phi} \\ \ddot{\theta} \\ \ddot{\psi} \end{Bmatrix} = \begin{Bmatrix} H_1 \\ H_2 \\ H_3 \end{Bmatrix} \qquad (3.3-1)$$

where the H_i are independent of the aerodynamic moments for forced tests and include these moment for free tests. Therefore, coupling the aerodynamic model with the motion equations requires first coupling a numerical integration scheme with the aerodynamic model. The integration technique chosen is Hamming's fourth-order predictor-corrector method as presented by Garnahan et al[1969]. This method was chosen over a Runge-Kutta technique because the aerodynamic model of Chapter II uses a constant step size.

The predictor-corrector technique requires the differential equations to be written in the form:

$$\frac{dX_i}{dt} = F_i(x_1, ..., x_n, t) \quad \text{for } i = 1,...,n. \qquad (3.3-2)$$

Therefore, Equation 3.3-1 is written as

$$\begin{Bmatrix} \dot{X}_1 \\ \dot{X}_2 \\ \dot{X}_3 \\ \dot{X}_4 \\ \dot{X}_5 \\ \dot{X}_6 \end{Bmatrix} = \begin{Bmatrix} \dot{\phi} \\ \ddot{\phi} \\ \dot{\theta} \\ \ddot{\theta} \\ \dot{\psi} \\ \ddot{\psi} \end{Bmatrix} = \begin{Bmatrix} X_2 \\ H_1 \\ X_4 \\ H_2 \\ X_6 \\ H_3 \end{Bmatrix} = \begin{Bmatrix} F_1 \\ F_2 \\ F_3 \\ F_4 \\ F_5 \\ F_6 \end{Bmatrix} \qquad (3.3-3)$$

This general procedure requires full knowledge of four previous time steps to predict the state at the next time. Assuming the states and the right hand side of Equation 3.3-3 are known at four previous time steps and designating them

$$X_{i,1}, X_{i,2}, X_{i,3}, X_{i,4}, \\ F_{i,1}, F_{i,2}, F_{i,3} \text{ and } F_{i,4}, \qquad (3.3-4)$$

the procedure follows the flow chart of Figure 42, where the equations referred to in the chart are

$$X_{i,5}^{p} = X_{i,1} + \frac{4\Delta t}{3}(2F_{i,4} - F_{i,3} + 2F_{i,2}), \qquad (3.3-5)$$

$$X_{i,5}^{1} = X_{i,5}^{p} + \frac{112}{9}E_{i,4}, \qquad (3.3-6)$$

$$X_{i,5}^{k+1} = \frac{1}{8}\left[9X_{i,4} - X_{i,2} + 3\Delta t\,(F_{i,5}^{k} + 2F_{i,4} - F_{i,3})\right], \qquad (3.3-7)$$

where k is the iteration number

$$E_{i,5} = \frac{9}{121}(X_{i,5}^{k+1} - X_{i,5}^{p}) \qquad (3.3-8)$$

and

$$X_{i,5} = X_{i,5}^{k+1} - E_{i,5}. \qquad (3.3-9)$$

The method presented in Figure 42. is based on the assumption that the solution is known at the four previous time steps, which is true only if three time steps have already been computed. For the first three steps, a starting procedure must be employed. The starting procedure chosen is based on a simple Taylor-series expansion. Using the initial conditions, designated by the subscript one, one can obtain the state at the first time step, designated by the subscript two, as follows:

$$X_{i,2} = X_{i,1} + \Delta t\, F_{i,1}. \qquad (3.3-10)$$

The right-hand side of Equation 3.3-3 ($F_{i,2}$) can then be computed by using the new state $X_{i,2}$. This information can be used to find the state at the second time step from the following:

$$X_{i,3} = \frac{1}{3}(4X_{i,2} - X_{i,1}) + \frac{2\Delta t}{3}(2F_{i,2} - F_{i,1}). \qquad (3.3-11)$$

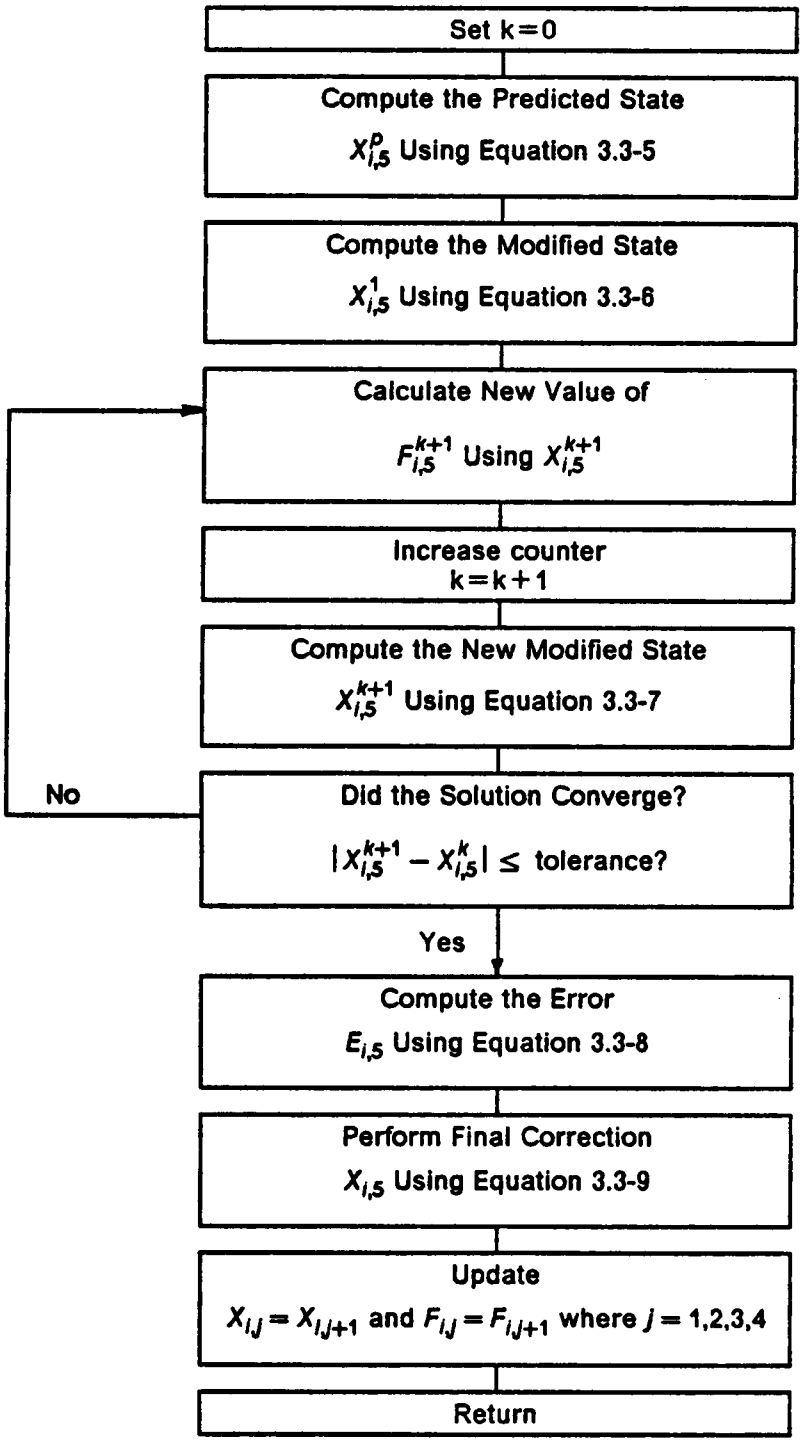

Figure 42. General Flow Chart of Predictor-Corrector Algorithm

This state can then be used to compute $F_{i,3}$. The state at the third time step is

$$X_{I,4} = \frac{1}{11}(18X_{I,3} - 9X_{I,2} + 2X_{I,1}) + \frac{6\Delta t}{11}(3F_{I,3} - 3F_{I,2} + F_{I,1}). \qquad (3.3-12)$$

Finally, $F_{I,4}$ can be found by using $X_{I,4}$. All the information needed for the general predictor-corrector method is now available, except $E_{I,3}$ which is set to zero before the general procedure is started. The flow chart of the entire numerical integration procedure is shown in Figure 43.

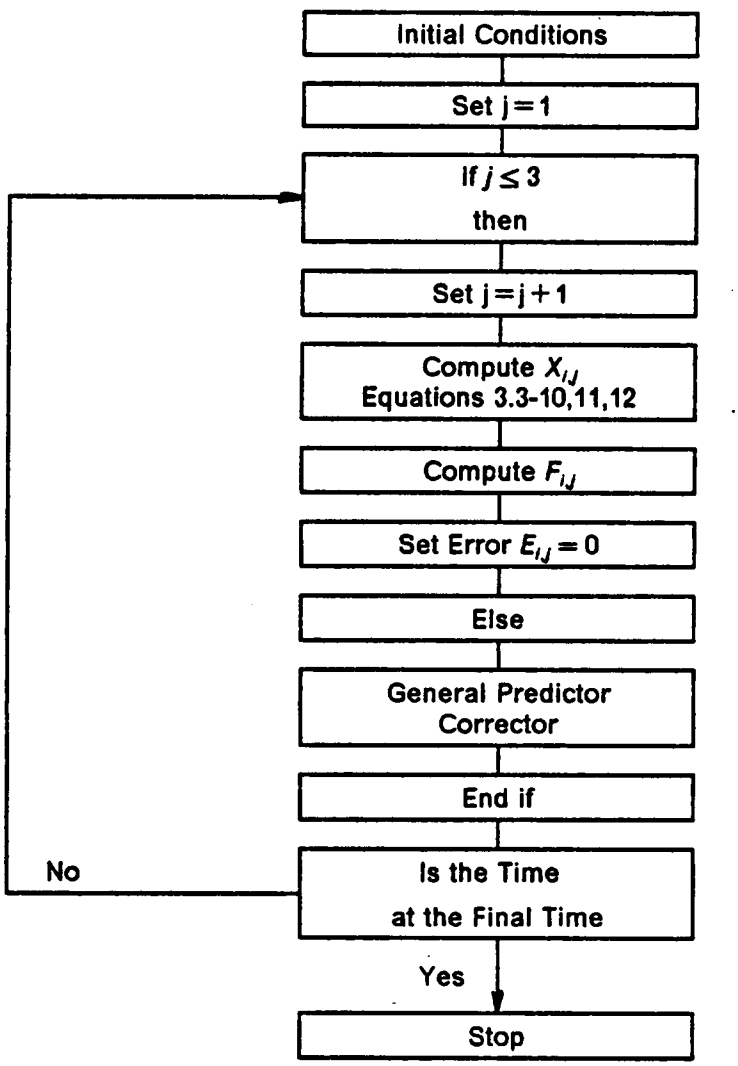

Figure 43. Entire Integration Flow Chart

The algorithm described in the flow charts of Figure 42 and Figure 43 was validated by solving the equation

$$\ddot{x} = -x \qquad (3.3-13)$$

with the initial conditions $x(0) = 1$ and $\dot{x}(0) = 0$. The results obtained from the predictor-corrector algorithm are compared with the analytical solution in Figure 44 for step sizes of 0.5 and 0.1. The comparison shows this method does very well for the smaller step but not as well for the larger step.

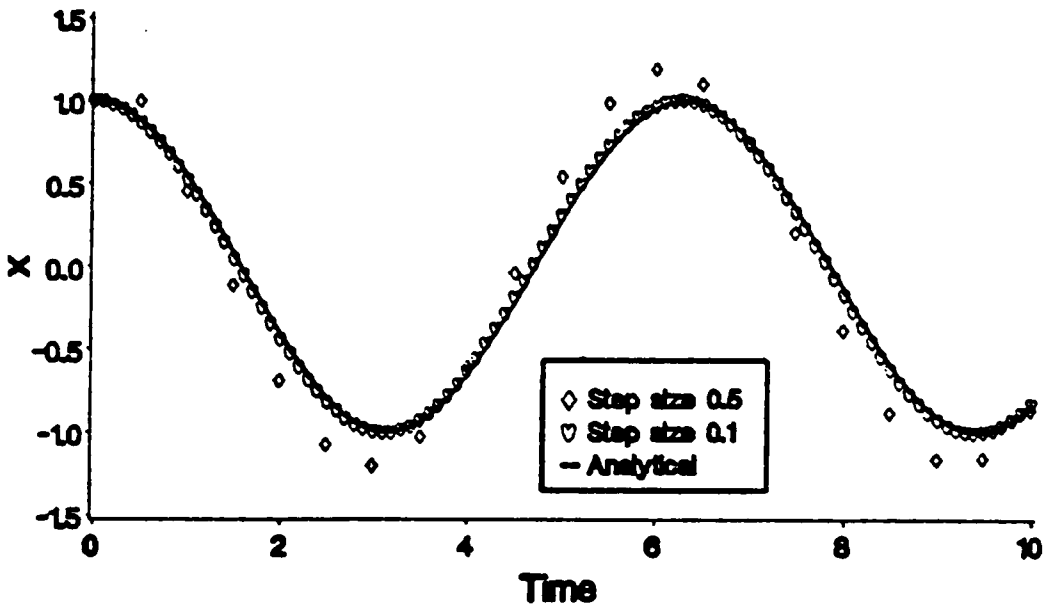

Figure 44. Validation of Numerical-Integration Scheme

So far, the integration technique has been discussed in general. That is, the technique has not been applied to the aerodynamic model. Three areas must be discussed in order to couple the differential-equation solver and the aerodynamic model. These areas are the determination of the position and angular velocity of the wing, the solution of the aerodynamic problem and the convection of the wake. The position and angular velocity of the wing are determined after the prediction and first modification has occurred, inside the predictor-corrector iteration loop. This placement allows the aerodynamic model to react to the current conditions as solved by the integration technique. The solution of the aerodynamic problem, which includes calculating the forces and moments, follows this step. The convection of the wake is placed after the final correction, or outside the predictor corrector iteration loop.

The actual flow for coupling the equations of motion and the aerodynamic model is shown below, where

Subroutine TAYLOR is the starting procedure Equations 3.3-10,11,12,

Subroutine PRAMOD finds the predicted and modified states Equations 3.3-5,6,

Subroutine OMEGAS computes the angular velocity Equation 3.2-4,

Subroutine CMATRX computes the direction cosine matrix Equation 3.2-2,

Subroutine SETRHS sets the right hand side of Equation 2.14-9,

Subroutine EINFLU computes the influence matrix of Equation 2.14-9,

Subroutine DIVERG computes the constraint matrix of Equation 2.14-9,

Subroutine REDOMA establishes the matrix Equation 2.14-10,

Subroutine DGEF and DGES solve the linear equations,

Subroutine FACTOR computes the c of Equation 2.4-20 the remaining components of the vorticity vector and checks for convergence of these,

Subroutine GAVERA finds the average circulations to be convected Equation 2.13-2,

Subroutine FORMOM computes the forces and moments as shown in Figure 17,

Subroutine IMWRIT prints out information during time step,

Subroutine RHSMOT computes the components of F_i,

Subroutine YFITER computes the corrected state Equation 3.3-7,

Subroutine ERRCOR computes the error and the final state for this iteration Equation 3.3-8,9,

Subroutine UPDATE moves the state and right hand sides of the motion back one in index

Subroutine CONVEC convects the wake without splitting Equation 2.13-5,

and Subroutine CONVE1 convects the wake with splitting Equations 2.13-5,8.

```
C       THE INITIALIZATION OF THE PROGRAM TAKES PLACE HERE
C             NSTIME -- STARTING NUMBER FOR THIS RUN
C             NTIME --- ENDING NUMBER FOR THIS RUN
C             NSTMOT -- THE NUMBER WHEN MOTION STARTS
C
C       THE MASTER LOOP
      DO 10 I=NSTIME,NTIME
         NCURTM=I
         NMOTIO=I-NSTMOT
         IF(NMOTIO.LT.0)THEN
C       BEFORE THE MOTION HAS STARTED
               CALL OMEGAS
               CALL CMATRX
               CALL SETRHS
   20          CONTINUE
                    CALL EINFLU
                    CALL DIVERG
                    CALL REDOMA
C       THIS IS A CANNED LINEAR EQUATION SOLVER
                    CALL DGEF(B,MUN,NUMB,IPVT)
                    CALL DGES(B,MUN,NUMB,IPVT,X)
C       FACTOR RETURNS IERROR=0 FOR CONVERGED IERROR=1 OTHERWISE
                    CALL FACTOR
                    CALL GAVERA
               IF(IERROR.NE.0)GOTO 20
         ELSE
               IF(NMOTIO.LT.3)THEN
                    CALL TAYLOR
                    NMOTIO=NMOTIO+1
               ELSE
                    CALL PRAMOD
                    NMOTIO=NMOTIO+1
   30               CONTINUE
                         CALL OMEGAS
                         CALL CMATRX
```

```
                        CALL SETRHS
 40                     CONTINUE
                            CALL EINFLU
                            CALL DIVERG
                            CALL REDOMA
                            CALL DGEF(B,MUN,NUMB,IPVT)
                            CALL DGES(B,MUN,NUMB,IPVT,X)
C       FACTOR RETURNS IERROR=0 FOR CONVERGED IERROR=1 OTHERWISE
                            CALL FACTOR
                             CALL GAVERA
                        IF(IERROR.NE.0)GOTO 40
                        CALL FORMOM
                        CALL RHSMOT
C       YFITER RETURNS IERROR=0 FOR CONVERGED IERROR=1 OTHERWISE
                        CALL YFITER
                    IF(IERROR.NE.0)GOTO 30
                    CALL ERRCOR
                END IF
                CALL OMEGAS
                CALL CMATRX
                CALL CTLMOV
                CALL SETRHS
 50             CONTINUE
                    CALL EINFLU
                    CALL DIVERG
                    CALL REDOMA
                    CALL DGEF(B,MUN,NUMB,IPVT)
                    CALL DGES(B,MUN,NUMB,IPVT,X)
C       FACTOR RETURNS IERROR=0 FOR CONVERGED IERROR=1 OTHERWISE
                    CALL FACTOR
                    CALL GAVERA
                IF(IERROR.NE.0)GOTO 50
            END IF
            CALL FORMOM
            CALL RHSMOT
```

```
            CALL IMWRIT
            TIME=TIME+DTIME
            CALL UPDATE
            IF(TIME.GT.CHORD)THEN
                 CALL CONVE1
            ELSE
                 CALL CONVEC
            END IF
C       SETTING THE WAKE STEPS
            NWPTS=NWPTS+1
C       LIMITING THE NUMBER OF WAKEPOINTS TO MAXWK
            IF(NWPTS.GE.MAXWK)NWPTS=MAXWK
   10 CONTINUE
```

Notice in this code there are three areas, before the motion starts, during the starting procedure and during the general predictor-corrector scheme. The first two sections require only one iterative loop, which is the iteration for non planar surfaces as discussed in Chapter II. The last section requires two iteration loops one for non planar effects and one for the predictor-corrector algorithm. The discussion of the placement of the aerodynamic subroutines relative to the solution of the motion equations, applies only during the last section.

3.4 Forced Oscillation Tests

The coupling of the aerodynamic model of Chapter II and the numerical integration scheme has been developed in Section 3.3. The forced oscillation tests can now be performed. The first test is a simple pitching motion of a high-aspect-ratio rectangular wing about its midchord. This wing was chosen to examine the effects of pitching a two-dimensional flat plate. The high-aspect-ratio wing has approximately the properties of a two-dimensional flat plate near the mid-span of the wing. For this test, the rectangular wing has an aspect ratio of

five and is represented with 320 elements. The wing is held fixed at 12 degrees angle of pitch until a steady-state is reached (20 chords). The steady-state normal-force coefficient is -0.783 and the pitching-moment coefficient about the leading edge is -0.201. The wing is then pitched by solving the differential equation

$$\ddot{\theta} = F_4 = -k\,(\theta - 10°) \qquad (3.4-1)$$

where $k = (\pi/10)^2$. This equation gives a period of twenty time steps. The dimensionless time step is one quarter of a chord. The evolution of the pitching motion, normal-force coefficient, and pitch-moment coefficient (calculated about the leading edge) is presented in Figure 45. The time period shown is from shortly before the motion starts until after three full cycles of the motion have been completed.

The pitching motion, as shown, is not exactly the solution of Equation 3.4-1. This discrepancy is caused by the relatively large step size. Because the motion is not described by Equation 3.4-1, the forces and moments presented also do not apply to that equation. It should be noted, that the motion presented in Figure 45 has nearly the correct period. From Figure 45, the normal force leads the motion by about 30 degrees, and the pitching moment leads the motion by about 60 degrees.

The position of the wake is shown at several time steps during the last cycle of the motion, in Figure 46. The effect of the motion can clearly be seen in this set of figures. The pitching motion results in the wave that propagates downstream of the wing. The numerical references on the plot of pitch angle as a function of time of Figure 46 correspond to the numbering on the right-hand side of the plots of the wake mesh.

The centerline pressure distributions for various times during the last cycle of the motion are presented in Figure 47. Again, the numerical references in the plot of pitch position correspond to the numbers near the pressure-distribution plots. The steady-state centerline pressure is compared with the analytical solution in the figure designated 1. The pressure determined by the present method shows favorable agreement with the analytical solution. The differences are due to the relative coarseness of the wing mesh and the wing not being truly two dimensional. As can be seen by examining the remaining pressure dis-

tributions, significant differences exist in the centerline loading for the same angular orientation, but different angular rates.

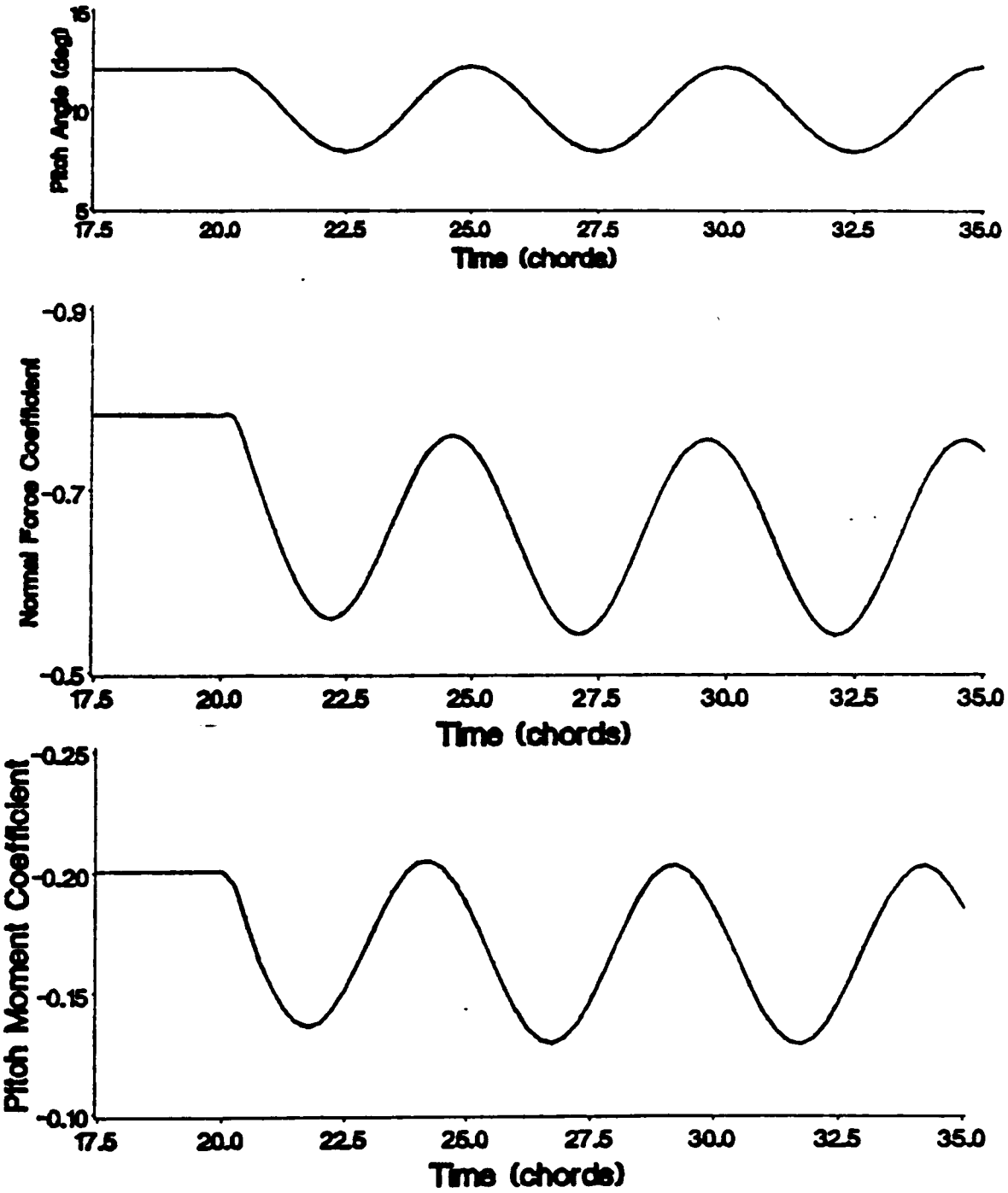

Figure 45. Aspect Ratio Five Rectangular Wing Pitching

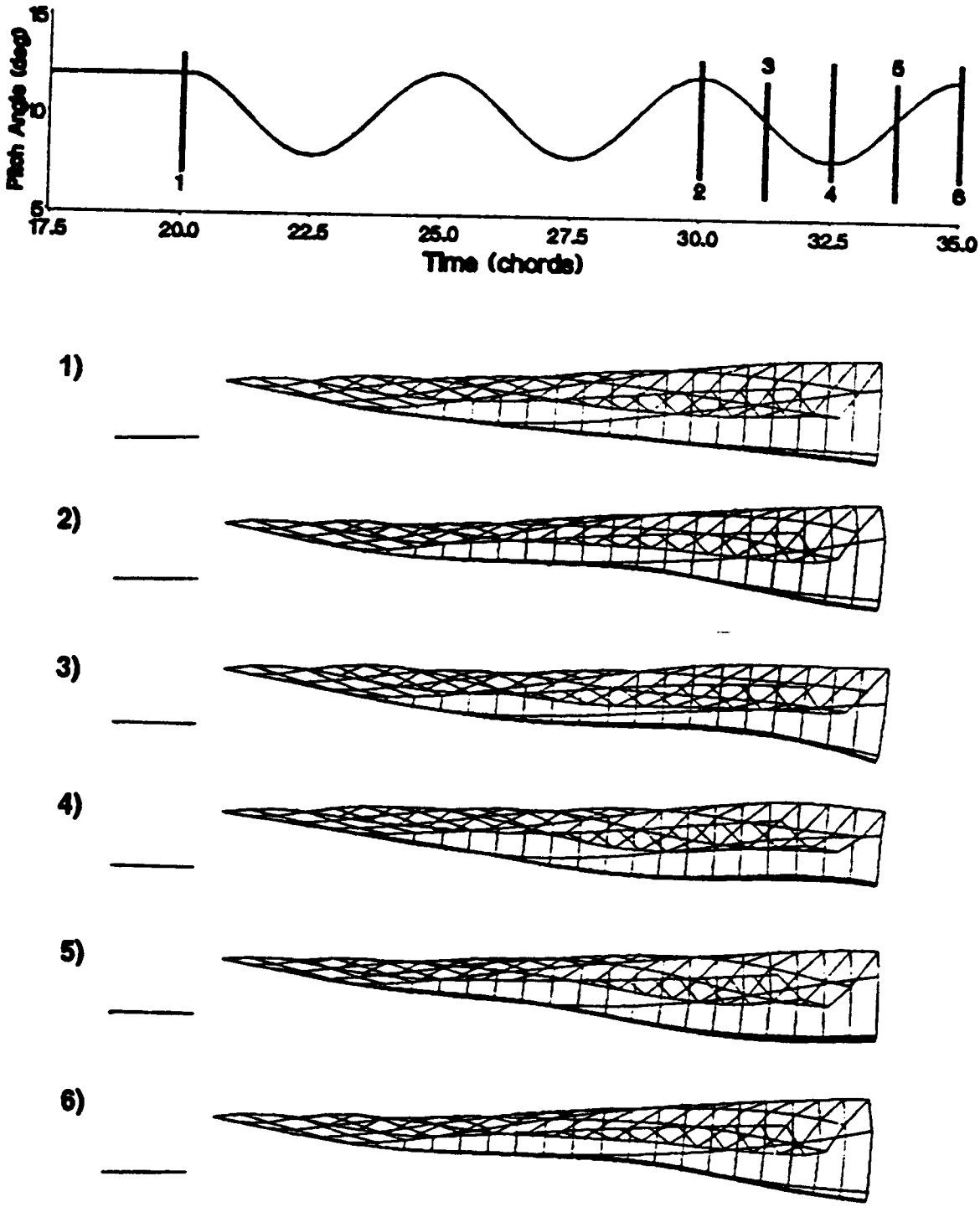

Figure 46. Wake Positions for Pitching Wing

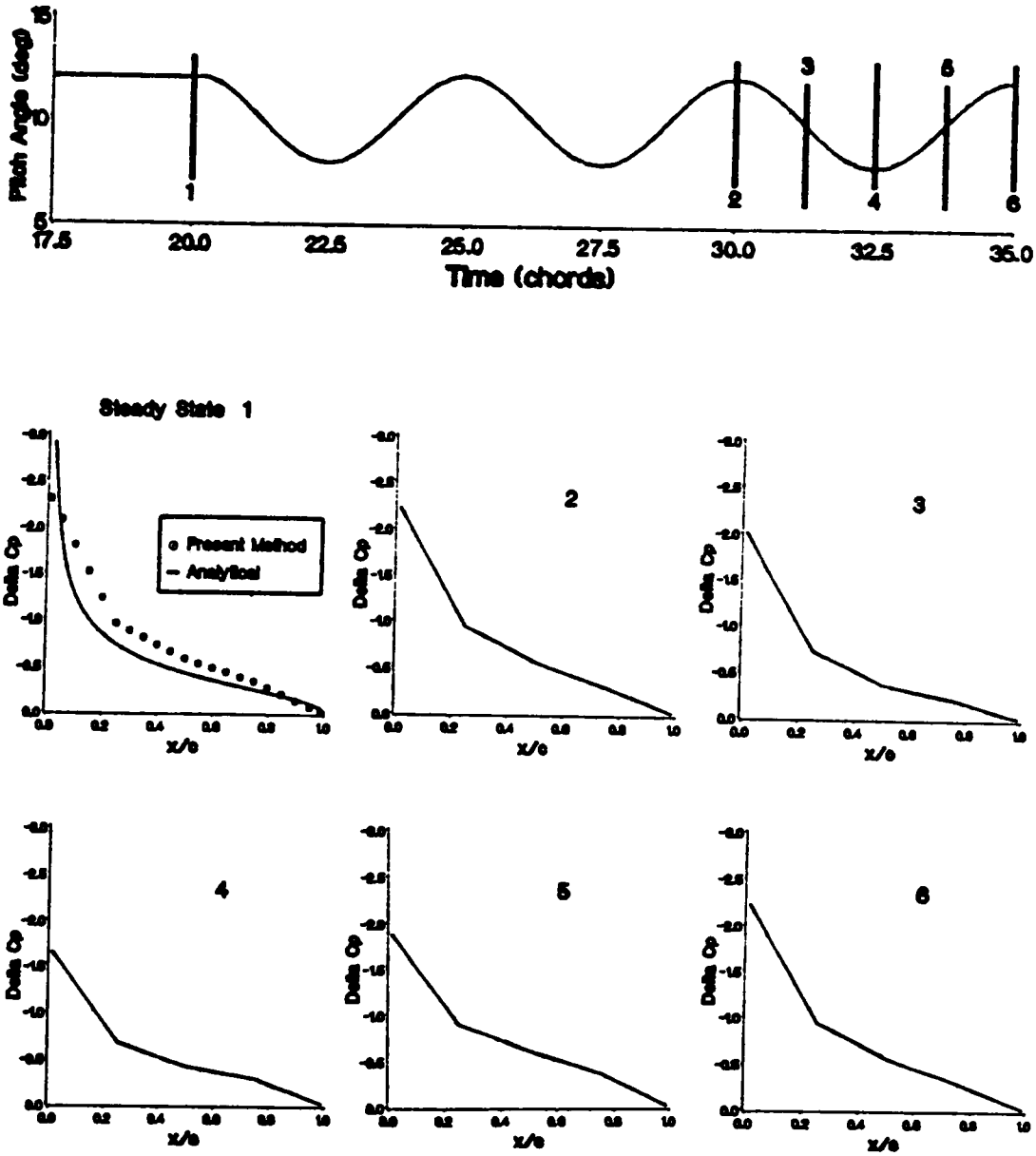

Figure 47. Centerline Pressure Distribution

The second set of pitching oscillation tests was performed to show the influence of the placement of the axis of rotation. For this test, a unit-aspect-ratio rectangular wing represented with 64 elements is oscillated using the same differential equation as for the first test. The axis of rotation is about three different chord positions: the leading edge, the midchord and the trailing edge. The pitching motion and the evolution of the normal-force coefficient are presented in Figure 48. Differences in the phase-angle between the motion and the force for the three axes exist, which can readily be explained by examining the motion. The angle of attack is initially 12 degrees for each. The rotation of the wing about the leading edge causes the trailing edge of the wing initially moves with the freestream; therefore, a lower apparent angle of attack is seen by the entire wing. This apparent angle of attack results in a significant loss of lift at the start of the motion. For rotation about the trailing edge, the initial effect is to raise the apparent angle of attack seen by the entire wing. Therefore, the loss of lift due to the overall pitching motion is delayed. The rotation about the midchord produces a higher apparent angle of attack on the front half of the wing but a lower angle of attack on the rear half. Thus, this curve should lie between the two extremes. These three situations are clearly visible in Figure 48.

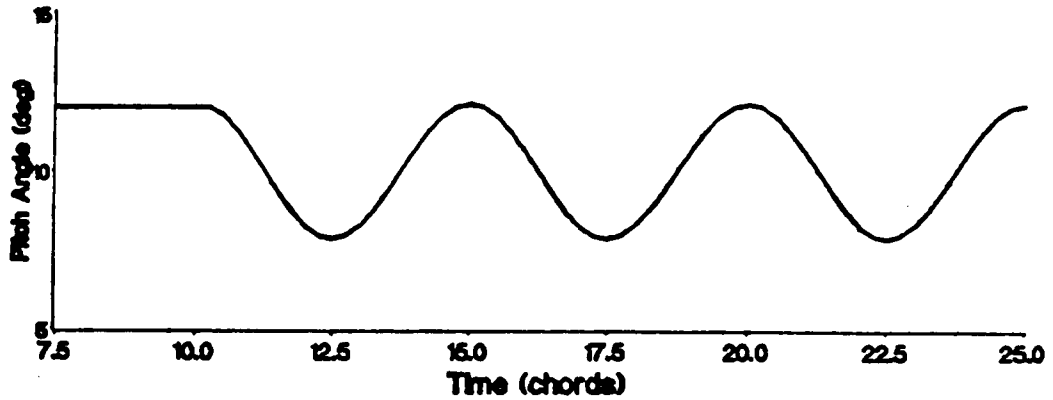

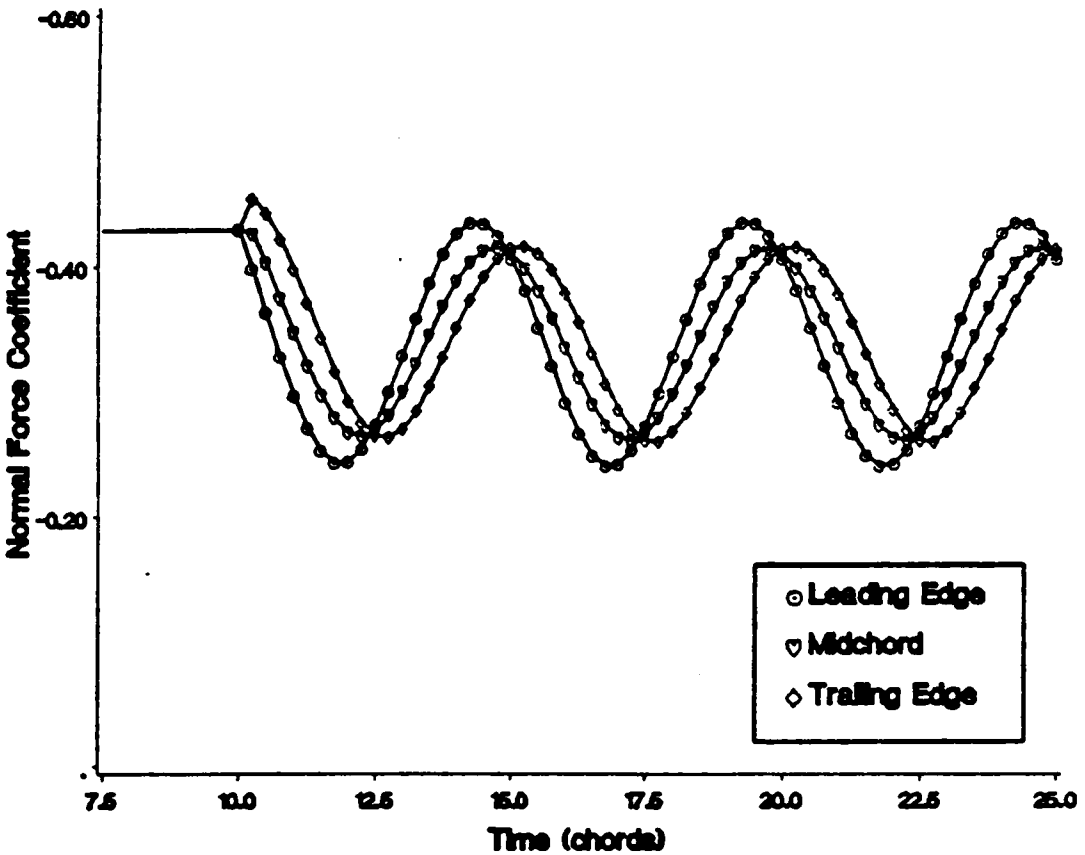

Figure 48. Normal Force as a Function of Time for Various Axes of Rotation

In order to analyze the results, the forces and moments were examined to determine their characteristics. The method of analysis is to calculate a least-square curve fit to the data to determine the average amplitude (A_{ave}), the relative amplitude (A) and phase shift (ϕ) from the motion. The assumed functional form for both the normal-force coefficient and pitch-moment coefficient is

$$x = A_{ave} + A\cos(\omega t + \phi) \qquad (3.4-2)$$

where A_{ave}, A and ϕ are determined by the least-square curve fit and ω is assumed to be the same as the pitching motion predicted by the predictor corrector algorithm. The period of the predicted motion was nearly the same as the period of the analytical solution. Thus, the assumption on ω is valid. The curve fit is compared to the normal-force coefficient during the last cycle of motion for pitching about the leading edge. These two curves are presented in Figure 49. The agreement is remarkable. Thus, simple harmonic pitching motion indeed results in a normal-force coefficient that is very nearly simple harmonic

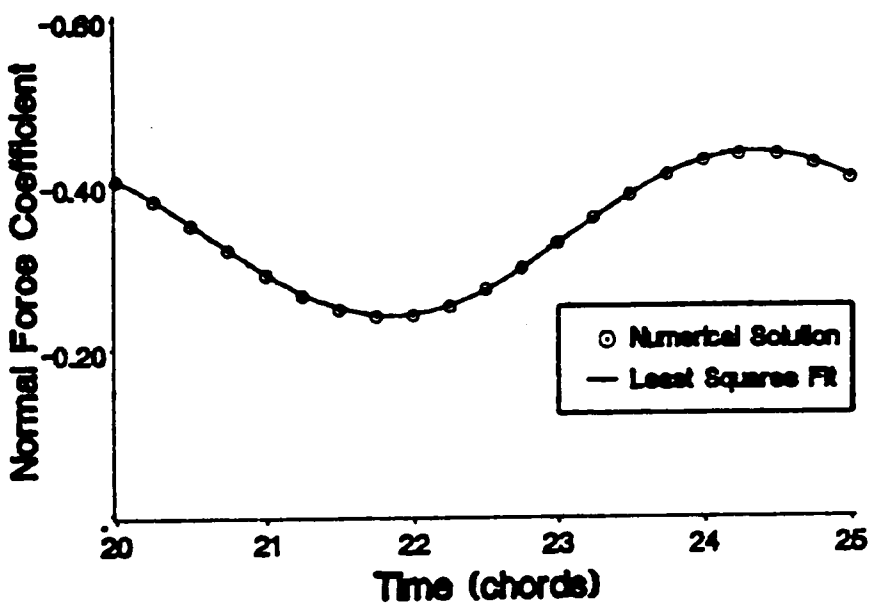

Figure 49. Least Square Curve Fit

The phase lead angles, relative amplitude and average amplitude are presented in Table 7 for the three axes of rotation of the unit-aspect-ratio wing and for the high-aspect-ratio wing of the first test. Table 7 was constructed by using the least-square curve fit described above applied to the last full cycle of the motion.

Table 7. Dependence of the Force on the Position of the Axis of Rotation

Normal Force Coefficient (C_{f_z})

Aspect Ratio	Axis of Rot.	ϕ	A	A_{ave}
1	0.0c	47.13	-0.0979	-0.3383
1	0.5c	21.62	-0.0772	-0.3381
1	1.0c	-10.90	-0.0782	-0.3385
5	0.5c	27.57	-0.1075	-0.6480

The pitching motion and the evolution of the pitching moment are presented in Figure 50. The pitch-moment coefficient is calculated about the leading edge of the wing. The phase lead angles, the relative amplitude and the average amplitude are presented in Table 8 for the three axes of rotation.

Table 8. Dependence of the Moment on the Position of the Axis of Rotation

Pitch Moment Coefficient (C_{m_y})

Aspect Ratio	Axis of Rot.	ϕ	A	A_{ave}
1	0.0c	66.46	-0.0329	-0.0871
1	0.5c	53.14	-0.0262	-0.0870
1	1.0c	32.88	-0.0217	-0.0869
5	0.5c	58.26	-0.0371	-0.1654

The results show virtually no difference in the average amplitude for both the force and moment. The relative amplitude of the force is smallest for pitching about the midchord, whereas the moment is smallest for pitching about the trailing edge. A substantial phase shift

for both the force and the moment for all three rotations exist. Also, for the three axes of rotation, the moment always leads the force.

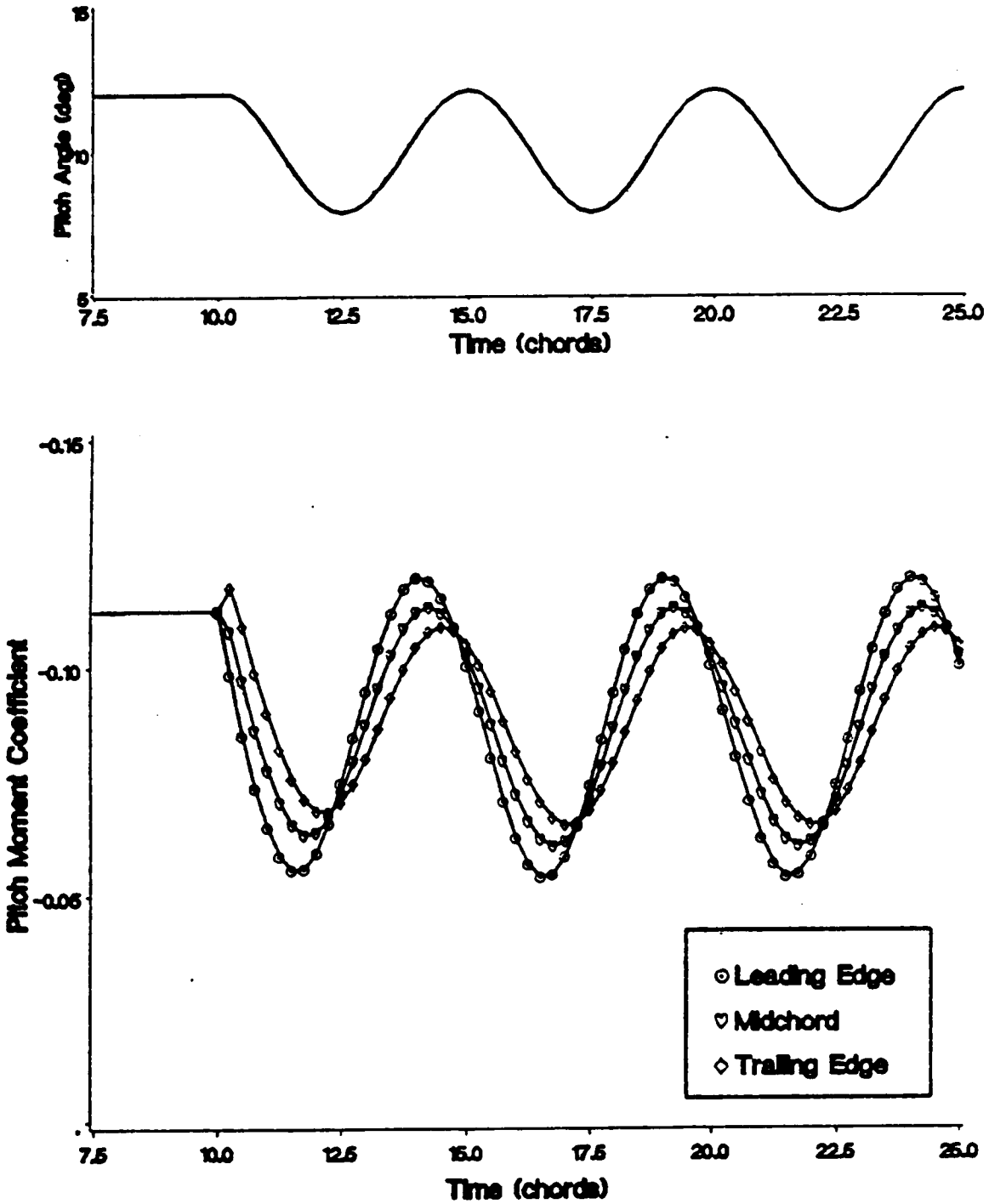

Figure 50. Pitch Moment as a Function of Time for Various Axes of Rotation

The pitching motion and contour plots of the pressure coefficient for the unit-aspect-ratio wing rotating about the midchord are shown in Figure 51 and Figure 52. The numerical references in the plot of the pitch position correspond to the numbers on top of the pressure contour plots. The pressure contour plots labeled two of Figure 51 is the same as the pressure contour plot labeled six of Figure 52. Thus, the cyclic motion produces cyclic pressure distributions.

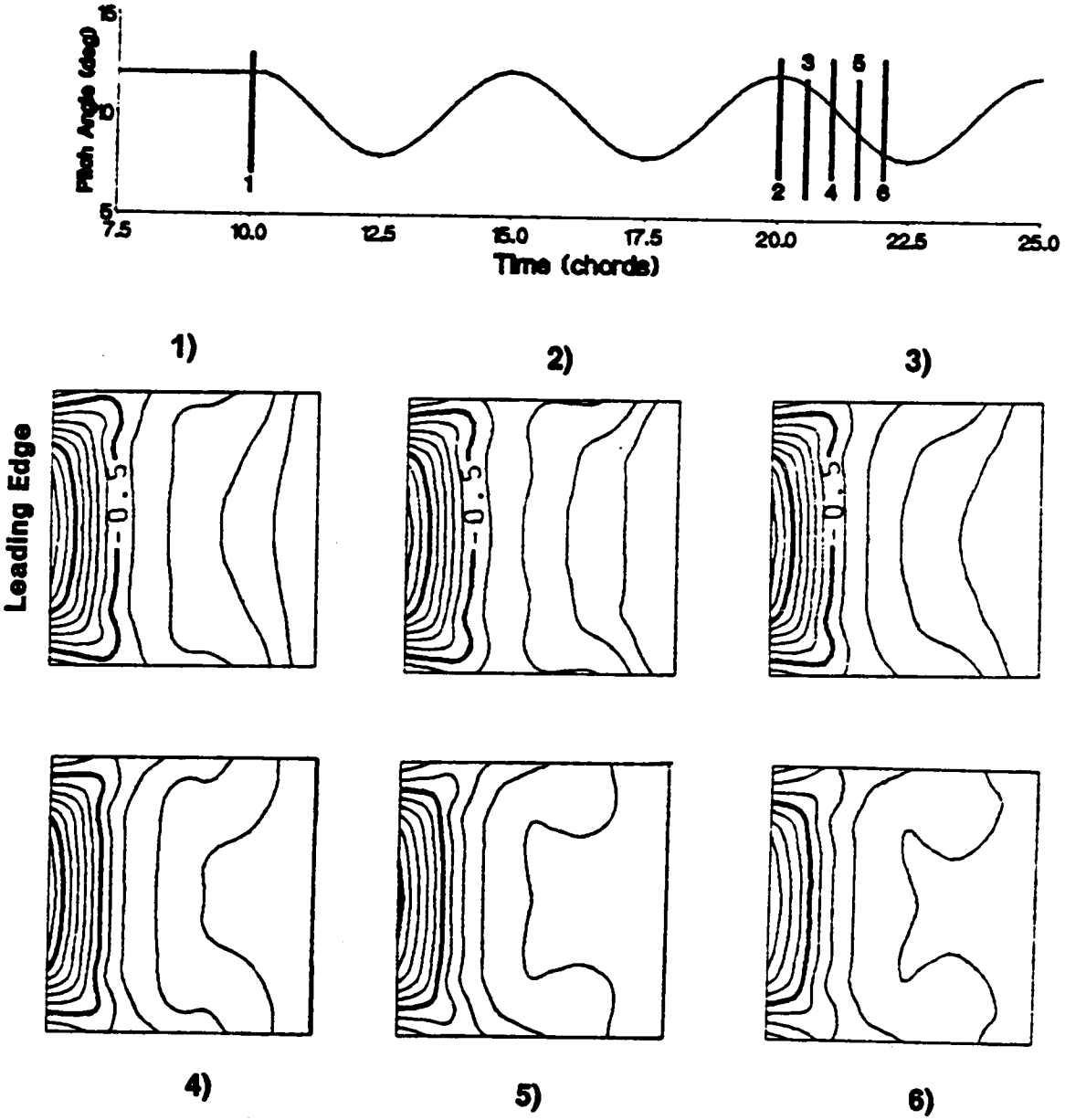

Figure 51. Pressure Contours for Oscillating Wing

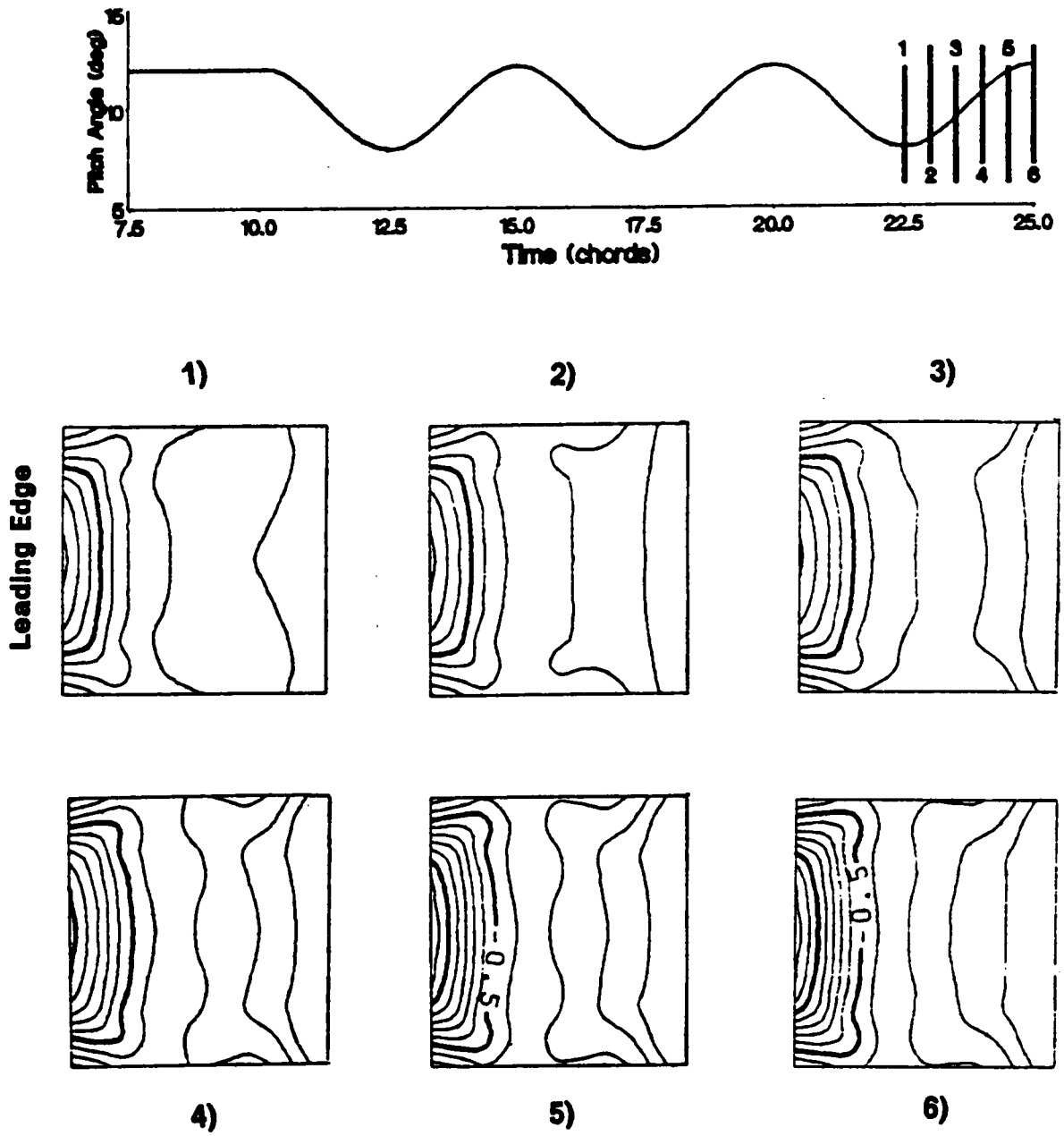

Figure 52. Pressure Contours for Oscillating Wing (cont.)

The last set of forced oscillation tests are for three delta wings. The results for pitch-moment coefficient are compared with the experimental results of Woodgate and Pugh [1963]. The three wings are of aspect ratio 0.654, 1.000, and 1.484. Woodgate and Pugh only present experimental data for wings of aspect ratio 0.654 and 1.484. The other wing is included for comparison. All three wings are approximated with 49 elements. The pitching motion for all tests is about the one quarter mean aerodynamic chord. The amplitude of the motion is one degree. The mean angle of attack is either 10 or 15 degrees. The reduced frequencies are either 0.50 or 1.01. The reduced frequency is defined by

$$\nu = \frac{\omega \bar{c}}{V_\infty} \qquad (3.4-3)$$

where ν is the reduced frequency, ω is the frequency, $\bar{c}$ is the mean aerodynamic chord and V_∞ is the reference velocity. The pitching motion and normal-force coefficient for all three wings are represented in Figure 53 for a pitching frequency of 1.01 at a mean angle of attack of 15 degrees. The comparable pitching-moment coefficient, calculated about the one quarter mean aerodynamic chord, is shown in Figure 54. The mean aerodynamic chord is defined as

$$\bar{c} = \frac{1}{S}\int_{-b/2}^{b/2} c^2(y)\, dy \qquad (3.4-4)$$

where $\bar{c}$ is the mean aerodynamic chord, S is the wing area, b is the wing span, and $c(y)$ is the chord length at a given span location. The results for a frequency of 0.50 at a mean angle of attack of 15 degrees for the normal-force coefficient and the pitch moment coefficient are shown in Figure 55 and Figure 56, respectively. One result of this test is that the method has difficulty predicting the loads for the larger-aspect-ratio wing.

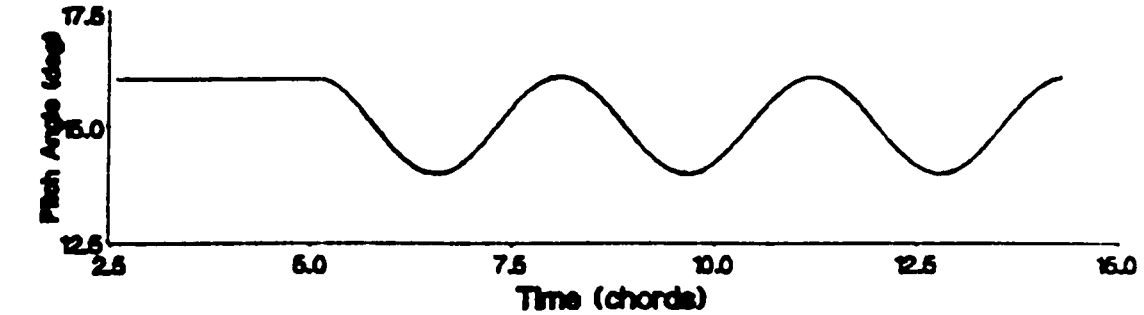

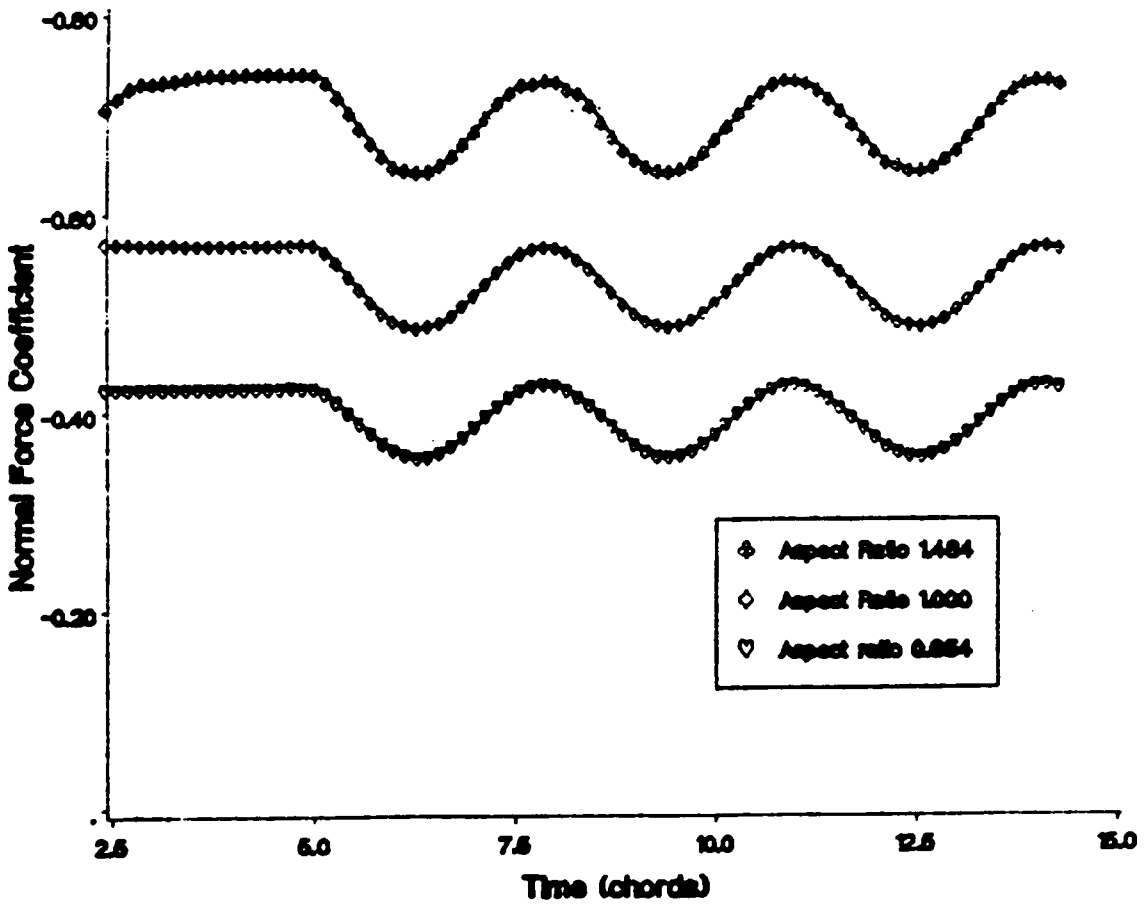

Figure 53. Normal Force as a Function of Time for a Reduced Frequency of 1.01

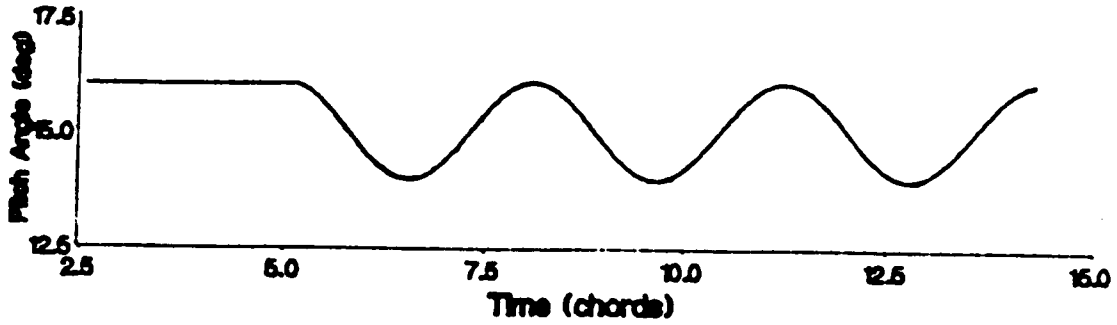

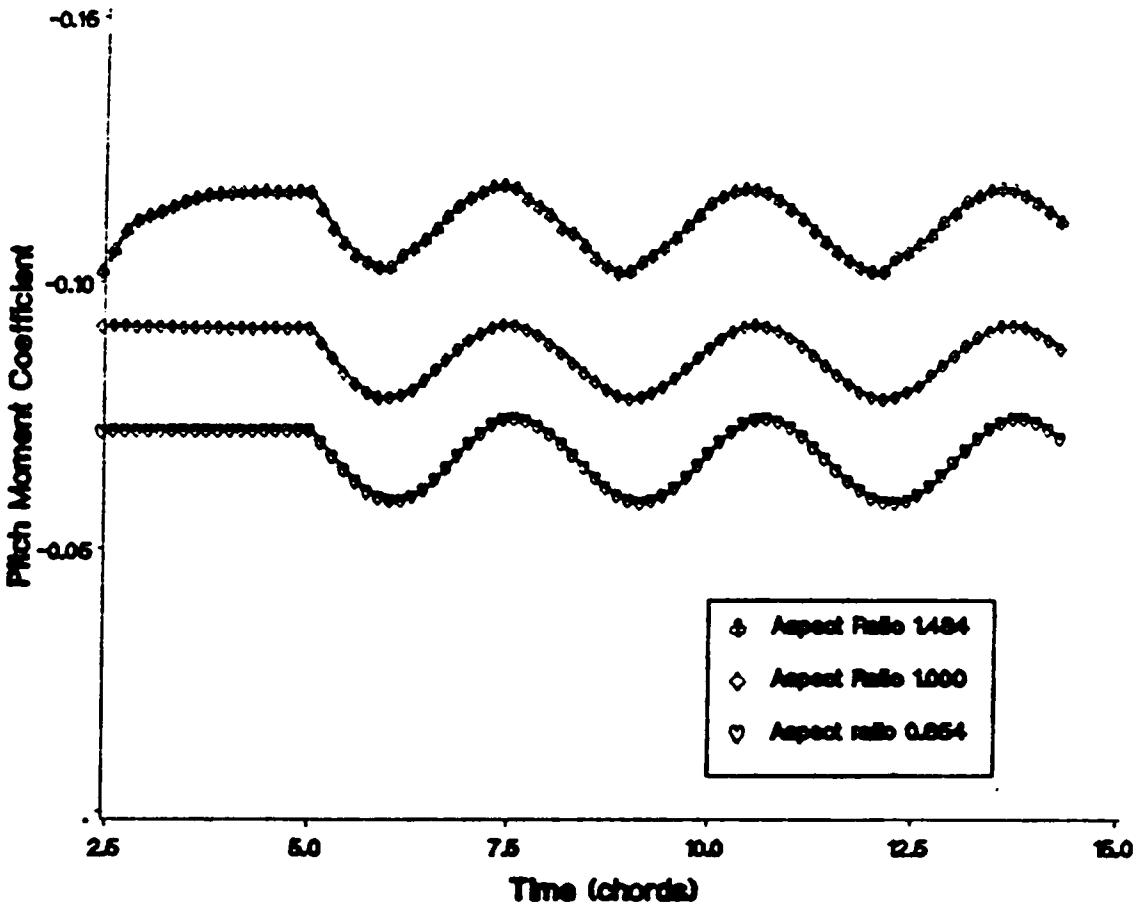

Figure 54. Pitch Moment as a Function of Time for a Reduced Frequency of 1.01

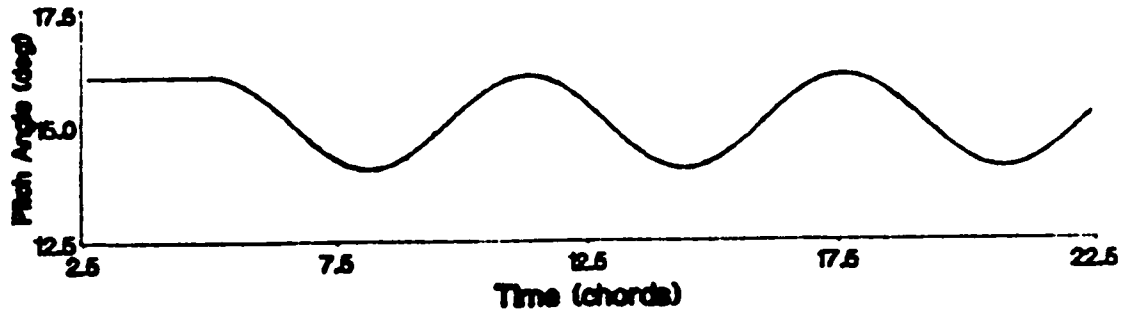

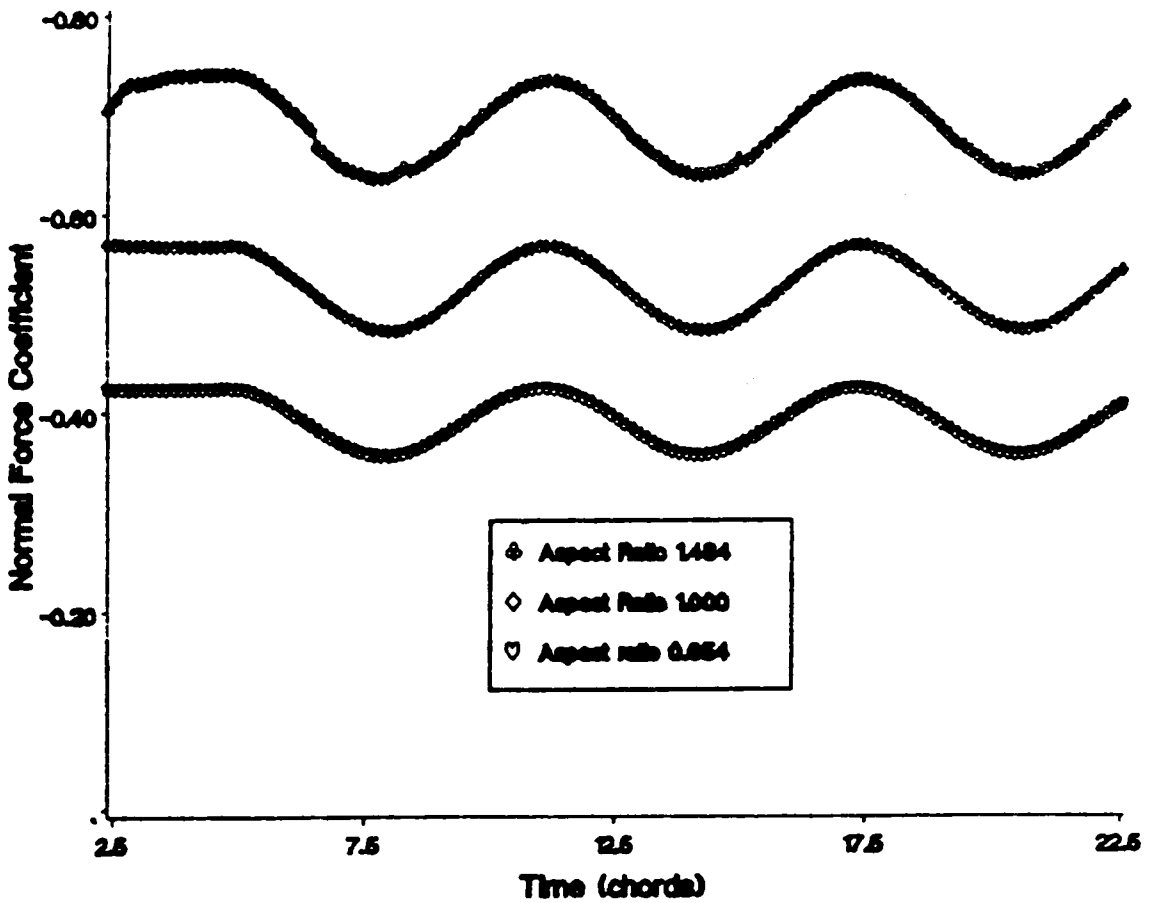

Figure 55. Normal Force as a Function of Time for a Reduced Frequency of 0.50

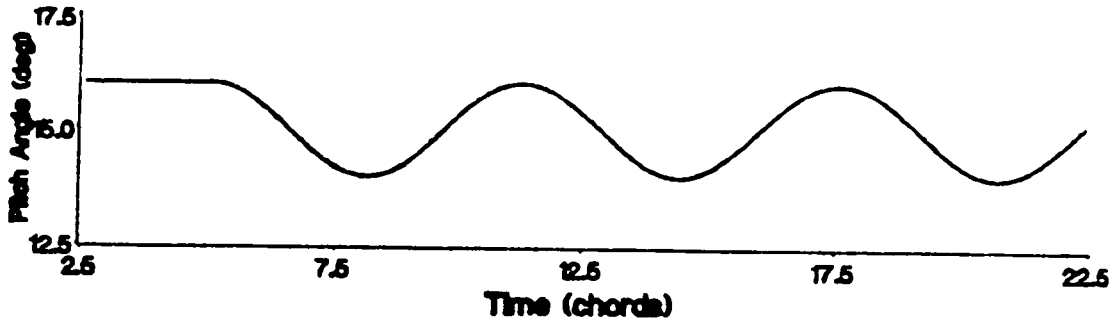

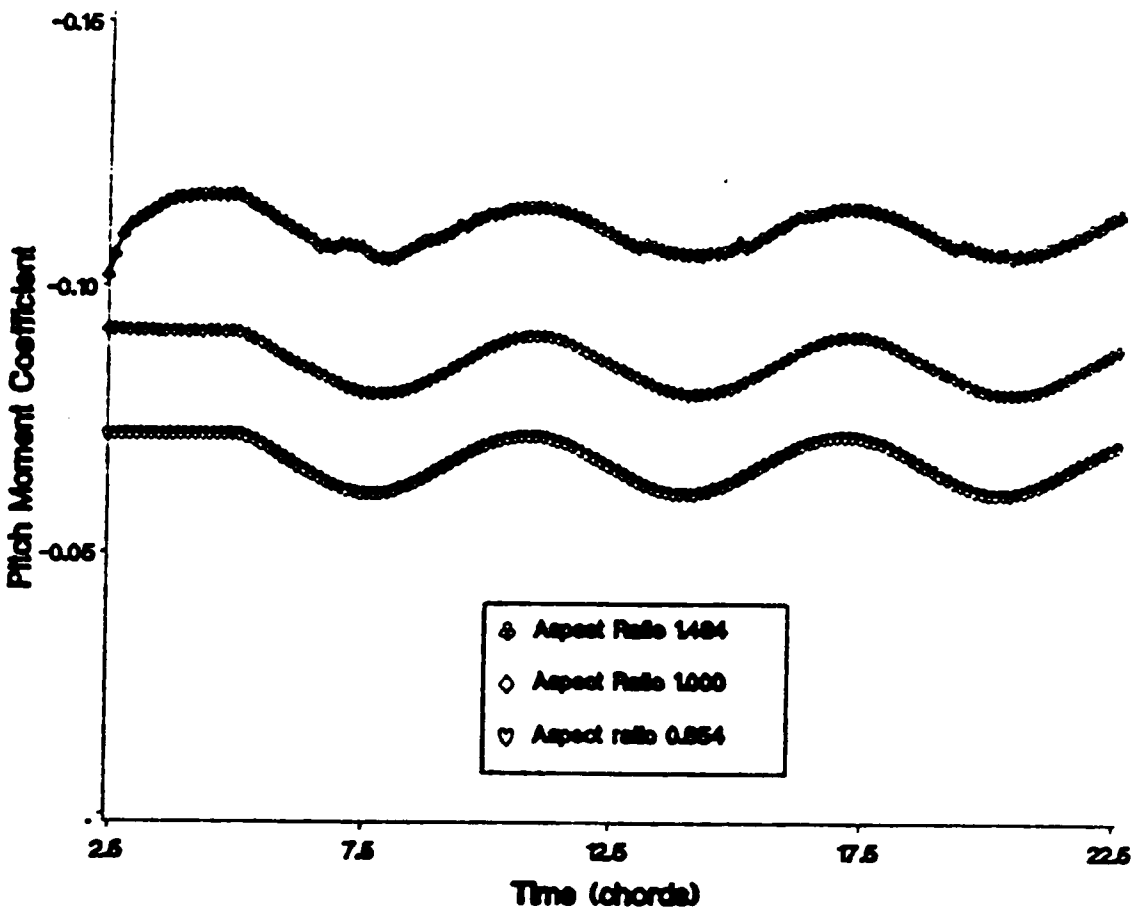

Figure 56. Pitch Moment as a Function of Time for a Reduced Frequency of 0.50

The computed normal-force coefficients for the three wings were approximated by fitting the force during the last cycle of motion with the function of Equation 3.4-2. The results of this analysis are presented in Table 9.

Table 9. Dependence of the Normal Force on Aspect Ratio and Frequency

Normal-Force Coefficient (C_{f_z})

Pitch Angle	Aspect Ratio	Freq. ν	ϕ	A	A_{ave}
10	0.654	0.50	23.696	-0.0253	-0.2417
10	0.654	1.01	42.970	-0.0339	-0.2420
10	1.000	0.50	13.681	-0.0347	-0.3344
10	1.000	1.01	35.091	-0.0357	-0.3346
10	1.484	0.50	6.141	-0.0470	-0.4106
10	1.484	1.01	24.262	-0.0401	-0.4112
15	0.654	0.50	12.051	-0.0337	-0.3905
15	0.654	1.01	28.536	-0.0367	-0.3907
15	1.000	0.50	7.725	-0.0421	-0.5248
15	1.000	1.01	27.591	-0.0404	-0.5251
15	1.484	0.50	7.552	-0.0470	-0.6857
15	1.484	1.01	32.282	-0.0462	-0.6858

The results of these tests show little effect caused by changing the aspect ratio. The results also show a significant change in the phase angle due to change in both frequency and aspect ratio.

The pitch-moment coefficient for the three wings are analyzed in the same manner as the normal force coefficient. The results of this analysis are presented in Table 10, along with the results of the experiment conducted by Woodgate and Pugh [1963]. Woodgate and Pugh oscillated in pitch two thin delta wings of aspect ratio 1.484 and 0.654 about two chord positions, 1.0 $\bar{c}$ and 1.5 $\bar{c}$. The pitch oscillations were at reduced frequencies ranging from 0.25 to 1.01. They measured the pitch moment with a sting balance. No correction was made to remove the moment required to produce the pitch motion.

Table 10. Moment Dependence on Aspect Ratio and Frequency

Pitch Moment Coefficient (C_{m_y})

			Present Method		Woodgate and Pugh	
Pitch Angle	Aspect Ratio	Freq. ν	A	ϕ	A	ϕ
10	0.654	0.50	-0.0054	38.568	-0.0054	50.18
10	0.654	1.01	-0.0087	63.199	-0.0102	66.72
10	1.000	0.50	-0.0058	20.876	—	—
10	1.000	1.01	-0.0067	67.454	—	—
10	1.484	0.50	-0.0080	0.475	-0.0058	55.93
10	1.484	1.01	-0.0033	49.904	-0.0109	69.52
15	0.654	0.50	-0.0055	27.303	-0.0068	50.94
15	0.654	1.01	-0.0080	62.189	-0.0108	69.91
15	1.000	0.50	-0.0054	17.581	—	—
15	1.000	1.01	-0.0069	73.504	—	—
15	1.484	0.50	-0.0045	22.641	-0.0052	49.93
15	1.484	1.01	-0.0076	87.682	-0.0104	78.24

The comparison shows the present method predicts a larger influence of the frequency on the phase shift than shown in the experiments. This difference may be caused by the experimental results including the inertial acceleration required to move the model.

3.5 Free Dynamic Equations

The forced oscillation tests have been completed. The next step in the development is to simulate the response of the wing to the forces and moments experienced during the free oscillation test. Before this step can be completed, the equations of motion have to be developed.

The assumptions are that the body is rigid and rotates about point c as shown in Figure 57.

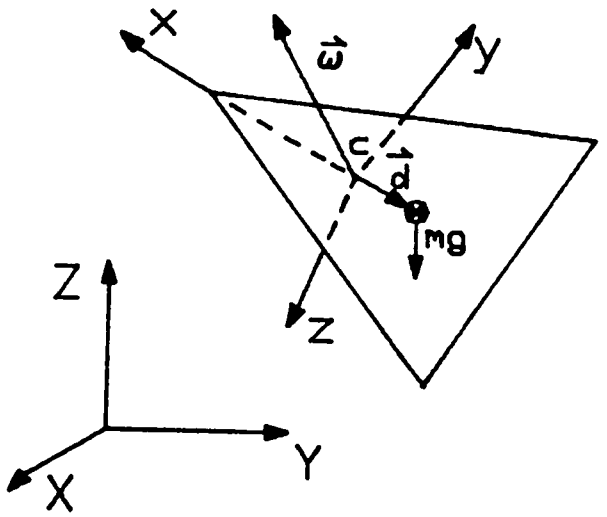

Figure 57. Coordinate Frames of Rotating Body

For such a body, the general vector set of governing equations are of the form

$$\vec{M}_c = [I_c]\dot{\vec{\omega}} + \vec{\omega} \times ([I_c] \cdot \vec{\omega}) \qquad (3.5-1)$$

where $\vec{M}_c$ is the external moment vector about point c, ω is the angular velocity vector, and $[I_c]$ is the inertia matrix about point c. For the special choice of principle axes

$$[I_c] = \begin{bmatrix} I_{xx} & 0 & 0 \\ 0 & I_{yy} & 0 \\ 0 & 0 & I_{zz} \end{bmatrix}. \qquad (3.5-2)$$

Then the individual differential equations of motion are

$$M_x = I_{xx}\dot{\omega}_x + (I_{zz} - I_{yy})\omega_z\omega_y \qquad (3.5-3)$$

$$M_y = I_{yy}\dot{\omega}_y + (I_{xx} - I_{zz})\omega_x\omega_z \qquad (3.5-4)$$

and

$$M_z = I_{zz}\dot{\omega}_z + (I_{yy} - I_{xx})\omega_y\omega_x. \qquad (3.5-5)$$

The kinematic relations are

$$\omega_x = \dot{\phi} - \dot{\psi}\sin\theta \qquad (3.5-6)$$

$$\omega_y = \dot{\theta}\cos\phi + \dot{\psi}\cos\theta\sin\phi \qquad (3.5-7)$$

and

$$\omega_z = -\dot{\theta}\sin\phi + \dot{\psi}\cos\theta\cos\phi. \qquad (3.5-8)$$

Differentiating the kinematic relations with respect to time results in

$$\dot{\omega}_x = \ddot{\phi} - \ddot{\psi}\sin\theta - \dot{\psi}\dot{\theta}\cos\theta \qquad (3.5-9)$$

$$\begin{aligned}\dot{\omega}_y = {} & \ddot{\theta}\cos\phi - \dot{\theta}\dot{\phi}\sin\phi + \ddot{\psi}\cos\theta\sin\phi \\ & - \dot{\psi}\dot{\theta}\sin\theta\sin\phi + \dot{\psi}\dot{\phi}\cos\theta\cos\phi\end{aligned} \qquad (3.5-10)$$

and

$$\begin{aligned}\dot{\omega}_z = {} & -\ddot{\theta}\sin\phi - \dot{\theta}\dot{\phi}\cos\phi + \ddot{\psi}\cos\theta\cos\phi \\ & - \dot{\psi}\dot{\theta}\sin\theta\cos\phi + \dot{\psi}\dot{\phi}\cos\theta\sin\phi\end{aligned} \qquad (3.5-11)$$

Equations 3.5-3 through 3.5-11 represent the second-order differential equations that predict the motion of the body responding to external moments.

The external moments about point c can be written as

$$\vec{M} = \vec{M}_A + \vec{M}_D + \vec{M}_G \qquad (3.5-12)$$

where $\vec{M}_A$ is the aerodynamic moment, $\vec{M}_D$ is the damping moment caused by any friction in the ball joint used to support the model and $\vec{M}_G$ is the moment caused by the center of gravity not being at the point of rotation. The aerodynamic moment in general is

$$\vec{M}_A = M_{A_x}\vec{i} + M_{A_y}\vec{j} + M_{A_z}\vec{k} \qquad (3.5-13)$$

where

$$M_{A_x} = \frac{1}{2}\rho U^2 SbC_{m_x}$$

$$M_{A_y} = \frac{1}{2}\rho U^2 S\bar{c}C_{m_y} \qquad (3.5-14)$$

and

$$M_{A_z} = \frac{1}{2}\rho U^2 SbC_{m_z}.$$

The aerodynamic moment coefficients are calculated by the method described in Chapter II.

The damping moment is

$$\vec{M}_D = M_{D_x}\vec{i} + M_{D_y}\vec{j} + M_{D_z}\vec{k} \qquad (3.5-15)$$

where

$$M_{D_x} = -\mu_x\omega_x = -\mu_x(\dot{\phi} - \dot{\psi}\sin\theta)$$

$$M_{D_y} = -\mu_y\omega_y = -\mu_y(\dot{\theta}\cos\phi + \dot{\psi}\cos\theta\sin\phi) \qquad (3.5-16)$$

$$M_{D_z} = -\mu_z\omega_z = -\mu_z(-\dot{\theta}\sin\phi + \dot{\psi}\cos\theta\cos\phi)$$

and μ is the damping coefficient.

The moment due to gravity is

$$\vec{M}_G = mg(\vec{d} \times \vec{K})$$

where m is the mass, g is the acceleration due to gravity, $\vec{d}$ is the distance from point c to the center of gravity, and $\vec{K}$ is the unit vector in the inertial Z direction. The inertial Z direction written in the body frame is

$$\vec{K} = -\sin\theta\,\vec{i} + \cos\theta\sin\phi\,\vec{j} + \cos\theta\cos\phi\,\vec{k}.$$

The distance to the center of gravity is, in general,

$$\vec{d} = d_x\vec{i} + d_y\vec{j} + d_z\vec{k}.$$

Therefore, the moment due to gravity is

$$\begin{aligned}\vec{M}_G = {} & mg(d_y\cos\theta\cos\phi - d_z\cos\theta\sin\phi)\vec{i} \\ & + mg(-d_z\sin\theta + d_x\cos\theta\sin\phi)\vec{j} \\ & + mg(-d_y\sin\theta + d_x\cos\theta\cos\phi)\vec{k}.\end{aligned} \qquad (3.5-17)$$

Next the equations of motion are nondimensionalized. The dimensionless time is

$$t^* = \frac{U}{L}t$$

where t is time in seconds, U is a reference velocity and L is a reference length. Equations 3.5-12 to 3.5-19 are then substituted into equations 3.5-3 to 3.5-5. This substitution and the change to dimensionless variables result in the equations

$$\begin{bmatrix} 1 & 0 & -\sin\theta \\ 0 & \cos\phi & \cos\theta\sin\phi \\ 0 & -\sin\phi & \cos\theta\cos\phi \end{bmatrix} \begin{Bmatrix} \ddot{\phi} \\ \ddot{\theta} \\ \ddot{\psi} \end{Bmatrix} = \begin{Bmatrix} R_x \\ R_y \\ R_z \end{Bmatrix} \qquad (3.5-18)$$

where

$$R_x = \frac{M_x}{I_{xx}} \frac{L^2}{U^2} - \frac{(I_{zz} - I_{yy})}{I_{xx}} \omega_z \omega_y + \dot{\psi}\dot{\theta} \cos\theta, \qquad (3.5-19)$$

$$R_y = \frac{M_y}{I_{yy}} \frac{L^2}{U^2} - \frac{(I_{xx} - I_{zz})}{I_{yy}} \omega_x \omega_z + \dot{\theta}\dot{\phi} \sin\phi + \dot{\psi}\dot{\theta} \sin\theta \sin\phi - \dot{\psi}\dot{\phi} \cos\theta \cos\phi$$

and

$$R_z = \frac{M_z}{I_{zz}} \frac{L^2}{U^2} - \frac{(I_{yy} - I_{xx})}{I_{zz}} \omega_y \omega_x + \dot{\theta}\dot{\phi} \cos\phi + \dot{\psi}\dot{\theta} \sin\theta \cos\phi + \dot{\psi}\dot{\phi} \cos\theta \sin\phi$$

Equation 3.5-18 can be used to solve for the second derivative of the Euler angles, as long as $\theta \neq \pm 90°$. The final equation is

$$\begin{Bmatrix} \ddot{\phi} \\ \ddot{\theta} \\ \ddot{\psi} \end{Bmatrix} = \begin{bmatrix} 1 & \tan\theta \sin\phi & \tan\theta \cos\phi \\ 0 & \cos\phi & -\sin\phi \\ 0 & \sec\theta \sin\phi & \sec\theta \cos\phi \end{bmatrix} \begin{Bmatrix} R_x \\ R_y \\ R_z \end{Bmatrix} \qquad (3.5-20)$$

The dimensionless differential equations, Equations 3.5-19 and 3.5-20, can now be written in the form needed by the predictor-corrector technique by simply converting the second order equations into two first order equations.

3.6 One-Dimensional Wing Rock

The equations of motion have been determined in Section 3.5. These equations can now be used in conjunction with the predictor-corrector method and the aerodynamic model, as presented in Section 3.4, to simulate a body in a wind tunnel that is free to rotate on a ball and socket. This complete coupling of the dynamic and aerodynamic models will be used to investigate one-dimensional wing rock of a slender delta wing. This simulation will be compared with the experimental results of Levin and Katz [1982]. Their experiment considered a thin delta wing of aspect ratio 0.707 free to roll about the mid-span.

The test equipment employed by Levin and Katz allowed the wing to roll only. Because the body is only free to roll, the equations of Section 3.5 can be significantly reduced. For one-dimensional roll motion the dimensionless equations reduce to

$$\ddot{\phi} = \frac{M_x}{I_{xx}} \frac{L^2}{U^2} \qquad (3.6-1)$$

and

$$\ddot{\theta} = \ddot{\psi} = 0$$

where

$$M_x = \frac{1}{2} \rho U^2 S b C_{m_x} - \mu_x \frac{U}{L} \dot{\phi}. \qquad (3.6-2)$$

Wing rock will be simulated at two flight conditions. In order to compare the results with the experiment, the actual physical properties for the model must be used. The conditions used in the simulation are shown in Table 11. The damping coefficient μ_x and the Moment of Inertia I_{xx} of Table 11 are assumed values since the physical values are not presented by Levin and Katz.

Table 11. Quantities Used in the Simulation of Wing Rock

Quantity	Magnitude	Units
ρ	1.2000	kg/m^3
U	15.000	m/s
S	0.0321	m^2
b	0.1500	m
μ_x	0.5×10^{-4}	
I_{xx}	1.3×10^{-4}	kg-m^2

The numerical experiment is carried out for a delta wing discretized with 25 elements or five rows of elements, which makes the reference length 0.0857 m. For this simulation the dimensionless equations are

$$\ddot{\phi} = 0.163C_{m_x} - 0.0022\dot{\phi} \qquad (3.6-3)$$

and

$$\ddot{\theta} = \ddot{\psi} = 0. \qquad (3.6-4)$$

Wing rock is investigated by holding the wing at an initial unsymmetric orientation until a steady state is reached. The wing is then released and allowed to roll freely about the mid span. The first set of initial conditions are

$$\phi(0) = 5^\circ \text{ and } \dot{\phi}(0) = 0. \qquad (3.6-5)$$

The pitch angle is 22.5 degrees. The results of this test are presented in Figure 58 through Figure 61. In Figure 58, the evolution of the roll position as a function of time after the wing is released is presented. In Figure 59 the evolution of the roll-moment coefficient as a function of time after the wing is released is presented. In Figure 60 and Figure 61 the evolution of the normal-force coefficient and the pitch-moment coefficient, respectively, as functions of time are shown. Clearly, wing rock has not developed for this set of initial conditions.

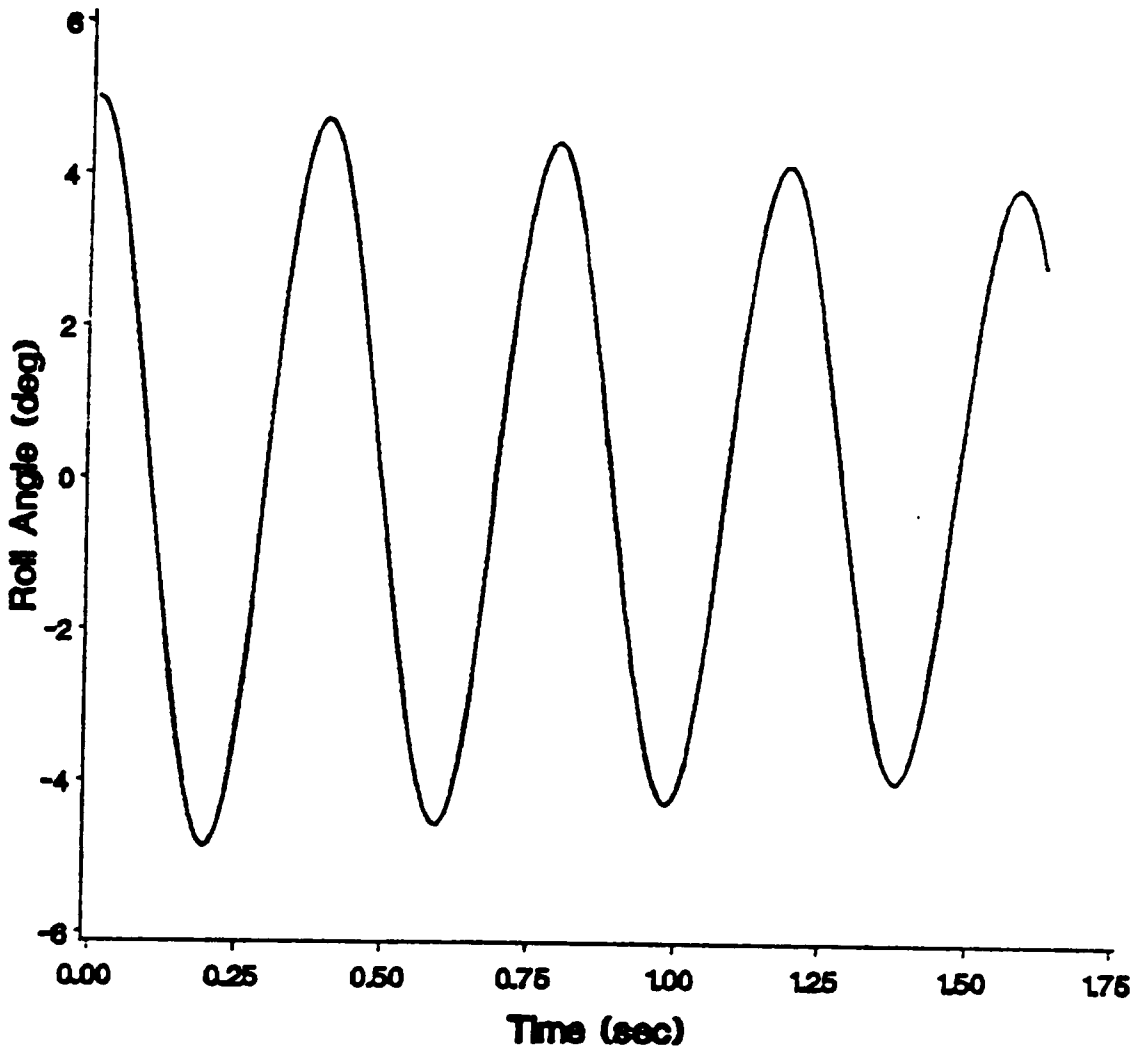

Figure 58. Roll Response for a Pitch Angle of 22.5 Degrees

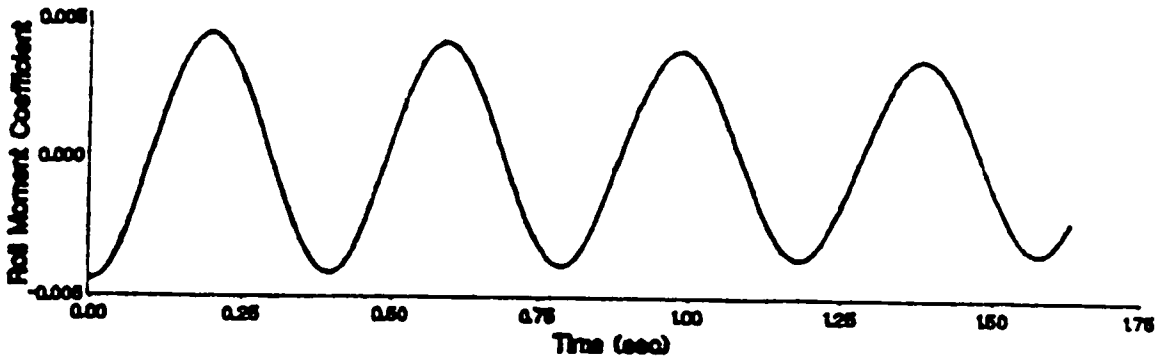

Figure 59. Roll Moment Evolution for a Pitch Angle of 22.5 Degrees

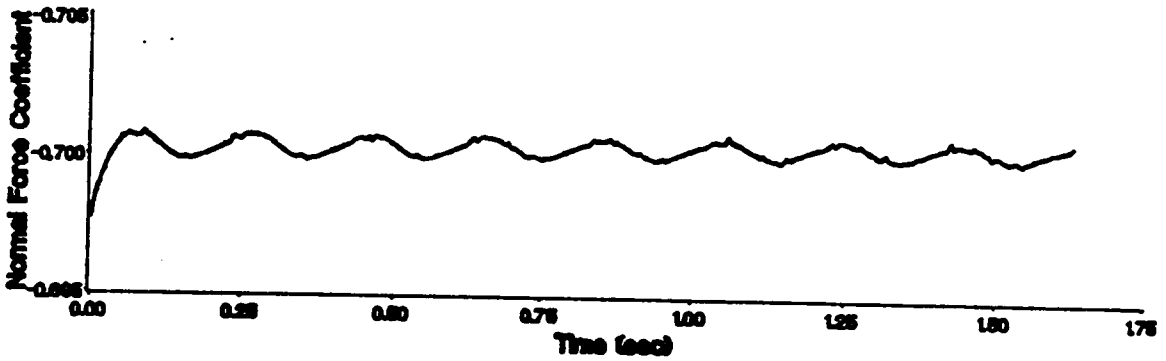

Figure 60. Normal Force Evolution for a Pitch Angle of 22.5 Degrees

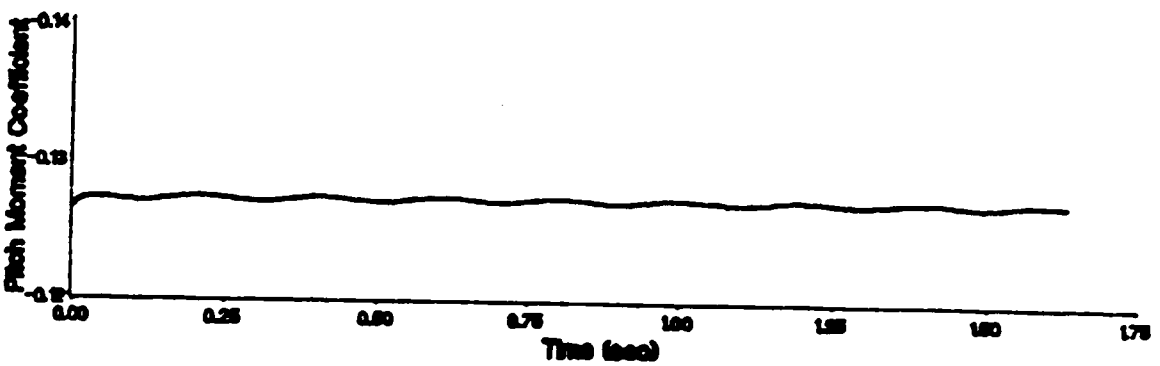

Figure 61. Pitch Moment Evolution for a Pitch Angle of 22.5 Degrees

The second set of initial conditions are also

$$\phi(0) = 5° \text{ and } \dot{\phi}(0) = 0. \qquad (3.6-6)$$

The pitch angle is 27.5 degrees The results of this test are presented in Figure 62 through Figure 67. Figure 62 presents the evolution of the roll position as a function of time. In Figure 63 the evolution of the roll-moment coefficient as a function of tim is shown. In Figure 64 the phase portrait of the motion is presented. In Figure 65 and Figure 66 the evolution of the normal-force coefficient and pitch-moment coefficient, respectively, as functions of time are presented. In Figure 67 the hysteresis of the roll-moment during the last cycle of the motion is shown. This set of initial conditions leads to the development of wing rock. The limit cycle amplitude is 29.6 and the period is 0.30 seconds. Levin and Katz determined experimentally the amplitude to be 30 degrees and the period was 0.33. They state, as the overall results of the experiments, that wing rock only occurred spontaneously for angles of attack greater than 25 degrees. Between 19 and 25 degrees, the wing rock motion could be maintained by developing a limit cycle behavior at a higher angle of attack and then lowering the pitch angle. The result of no spontaneous wing rock below 25 degrees for an aspect ratio 0.7 flat delta wing agrees with the results of Nguyen, Yip and Chambers [1981] . Clearly the results of the dynamic simulation presented in this section agree quantitatively with the available experimental data. These results may not be in complete agreement with the experiments because of the damping factor employed, the discrepancy in the predicted period and the slow growth rate. The reason the damping factor was to closer approximate the experimental results, without the damping the limit cycle amplitude was approximately 37 degrees.

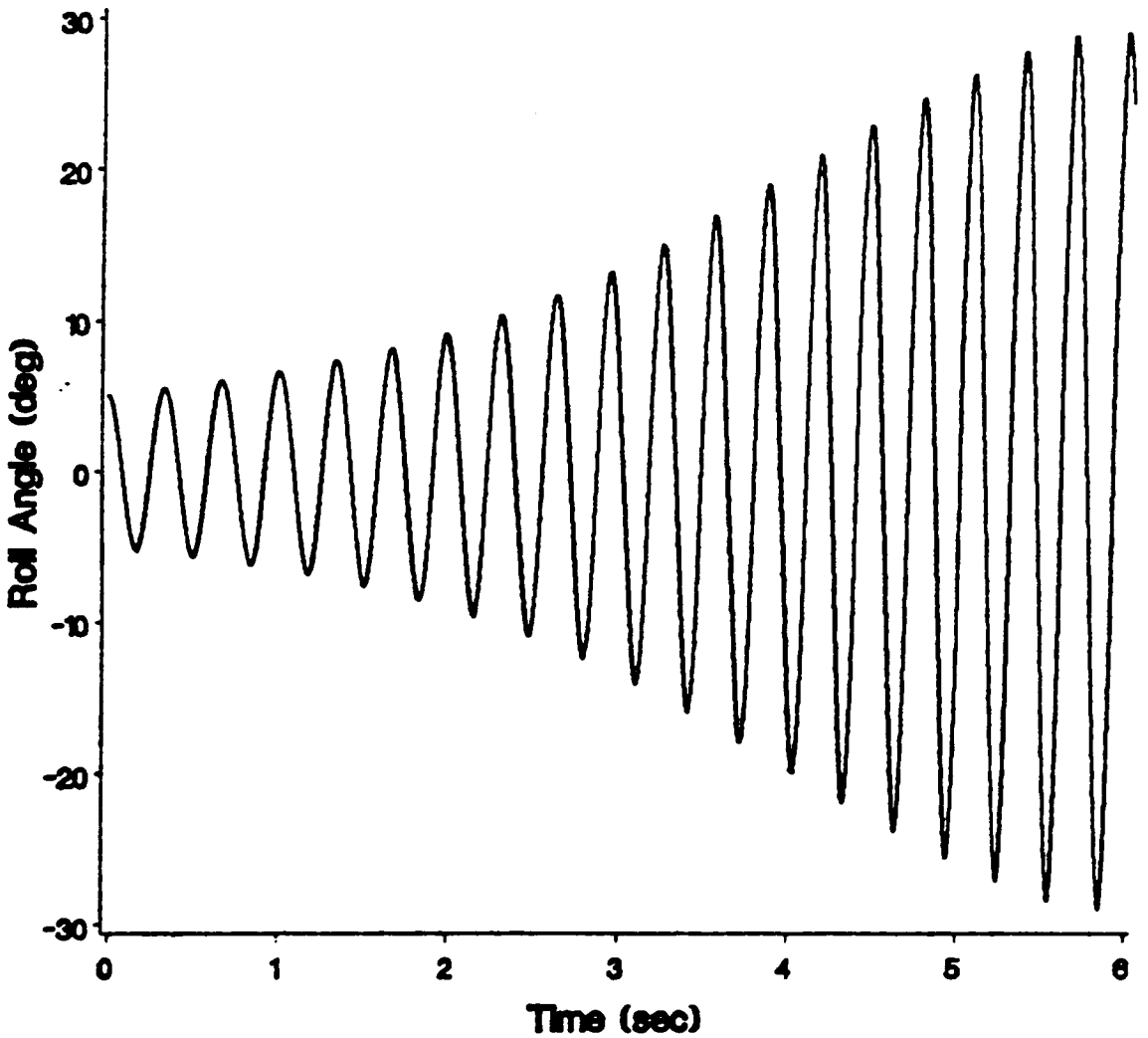

Figure 62. Roll Response for a Pitch Angle of 27.5 Degrees

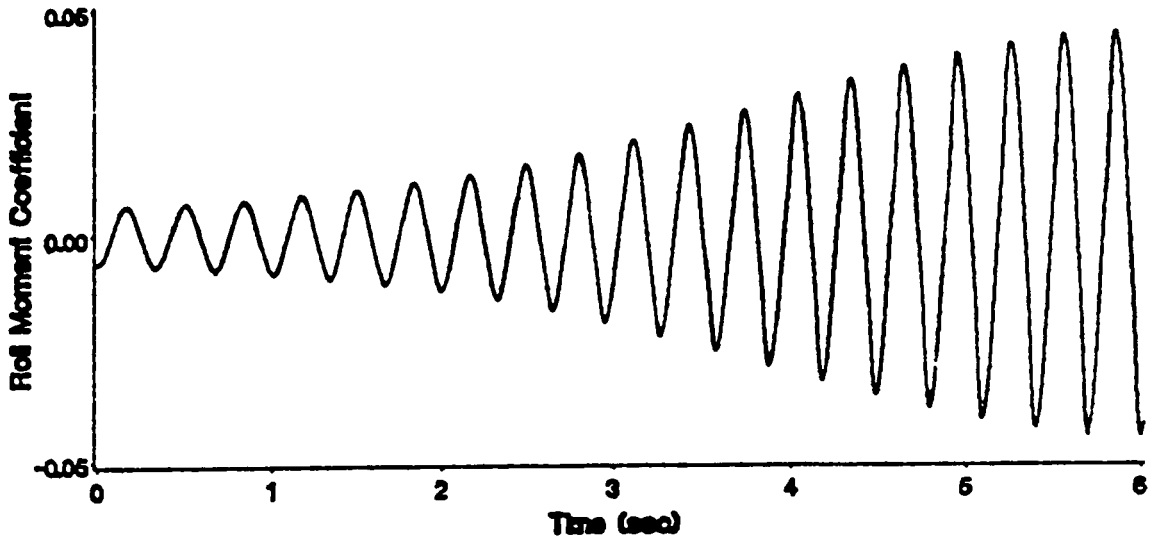

Figure 63. Roll Moment Evolution for a Pitch Angle of 27.5 Degrees

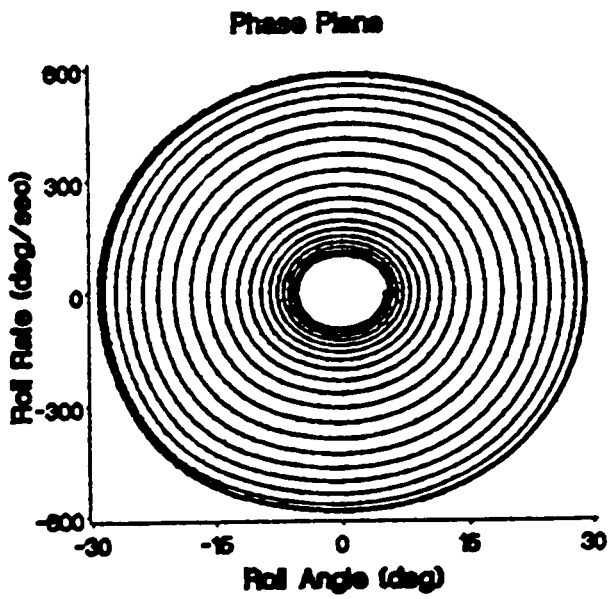

Figure 64. Phase Portrait for a Pitch Angle of 27.5 Degrees

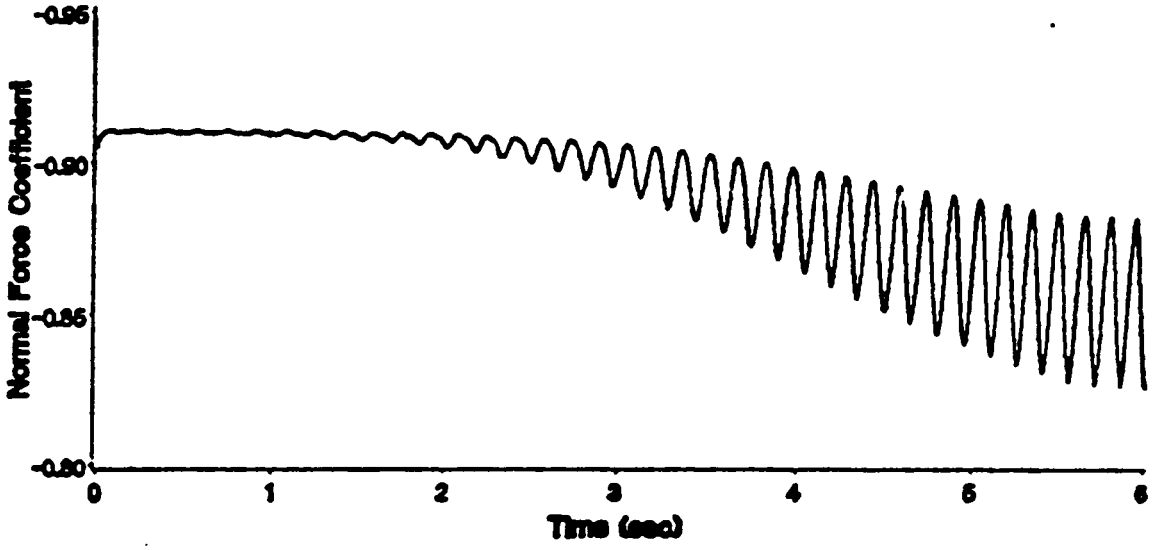

Figure 65. Normal Force Evolution for a Pitch Angle of 27.5 Degrees

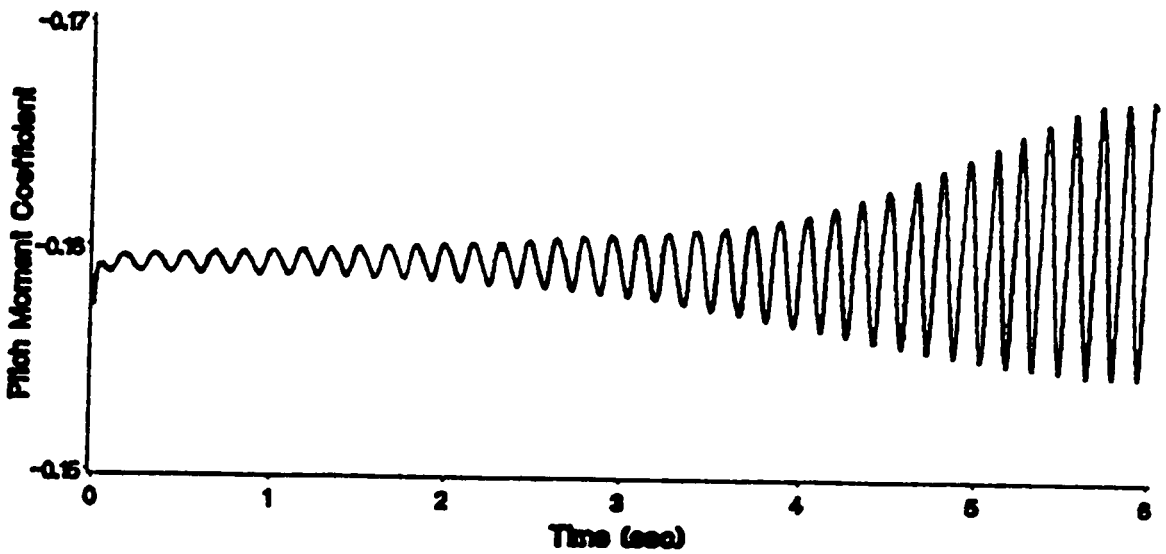

Figure 66. Pitch Moment Evolution for a Pitch Angle of 27.5 Degrees

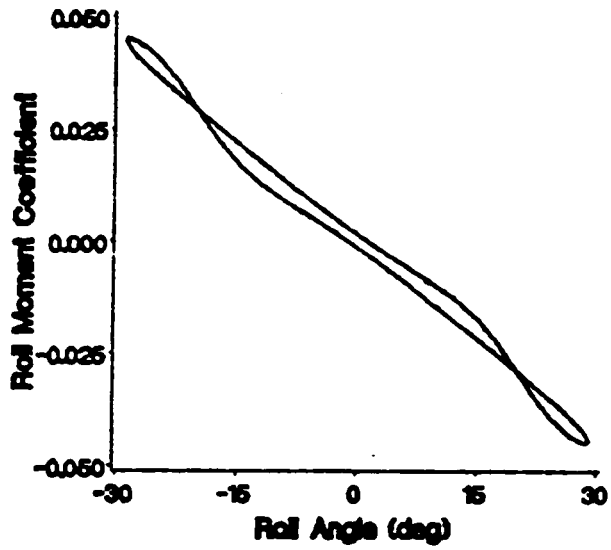

Figure 67. Roll Moment Hysteresis for a Pitch Angle of 27.5 Degrees

3.7 Conclusions of Dynamic/Aerodynamic Coupling

In this chapter the complete development of the method used to couple the equations of motion and the aerodynamic model was presented. This coupled model was used to simulate both free and forced wind-tunnel experiments. The results show that the coupling is indeed a viable method for predicting a wind-tunnel environment and wing rock of slender delta wings.

Chapter IV

Control Model

4.1 Introduction

The aerodynamic model of Chapter II was coupled with the equations of motion in Chapter III. This coupled system was used to determine the motion of a slender delta wing mounted on a free-to-roll sting in a wind tunnel. The goal of this research is not only to predict the motion, but also to control it. In this chapter the problem of simulating control of the wing by adding control-surface motion to the aerodynamic/dynamic model is addressed.

In Section 4.2 the method used to couple the control-surface movement with the aerodynamic system is described. In Section 4.3 the control surface effectiveness will be examined. In Section 4.4, the minimum-time optimal control problem to change pitch orientation is solved by using a simplified, linearized model. Then this control law is evaluated by using it in the full system model. The same maneuver of changing pitch angles will be accomplished by using feedback control in Section 4.5. Finally, in Section 4.6 the wing rock predicted in Section 3.6 will be suppressed by using feedback control.

4.2 Control Surface Motion

Throughout this chapter, the test wing is a thin delta wing with two control surfaces located along the trailing edge. These surfaces can move independently of each other, but for the purposes of controlling independent degrees of freedom, they either move in tandem as flaps, or they move asymmetrically as ailerons. The symmetric movement is used to control the pitch orientation and the asymmetric movement is used to control the roll motion. The flow is assumed to separate along all the edges of the wing, except for the two nonconvecting cores on each side of the centerline near the apex, and the control surfaces, but it does not separate along the hinge line. Thus, the transition from the wing to the control surface is

It is assumed the movement of the control surfaces does not alter the moment of inertia characteristics of the wing.

The coordinate system used to define the motion of the control surfaces is shown in Figure 68. The positive deflection is down.

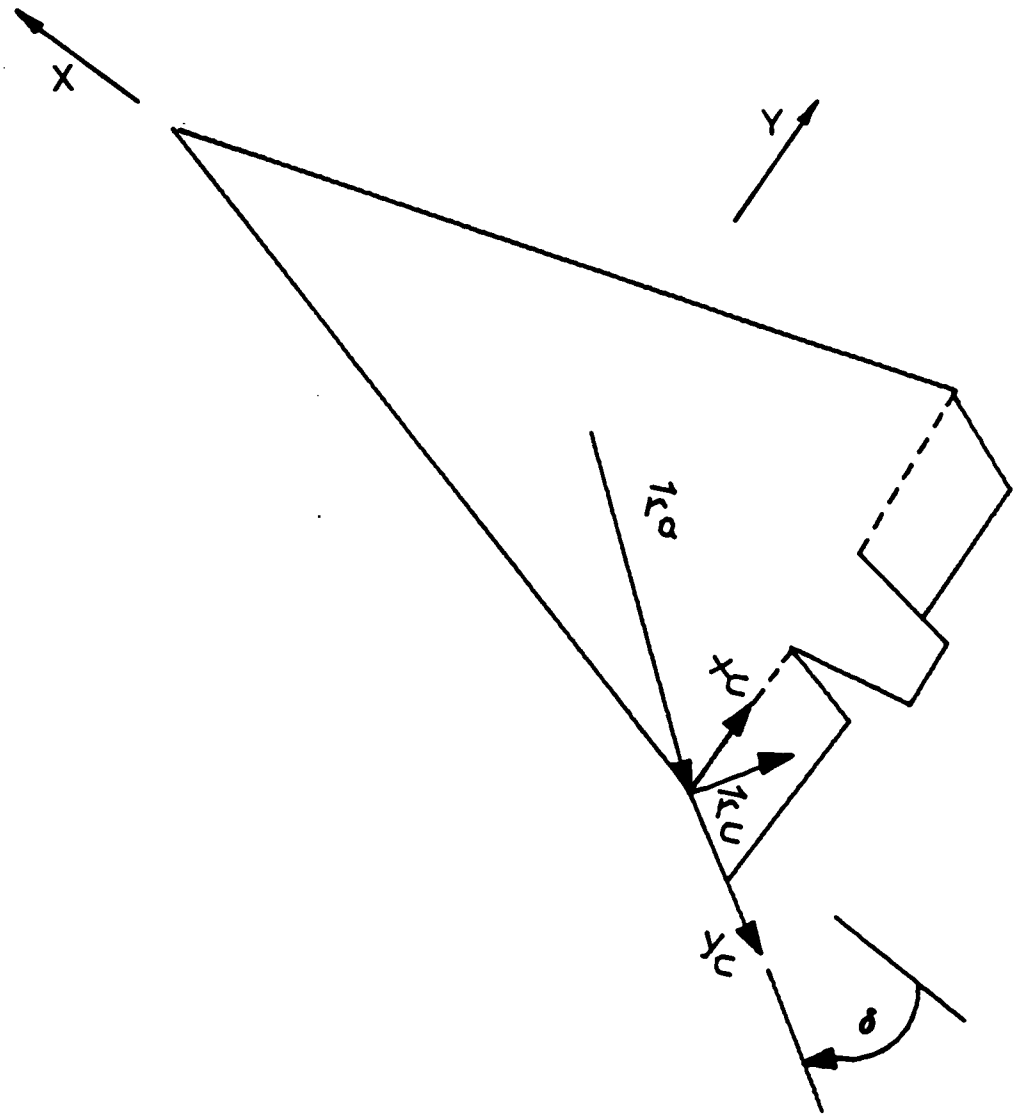

Figure 68. Control Surface Coordinate Frames

The unit vectors of the coordinate systems are designated $\vec{i}, \vec{j}$ and $\vec{k}$ for the body-fixed reference frame, $\vec{i}_c, \vec{j}_c$ and $\vec{k}_c$ for the control surface, and $\vec{i}_{co}, \vec{j}_{co}$ and $\vec{k}_{co}$ for the control surface when $\delta = 0$. The coordinate frame of the control surface is related to the body-fixed frame by

$$\begin{Bmatrix} \vec{i}_c \\ \vec{j}_c \\ \vec{k}_c \end{Bmatrix} = [C] \begin{Bmatrix} \vec{i} \\ \vec{j} \\ \vec{k} \end{Bmatrix} \qquad (4.2-1)$$

where the direction cosine matrix, $[C]$, is composed of two matrices. The element of these matrices are the direction cosines of the control surface when $\delta = 0$, designated $[C_o]$, and the direction cosines when δ is nonzero, designated $[C_\delta]$. That is,

$$[C] = [C_\delta][C_o] \qquad (4.2-2)$$

where

$$\begin{Bmatrix} \vec{i}_{co} \\ \vec{j}_{co} \\ \vec{k}_{co} \end{Bmatrix} = [C_o] \begin{Bmatrix} \vec{i} \\ \vec{j} \\ \vec{k} \end{Bmatrix} \qquad (4.2-3)$$

and

$$\begin{Bmatrix} \vec{i}_c \\ \vec{j}_c \\ \vec{k}_c \end{Bmatrix} = [C_\delta] \begin{Bmatrix} \vec{i}_{co} \\ \vec{j}_{co} \\ \vec{k}_{co} \end{Bmatrix} \qquad (4.2-4)$$

Because the rotation of the control surface is about the local $\vec{i}_e$ direction through an angle δ

$$[C_\delta] = \begin{bmatrix} 1 & 0 & 0 \\ 0 & \cos\delta & \sin\delta \\ 0 & -\sin\delta & \cos\delta \end{bmatrix}. \qquad (4.2-5)$$

Two quantities must be determined to implement moving the surfaces in the body reference frame. These quantities are the position of the surface and the velocity of the points on the surface relative to the body fixed frame. The position is needed to form the influence matrix (Equation 2.5-2). The velocity is needed to form the right-hand side of the no-

penetration condition (Equation 2.5-2), to form the Kutta condition (Equation 2.10-23), and to calculate the surface pressure (Equation 2.10-26).

The position of a point on the surface is

$$\vec{r} = \vec{r}_a + \vec{r}_c \qquad (4.2-6)$$

where $\vec{r}_a$ is the location of the origin of the control-surface reference frame (written in the body-fixed frame) and

$$\vec{r}_c = x_c \vec{i} + y_c \vec{j} + z_c \vec{k}. \qquad (4.2-7)$$

One means of identifying the position is to use the original position of the point on the surface and the angle of rotation. Because all positions are written in the body-fixed reference frame, the original position of the point on the surface is

$$\vec{r}_{co} = x_o \vec{i} + y_o \vec{j} + z_o \vec{k}.$$

or

$$\vec{r}_{co} = [x_o, y_o, z_o][C_o]^T \begin{Bmatrix} \vec{i}_{co} \\ \vec{j}_{co} \\ \vec{k}_{co} \end{Bmatrix}. \qquad (4.2-8)$$

When the surface is rotated, the position written in the surface reference frame does not change. Therefore, the position vector at the current position is

$$\vec{r}_c = [x_o, y_o, z_o][C_o]^T \begin{Bmatrix} \vec{i}_c \\ \vec{j}_c \\ \vec{k}_c \end{Bmatrix}$$

or

$$\vec{r}_c = [x_o, y_o, z_o][C_o]^T[C_\delta][C_o]\begin{Bmatrix}\vec{i}\\ \vec{j}\\ \vec{k}\end{Bmatrix}. \qquad (4.2-9)$$

As mentioned earlier, the control surface is rotating about the hinge line and in the $\vec{i}_c$ direction. The velocity at a point on the control surface is

$$\vec{v}_c = \dot{\delta}\,\vec{i}_c \times \vec{r}_c \qquad (4.2-10)$$

where $\dot{\delta}$ is the angular rotation rate of the surface. The angular rotation rate, written in the body-fixed reference frame, $\vec{\omega}_c$, is

$$\vec{\omega}_c = \omega_{cx}\vec{i} + \omega_{cy}\vec{j} + \omega_{cz}\vec{k} = \dot{\delta}\,\vec{i}_c = \dot{\delta}\,\vec{i}_{co}. \qquad (4.2-11)$$

The position and velocity of all points on the control surface can now be determined given the original position, the location of the hinge line, the current angular displacement and the current angular rate.

Because positioning the control surface is basically the same as positioning the wing, the control surface position will be calculated directly after calculating the body angular rates (subroutine OMEGAS). The calculation of the direction cosine matrix of Equation 4.2-2, $[C]$, is included in the subroutine that calculates the direction cosine matrix between the body-fixed and the inertial frames (subroutine CMATRX). The angular rate, $\vec{\omega}_c$, is determined in the routine that calculates the body angular rates (subroutine OMEGAS).

The determination of the deflection angle, δ, and the deflection rate, $\dot{\delta}$, will now be discussed. Physically, the angular deflection and angular deflection rate of the control surfaces are input into the system as a commanded deflection angle, δ_c. This commanded input then produces a deflection through a servo mechanism. In this presentation, the servo mechanism is modeled by the following second-order differential equation:

$$\ddot{\delta} = C_1\dot{\delta} + C_2(\delta - \delta_c). \qquad (4.2-12)$$

The commanded deflection angle is known throughout the flight either explicitly for an open-loop system or implicitly for a closed-loop system. The values of C_1 and C_2 will be presented during the specific applications of Section 4.4 through 4.6.

In order to make the model more realistic, the deflection angle was limited to $\pm 25°$ for all applications. These limits where chosen arbitrarily because no specific physical system was modeled. However, the same procedure could be used to limit the deflection angle or rate for any limits.

The deflection angle is limited in the differential-equation solver by including conditional statements on the magnitude of the deflection in the subroutines TAYLOR, YFITER, PRAMOD and ERRCOR. When the limit is exceeded, within these routines, the deflection angle is set to the limit and the angular rate is set to zero. In order for the numerical integration scheme to converge, the subroutine YFITER must also include limiting the new predicted solution and stopping the iteration if the new solution is beyond the specified limits.

4.3 Control Surface Effectiveness

The method used to couple the control-surface with the aerodynamic and dynamic model has been presented. Before the design of a control system is discussed, the control-surface effectiveness is investigated.

The effectiveness will be investigated with two sets of steady-state conditions. First, the effect of surface size will be determined. Second, the effect of the deflection angle magnitude will be presented. A unit-aspect-ratio delta wing set at twenty degrees pitch is used to determine the effect of the control surface size. Both flap and aileron deflections will be examined. First the surfaces are used as flaps and are set at negative 10 degrees. The lift (C_L) , drag (C_D) , pitch moment (C_m) , and hinge moment (C_h) coefficients are presented in Table 12. The pitch-moment coefficient is calculated about .568 c, which is the location of the center of gravity for the wing of Sections 4.4 and 4.5.

Table 12. Flap Size Effectiveness for a Pitch Angle of 20 Degrees

S_f/S	C_L	C_D	C_m	C_h
0.000	0.677	0.246	-0.0339	N/A
0.172	0.550	0.199	0.0246	-0.011
0.204	0.527	0.187	0.0124	-0.045
0.240	0.522	0.182	-0.0110	-0.075

S_f: Total area of both flaps
S: Total area of wing including flaps

The hinge moment is calculated about the hinge axis. The hinge-moment coefficient is defined as

$$C_h = \frac{1}{2}\rho U^2 S_1 c_1 M_h \qquad (4.3-1)$$

where S_1 is the surface area of one flap and c_1 is the chord of that flap. As expected, the larger flaps produce larger effects on the lift and drag characteristics. Because the rotation of the vorticity vector at the node is applied along the hinge line, the requirement that the derivative of the circulation along the edge be continuous is satisfied automatically at the node on the hinge line's outside edge. This requirement is imposed at the other nine corners of the wing using the constraint equations.

The effect of surface size for aileron deflections is investigated by setting the port surface, δ_p, at positive 10 degrees and the starboard surface, δ_s , at negative 10 degrees. The lift, rolling moment, pitching moment, yawing moment, starboard hinge moment, C_{h_s} and port hinge moment, C_{h_p} coefficients are presented in Table 13.

Table 13. Aileron Size Effectiveness for a Pitch Angle of 20 Degrees

S_f/S	C_L	C_l	C_n	C_{hs}	C_{hp}
0.000	0.677	0.0000	0.0000	N/A	N/A
0.149	0.664	0.0013	-0.0008	-0.0454	-0.0406
0.172	0.657	0.0092	-0.0007	-0.0588	-0.0530
0.204	0.663	0.0071	-0.0019	-0.0819	-0.0376

The deflection used to produce Table 13 is defined as a positive aileron deflection. The aileron deflection angle, δ_A, is defined as

$$\delta_A = \frac{(\delta_p - \delta_s)}{2}. \qquad (4.3-2)$$

That is, a positive aileron deflection produces a positive roll moment. The yaw moment is negative as expected for a pitched up wing with positive aileron deflection.

The effect of the flap deflection magnitude will be determined by using a unit aspect ratio delta wing with 25 elements at angle of attack of 5, 10, 15 and 20 degrees. The flaps are set at angles ranging from 25 degrees to -25 degrees in 5 degree increments. The results of these tests are presented in Figure 69 through Figure 73. Figure 69 shows the lift coefficient, Figure 70 presents the drag coefficient and Figure 71 shows the pitch-moment coefficient. These figures show that the effect of the flap angle on the lift and drag are nearly linear. The effectiveness of the flap over the range of angles of attack is shown in Figure 72 and Figure 73.

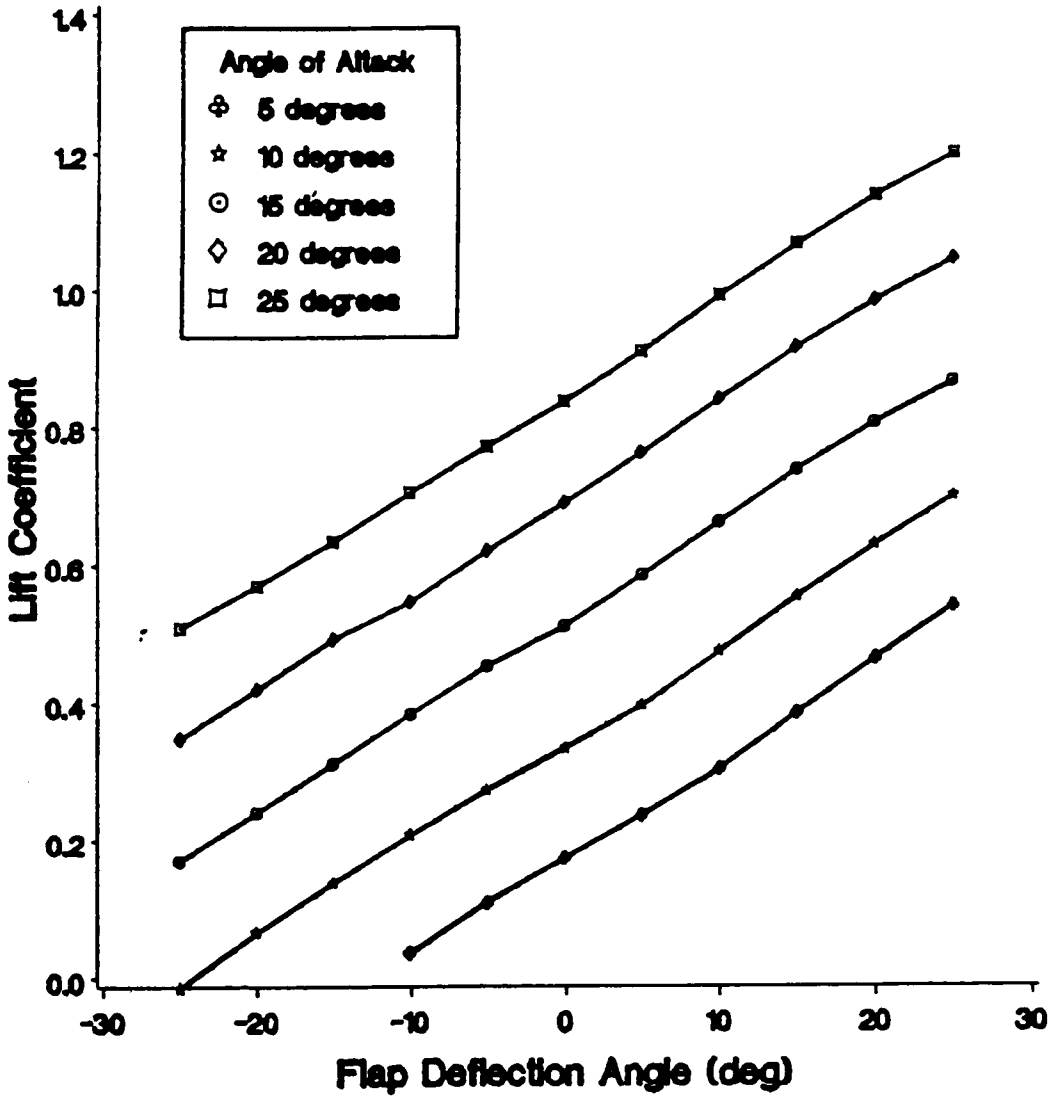

Figure 69. Lift Coefficient as a Function of Flap Deflection

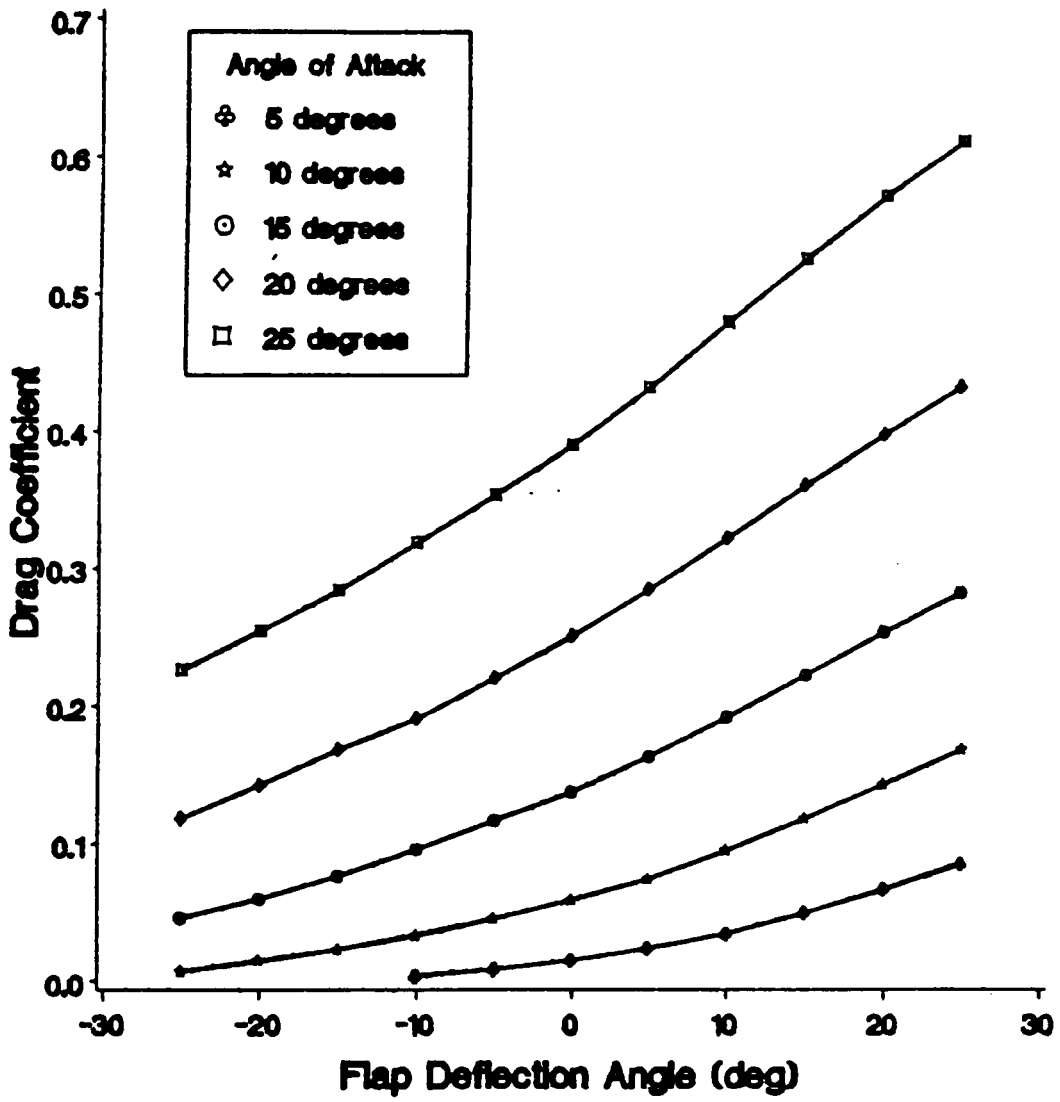

Figure 70. Drag Coefficient as a Function of Flap Deflection

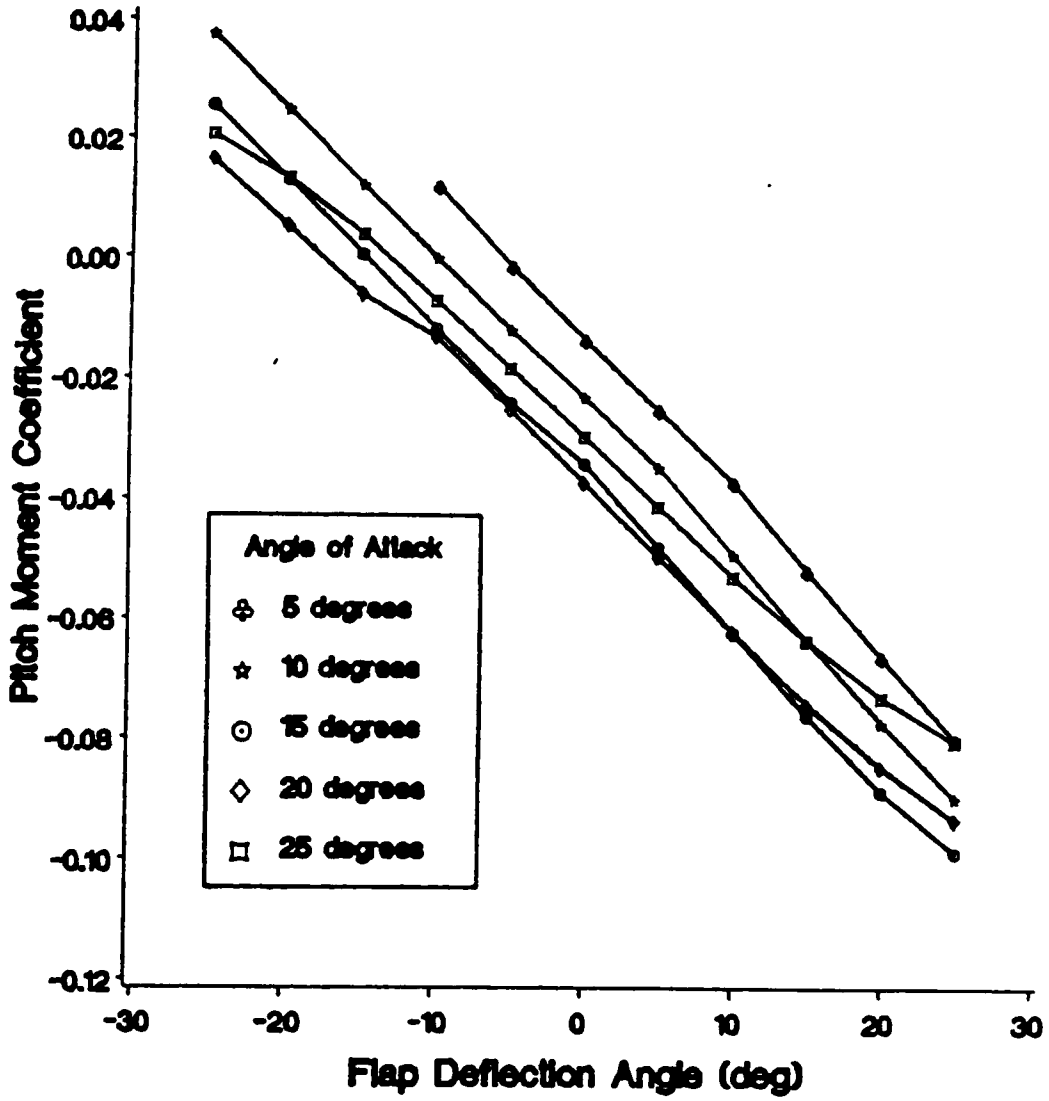

Figure 71. Pitch Moment Coefficient as a Function of Flap Deflection

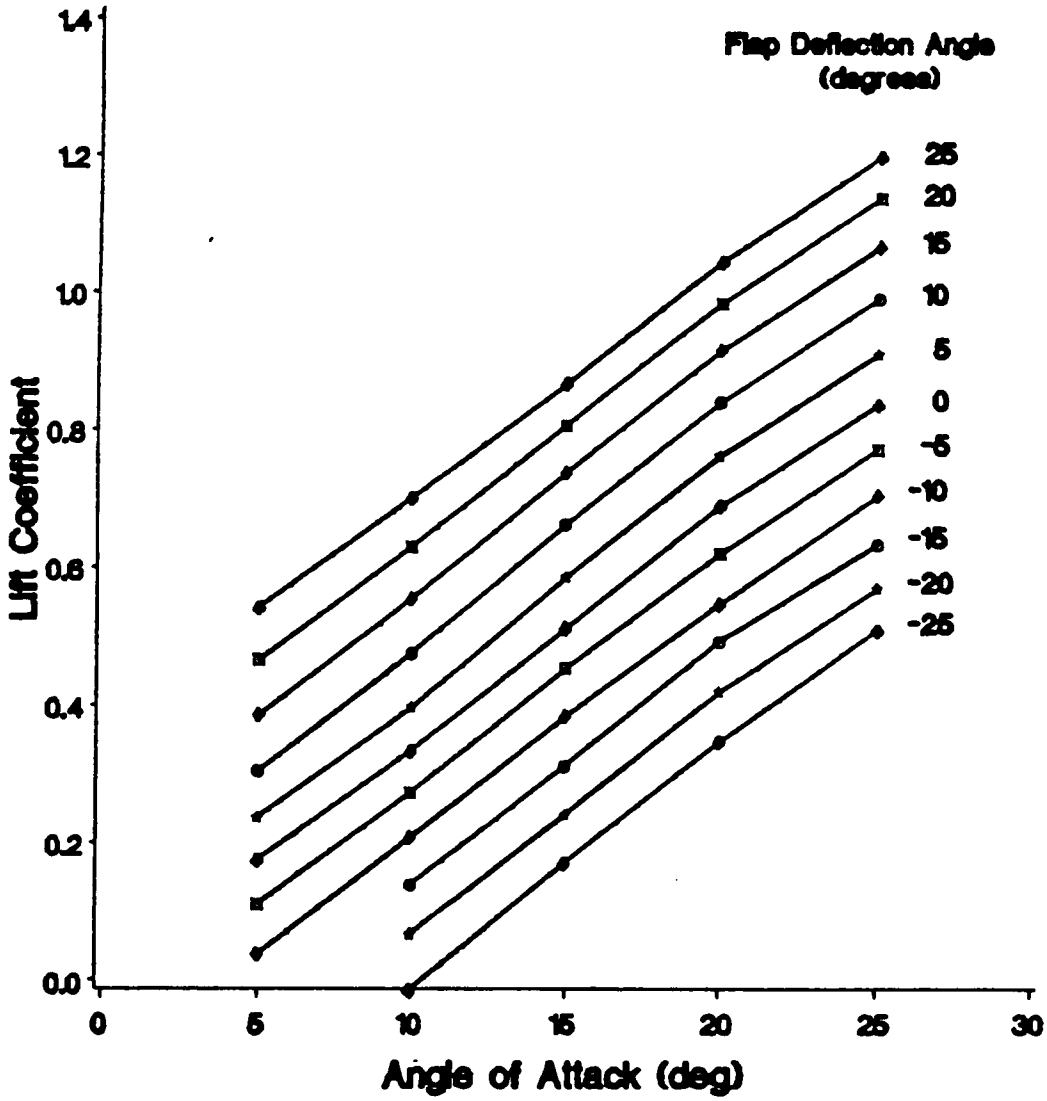

Figure 72. Lift Coefficient as a Function of Angle of Attack

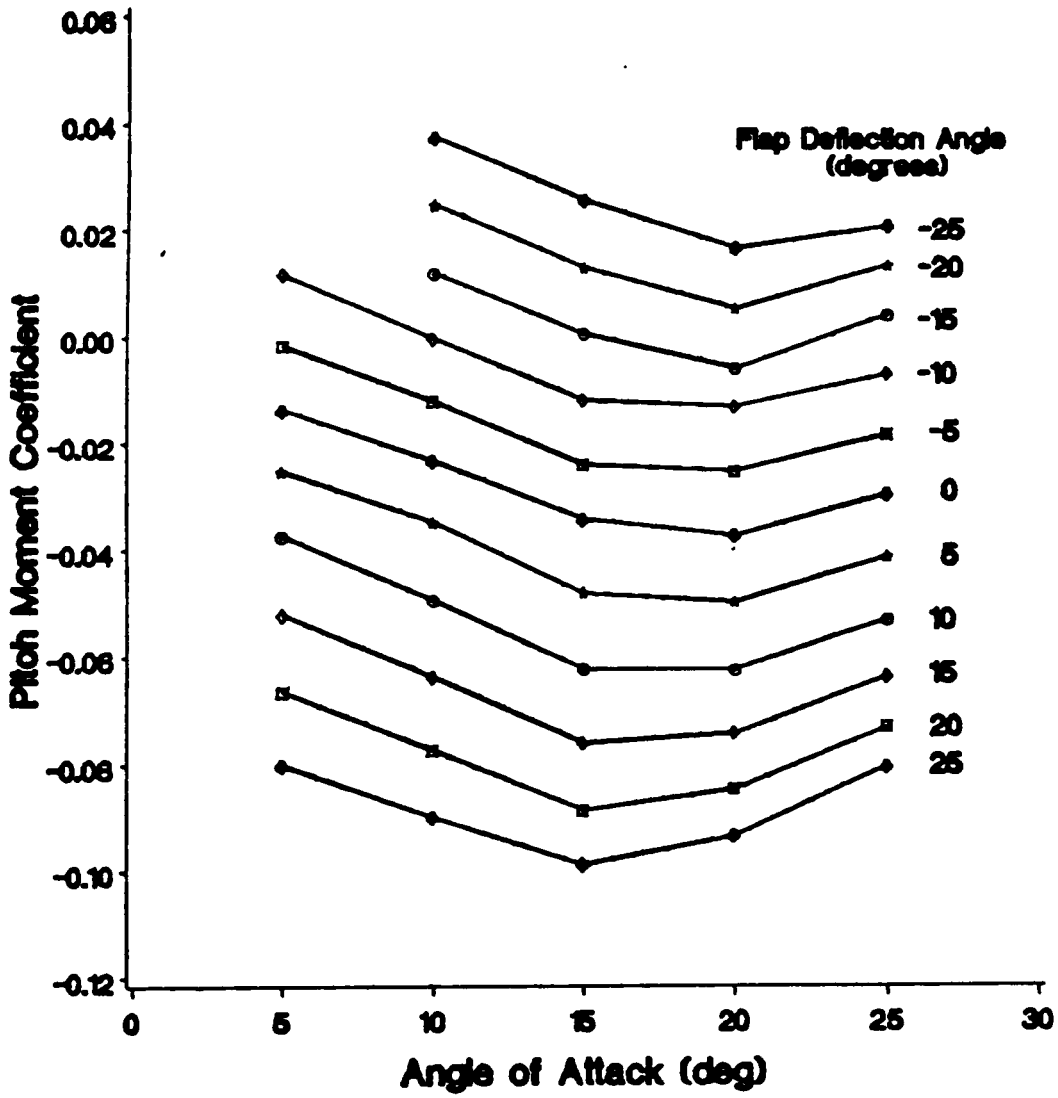

Figure 73. Pitch Moment Coefficient as a Function of Angle of Attack

The aileron effectiveness is determined by setting the port and starboard surfaces at asymmetric positions such that the aileron deflection ranges from -5 to 25 degrees. The angle of attack is 20 degrees and 81 elements are used for the wing. The results of this set of tests are presented in Figure 74 through Figure 77.

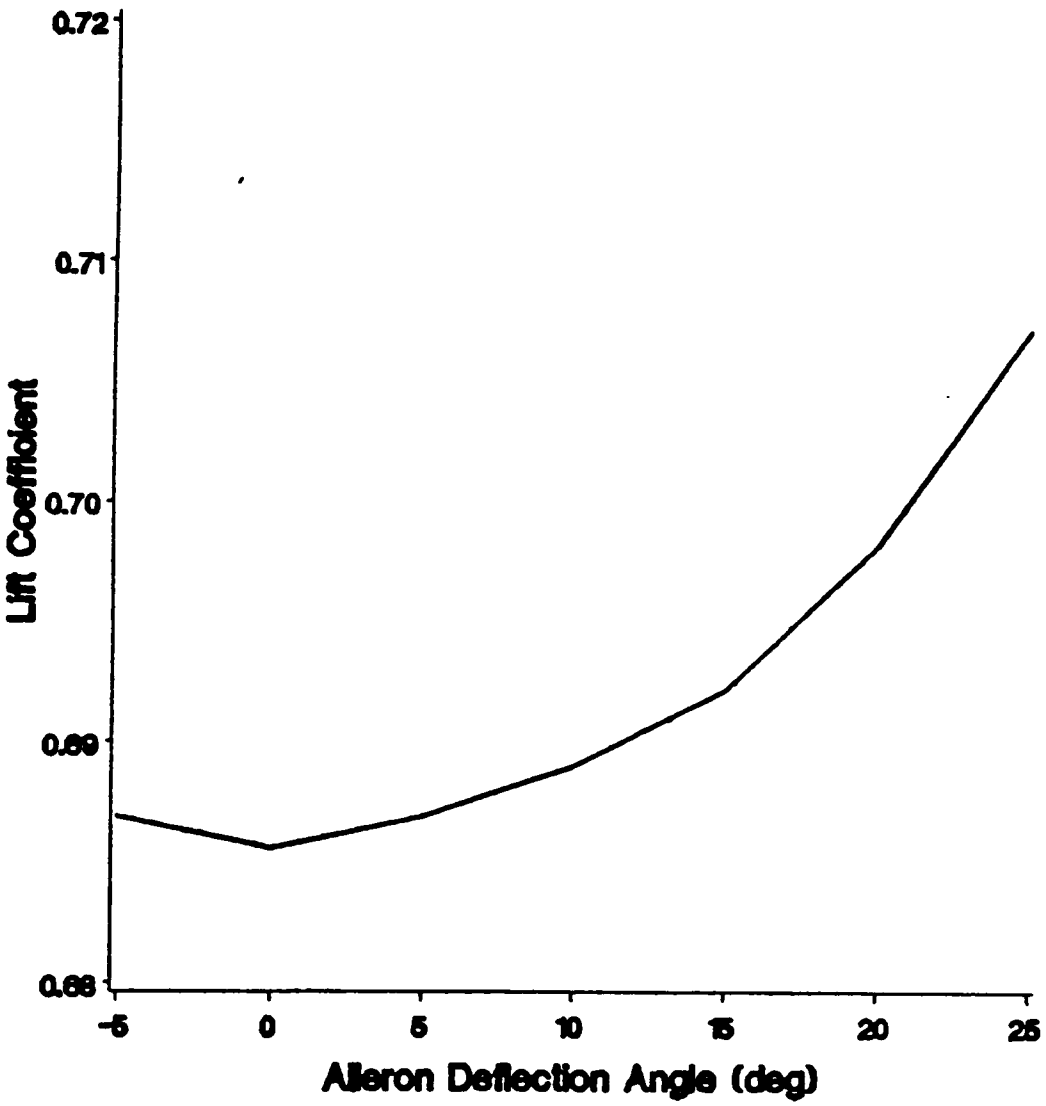

Figure 74. Lift Coefficient as a Function of Aileron Deflection

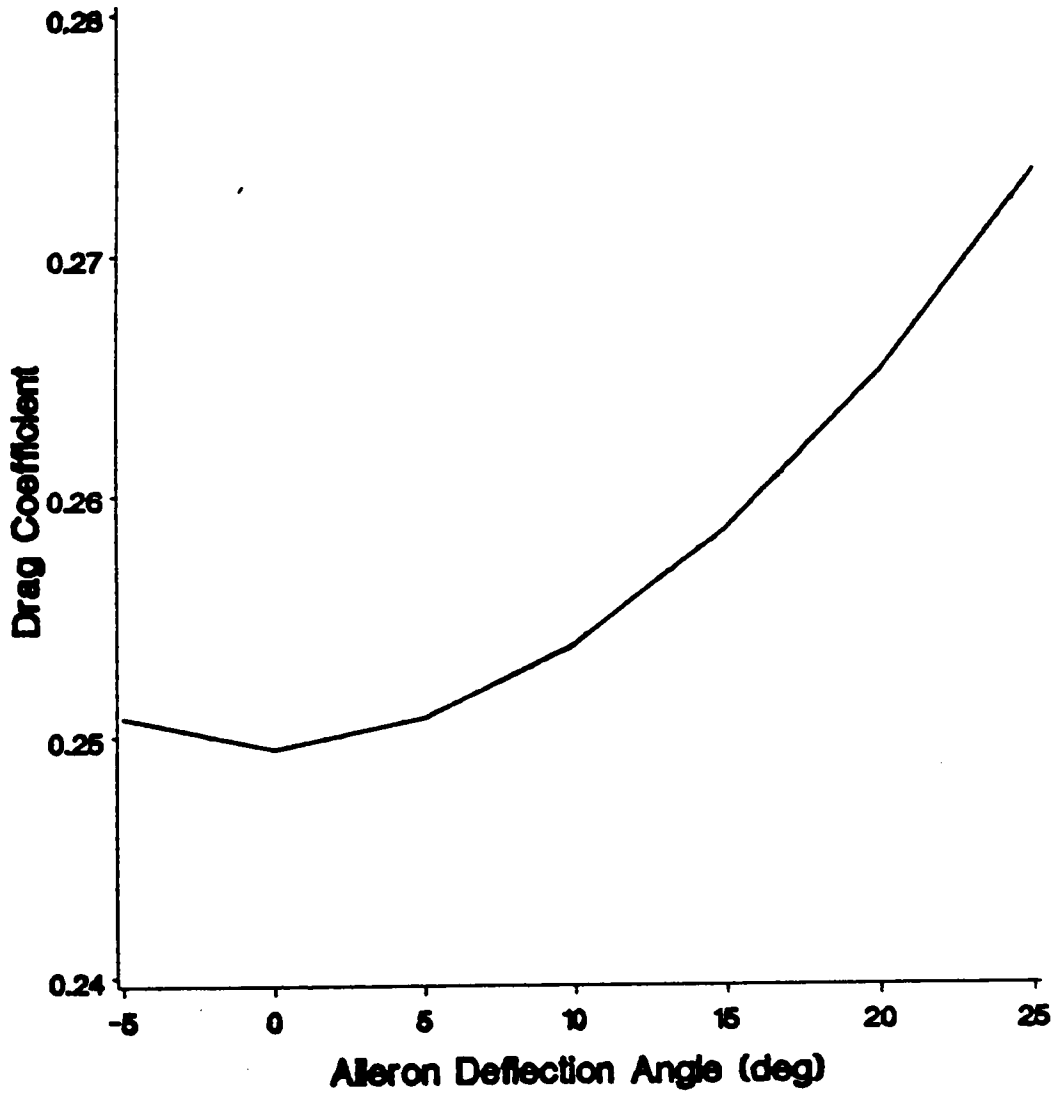

Figure 75. Drag Coefficient as a Function of Aileron Deflection

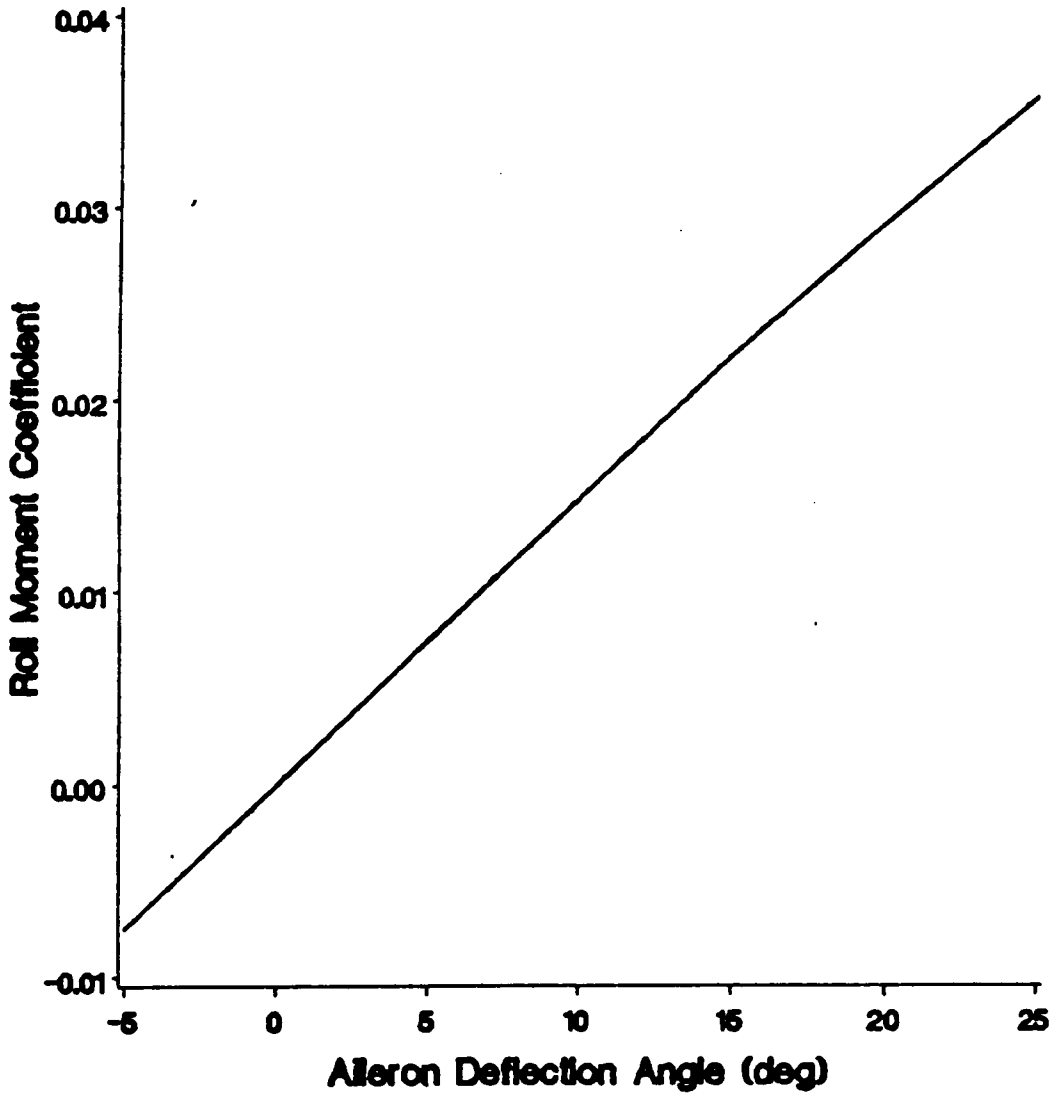

Figure 76. Roll Moment Coefficient as a Function of Aileron Deflection

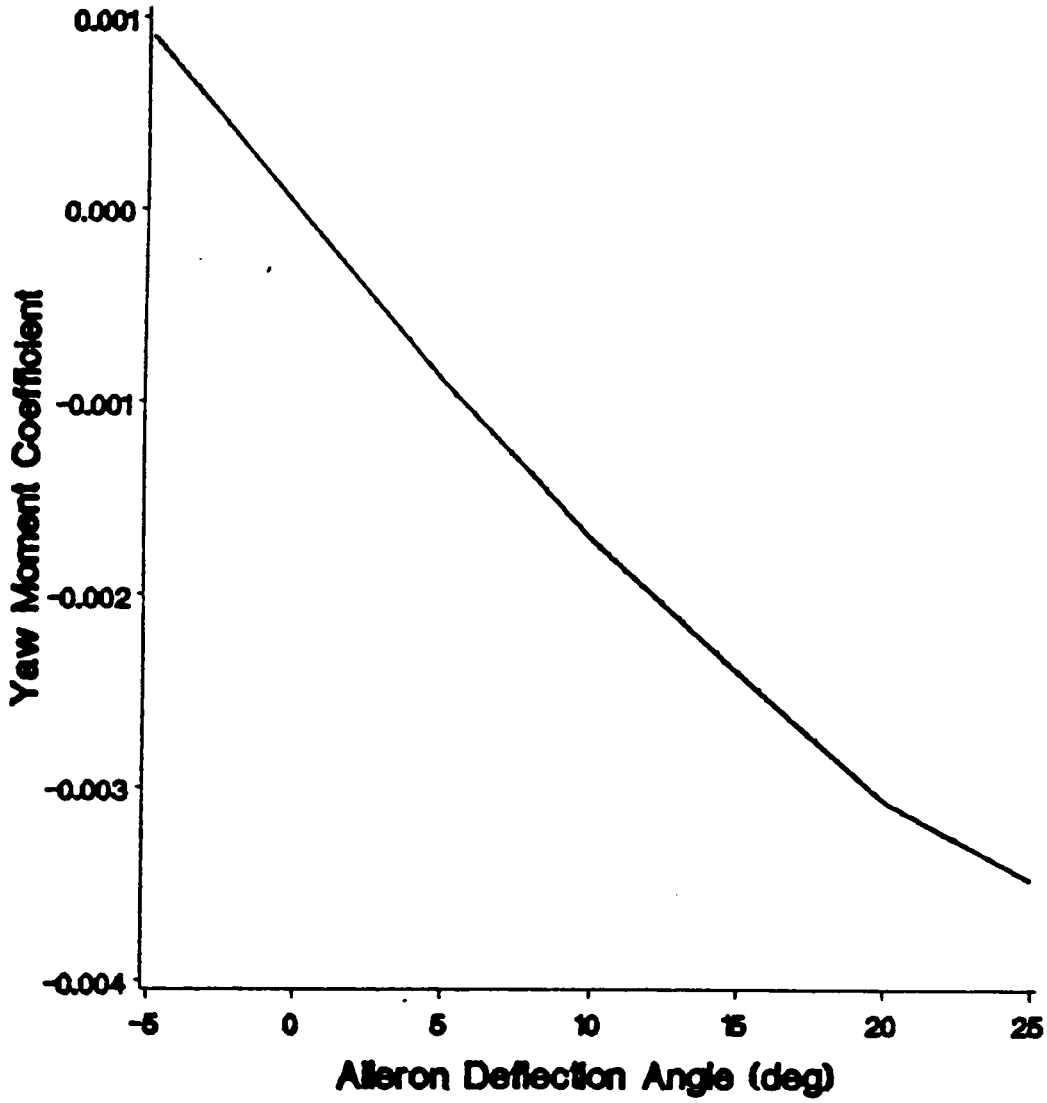

Figure 77. Yaw Moment Coefficient as a Function of Aileron Deflection

4.4 Optimal Control Problem

In this section, the minimum-time, optimal-control problem for changing pitch orientation is examined. First, the linear model will be created by using the results of Section 4.3. A linear model was chosen because for such a model the optimal solution is known. This simplified model is then used to determine the minimum-time control law. The usefulness of this law is then examined by implementing it in the full nonlinear, unsteady simulation. For this experiment, the wing was only allowed to rotate in pitch about the center of gravity.

The physical system selected to be investigated is similar to the wind-tunnel model used by McKinney and Drake [1948] . This system is used because McKinney and Drake provide a complete set of weight and balance characteristics for a unit-aspect-ratio wing with control surfaces. The physical characteristics for this simulation are listed in Table 14.

Table 14. Test Wing Characteristics

Quantity	Magnitude	Units
W	0.925	kg
S	0.248	m^2
b	0.498	m
c	0.996	m
c_{cg}	0.566	m
$\bar{c}$	0.663	m
I_{xx}	0.969	kg-m^2
I_{yy}	9.413	kg-m^2
I_{zz}	9.758	kg-m^2
V	15.47	m/s
ρ	1.200	kg/m^3

The servo mechanism constants where chosen to be $C_1 = -0.00515$ and $C_2 = -0.000033$. These constants yield a damped servo system.

The wing used in this development is not quite the same as the model used by McKinney and Drake because the flaps are much larger and no tail surface exists for the

current model. The wing for this development is represented by 25 elements and the ratio of the control surface area to the wing area, S_f/S, is 0.240. Because 25 elements are used, the chord length is five units. Therefore, the reference length, L, is 0.1992 m. The dimensionless servo equation is then

$$\ddot{\delta} = -\frac{C_1 L}{V}\dot{\delta} - \frac{C_2 L^2}{V^2}(\delta - \delta_c) \qquad (4.4-1)$$

or

$$\ddot{\delta} = -0.4\dot{\delta} - 0.2(\delta - \delta_c) \qquad (4.4-2)$$

This equation is not used in the development of the optimal control law to further simplify the calculations. It is used when the control law is validated in the full simulation and in the feedback systems.

The optimal control problem is to pitch the wing from 10 to 15 degrees in the minimal time, subject to the constraint that the flaps are limited to $\pm$ 25 degrees. The linear model used to approximate the wing motion is

$$\ddot{\theta} = \frac{M_y}{I_{yy}} \qquad (4.4-3)$$

where

$$M_y = M_\theta\,\theta + M_\delta\,\delta + M_o. \qquad (4.4-4)$$

The steady state results presented in Figure 71 are use to derive the linear model. At an angle of attack of 10 degrees the entire range of flap deflections is used to find the linear model for the flap effectiveness. The linear model at 10 degrees angle of attack is

$$C_{m_y} = -0.02208 - 0.00232\,\delta \qquad (4.4-5)$$

where δ has units of degrees. The entire range of flap deflection angles is again used to find the linear model at 15 degrees angle of attack. The linear model at 15 degrees angle of attack is

$$C_{m_y} = -0.02755 - 0.00212\,\delta \qquad (4.4-6)$$

The average slope is used for the entire range of angles of attack, that is the effect of angle of attack and flap deflection are assumed to be independent. The constants of Equations 4.4-5 and 4.4-6 depend on the angle of attack. A linear regression is performed on the two constants of Equations 4.4-5 and 4.4-6 to determine the influence of the angle of attack on the pitch-moment coefficient. The total linear pitch-moment coefficient calculated about the center of gravity is

$$C_{m_y} = -0.01114 - 0.00109\,\theta - 0.00222\,\delta \qquad (4.4-7)$$

where both δ and θ have units of degrees. The trim flap settings for the linear model are $\delta = -9.928°$ for 10 degrees pitch and $\delta = -12.382°$ for 15 degrees pitch. For comparison the trim flap settings for the nonlinear model are $\delta = -8.989°$ for 10 degrees pitch and $\delta = -12.533°$ for 15 degrees pitch.

The state and control variables are defined as

$$x_1 = \theta - 15.0° = \theta - 0.26180 \qquad (4.4-8)$$

$$x_2 = \dot{\theta} \qquad (4.4-9)$$

and

$$u = \delta + 12.382° = \delta + 0.21611. \qquad (4.4-10)$$

For this development the servo equation is not used. That is, the actual deflection angle is assumed to be the commanded deflection angle. The equation of motion is

$$\ddot{\theta} = \frac{1}{2}\rho V^2 S\bar{c}\frac{C_{m_y}}{I_{yy}} \qquad (4.4-11)$$

or

$$\ddot{\theta} = -0.02794 - 0.15682\theta - 0.31976\delta \qquad (4.4-12)$$

where both θ and δ now have units of radians. In terms of the state variables Equation 4.4-12 can be written as

$$\dot{x}_2 = -0.02794 - 0.15682(x_1 + 0.26180) - 0.31976(u - 0.21612) \qquad (4.4-13)$$

Therefore, the state space representation of the system is

$$\begin{Bmatrix}\dot{x}_1\\ \dot{x}_2\end{Bmatrix} = \begin{bmatrix} 0.00000 & 1.00000 \\ -0.15682 & 0.00000 \end{bmatrix}\begin{Bmatrix}x_1\\ x_2\end{Bmatrix} + \begin{Bmatrix}0.00000\\ 0.31976\end{Bmatrix}u, \qquad (4.4-14)$$

subject to

$$-0.22022 \le u \le 0.65244. \qquad (4.4-15)$$

The initial and final states are:

$$\begin{aligned} x_1(0) &= -0.08727 \text{ radians} \\ x_2(0) &= 0.00000 \text{ rad/sec} \\ x_1(t_f) &= 0.00000 \text{ radians and} \\ x_2(t_f) &= 0.00000 \text{ rad/sec.} \end{aligned} \qquad (4.4-16)$$

The optimal solution is "Bang-Bang" control, Hermes and LaSalle [1969] . The switching times are defined by

$$\sin(\omega t + \phi) = 0, \qquad (4.4-17)$$

where $\omega^2 = 0.15682$ and $-\pi \leq \phi \leq \pi$. That is, the switching times are 15.87 seconds apart. The final state can be reached in 1.73 seconds by using one switching time at 1.24 seconds. The optimal control law is

$$\begin{aligned} u^* &= -0.0428 && t < 0 \\ u^* &= -0.2202 && 0 \leq t < 1.24 \\ u^* &= 0.6524 && 1.24 \leq t < 1.73 \\ u^* &= 0.0000 && t \geq 1.73 \end{aligned} \qquad (4.4-18)$$

where u^* is the optimal control. Because the trim conditions are not the same for the linear model as for the full model, the control law was changed to

$$\begin{aligned} \delta_c^* &= -0.15689 && t < 0 \\ \delta_c^* &= -0.43633 && 0 \leq t < 1.24 \\ \delta_c^* &= 0.43633 && 1.24 \leq t < 1.73 \\ \delta_c^* &= -0.21875 && t \geq 1.73 \end{aligned} \qquad (4.4-19)$$

where δ_e^* is the commanded flap deflection angle. The validation incorporated the servo equation with the equations of motion. This control law was validated by setting δ_e at the start of the time set in the nonlinear unsteady method. The resulting pitch angle is shown in Figure 78. The actual run consisted of two sections, first the wing was held fixed at 10 degrees pitch until a steady state was reached (10 chords of dimensionless time). After this time the control law of Equation 4.4-19 was used. The starting time is set at 20 chords of dimensionless time.

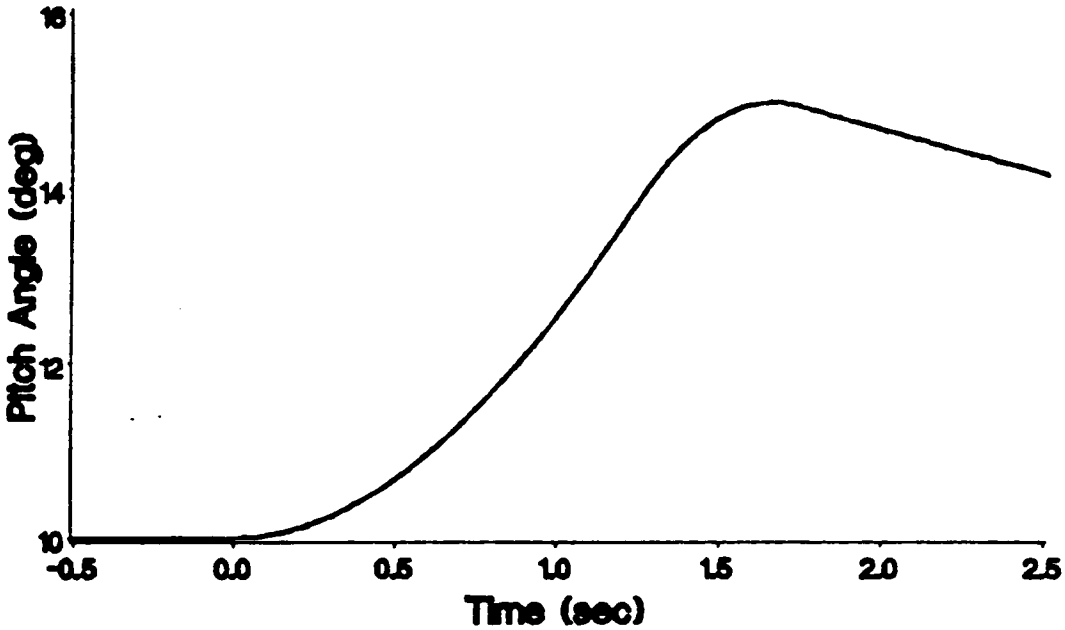

Figure 78. Linear Optimal Control Law in Full System Simulation

Obviously, the control law was not correct since the final state was not reached at the final time. However, this control law is not far from the optimal. The switching time and final time were adjusted slightly until the final state was reached. The best control law for only one switching time is

$$\begin{aligned} \delta_c^* &= -0.15689 && t < 0 \\ \delta_c^* &= -0.43633 && 0 \le t < 1.25 \\ \delta_c^* &= 0.43633 && 1.25 \le t < 1.66 \\ \delta_c^* &= -0.21875 && t \ge 1.66 \end{aligned} \qquad (4.4-20)$$

This control law is not optimal because only one switching time is used. A better solution would be found by including more switches near the final time. Nevertheless the control law of Equation 4.4-20 will be referred to as the optimal control law. The pitch motion for the op-

timal control is presented in Figure 79. The commanded and actual flap deflection angles are shown in Figure 80. The commanded flap deflection is the curve that changes instantaneously. The lift, drag, pitch moment and hinge moment coefficients are shown in Figure 81 trough Figure 84, respectively. The slight irregularities in the figures occur when the flap moves through the plane of the wing. This change in position causes dramatic changes in the flow near the control surfaces.

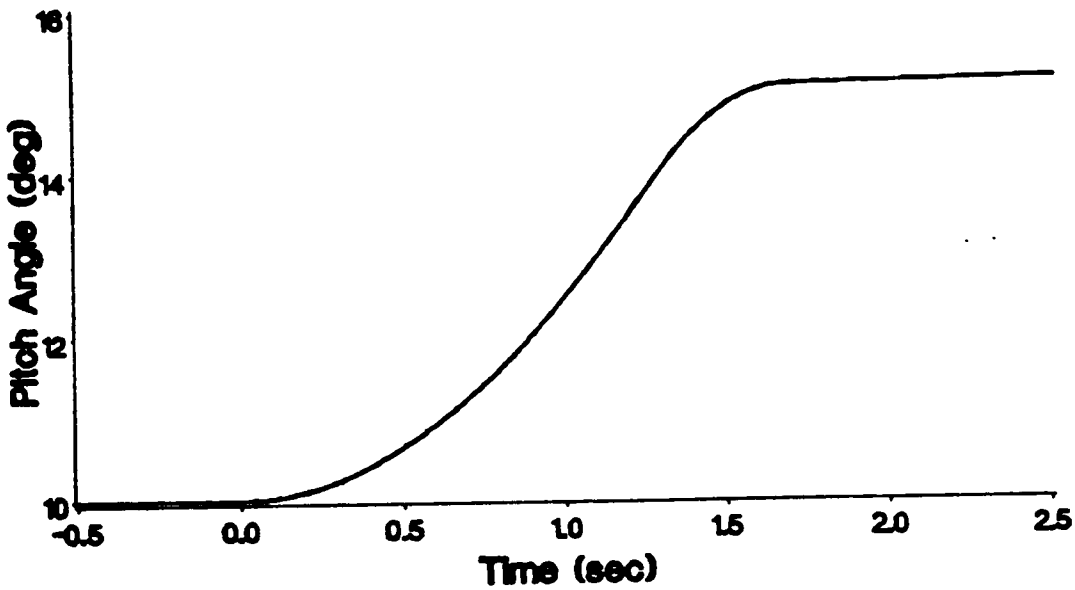

Figure 79. Optimal Control Pitch Angle

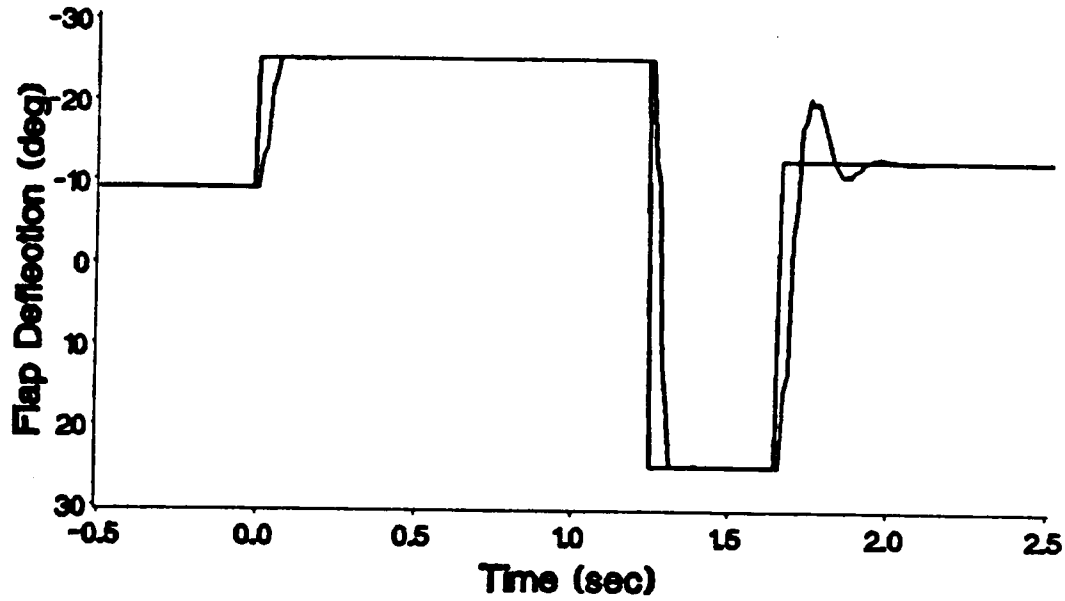

Figure 80. Optimal Control Flap Deflection

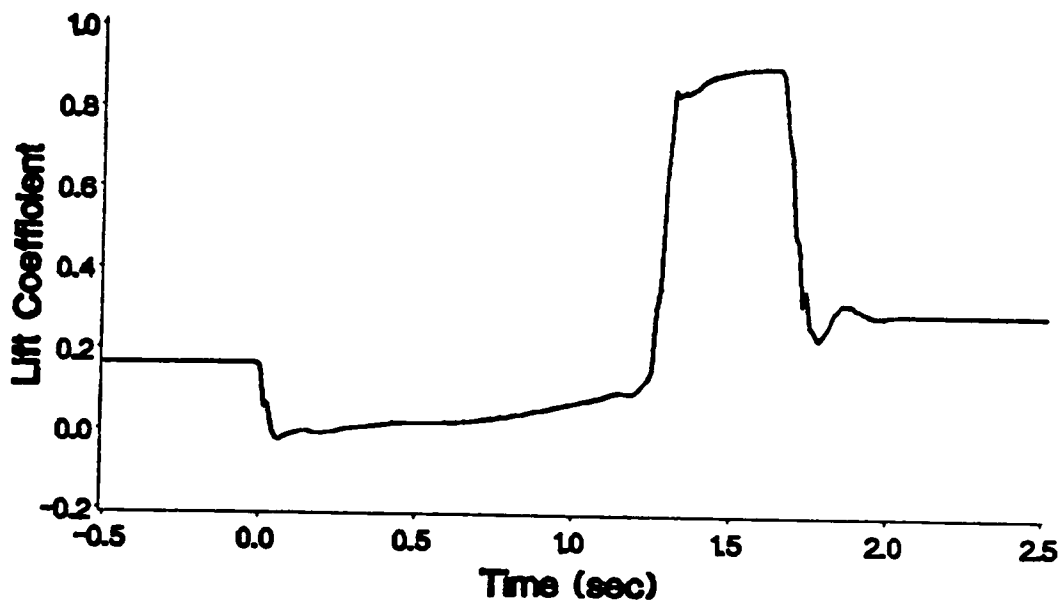

Figure 81. Optimal Control Lift Coefficient

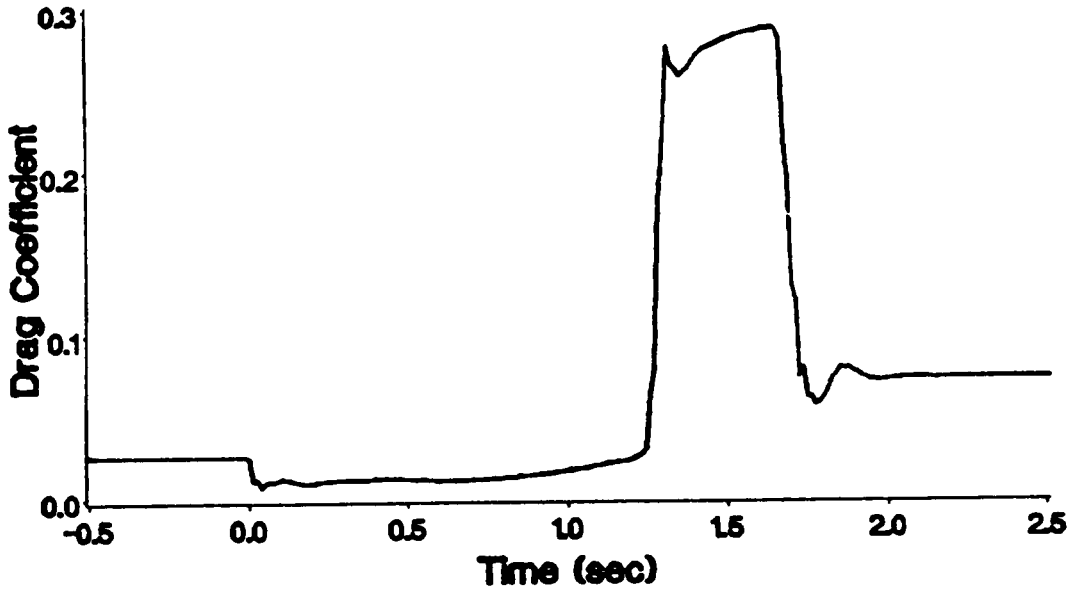

Figure 82. Optimal Control Drag Coefficient

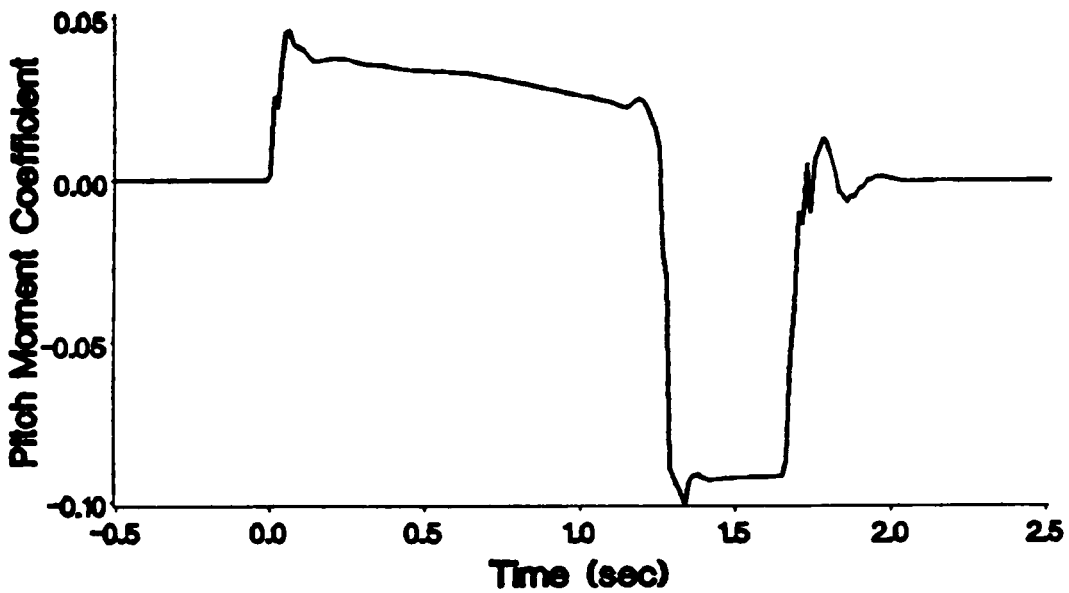

Figure 83. Optimal Control Pitch Moment Coefficient

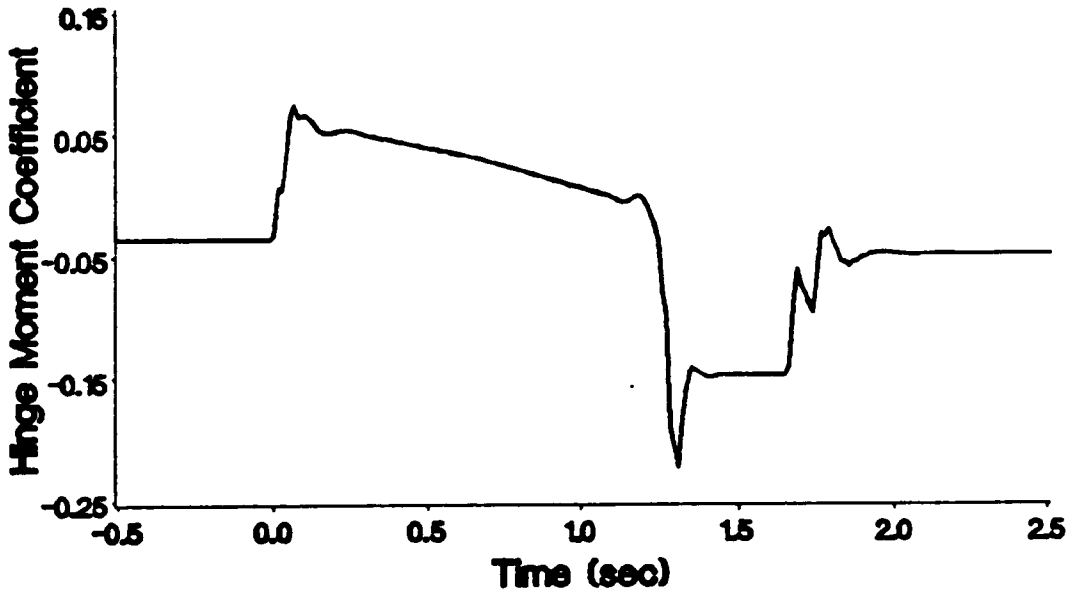

Figure 84. Optimal Control Hinge Moment Coefficient

4.5 Feedback Control of Pitch Orientation

The best solution to change from 10 degrees pitch to 15 degrees pitch has been developed in Section 4.4. This solution is applicable only for the stated conditions. A more realistic means of producing the desired motion is to use feedback control. The block diagram of the system with feedback loops is shown in Figure 85.

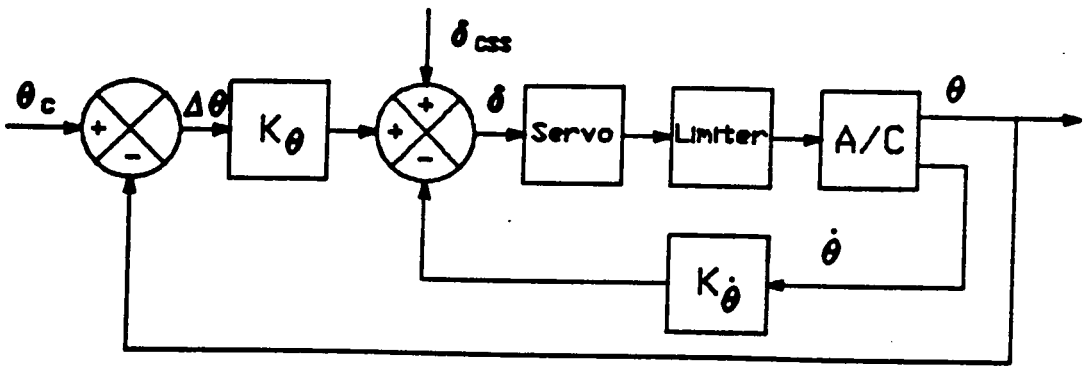

Figure 85. Feedback System to Change Pitch Orientation

Again, the motion of the wing is restricted to one degree of freedom in pitch. The dimensionless gains are chosen to be $K_\theta = 17.50$ and $K_{\dot{\theta}} = 677$. Therefore, the dimensionless flap equation is

$$\delta_c = 17.5(\theta_c - \theta) - 677\dot{\theta} + \delta_{css}. \qquad (4.5-1)$$

where δ_{css} is the steady state commanded flap deflection. The dimensionless equations used in this simulation are

$$\ddot{\theta} = R_y \qquad (4.5-2)$$

$$\ddot{\delta} = -0.4\dot{\delta} - 0.2(\delta - \delta_c) \qquad (4.5-3)$$

$$\delta_s = \delta \qquad (4.5-4)$$

and

$$\delta_p = \delta \tag{4.5-5}$$

where

$$R_y = \frac{1}{2}\rho S\bar{c}L^2\frac{C_{m_y}}{I_{yy}} = 0.000416C_{m_y}, \tag{4.5-6}$$

δ_s is the starboard deflection, and δ_p is the port deflection. The feedback control law is implemented by setting the commanded deflection at the start of the time step, and then holding it constant through that time step.

The results of implementing this feedback control law are presented in Figure 86 through Figure 91 where the pitch angle, flap-deflection angle, lift coefficient, drag coefficient, pitch-moment coefficient, and hinge-moment coefficient, respectively, are shown as functions of time. These figures present time with units of seconds, for direct comparison with the figures developed by using the optimal control law.

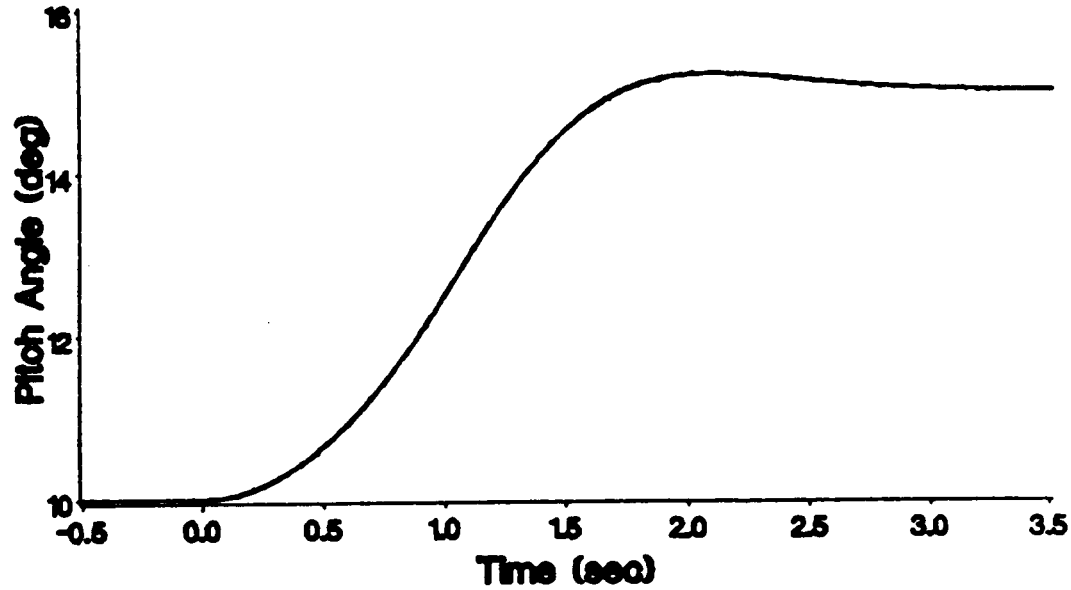

Figure 86. Feedback Control Pitch Angle

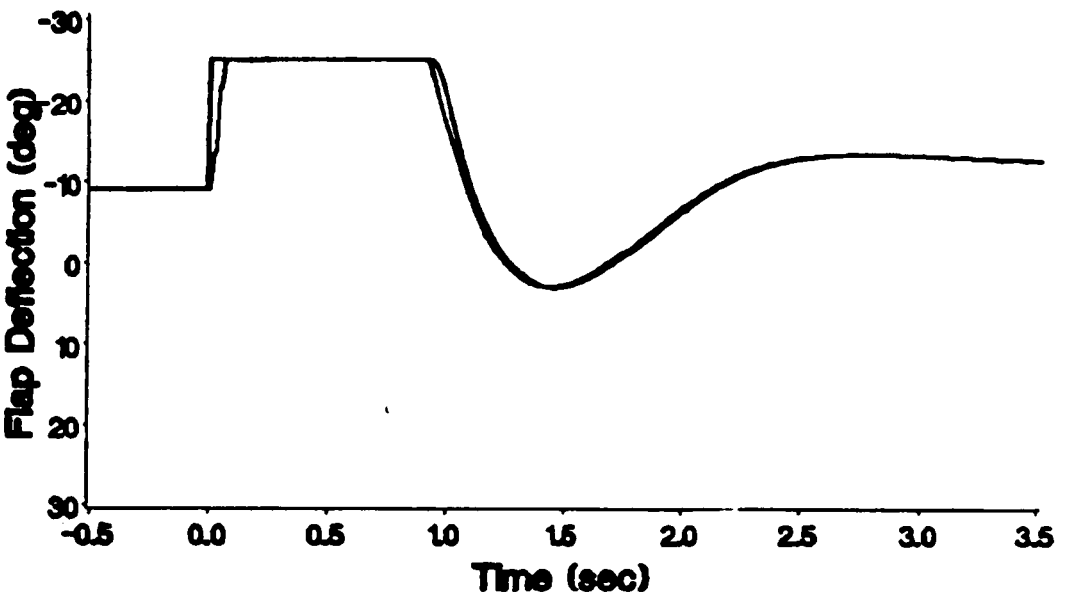

Figure 87. Feedback Control Flap Deflection

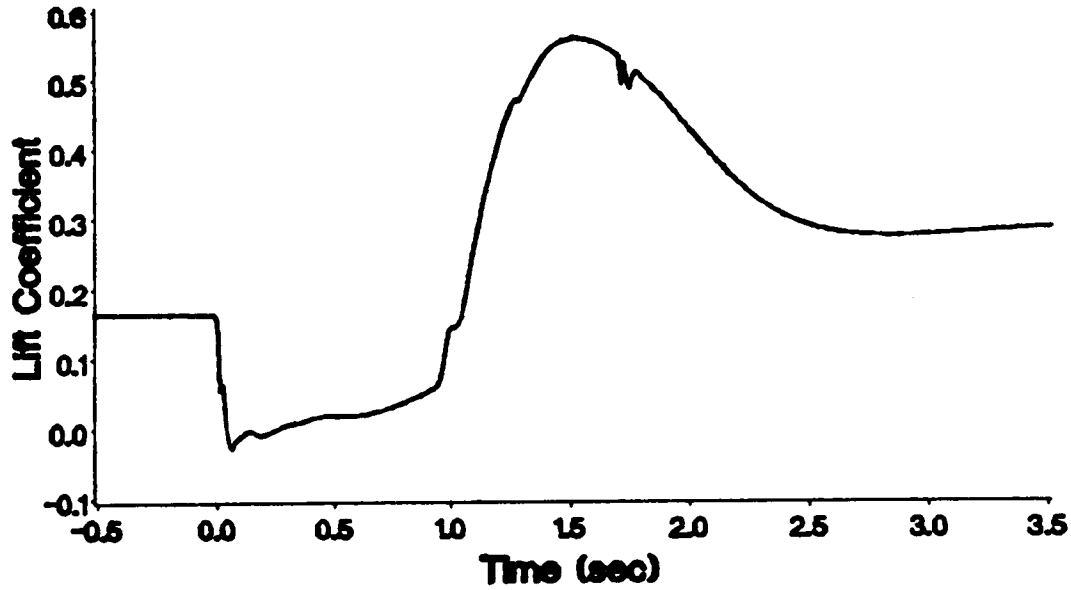

Figure 88. Feedback Control Lift Coefficient

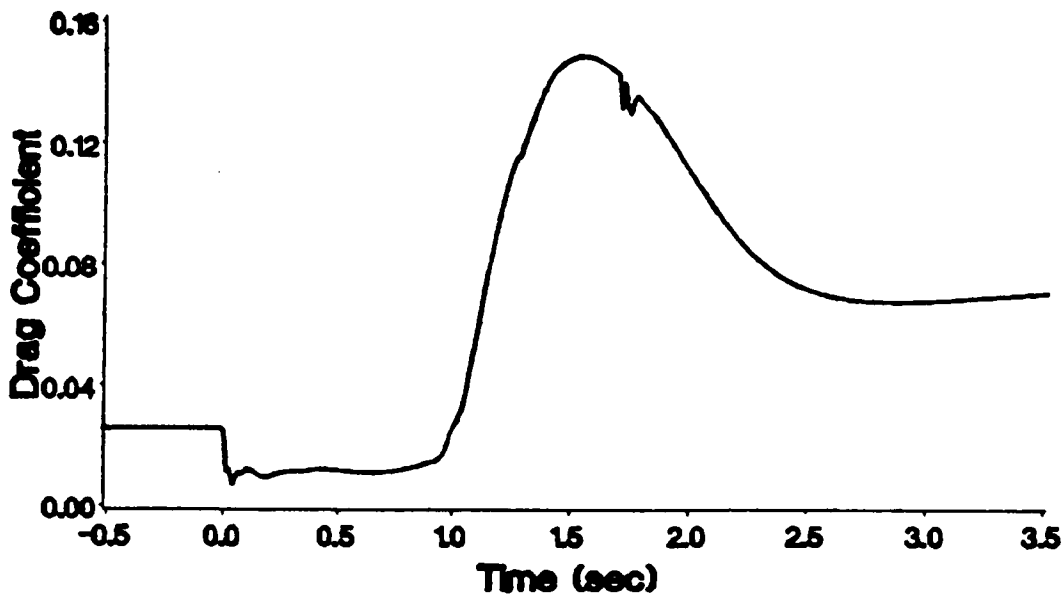

Figure 89. Feedback Control Drag Coefficient

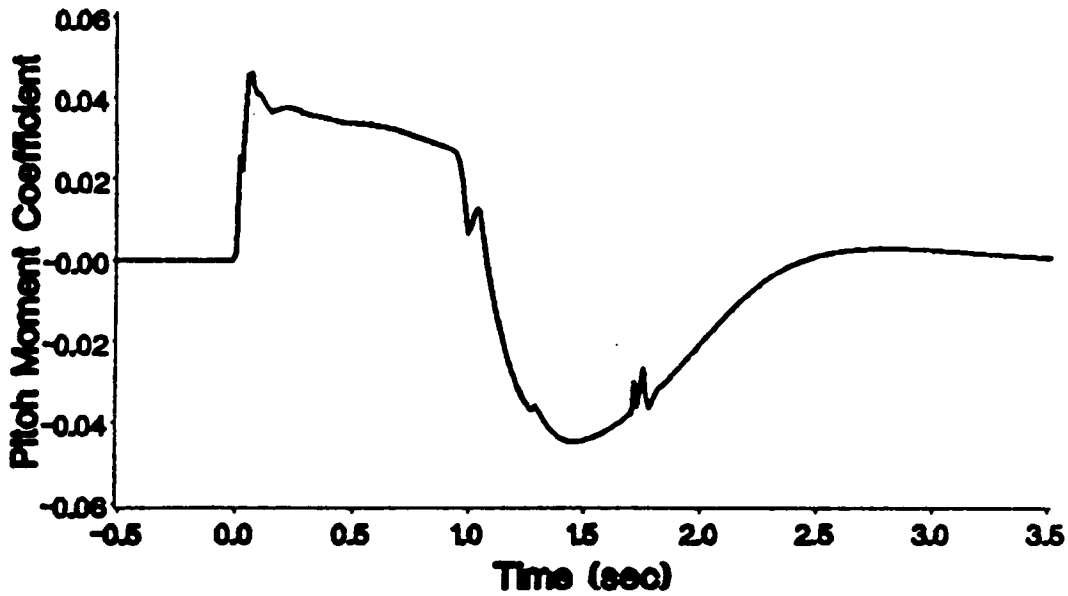

Figure 90. Feedback Control Pitch-Moment Coefficient

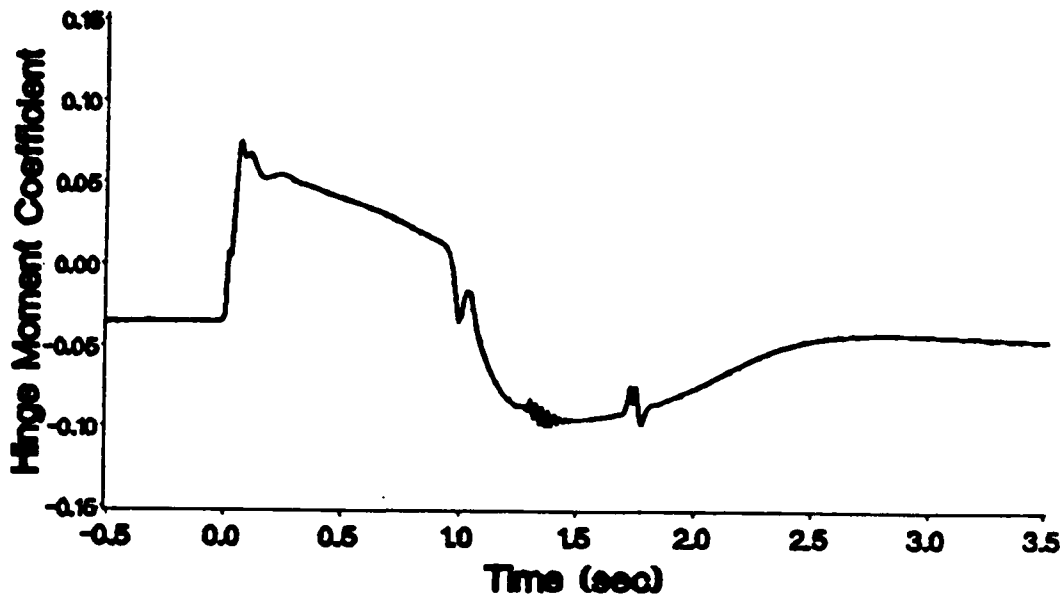

Figure 91. Feedback Control Hinge-Moment Coefficient

4.6 Feedback Control of Wing Rock

The applicability of using feedback control to change pitch orientation was demonstrated in Section 4.5. The use of feedback control will now be used to suppress the wing rock motion predicted in Section 3.6. All the physical conditions are the same as used in Section 3.6, except the damping term was set to zero. The feedback block diagram is shown in Figure 92.

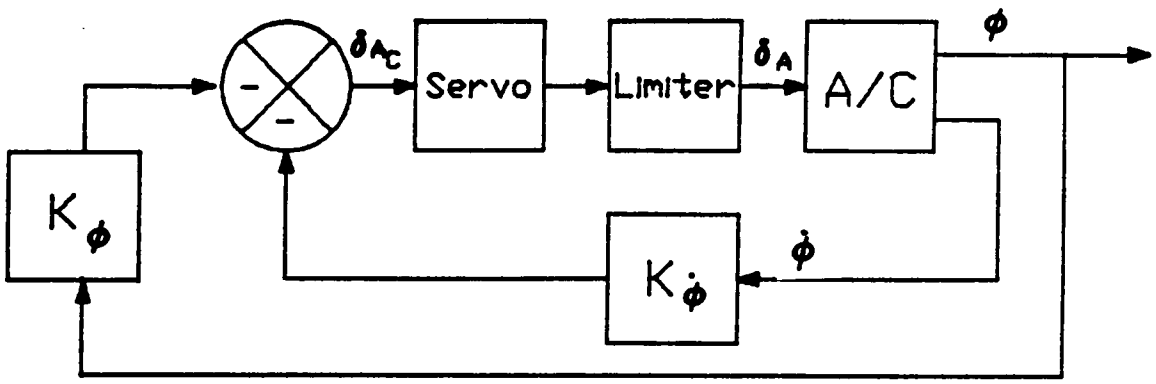

Figure 92. Feedback System to Suppress Wing Rock

The motion of the wing is restricted to one degree of freedom in roll. The dimensionless gains are chosen to be $K_\phi = 1.0$. and $K_{\dot\phi} = 20.0$. Therefore, the dimensionless feedback equation is

$$\delta_{A_c} = -1.0\phi - 20.0\dot{\phi}. \qquad (4.6-1)$$

This simple control law results from the command roll angle and the steady aileron deflection angle both being zero. The dimensionless equations used in this simulation are

$$\ddot{\phi} = R_x \qquad (4.6-2)$$

$$\ddot{\delta}_A = -0.4\dot{\delta}_A - 0.2(\delta_A - \delta_{A_c}) \qquad (4.6-3)$$

$$\delta_s = \delta_A \qquad (4.6-4)$$

and

$$\delta_p = -\delta_A \tag{4.6-5}$$

where

$$R_x = \frac{1}{2}\rho SbL^2 \frac{C_{m_x}}{I_{xx}} = 0.16342 C_{m_x}. \tag{4.5-6}$$

The initial conditions are

$$\begin{aligned} &\phi(0) = 5^\circ \,,\ \dot{\phi}(0) = 0 \,, \\ &\delta_{A_c}(0) = 0 \,,\ \delta_A(0) = 0 \text{ and } \dot{\delta}_A(0) = 0. \end{aligned} \tag{4.6-7}$$

The angle of attack is 27.5 degrees. This case is the same one that produced the wing rock of Section 3.6. The wing rock results were presented in Figure 62 through Figure 67. The simulation is run to a steady state at these initial conditions (10 chords). The wing is then released. The resulting roll motion is shown in Figure 93. The port aileron deflection is presented in Figure 94. The lift, rolling moment, yaw moment, starboard hinge moment and port hinge moment coefficients are shown in Figure 95 through Figure 99. From these figures, the rocking motion is shown to be suppressed. Again, areas exist where the predicted loads are not smooth. This situation is caused by the ailerons repeatedly passing through the plane of the wing.

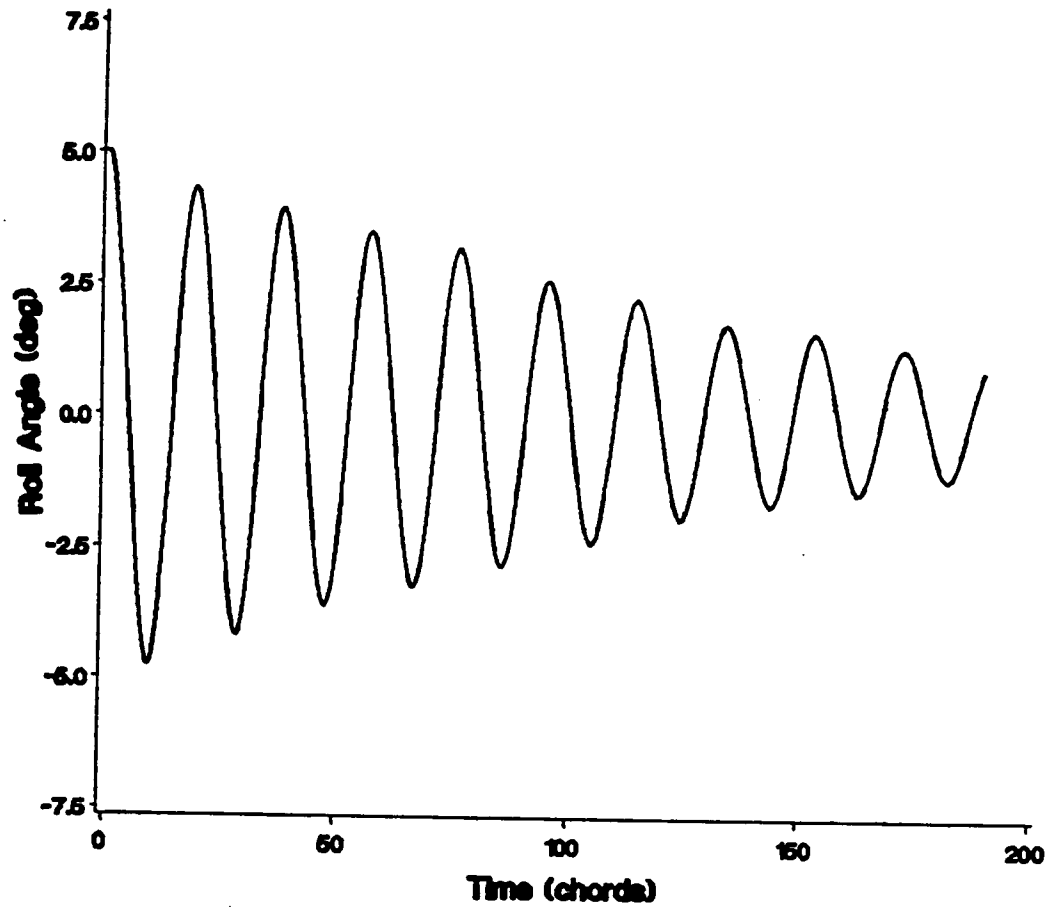

Figure 93. Feedback System Roll Angle

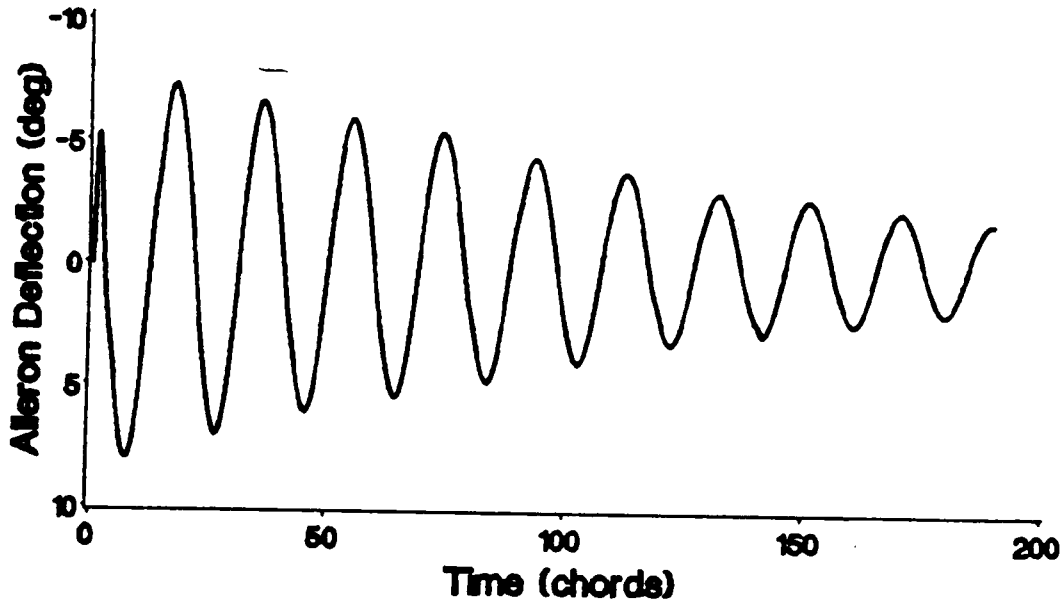

Figure 94. Feedback System Port Aileron Deflection

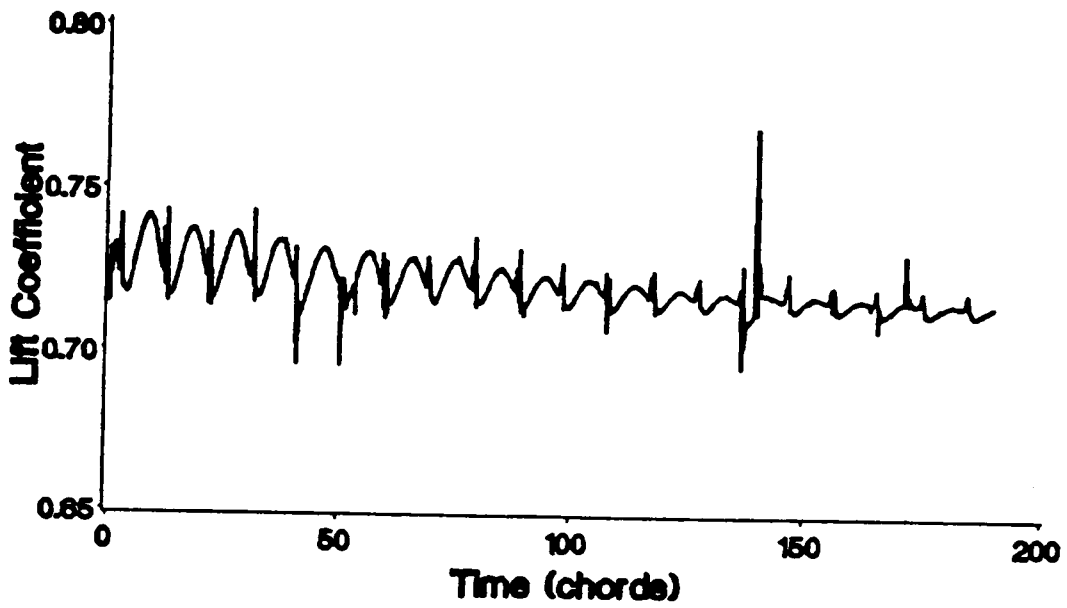

Figure 95. Feedback System Lift Coefficient

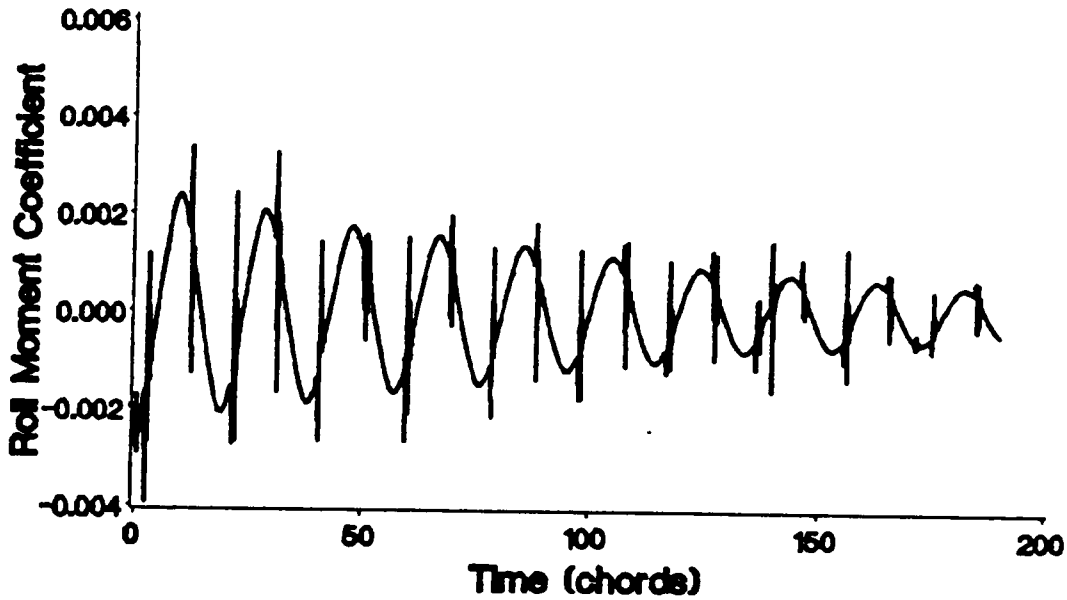

Figure 96. Feedback System Roll Moment Coefficient

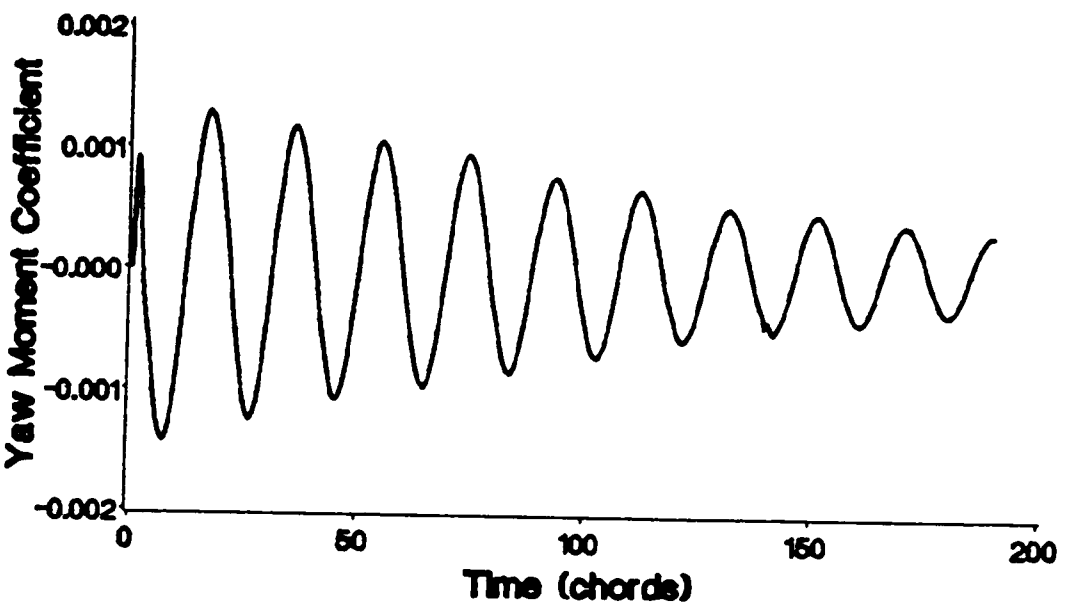

Figure 97. Feedback System Yaw Moment Coefficient

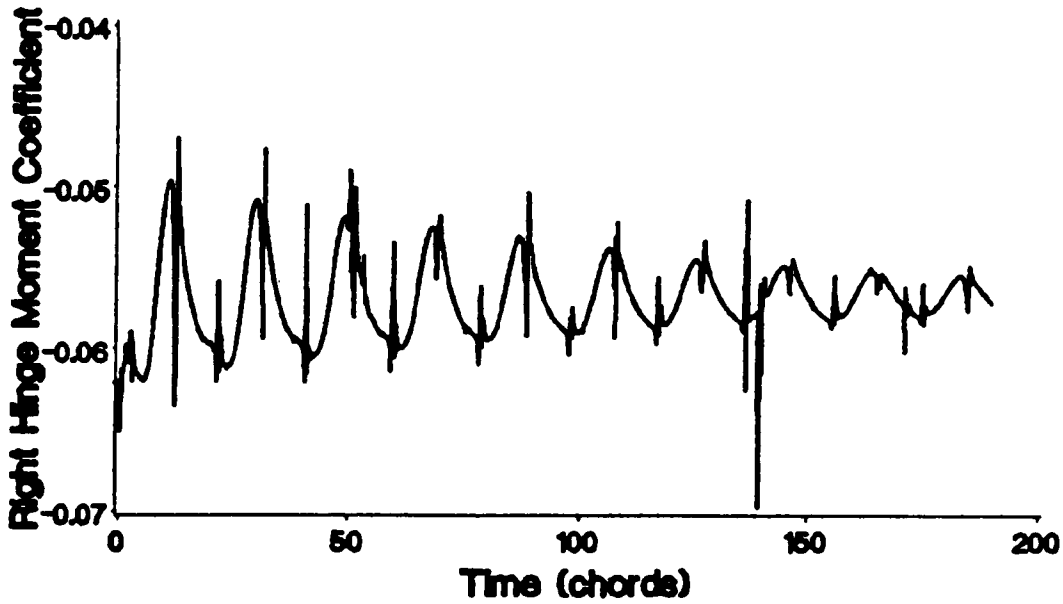

Figure 98. Feedback System Starboard Hinge Moment Coefficient

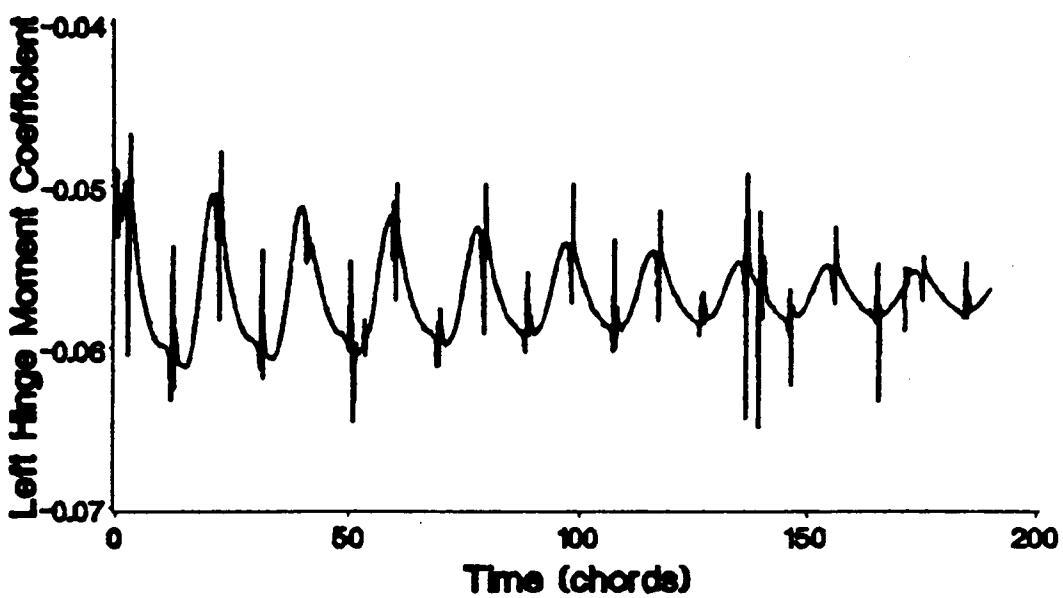

Figure 99. Feedback System Port Hinge Moment Coefficient

4.7 Conclusions for the Control Model

The nonlinear, unsteady aerodynamic/dynamic model was coupled with movement of control surfaces to produce desired changes in the orientation. Two types of control laws were developed, an open-loop near optimal and a closed-loop feedback system. The examples presented in this chapter illustrate the usefulness of the total system model.

As for the examples chosen, the feedback developed to change orientations is rather robust in that most gain settings produce reasonable results. The only problems occur when the flaps are used to maintain a large angle of attack (greater then 20 degrees). At these large pitch angles, the negative flap deflections lose their effectiveness. The control of the wing rock is not as simple. The gains selected are in a relatively narrow band of values where the rocking motion is suppressed. For small gains, the ailerons are not moved enough to be effective and for high gains, the actual deflection lags the commanded deflection by a significant amount. Thus instead of suppressing the motion the ailerons can actually add to the divergence rate of the motion.

Chapter V

Conclusions and Recommendations

5.1 Introduction

A completely unsteady aerodynamic model based on a vortex-panel method was developed. This model was coupled with equations of motion so that forced and free wind-tunnel tests could be simulated. The aerodynamic/dynamic model was also coupled with control laws that govern the motion of the control surfaces so that specified maneuvers could be performed.

5.2 Conclusions

The vortex-panel method developed in Chapter II provides a reasonably reliable unsteady aerodynamic model. The solution for closed nonlifting bodies is very accurate, especially when one considers the small number of elements used in the examples. One reason for the accuracy with so few panels is the rotation of the vorticity vector at the nodes of the surface mesh. Applying this method to closed bodies with sharp corners could give erroneous results, because the rotation of the vorticity vector assumes the surface is smooth

The method developed for thin lifting surfaces has several additional requirements beyond those needed for nonlifting closed bodies, all of which must be included for accurate simulation. These requirements are that a variable vortex core system must be included along the edge, the edge cores must be continuous through the first derivative, and the Kutta condition (no pressure jump from the upper to the lower surface) must be imposed at the trailing edge. Using these conditions, one finds that the results for thin flat rectangular surfaces are very accurate. No problems were encountered for this planform. The simulation of flows over delta planforms is not as robust. The method can be used to predict accurate solutions for this type of wing, but the solutions are influenced by the offset distance above the wing and the number of cores convected from the sides of the wing. For delta wings, the method performed

better for the lower aspect ratio wings. As noted in the forced oscillation tests, the higher aspect ratio wing did not have smooth aerodynamic characteristics. The adaptive grid technique, described in Section 2.13, is not unique to this method. It could be applied in any progressively formed vortex filament model of a wake.

The coupling of the dynamic equations of motion with the aerodynamic model is straightforward. This method can be used in conjunction with any aerodynamic model.

The addition of the control surfaces and the implementation of the control laws are also relatively straightforward. Though this work was the first attempt to couple the aerodynamic/dynamic simulation with a control law, few problems were experienced.

5.3 Recommendations

Several areas should be examined to either improve or extend the method. The improvements are needed in the aerodynamic model. The extensions are areas outside the scope of this investigation that will further the usefulness of the method.

Three areas exist that should be examined for improvement of the present aerodynamic model. These improvements are implementing the constraint equations, positioning the wake, and developing a better adaptive grid technique for the wake.

The constraint equations were imposed by the use of weighting factors. This method was chosen because it is easy to implement. The weights on these equations were found to be significantly larger than the no-penetration conditions. This weighting provided solutions that were insensitive to the specific weight employed. This result suggests that these equations should be imposed exactly. The method of weighted constraints cannot satisfy equality constraints exactly. One possible method would be to use Lagrange multipliers. A problem with imposing the constraints by using a Lagrange multiplier technique may exist because all the divergenceless equations are not independent. A better method may be to use a method of direct substitution.

In the current method the positioning of the wake was implemented by approximating the position by a first order finite difference formula. This approximation is inconsistent with the solution of the dynamic equations which are approximated with a fourth order predictor

corrector algorithm. This inconsistency could be removed by using a higher order approximation for the position. The problem with higher order approximations is that they require iteration. The positioning of the wake already uses the majority of the computer time during processing. Therefore the cost of a method that requires iteration might outweigh the benefits. Nevertheless, the impact of using a higher-order method should be investigated to determine the cost and benefit.

The adaptive grid technique developed for splitting the wake as it spreads should be re-examined. The method presented in Section 2.13 was found to provide a smoother wake than the approach used in the vortex-lattice techniques. The basic problems are with the implementation of the method. First, the splitting was implemented by assuming that after the wake element splits, the parts never rejoin. This assumption is valid, but was not implemented correctly for unsteady conditions. The current method identified a specific element of the wake by its position relative to the wing and once it split, it remained split. With the wing moving in an unsteady manner at one time the element might require adapting the grid. However, as time progresses, this split convects downstream and the element currently occupying the position relative to the wing may or may not split. For this reason, splitting in the wake was not used during the unsteady tests. The second problem with the implementation for splitting the wake is that a crossflow of circulation exists wherever a split occurs. This phenomeon is caused by one ring of circulation in the wake adjoining two rings at a split point. Because the one circulation cannot equal both downstream circulations a crossflow exists in the steady state. Physically, this situation should not be the case, but in order to satisfy the conservation of circulation requirements using the equations of Section 2.13, crossflow results. Some rectification of the physical system with the model needs to be developed.

The potential for extending the current method seems great. Several other areas should be developed. The first of these areas is to couple the current model with a structural model to provide a general unsteady aeroelastic model. The current method would be a good choice for the aerodynamic half of the model because the pressure is continuous on the body.

The second area to be developed is that the model should be extended to closed bodies with separation. This model would not have many problems with wing shapes because

the separation line is known. The model could be coupled with the boundary-layer equations to predict separation from the surface of a smooth body. As a by-product of this coupling, the form drag could be estimated.

The third area is to re-examine the basic form of the wake. The discretized wake used in this work is a good approximation to the wake surface, but it seems reasonable that a continuous vortex sheet would provide a better wake model. Before this improvement could be implemented the method of reducing the vortex strength of the wake sheet as it spreads will have to be developed.

The remaining areas are as follows. The model could easily be used to investigate ground effects, which could be done with images.

Next the model could be taken out of the wind tunnel and into the world. That is, the three position degrees of freedom should be included in the dynamic simulation. This possibility is not as straightforward as simply adding more differential equations, because the dimensionless equations require a constant reference velocity and the integration technique requires a constant step size. These problems might be circumvented by using the idea of computer-aided design programs that work entirely in physical units rather than scaled rules and using an integration scheme where the step size cannot be adjusted by the algorithm but is not constant for the entire test.

The final recommendation is completely aside from the development of this or any other aerodynamic model. Unsteady wind-tunnel experiments must be performed so that a means for validating unsteady computer simulations exists.

Appendix I

Velocity Induced by a Triangular Element

I.1 Integral Equations

The velocity induced by a general triangular element can in general, be written in the following form:

$$\vec{V}_d = V_x \vec{i} + V_y \vec{j} + V_z \vec{k},$$

where $\vec{V}_d$ is the velocity and $\vec{i}, \vec{j}$ and $\vec{k}$ are the unit vectors of the local coordinate frame of the element. As shown in Chapter II, the velocity induced by a vortex sheet can be written as

$$\vec{V}_d = \frac{1}{4\pi} \text{ curl} \iint_S \frac{\vec{\gamma}}{|\vec{r} - \vec{s}|} \, d\sigma.$$

where γ is the integral of the vorticity across the thickness of the sheet

$$\vec{\gamma} = \gamma_x \vec{i} + \gamma_y \vec{j},$$

The actual vorticity is approximated by the linear function

$$\vec{\gamma} = (\gamma_{x1} f_1 + \gamma_{x2} f_2 + \gamma_{x3} f_3) \vec{i} + (\gamma_{y1} f_1 + \gamma_{y2} f_2 + \gamma_{y3} f_3) \vec{j}$$

where γ_{xi} and γ_{yi} are unknown constants and the f_i are the following basis functions:

$$f_1 = a_1 x + b_1 y + 1$$

$$f_2 = a_2 x + b_2 y$$

$$f_3 = a_3 x + b_3 y$$

where

$$a_1 = -\frac{1}{a}\ ,\quad b_1 = \frac{b-a}{ac}\ ,\quad a_2 = \frac{1}{a}\ ,\quad b_2 = -\frac{b}{ac}\ ,\quad a_3 = 0 \quad \text{and} \quad b_3 = \frac{1}{c}\ .$$

The position vector to the point where the velocity is to be calculated is

$$\vec{r} = x_p\vec{i} + y_p\vec{j} + z_p\vec{k}$$

and the position vector to a point on the sheet is

$$\vec{s} = x\vec{i} + y\vec{j}\ .$$

For convenience we let

$$r^2 = |\vec{r} - \vec{s}\,|^2 = (x_p - x)^2 + (y_p - y)^2 + z_p^2.$$

In terms of the basis functions

$$f_1 = a_1x + b_1y + 1$$

$$f_2 = a_2x + b_2y$$

$$f_3 = a_3x + b_3y,$$

the linear variation of the vorticity on the element is

$$\vec{\gamma} = [\gamma_{x1}f_1 + \gamma_{x2}f_2 + \gamma_{x3}f_3]\vec{i} + [\gamma_{y1}f_1 + \gamma_{y2}f_2 + \gamma_{y3}f_3]\vec{j}\ .$$

Then the induced velocity is approximated by

$$\vec{V}_d = \frac{1}{4\pi}\ \text{curl} \iint_S \frac{1}{r}[(\gamma_{x1}\vec{i} + \gamma_{y1}\vec{j})f_1 + (\gamma_{x2}\vec{i} + \gamma_{y2}\vec{j})f_2 + (\gamma_{x3}\vec{i} + \gamma_{y3}\vec{j})f_3]\ dxdy.$$

Because γ_{xi}, γ_{yi}, a_i and b_i are constant, the velocity can be written as

$$\vec{V}_d = \frac{1}{4\pi}\,\mathrm{curl}\{[(\gamma_{x1}\vec{i} + \gamma_{y1}\vec{j})a_1 + (\gamma_{x2}\vec{i} + \gamma_{y2}\vec{j})a_2 + (\gamma_{x3}\vec{i} + \gamma_{y3}\vec{j})a_3]\iint_S \frac{x}{r}\,dxdy$$
$$+ [(\gamma_{x1}\vec{i} + \gamma_{y1}\vec{j})b_1 + (\gamma_{x2}\vec{i} + \gamma_{y2}\vec{j})b_2 + (\gamma_{x3}\vec{i} + \gamma_{y3}\vec{j})b_3]\iint_S \frac{y}{r}\,dxdy$$
$$+ (\gamma_{x1}\vec{i} + \gamma_{y1}\vec{j})\iint_S \frac{1}{r}\,dxdy\}.$$

Adding and subtracting x_p from the first integral, y_p from the second and using the fact that neither of these depends on x or y, one can write the velocity vector as follows

$$\vec{V}_d = \frac{1}{4\pi}\,\mathrm{curl}\{[(\gamma_{x1}\vec{i} + \gamma_{y1}\vec{j})a_1 + (\gamma_{x2}\vec{i} + \gamma_{y2}\vec{j})a_2 + (\gamma_{x3}\vec{i} + \gamma_{y3}\vec{j})a_3]\iint_S \frac{x - x_p}{r}\,dxdy$$
$$+ [(\gamma_{x1}\vec{i} + \gamma_{y1}\vec{j})b_1 + (\gamma_{x2}\vec{i} + \gamma_{y2}\vec{j})b_2 + (\gamma_{x3}\vec{i} + \gamma_{y3}\vec{j})b_3]\iint_S \frac{y - y_p}{r}\,dxdy$$
$$+ [(\gamma_{x1}\vec{i} + \gamma_{y1}\vec{j})(a_1x_p + b_1y_p + 1) + (\gamma_{x2}\vec{i} + \gamma_{y2}\vec{j})(a_2x_p + b_2y_p)$$
$$+ (\gamma_{x3}\vec{i} + \gamma_{y3}\vec{j})(a_3x_p + b_3y_p)]\iint_S \frac{1}{r}\,dxdy\}.$$

Index notation can be used to reduce the expression above to

$$\vec{V}_d = \frac{1}{4\pi}\,\mathrm{curl}\sum_{n=1}^{3}(\gamma_{xn}\vec{i} + \gamma_{yn}\vec{j})B_n$$

where

$$B_n = a_n\iint_S \frac{x - x_p}{r}\,dxdy + b_n\iint_S \frac{y - y_p}{r}\,dxdy + (a_nx_p + b_ny_p + \delta_{n1})\iint_S \frac{1}{r}\,dxdy$$

and δ_{n1} is the Kronecker delta.

Expanding the curl results in

$$V_x = -\frac{1}{4\pi}\sum_{n=1}^{3}\gamma_{yn}\frac{\partial B_n}{\partial z_p}$$

$$V_y = \frac{1}{4\pi} \sum_{n=1}^{3} \gamma_{xn} \frac{\partial B_n}{\partial z_p}$$

$$V_z = \frac{1}{4\pi} \sum_{n=1}^{3} \left[\gamma_{yn} \frac{\partial B_n}{\partial x_p} - \gamma_{xn} \frac{\partial B_n}{\partial y_p} \right]$$

where

$$\frac{\partial B_n}{\partial x_p} = a_n \frac{\partial}{\partial x_p} \iint_S \frac{x - x_p}{r} \, dxdy + b_n \frac{\partial}{\partial x_p} \iint_S \frac{y - y_p}{r} \, dxdy + (a_n x_p + b_n y_p + \delta_{n1}) \frac{\partial}{\partial x_p} \iint_S \frac{1}{r} \, dxdy + a_n \iint_S \frac{1}{r} \, dxdy$$

$$\frac{\partial B_n}{\partial y_p} = a_n \frac{\partial}{\partial y_p} \iint_S \frac{x - x_p}{r} \, dxdy + b_n \frac{\partial}{\partial y_p} \iint_S \frac{y - y_p}{r} \, dxdy + (a_n x_p + b_n y_p + \delta_{n1}) \frac{\partial}{\partial y_p} \iint_S \frac{1}{r} \, dxdy + b_n \iint_S \frac{1}{r} \, dxdy$$

and

$$\frac{\partial B_n}{\partial z_p} = a_n \frac{\partial}{\partial z_p} \iint_S \frac{x - x_p}{r} \, dxdy + b_n \frac{\partial}{\partial z_p} \iint_S \frac{y - y_p}{r} \, dxdy + (a_n x_p + b_n y_p + \delta_{n1}) \frac{\partial}{\partial z_p} \iint_S \frac{1}{r} \, dxdy.$$

Next some new notation is introduced:

$$I_1 = \frac{\partial}{\partial x_p} \iint_S \frac{x - x_p}{r} \, dxdy$$

$$I_2 = \frac{\partial}{\partial y_p} \iint_S \frac{x - x_p}{r} \, dxdy$$

$$I_3 = \frac{\partial}{\partial z_p} \iint_S \frac{x - x_p}{r} \, dxdy$$

$$I_4 = \frac{\partial}{\partial x_p} \iint_S \frac{y - y_p}{r} \, dxdy$$

$$I_5 = \frac{\partial}{\partial y_p} \iint_S \frac{y - y_p}{r} \, dxdy$$

$$I_6 = \frac{\partial}{\partial z_p} \iint_S \frac{y - y_p}{r} \, dxdy$$

$$I_7 = \frac{\partial}{\partial x_p} \iint_S \frac{1}{r} \, dxdy$$

$$I_8 = \frac{\partial}{\partial y_p} \iint_S \frac{1}{r} \, dxdy$$

$$I_9 = \frac{\partial}{\partial z_p} \iint_S \frac{1}{r} \, dxdy$$

$$I_{10} = \iint_S \frac{1}{r} \, dxdy.$$

In terms of the new notation, the velocity components are

$$\begin{aligned} V_x = -\frac{1}{4\pi} [& \gamma_{y1}(a_1 I_3 + b_1 I_6 + a_1 x_p I_9 + b_1 y_p I_9 + I_9) \\ & + \gamma_{y2}(a_2 I_3 + b_2 I_6 + a_2 x_p I_9 + b_2 y_p I_9) \\ & + \gamma_{y3}(a_3 I_3 + b_3 I_6 + a_3 x_p I_9 + b_3 y_p I_9)] \end{aligned}$$

$$V_y = \frac{1}{4\pi}\left[\gamma_{x1}(a_1 I_3 + b_1 I_6 + a_1 x_p I_9 + b_1 y_p I_9 + I_9) + \gamma_{x2}(a_2 I_3 + b_2 I_6 + a_2 x_p I_9 + b_2 y_p I_9) + \gamma_{x3}(a_3 I_3 + b_3 I_6 + a_3 x_p I_9 + b_3 y_p I_9)\right]$$

and

$$\begin{aligned} V_z = \frac{1}{4\pi}\Big[& \gamma_{y1}(a_1 I_1 + b_1 I_4 + a_1 x_p I_7 + b_1 y_p I_7 + I_7 + a_1 I_{10}) \\ & - \gamma_{x1}(a_1 I_2 + b_1 I_5 + a_1 x_p I_8 + b_1 y_p I_8 + I_8 + b_1 I_{10}) \\ & + \gamma_{y2}(a_2 I_1 + b_2 I_4 + a_2 x_p I_7 + b_2 y_p I_7 + a_2 I_{10}) \\ & - \gamma_{x2}(a_2 I_2 + b_2 I_5 + a_2 x_p I_8 + b_2 y_p I_8 + b_2 I_{10}) \\ & + \gamma_{y3}(a_3 I_1 + b_3 I_4 + a_3 x_p I_7 + b_3 y_p I_7 + a_3 I_{10}) \\ & - \gamma_{x3}(a_3 I_2 + b_3 I_5 + a_3 x_p I_8 + b_3 y_p I_8 + b_3 I_{10})\Big]. \end{aligned}$$

I.2 Evaluation of the Integrals

The components of the disturbance velocity have been expressed in terms of the integrals I_1 through I_{10}. In this section these integrals will be evaluated. The first integral is

$$I_1 = \frac{\partial}{\partial x_p}\iint_S \frac{x - x_p}{r}\, dxdy.$$

With the definition of $\vec{r}$, I_1 can be rewritten as

$$I_1 = \frac{\partial}{\partial x_p}\iint_S \frac{x - x_p}{[(x - x_p)^2 + (y - y_p)^2 + z_p^2]^{1/2}}\, dxdy.$$

The general triangular element, area S, is shown in Figure 100. The integral over the area of the triangle is then

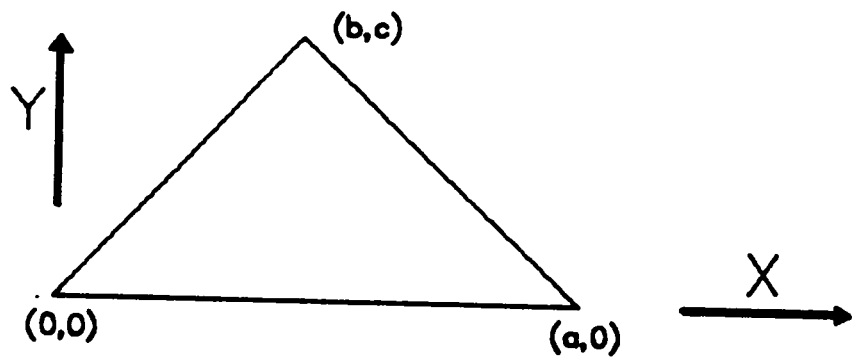

Figure 100. Triangular Element

$$I_1 = \frac{\partial}{\partial x_p} \int_0^c \int_{\frac{b}{c}y}^{\frac{b-a}{c}y+a} \frac{x - x_p}{[(x-x_p)^2 + (y-y_p)^2 + z_p^2]^{1/2}} \, dx dy.$$

Let

$$u = [(x-x_p)^2 + (y-y_p)^2 + z_p^2],$$

then I_1 can be written as

$$I_1 = \frac{\partial}{\partial x_p} \int_0^c \int_{\frac{b}{c}y}^{\frac{b-a}{c}y+a} \frac{du}{2u^{1/2}} \, dy$$

$$= \frac{\partial}{\partial x_p} \int_0^c u^{1/2} \Big|_{\frac{b}{c}y}^{\frac{b-a}{c}y+a} dy$$

$$= \int_0^c \frac{\partial}{\partial x_p} [(\frac{b-a}{c}y + a - x_p)^2 + (y-y_p)^2 + z_p^2]^{1/2}$$
$$- \frac{\partial}{\partial x_p} [(\frac{b}{c}y - x_p)^2 + (y-y_p)^2 + z_p^2]^{1/2} \, dy,$$

$$
\begin{aligned}
I_1 = {} & (x_p - a)\int_0^c [(\tfrac{b-a}{c}y + a - x_p)^2 + (y - y_p)^2 + z_p^2]^{-1/2}\,dy \\
& + \tfrac{a-b}{c}\int_0^c y\,[(\tfrac{b-a}{c}y + a - x_p)^2 + (y - y_p)^2 + z_p^2]^{-1/2}\,dy \\
& - x_p\int_0^c [(\tfrac{b}{c}y - x_p)^2 + (y - y_p)^2 + z_p^2]^{-1/2}\,dy \\
& + \tfrac{b}{c}\int_0^c y\,[(\tfrac{b}{c}y - x_p)^2 + (y - y_p)^2 + z_p^2]^{-1/2}\,dy.
\end{aligned}
$$

Next let

$$H_1 = \int_0^c [(\tfrac{b-a}{c}y + a - x_p)^2 + (y - y_p)^2 + z_p^2]^{-1/2}\,dy$$

$$H_2 = \int_0^c y\,[(\tfrac{b-a}{c}y + a - x_p)^2 + (y - y_p)^2 + z_p^2]^{-1/2}\,dy$$

$$H_3 = \int_0^c [(\tfrac{b}{c}y - x_p)^2 + (y - y_p)^2 + z_p^2]^{-1/2}\,dy$$

$$H_4 = \int_0^c y\,[(\tfrac{b}{c}y - x_p)^2 + (y - y_p)^2 + z_p^2]^{-1/2}\,dy,$$

then I_1 can be written as

$$I_1 = (x_p - a)H_1 + \left(\frac{a-b}{c}\right)H_2 - x_pH_3 + \frac{b}{c}H_4.$$

Next the evaluation of H_1:

$$H_1 = \int_0^c [(\tfrac{b-a}{c}y + a - x_p)^2 + (y - y_p)^2 + z_p^2]^{-1/2}\,dy.$$

After expanding the squares and collecting terms, one finds

$$H_1 = \int_0^c \left\{ \left[\left(\frac{b-a}{c} \right)^2 + 1 \right] y^2 + 2 \left[\left(\frac{b-a}{c} \right)(a - x_p) - y_p \right] y + (a - x_p)^2 + y_p^2 + z_p^2 \right\}^{-1/2} dy.$$

Defining

$$\alpha_1 = \left(\frac{b-a}{c} \right)^2 + 1 = \left(\frac{a-b}{c} \right)^2 + 1$$

$$\alpha_2 = \left(\frac{b-a}{c} \right)(a - x_p) - y_p$$

and

$$r_3^2 = (a - x_p)^2 + y_p^2 + z_p^2.$$

We note that r_3 is the distance from the vertex at (a,0) to the field point (x_p, y_p, z_p). One can write

$$H_1 = \int_0^c [\alpha_1 y^2 + 2\alpha_2 y + r_3^2]^{-1/2} dy.$$

Completing the square results in

$$H_1 = \frac{1}{\sqrt{\alpha_1}} \int_0^c \left[\left(y + \frac{\alpha_2}{\alpha_1} \right)^2 - \left(\frac{\alpha_2}{\alpha_1} \right)^2 + \frac{r_3^2}{\alpha_1} \right]^{-1/2} dy.$$

In general,

$$\int [u^2 + a^2]^{-1/2} du = \ln[u + (u^2 + a^2)^{1/2}],$$

it follows that

$$H_1 = = \frac{1}{\sqrt{\alpha_1}} \ln\left\{ \frac{c\alpha_1 + \alpha_2 + \left[(c\alpha_1 + \alpha_2)^2 - \alpha_2^2 + r_3^2\alpha_1\right]^{1/2}}{\alpha_2 + \sqrt{\alpha_1}\, r_3} \right\}.$$

Now letting

$$r_2^2 = c^2\alpha_1 + 2c\alpha_2 + r_3^2,$$

$$= (x_p - b)^2 + (y_p - c)^2 + z_p.$$

We note that r_2 is the distance from the vertex (b,c) to the field point (x_p, y_p, z_p). Then

$$H_1 = \frac{1}{\sqrt{\alpha_1}} \ln\left\{ \frac{c\alpha_1 + \alpha_2 + \sqrt{\alpha_1}\, r_2}{\alpha_2 + \sqrt{\alpha_1}\, r_3} \right\}.$$

Now the evaluation of H_2:

$$H_2 = \int_0^c y\left[\left(\frac{b-a}{c}y + a - x_p\right)^2 + (y - y_p)^2 + z_p^2\right]^{-1/2} dy$$

$$= \frac{1}{\sqrt{\alpha_1}} \int_0^c y\left[\left(y + \frac{\alpha_2}{\alpha_1}\right)^2 - \left(\frac{\alpha_2}{\alpha_1}\right)^2 + \frac{r_3^2}{\alpha_1}\right]^{-1/2} dy.$$

Adding and subtracting $\frac{\alpha_2}{\alpha_1}$ to the first factor in the integral results in

$$H_2 = \frac{1}{\sqrt{\alpha_1}} \int_0^c \left(y + \frac{\alpha_2}{\alpha_1}\right)\left[\left(y + \frac{\alpha_2}{\alpha_1}\right)^2 - \left(\frac{\alpha_2}{\alpha_1}\right)^2 + \frac{r_3^2}{\alpha_1}\right]^{-1/2} dy$$
$$- \frac{1}{\sqrt{\alpha_1}} \int_0^c \frac{\alpha_2}{\alpha_1}\left[\left(y + \frac{\alpha_2}{\alpha_1}\right)^2 - \left(\frac{\alpha_2}{\alpha_1}\right)^2 + \frac{r_3^2}{\alpha_1}\right]^{-1/2} dy.$$

The variable substitution

$$u = \left(y + \frac{\alpha_2}{\alpha_1}\right)^2 - \left(\frac{\alpha_2}{\alpha_1}\right)^2 + \frac{r_3^2}{\alpha_1}$$

yields

$$H_2 = \frac{1}{\sqrt{\alpha_1}} \int_0^c \frac{du}{2u^{1/2}} - \frac{\alpha_2}{\alpha_1} H_1$$

$$= \frac{1}{\sqrt{\alpha_1}} u^{1/2} \Big|_0^c - \frac{\alpha_2}{\alpha_1} H_1$$

$$= \frac{1}{\sqrt{\alpha_1}} \left[\left[\left(c + \frac{\alpha_2}{\alpha_1} \right)^2 - \left(\frac{\alpha_2}{\alpha_1} \right)^2 + \frac{r_3^2}{\alpha_1} \right]^{1/2} - \left[\left(\frac{\alpha_2}{\alpha_1} \right)^2 - \left(\frac{\alpha_2}{\alpha_1} \right)^2 + \frac{r_3^2}{\alpha_1} \right]^{1/2} \right] - \frac{\alpha_2}{\alpha_1} H_1$$

$$= \frac{1}{\alpha_1} \left[\frac{1}{\sqrt{\alpha_1}} \left[(c\alpha_1 + \alpha_2)^2 - (\alpha_2)^2 + r_3^2 \alpha_1 \right]^{1/2} - r_3 \right] - \frac{\alpha_2}{\alpha_1} H_1.$$

The definition of r_2 gives

$$H_2 = \frac{1}{\alpha_1} (r_2 - r_3) - \frac{\alpha_2}{\alpha_1} H_1.$$

Now the evaluation of H_3:

$$H_3 = \int_0^c \left[\left(\frac{b}{c} y - x_p \right)^2 + (y - y_p)^2 + z_p^2 \right]^{-1/2} dy$$

which can be rewritten as

$$H_3 = \frac{1}{\sqrt{\alpha_3}} \int_0^c \left[y^2 - 2 \frac{\alpha_4}{\alpha_3} y + \frac{r_1^2}{\alpha_3} \right]^{-1/2} dy.$$

where

$$\alpha_3 = \left(\frac{b}{c} \right)^2 + 1$$

$$\alpha_4 = \left(\frac{b}{c} \right) x_p + y_p$$

and

$$r_1^2 = x_p^2 + y_p^2 + z_p^2.$$

We note that r_1 is the distance from the vertex (0,0) to the field point (x_p, y_p, z_p). Completing the square results in

$$H_3 = \frac{1}{\sqrt{\alpha_3}} \int_0^c \left[\left(y - \frac{\alpha_4}{\alpha_3} \right)^2 - \left(\frac{\alpha_4}{\alpha_3} \right)^2 + \frac{r_1^2}{\alpha_3} \right]^{-1/2} dy$$

$$= \frac{1}{\sqrt{\alpha_3}} \ln \left\{ \frac{\left(c - \frac{\alpha_4}{\alpha_3} \right) + \left[\left(c - \frac{\alpha_4}{\alpha_3} \right)^2 - \left(\frac{\alpha_4}{\alpha_3} \right)^2 + \frac{r_3^2}{\alpha_3} \right]^{1/2}}{\frac{\alpha_4}{\alpha_3} + \left[\left(\frac{\alpha_4}{\alpha_3} \right)^2 - \left(\frac{\alpha_4}{\alpha_3} \right)^2 + \frac{r_1^2}{\alpha_3} \right]^{1/2}} \right\}$$

$$= \frac{1}{\sqrt{\alpha_3}} \ln \left\{ \frac{c\alpha_3 - \alpha_4 + \left[(c\alpha_3 - \alpha_4)^2 - \alpha_4^2 + r_1^2 \alpha_3 \right]^{1/2}}{-\alpha_4 + \sqrt{\alpha_3}\, r_1} \right\}.$$

The definition of r_1, α_3 and α_4 can be used to reduce the square-root term in the numerator to

$$(c\alpha_3 - \alpha_4)^2 - \alpha_4^2 + r_1^2 \alpha_3 = \alpha_3 \left[b^2 + c^2 - 2c(bx_p + cy_p) + x_p^2 + y_p^2 + z_p^2 \right]$$

$$= \alpha_3 \left[(x_p - b)^2 + (y_p - c)^2 + z_p^2 \right].$$

then

$$H_3 = \frac{1}{\sqrt{\alpha_3}} \ln \left\{ \frac{c\alpha_3 - \alpha_4 + \sqrt{\alpha_3}\, r_2}{-\alpha_4 + \sqrt{\alpha_3}\, r_1} \right\}.$$

Finally the evaluation of H_4:

$$H_4 = \int_0^c y \left[\left(\frac{b}{c} y - x_p \right)^2 + (y - y_p)^2 + z_p^2 \right]^{-1/2} dy$$

$$H_4 = \int_0^c y\left[\left(\left(\frac{b}{c}\right)^2 + 1\right)y^2 - 2\left(\frac{bx_p}{c} + y_p\right)y + x_p^2 - y_p^2 + z_p^2\right]^{-1/2} dy$$

$$= \int_0^c \frac{y}{[\alpha_3 y^2 - 2\alpha_4 y + r_1^2]^{1/2}}\, dy.$$

Adding and subtracting $\frac{\alpha_4}{\alpha_3}$ to the factor in the numerator yields

$$H_4 = \frac{1}{\sqrt{\alpha_3}} \int_0^c \left(y - \frac{\alpha_4}{\alpha_3}\right)\left[\left(y - \frac{\alpha_4}{\alpha_3}\right)^2 - \left(\frac{\alpha_4}{\alpha_3}\right)^2 + \frac{r_1^2}{\alpha_3}\right]^{-1/2} dy$$
$$+ \frac{1}{\sqrt{\alpha_3}} \int_0^c \frac{\alpha_4}{\alpha_3}\left[\left(\frac{\alpha_4}{\alpha_3}\right)^2 - \left(\frac{\alpha_4}{\alpha_3}\right)^2 + \frac{r_1^2}{\alpha_3}\right]^{-1/2} dy$$

$$= \frac{1}{\sqrt{\alpha_3}}\left[\left(y - \frac{\alpha_4}{\alpha_3}\right)^2 - \left(\frac{\alpha_4}{\alpha_3}\right)^2 + \frac{r_1^2}{\alpha_3}\right]^{1/2}\Big|_0^c + \frac{\alpha_4}{\alpha_3} H_3$$

$$= \frac{1}{\alpha_3}\left[\left[\frac{(c\alpha_3 - \alpha_4)^2}{\alpha_3} - \frac{\alpha_4^2}{\alpha_3} + r_1^2\right]^{1/2} - r_1\right] + \frac{\alpha_4}{\alpha_3} H_3.$$

The previously derived relation of r_2 can be used to obtain

$$H_4 = \frac{1}{\alpha_3}(r_2 - r_1) + \frac{\alpha_4}{\alpha_3} H_3.$$

This completes the evaluation of the first integral.

The second integral is

$$I_2 = \frac{\partial}{\partial y_p} \iint_S \frac{x - x_p}{r}\, dxdy.$$

Following the same procedure as for I_1, one can obtain

$$I_2 = \frac{\partial}{\partial y_p} \int_0^c \int_{\frac{b}{c}y}^{\frac{b-a}{c}y+a} \frac{x - x_p}{[(x-x_p)^2 + (y-y_p)^2 + z_p^2]^{1/2}} \, dx dy$$

$$= \int_0^c \frac{\partial}{\partial y_p} [(\frac{b-a}{c}y + a - x_p)^2 + (y-y_p)^2 + z_p^2]^{1/2}$$
$$- \frac{\partial}{\partial y_p} [(\frac{b}{c}y - x_p)^2 + (y-y_p)^2 + z_p^2]^{1/2} \, dy$$

$$= -\int_0^c (y-y_p)\Big\{[(\frac{b-a}{c}y + a - x_p)^2 + (y-y_p)^2 + z_p^2]^{-1/2}$$
$$- [(\frac{b}{c}y - x_p)^2 + (y-y_p)^2 + z_p^2]^{-1/2} \, dy\Big\}$$

$$= y_p \int_0^c [(\frac{b-a}{c}y + a - x_p)^2 + (y-y_p)^2 + z_p^2]^{-1/2} \, dy$$
$$- \int_0^c y [(\frac{b-a}{c}y + a - x_p)^2 + (y-y_p)^2 + z_p^2]^{-1/2} \, dy$$
$$- y_p \int_0^c [(\frac{b}{c}y - x_p)^2 + (y-y_p)^2 + z_p^2]^{-1/2} \, dy$$
$$+ \int_0^c y [(\frac{b}{c}y - x_p)^2 + (y-y_p)^2 + z_p^2]^{-1/2} \, dy.$$

Then using the definitions of the H_i, one can write

$$I_2 = y_p(H_1 - H_3) + H_4 - H_2.$$

The third integral is

$$I_3 = \frac{\partial}{\partial z_p} \iint_S \frac{x - x_p}{r} \, dx dy.$$

Following the same procedure, one can write

$$I_3 = \frac{\partial}{\partial z_p} \int_0^c \int_{\frac{b}{c}y}^{\frac{b-a}{c}y+a} \frac{x - x_p}{[(x-x_p)^2 + (y-y_p)^2 + z_p^2]^{1/2}} \, dx dy$$

$$I_3 = \int_0^c \Big\{ z_p[(\frac{b-a}{c}y + a - x_p)^2 + (y-y_p)^2 + z_p^2]^{-1/2} - z_p[(\frac{b}{c}y - x_p)^2 + (y-y_p)^2 + z_p^2]^{-1/2} \Big\}\, dy$$

$$= z_p \int_0^c [(\frac{b-a}{c}y + a - x_p)^2 + (y-y_p)^2 + z_p^2]^{-1/2}\, dy - z_p \int_0^c [(\frac{b}{c}y - x_p)^2 + (y-y_p)^2 + z_p^2]^{-1/2}\, dy.$$

Then

$$I_3 = z_p(H_1 - H_3).$$

The fourth integral is

$$I_4 = \frac{\partial}{\partial x_p} \iint_S \frac{y - y_p}{r}\, dxdy$$

In the local coordinate frame of the triangular element, the longest side of the triangle is always placed along the positive x axis. This allows the integral to be easily written integrating with respect to y first.

$$I_4 = \frac{\partial}{\partial x_p} \int_0^b \int_0^{\frac{c}{b}x} \frac{y - y_p}{[(x-x_p)^2 + (y-y_p)^2 + z_p^2]^{1/2}}\, dydx + \frac{\partial}{\partial x_p} \int_b^a \int_0^{\frac{c}{(b-a)}(x-a)} \frac{y - y_p}{[(x-x_p)^2 + (y-y_p)^2 + z_p^2]^{1/2}}\, dydx.$$

Evaluating the inside integral results in

$$I_4 = \int_0^b \frac{\partial}{\partial x_p}\left[(x-x_p)^2 + \left(\frac{c}{b}x - y_p\right)^2 + z_p^2\right]^{1/2} dx$$
$$- \int_0^b \frac{\partial}{\partial x_p}\left[(x-x_p)^2 + y_p^2 + z_p^2\right]^{1/2} dx$$
$$+ \int_b^a \frac{\partial}{\partial x_p}\left[(x-x_p)^2 + \left(\frac{c}{b-a}(x-a) - y_p\right)^2 + z_p^2\right]^{1/2} dx$$
$$- \int_b^a \frac{\partial}{\partial x_p}\left[(x-x_p)^2 + y_p^2 + z_p^2\right]^{1/2} dx.,$$

Note

$$\frac{\partial}{\partial x_p}\left[(x-x_p)^2 + y_p^2 + z_p^2\right]^{1/2} = -\frac{\partial}{\partial x_p}\left[(x-x_p)^2 + y_p^2 + z_p^2\right]^{1/2},$$

therefore

$$-\int_0^a \frac{\partial}{\partial x_p}\left[(x-x_p)^2 + y_p^2 + z_p^2\right]^{1/2} dx = \int_0^a \frac{\partial}{\partial x_p}\left[(x-x_p)^2 + y_p^2 + z_p^2\right]^{1/2} dx$$

$$= r_3 - r_1.$$

The second and fourth integrals can be combined into one integral from 0 to a, then

$$I_4 = \int_0^b \frac{\partial}{\partial x_p}\left[(x-x_p)^2 + \left(\frac{c}{b}x - y_p\right)^2 + z_p^2\right]^{1/2} dx$$
$$+ \int_b^a \frac{\partial}{\partial x_p}\left[(x-x_p)^2 + \left(\frac{c}{b-a}(x-a) - y_p\right)^2 + z_p^2\right]^{1/2} dx$$
$$- \int_0^a \frac{\partial}{\partial x_p}\left[(x-x_p)^2 + y_p^2 + z_p^2\right]^{1/2} dx.$$

which can be rewritten as

$$I_4 = -\int_0^b (x - x_p)[(x - x_p)^2 + (\frac{c}{b}x - y_p)^2 + z_p^2]^{-1/2}\,dx$$
$$-\int_b^a (x - x_p)[(x - x_p)^2 + \left(\frac{c}{b-a}(x-a) - y_p\right)^2 + z_p^2]^{-1/2}\,dx$$
$$+\int_0^a (x - x_p)[(x - x_p)^2 + y_p^2 + z_p^2]^{-1/2}\,dx.$$

Next let

$$H_5 = \int_0^b [(x - x_p)^2 + (\frac{c}{b}x - y_p)^2 + z_p^2]^{-1/2}\,dx$$

$$H_6 = \int_0^b x\,[(x - x_p)^2 + (\frac{c}{b}x - y_p)^2 + z_p^2]^{-1/2}\,dx$$

$$H_7 = \int_b^a [(x - x_p)^2 + \left(\frac{c}{b-a}(x-a) - y_p\right)^2 + z_p^2]^{-1/2}\,dx$$

and

$$H_8 = \int_b^a x\,[(x - x_p)^2 + \left(\frac{c}{b-a}(x-a) - y_p\right)^2 + z_p^2]^{-1/2}\,dx.$$

Then

$$I_4 = x_p H_5 - H_6 + x_p H_7 - H_8 + \int_0^a (x - x_p)[(x - x_p)^2 + y_p^2 + z_p^2]^{-1/2}\,dx.$$

Therefore, the fourth integral is

$$I_4 = x_p H_5 - H_6 + x_p H_7 - H_8 + r_3 - r_1.$$

Now the evaluation of H_5:

$$H_5 = \int_0^b [(x - x_p)^2 + (\frac{c}{b}x - y_p)^2 + z_p^2]^{-1/2}\, dx.$$

Expanding the squares and collecting terms results in

$$H_5 = \int_0^b \left[\left[(\frac{c}{b})^2 + 1\right]x^2 - 2\left[x_p + \frac{c}{b}y_p\right]x + x_p^2 + y_p^2 + z_p^2\right]^{-1/2} dx.$$

Let

$$\alpha_5 = (\frac{c}{b})^2 + 1$$

and

$$\alpha_6 = x_p + \frac{c}{b}y_p$$

then substitution yields

$$H_5 = \frac{1}{\sqrt{\alpha_5}} \int_0^b \left[x^2 - 2\frac{\alpha_6}{\alpha_5}x + \frac{r_1^2}{\alpha_5}\right]^{-1/2} dx$$

$$= \frac{1}{\sqrt{\alpha_5}} \int_0^b \left[\left(x - \frac{\alpha_6}{\alpha_5}\right)^2 - \left(\frac{\alpha_6}{\alpha_5}\right)^2 + \frac{r_1^2}{\alpha_5}\right]^{-1/2} dx$$

$$= \frac{1}{\sqrt{\alpha_5}} \ln\left\{ \frac{\left(b - \frac{\alpha_6}{\alpha_5}\right) + \left[\left(b - \frac{\alpha_6}{\alpha_5}\right)^2 - \left(\frac{\alpha_6}{\alpha_5}\right)^2 + \frac{r_1^2}{\alpha_5}\right]^{1/2}}{-\frac{\alpha_6}{\alpha_5} + \left[\left(\frac{\alpha_6}{\alpha_5}\right)^2 - \left(\frac{\alpha_6}{\alpha_5}\right)^2 + \frac{r_1^2}{\alpha_5}\right]^{1/2}} \right\}$$

$$= \frac{1}{\sqrt{\alpha_5}} \ln\left\{ \frac{b\alpha_5 - \alpha_6 + \left[(b\alpha_5 - \alpha_6)^2 - \alpha_6^2 + r_1^2\alpha_5\right]^{1/2}}{-\alpha_6 + \sqrt{\alpha_5}\, r_1} \right\}.$$

Considering the square-root term in the numerator, one finds

$$\left[(b\alpha_5 - \alpha_6)^2 - \alpha_6^2 + r_1^2\alpha_5\right]^{1/2} = \left[b^2\alpha_5^2 - 2b\alpha_5\alpha_6 + \alpha_6^2 - \alpha_6^2 + r_1^2\alpha_5\right]^{1/2}$$

$$= \sqrt{\alpha_5}\left[b^2\alpha_5 - 2b\alpha_6 + r_1^2\right]^{1/2}$$

$$= \sqrt{\alpha_5}\left[b^2 + c^2 - 2bx_p - 2cy_p + x_p^2 + y_p^2 + z_p^2\right]^{1/2}$$

$$= \sqrt{\alpha_5}\left[(b - x_p)^2 + (c - y_p)^2 + z_p^2\right]^{1/2}$$

$$= \sqrt{\alpha_5}\, r_2.$$

The result is

$$H_5 = \frac{1}{\sqrt{\alpha_5}} \ln\left\{\frac{b\alpha_5 - \alpha_6 + \sqrt{\alpha_5}\, r_2}{-\alpha_6 + \sqrt{\alpha_5}\, r_1}\right\}.$$

Next it will be shown that

$$\frac{b\alpha_5 - \alpha_6 + \sqrt{\alpha_5}\, r_2}{-\alpha_6 + \sqrt{\alpha_5}\, r_1} = \frac{c\alpha_3 - \alpha_4 + \sqrt{\alpha_3}\, r_2}{-\alpha_4 + \sqrt{\alpha_3}\, r_1}$$

This will be proved by showing that

$$(b\alpha_5 - \alpha_6 + \sqrt{\alpha_5}\, r_2)(\sqrt{\alpha_3}\, r_1 - \alpha_4) = (c\alpha_3 - \alpha_4 + \sqrt{\alpha_3}\, r_2)(\sqrt{\alpha_5}\, r_1 - \alpha_6)$$

is an identity. Multiplying out both sides of the equation

$$\alpha_5\sqrt{\alpha_3}\, br_1 - \alpha_6\sqrt{\alpha_3}\, r_1 + \sqrt{\alpha_5}\sqrt{\alpha_3}\, r_1 r_2 - \alpha_4\alpha_5 b + \alpha_6\alpha_4 - \alpha_4\sqrt{\alpha_5}\, r_2 =$$
$$\alpha_3\sqrt{\alpha_5}\, br_1 - \alpha_4\sqrt{\alpha_5}\, r_1 + \sqrt{\alpha_5}\sqrt{\alpha_3}\, r_1 r_2 - \alpha_3\alpha_6 c + \alpha_6\alpha_4 - \alpha_6\sqrt{\alpha_3}\, r_2$$

Collecting terms

$$[\alpha_6\sqrt{\alpha_3} - \alpha_4\sqrt{\alpha_5}\,]r_1 + [\alpha_4\alpha_5 b - \alpha_3\alpha_6 c] - [\alpha_6\sqrt{\alpha_3} - \alpha_4\sqrt{\alpha_5}\,]r_2 = 0.$$

First,

$$\alpha_6\sqrt{\alpha_3} - \alpha_4\sqrt{\alpha_5} = \left(x_p + \frac{c}{b}y_p\right)\left(\frac{b^2+c^2}{c^2}\right)^{1/2} - \left(\frac{b}{c}x_p + y_p\right)\left(\frac{c^2+b^2}{b^2}\right)^{1/2}$$

$$= \left(\frac{x_p}{c} + \frac{y_p}{b}\right)(b^2+c^2)^{1/2} - \left(\frac{x_p}{c} + \frac{y_p}{b}\right)(c^2+b^2)^{1/2} = 0,$$

and second

$$\alpha_4\alpha_5 b - \alpha_3\alpha_6 c = \left(\frac{b}{c}x_p + y_p\right)\left(\frac{c^2+b^2}{b^2}\right)b - \left(x_p + \frac{c}{b}y_p\right)\left(\frac{b^2+c^2}{c^2}\right)c$$

$$= \left(\frac{x_p}{c} + \frac{y_p}{b}\right)(c^2+b^2) - \left(\frac{x_p}{c} + \frac{y_p}{b}\right)(b^2+c^2) = 0.$$

Therefore,

$$H_5 = \frac{1}{\sqrt{\alpha_5}} \ln\left\{\frac{c\alpha_3 - \alpha_4 + \sqrt{\alpha_3}\, r_2}{-\alpha_4 + \sqrt{\alpha_3}\, r_1}\right\}$$

$$= \frac{1}{\sqrt{\alpha_5}}\sqrt{\alpha_3}\, H_3$$

$$= \left(\frac{b^2}{c^2}\right)^{1/2} H_3$$

and finally because b and c are both positive

$$H_5 = \frac{b}{c} H_3.$$

Next the evaluation of H_6:

$$H_6 = \int_0^b x\,[(x - x_p)^2 + \left(\frac{c}{b}x - y_p\right)^2 + z_p^2]^{-1/2}\, dx$$

$$H_6 = \frac{1}{\sqrt{\alpha_5}} \int_0^b x \left[x^2 - 2\frac{\alpha_6}{\alpha_5} x + \frac{r_1^2}{\alpha_5} \right]^{-1/2} dx$$

$$= \frac{1}{\sqrt{\alpha_5}} \int_0^b x \left[\left(x - \frac{\alpha_6}{\alpha_5} \right)^2 - \left(\frac{\alpha_6}{\alpha_5} \right)^2 + \frac{r_1^2}{\alpha_5} \right]^{-1/2} dx$$

$$= \frac{1}{\sqrt{\alpha_5}} \int_0^b \left(x - \frac{\alpha_6}{\alpha_5} \right) \left[\left(x - \frac{\alpha_6}{\alpha_5} \right)^2 - \left(\frac{\alpha_6}{\alpha_5} \right)^2 + \frac{r_1^2}{\alpha_5} \right]^{-1/2} dx$$
$$+ \frac{1}{\sqrt{\alpha_5}} \frac{\alpha_6}{\alpha_5} \int_0^b \left[\left(x - \frac{\alpha_6}{\alpha_5} \right)^2 - \left(\frac{\alpha_6}{\alpha_5} \right)^2 + \frac{r_1^2}{\alpha_5} \right]^{-1/2} dx$$

$$= \frac{1}{\sqrt{\alpha_5}} \left[\left(b - \frac{\alpha_6}{\alpha_5} \right)^2 - \left(\frac{\alpha_6}{\alpha_5} \right)^2 + \frac{r_1^2}{\alpha_5} \right]^{1/2} + \frac{1}{\sqrt{\alpha_5}} \left[\left(\frac{\alpha_6}{\alpha_5} \right)^2 - \left(\frac{\alpha_6}{\alpha_5} \right)^2 + \frac{r_1^2}{\alpha_5} \right]^{1/2} + \frac{\alpha_6}{\alpha_5} H_5$$

$$= \frac{1}{\alpha_5} \left[b^2 \alpha_5 - 2b\alpha_6 + r_1^2 \right]^{1/2} - \frac{r_1}{\alpha_5} + \frac{\alpha_6}{\alpha_5} H_5.$$

Then using the definition of r_2

$$H_6 = \frac{1}{\alpha_5} (r_2 - r_1) + \frac{\alpha_6}{\alpha_5} H_5.$$

The evaluation of H_7:

$$H_7 = \int_b^a \left[(x - x_p)^2 + \left(\frac{c}{b-a} (x - a) - y_p \right)^2 + z_p^2 \right]^{-1/2} dx$$

Expanding the squares and collecting terms, one can obtain

$$H_7 = \int_b^a \left[\left(1 + \left(\frac{c}{b-a} \right)^2 \right) x^2 - 2 \left(x_p + a \left(\frac{c}{b-a} \right)^2 + \frac{c}{b-a} y_p \right) x \right.$$
$$\left. + x_p^2 + \left(\frac{c}{b-a} \right)^2 a^2 + 2\frac{ca}{b-a} y_p + y_p^2 + z_p^2 \right]^{-1/2} dx.$$

We introduce the following definitions:

$$\alpha_7 = 1 + \left(\frac{c}{b-a}\right)^2$$

$$\alpha_8 = x_p + a\left(\frac{c}{b-a}\right)^2 + \frac{c}{b-a} y_p$$

and

$$\alpha_9 = \left(\frac{c}{b-a}\right)^2 a^2 + 2\frac{ca}{b-a} y_p,$$

results in

$$H_7 = \int_b^a \left[\alpha_7 x^2 - 2\alpha_8 x + \alpha_9 + x_p^2 + y_p^2 + z_p^2\right]^{-1/2} dx$$

$$= \frac{1}{\sqrt{\alpha_7}} \int_b^a \left[\left(x - \frac{\alpha_8}{\alpha_7}\right)^2 - \left(\frac{\alpha_8}{\alpha_7}\right)^2 + \frac{\alpha_9}{\alpha_7} + \frac{r_1^2}{\alpha_7}\right]^{-1/2} dx$$

$$= \frac{1}{\sqrt{\alpha_7}} \ln\left\{\frac{\left(a - \frac{\alpha_8}{\alpha_7}\right) + \left[\left(a - \frac{\alpha_8}{\alpha_7}\right)^2 - \left(\frac{\alpha_8}{\alpha_7}\right)^2 + \frac{\alpha_9}{\alpha_7} + \frac{r_1^2}{\alpha_7}\right]^{1/2}}{\left(b - \frac{\alpha_8}{\alpha_7}\right) + \left[\left(b - \frac{\alpha_8}{\alpha_7}\right)^2 - \left(\frac{\alpha_8}{\alpha_7}\right)^2 + \frac{\alpha_9}{\alpha_7} + \frac{r_1^2}{\alpha_7}\right]^{1/2}}\right\}.$$

Examining the term under the radical in the numerator, one finds that

$$\left(a - \frac{\alpha_8}{\alpha_7}\right)^2 - \left(\frac{\alpha_8}{\alpha_7}\right)^2 + \frac{\alpha_9}{\alpha_7} + \frac{r_1^2}{\alpha_7} = \frac{1}{\alpha_7}\left[\alpha_7 a^2 - 2\alpha_8 a + \frac{c^2 a^2}{(b-a)^2} + 2\frac{ca}{b-a} y_p + r_1^2\right]$$

$$= \frac{1}{\alpha_7}\left[a^2 + \frac{a^2 c^2}{(b-a)^2} - 2ax_p - 2\frac{a^2 c^2}{(b-a)^2} - 2\frac{ca}{b-a} y_p + \frac{c^2 a^2}{(b-a)^2} + 2\frac{ca}{b-a} y_p + r_1^2\right]$$

$$= \frac{1}{\alpha_7}\left[a^2 - 2ax_p + x_p^2 + y_p^2 + z_p^2\right]$$

$$= \frac{1}{\alpha_7}\left[(a - x_p)^2 + y_p^2 + z_p^2\right]$$

therefore,

$$\left(a - \frac{\alpha_8}{\alpha_7}\right)^2 - \left(\frac{\alpha_8}{\alpha_7}\right)^2 + \frac{\alpha_9}{\alpha_7} + \frac{r_1^2}{\alpha_7} = \frac{1}{\alpha_7} r_3^2.$$

Next examining the square-root term in the denominator, one finds that

$$\left(b - \frac{\alpha_8}{\alpha_7}\right)^2 - \left(\frac{\alpha_8}{\alpha_7}\right)^2 + \frac{\alpha_9}{\alpha_7} + \frac{r_1^2}{\alpha_7} = \frac{1}{\alpha_7}\left[\alpha_7 b^2 - 2\alpha_8 b + \frac{c^2 a^2}{(b-a)^2} + 2\frac{ca}{b-a} y_p + r_1^2\right]$$

$$= \frac{1}{\alpha_7}\left[b^2 + \frac{b^2 c^2}{(b-a)^2} - 2bx_p - 2\frac{abc^2}{(b-a)^2} - 2\frac{bc}{b-a} y_p + \frac{c^2 a^2}{(b-a)^2} + 2\frac{ca}{b-a} y_p + r_1^2\right]$$

$$= \frac{1}{\alpha_7}\left[b^2 - 2bx_p + \frac{c^2(b^2 - 2ab + a^2)}{(b-a)^2} - 2\frac{c(b-a)}{b-a} y_p + r_1^2\right]$$

$$= \frac{1}{\alpha_7}\left[b^2 - 2bx_p + c^2 - 2cy_p + x_p^2 + y_p^2 + z_p^2\right]$$

$$= \frac{1}{\alpha_7}\left[(b - x_p)^2 + (c - y_p)^2 + z_p^2\right]$$

therefore

$$\left(b - \frac{\alpha_8}{\alpha_7}\right)^2 - \left(\frac{\alpha_8}{\alpha_7}\right)^2 + \frac{\alpha_9}{\alpha_7} + \frac{r_1^2}{\alpha_7} = \frac{1}{\alpha_7} r_2^2,$$

then

$$H_7 = \frac{1}{\sqrt{\alpha_7}} \ln\left\{\frac{a - \frac{\alpha_8}{\alpha_7} + \frac{r_3}{\sqrt{\alpha_7}}}{b - \frac{\alpha_8}{\alpha_7} + \frac{r_2}{\sqrt{\alpha_7}}}\right\}.$$

$$H_7 = \frac{1}{\sqrt{\alpha_7}} \ln\left\{ \frac{\alpha_7 a - \alpha_8 + \sqrt{\alpha_7}\, r_3}{\alpha_7 b - \alpha_8 + \sqrt{\alpha_7}\, r_2} \right\}$$

One can show that

$$\frac{\alpha_7 a - \alpha_8 + \sqrt{\alpha_7}\, r_3}{\alpha_7 b - \alpha_8 + \sqrt{\alpha_7}\, r_2} = \frac{\alpha_1 c + \alpha_2 + \sqrt{\alpha_1}\, r_2}{\alpha_2 + \sqrt{\alpha_1}\, r_3}.$$

This is done by showing that both sides of the equation equal the same expression. First showing

$$\frac{\alpha_1 c + \alpha_2 + \sqrt{\alpha_1}\, r_2}{\alpha_2 + \sqrt{\alpha_1}\, r_3} = \frac{\sqrt{\alpha_1}\, r_3 - \alpha_2}{\sqrt{\alpha_1}\, r_2 - \alpha_2 - c\alpha_1}.$$

Clearing the denominators gives

$$(\alpha_1 c + \alpha_2 + \sqrt{\alpha_1}\, r_2)(\sqrt{\alpha_1}\, r_2 - \alpha_2 - c\alpha_1) = (\alpha_2 + \sqrt{\alpha_1}\, r_3)(\sqrt{\alpha_1}\, r_3 - \alpha_2).$$

Multiplying out both sides of the equation results in

$$\begin{aligned} &\alpha_1 r_2^2 - r_2\sqrt{\alpha_1}\,\alpha_2 + r_2\sqrt{\alpha_1}\,\alpha_2 - r_2\sqrt{\alpha_1}\,c\alpha_1 + r_2\sqrt{\alpha_1}\,c\alpha_1 - \alpha_2^2 - 2c\alpha_2\alpha_1 - c^2\alpha_1^2 \\ &\quad = r_3^2\alpha_1 - r_3\sqrt{\alpha_1} + r_3\sqrt{\alpha_1} - \alpha_2^2, \end{aligned}$$

which can be reduced to

$$\alpha_1 r_2^2 - 2c\alpha_2\alpha_1 - c^2\alpha_1^2 = r_3^2\alpha_1.$$

Then

$$\alpha_1(r_2^2 - 2c\alpha_2 - c^2\alpha_1) = r_3^2\alpha_1.$$

Canceling α_1 and using the definitions, one can show

$$(b - x_p)^2 + (c - y_p)^2 + z_p^2 - 2c\left[\frac{(b-a)}{c}(a - x_p) - y_p\right] - (b-a)^2 - c^2 = r_3^2.$$

It follows that

$$b^2 - 2bx_p + x_p^2 + c^2 - 2cy_p + y_p^2 + z_p^2$$
$$+ 2bx_p - 2ba + 2a^2 - 2ax_p + 2cy_p - b^2 + 2ba - a^2 - c^2 = r_3^2.$$

Canceling again leads to

$$x_p^2 + y_p^2 + z_p^2 + 2a^2 - 2ax_p - a^2 = r_3^2,$$

and then regrouping the terms results in

$$(a - x_p)^2 + y_p^2 + z_p^2 = r_3^2,$$

which is the definition of r_3 given earlier. In order to show the original premise, the following must also be true:

$$\frac{\alpha_7 a - \alpha_8 + \sqrt{\alpha_7}\, r_3}{\alpha_7 b - \alpha_8 + \sqrt{\alpha_7}\, r_2} = \frac{\sqrt{\alpha_1}\, r_3 - \alpha_2}{\sqrt{\alpha_1}\, r_2 - \alpha_2 - c\alpha_1}.$$

This will be shown by expanding both sides of the equation. First

$$\frac{\alpha_7 a - \alpha_8 + + \sqrt{\alpha_7}\, r_3}{\alpha_7 b - \alpha_8 + \sqrt{\alpha_7}\, r_2} = \frac{\left[1 + \left(\frac{c}{b-a}\right)^2\right] a - x_p - a\left(\frac{c}{b-a}\right)^2 - \frac{c}{b-a} y_p + \sqrt{\alpha_7}\, r_3}{\left[1 + \left(\frac{c}{b-a}\right)^2\right] b - x_p - a\left(\frac{c}{b-a}\right)^2 - \frac{c}{b-a} y_p + \sqrt{\alpha_7}\, r_2},$$

The local coordinate system is introduced in such a way that $a > b$, always; thus,

$$\sqrt{\alpha_7} = \left[\frac{(b-a)^2 + c^2}{(b-a)^2}\right]^{1/2}$$
$$= \frac{\sqrt{(b-a)^2 + c^2}}{|b-a|}$$
$$= \frac{\sqrt{(b-a)^2 + c^2}}{a-b}.$$

Multiplying top and bottom by $a-b$ yields

$$\frac{\alpha_7 a-\alpha_8++\sqrt{\alpha_7}\,r_3}{\alpha_7 b-\alpha_8+\sqrt{\alpha_7}\,r_2}=\frac{a(a-b)-x_p(a-b)+y_pc+\sqrt{(b-a)^2+c^2}\,r_3}{b(a-b)-c^2-x_p(a-b)+y_pc+\sqrt{(b-a)^2+c^2}\,r_2},$$

and expanding the other side of the equation yields

$$\frac{\sqrt{\alpha_1}\,r_3-\alpha_2}{\sqrt{\alpha_1}\,r_2-\alpha_2-c\alpha_1}=\frac{-\left[(a-x_p)\dfrac{b-a}{c}-y_p\right]+\dfrac{\sqrt{(b-a)^2+c^2}}{c}r_3}{-\left[(a-x_p)\dfrac{b-a}{c}-y_p\right]-c\left[\dfrac{(b-a)^2+c^2}{c^2}\right]+\dfrac{\sqrt{(b-a)^2+c^2}}{c}r_2}.$$

Multiplying top and bottom by c yields

$$\frac{\sqrt{\alpha_1}\,r_3-\alpha_2}{\sqrt{\alpha_1}\,r_2-\alpha_2-c\alpha_1}=\frac{(a-x_p)(a-b)+y_pc+\sqrt{(b-a)^2+c^2}\,r_3}{a(a-b)-x_p(a-b)+y_pc-(a-b)^2-c^2+\sqrt{(b-a)^2+c^2}\,r_2}$$

$$=\frac{(a-x_p)(a-b)+y_pc+\sqrt{(b-a)^2+c^2}\,r_3}{a^2-ab-b^2+2ab-a^2-c^2-x_p(a-b)+y_pc+\sqrt{(b-a)^2+c^2}\,r_2}$$

$$=\frac{(a-x_p)(a-b)+y_pc+\sqrt{(b-a)^2+c^2}\,r_3}{ab-b^2-c^2-x_p(a-b)+y_pc+\sqrt{(b-a)^2+c^2}\,r_2}$$

$$=\frac{(a-x_p)(a-b)+y_pc+\sqrt{(b-a)^2+c^2}\,r_3}{b(a-b)-c^2-x_p(a-b)+y_pc+\sqrt{(b-a)^2+c^2}\,r_2}.$$

Because both sides of the original equation are equal to the same expression the proof is complete. Therefore

$$H_7=\frac{1}{\sqrt{\alpha_7}}\ln\left\{\frac{\alpha_1 c+\alpha_2+\sqrt{\alpha_1}\,r_2}{\alpha_2+\sqrt{\alpha_1}\,r_3}\right\}$$

$$H_7 = \frac{1}{\sqrt{\alpha_7}} \sqrt{\alpha_1}\, H_1$$

$$= \frac{\left[\frac{(a-b)^2 + c^2}{c^2} \right]^{1/2}}{\left[\frac{(b-a)^2 + c^2}{(b-a)^2} \right]^{1/2}} H_1$$

$$= \frac{\sqrt{(b-a)^2}}{\sqrt{c^2}} H_1$$

$$= \frac{|b-a|}{c} H_1.$$

With the restriction on the orientation of the triangle, it follows that

$$H_7 = \frac{a-b}{c} H_1.$$

The evaluation of H_8:

$$H_8 = \int_b^a x[(x - x_p)^2 + (\frac{c}{b-a}(x-a) - y_p)^2 + z_p^2]^{-1/2}\, dx$$

$$= \int_b^a x\left[\alpha_7 x^2 - 2\alpha_8 x + \alpha_9 + r_1^2\right]^{-1/2} dx$$

$$= \frac{1}{\sqrt{\alpha_7}} \int_b^a x\left[\left(x - \frac{\alpha_8}{\alpha_7}\right)^2 - \left(\frac{\alpha_8}{\alpha_7}\right)^2 + \frac{\alpha_9}{\alpha_7} + \frac{r_1^2}{\alpha_7}\right]^{-1/2} dx$$

$$= \frac{1}{\sqrt{\alpha_7}} \int_b^a \left(x - \frac{\alpha_8}{\alpha_7}\right)\left[\left(x - \frac{\alpha_8}{\alpha_7}\right)^2 - \left(\frac{\alpha_8}{\alpha_7}\right)^2 + \frac{\alpha_9}{\alpha_7} + \frac{r_1^2}{\alpha_7}\right]^{-1/2} dx$$
$$+ \frac{1}{\sqrt{\alpha_7}} \int_b^a \frac{\alpha_8}{\alpha_7}\left[\left(x - \frac{\alpha_8}{\alpha_7}\right)^2 - \left(\frac{\alpha_8}{\alpha_7}\right)^2 + \frac{\alpha_9}{\alpha_7} + \frac{r_1^2}{\alpha_7}\right]^{-1/2} dx$$

$$H_8 = \frac{1}{\sqrt{\alpha_7}}\left[\left(x - \frac{\alpha_8}{\alpha_7}\right)^2 - \left(\frac{\alpha_8}{\alpha_7}\right)^2 + \frac{\alpha_9}{\alpha_7} + \frac{r_1^2}{\alpha_7}\right]^{1/2}\Big|_b^a + \frac{\alpha_8}{\alpha_7} H_7$$

$$= \frac{1}{\sqrt{\alpha_7}}\left[\left(a - \frac{\alpha_8}{\alpha_7}\right)^2 - \left(\frac{\alpha_8}{\alpha_7}\right)^2 + \frac{\alpha_9}{\alpha_7} + \frac{r_1^2}{\alpha_7}\right]^{1/2}$$
$$+ \frac{1}{\sqrt{\alpha_7}}\left[\left(b - \frac{\alpha_8}{\alpha_7}\right)^2 - \left(\frac{\alpha_8}{\alpha_7}\right)^2 + \frac{\alpha_9}{\alpha_7} + \frac{r_1^2}{\alpha_7}\right]^{1/2} + \frac{\alpha_8}{\alpha_7} H_7$$

As shown before this reduces to

$$H_8 = \frac{1}{\sqrt{\alpha_7}}\left[\frac{r_3}{\sqrt{\alpha_7}} - \frac{r_2}{\sqrt{\alpha_7}}\right] + \frac{\alpha_8}{\alpha_7} H_7,$$

then

$$H_8 = \frac{r_3 - r_2}{\alpha_7} + \frac{\alpha_8}{\alpha_7} H_7.$$

This completes the evaluation of I_4.

The evaluation of I_5:

$$I_5 = \frac{\partial}{\partial y_p}\iint_S \frac{y - y_p}{r}\,dxdy.$$

Integrating in the y direction first, one can rewrite the integral as

$$I_5 = \frac{\partial}{\partial y_p}\int_0^b \int_0^{\frac{c}{b}x} \frac{y - y_p}{[(x - x_p)^2 + (y - y_p)^2 + z_p^2]^{1/2}}\,dydx$$
$$+ \frac{\partial}{\partial y_p}\int_b^a \int_0^{\frac{c}{(b-a)}(x-a)} \frac{y - y_p}{[(x - x_p)^2 + (y - y_p)^2 + z_p^2]^{1/2}}\,dydx.$$

$$I_5 = \int_0^b \frac{\partial}{\partial y_p}[(x-x_p)^2 + (\frac{c}{b}x - y_p)^2 + z_p^2]^{1/2}\,dx$$
$$- \int_0^b \frac{\partial}{\partial y_p}[(x-x_p)^2 + y_p^2 + z_p^2]^{1/2}\,dx$$
$$+ \int_b^a \frac{\partial}{\partial y_p}[(x-x_p)^2 + \left(\frac{c}{b-a}(x-a) - y_p\right)^2 + z_p^2]^{1/2}\,dx$$
$$- \int_b^a \frac{\partial}{\partial y_p}[(x-x_p)^2 + y_p^2 + z_p^2]^{1/2}\,dx$$

The second and fourth integrals can be combined into one integral from 0 to a :

$$I_5 = \int_0^b \frac{\partial}{\partial y_p}[(x-x_p)^2 + (\frac{c}{b}x - y_p)^2 + z_p^2]^{1/2}\,dx$$
$$+ \int_b^a \frac{\partial}{\partial y_p}[(x-x_p)^2 + \left(\frac{c}{b-a}(x-a) - y_p\right)^2 + z_p^2]^{1/2}\,dx$$
$$- \int_0^a \frac{\partial}{\partial y_p}[(x-x_p)^2 + y_p^2 + z_p^2]^{1/2}\,dx,$$

which reduces to

$$I_5 = \int_0^b -(\frac{c}{b}x - y_p)[(x-x_p)^2 + (\frac{c}{b}x - y_p)^2 + z_p^2]^{-1/2}\,dx$$
$$+ \int_0^b -\left(\frac{c}{b-a}(x-a) - y_p\right)[(x-x_p)^2 + \left(\frac{c}{b-a}(x-a) - y_p\right)^2 + z_p^2]^{-1/2}\,dx$$
$$- \int_0^a y_p[(x-x_p)^2 + y_p^2 + z_p^2]^{-1/2}\,dx.$$

Taking the constants outside the integrals yields

$$I_5 = y_p \int_0^b [(x - x_p)^2 + (\frac{c}{b}x - y_p)^2 + z_p^2]^{-1/2}\, dx$$
$$- \frac{c}{b} \int_0^b x[(x - x_p)^2 + (\frac{c}{b}x - y_p)^2 + z_p^2]^{-1/2}\, dx$$
$$+ [y_p + \frac{ac}{b-a}] \int_0^b [(x - x_p)^2 + \left(\frac{c}{b-a}(x-a) - y_p\right)^2 + z_p^2]^{-1/2}\, dx$$
$$- \frac{c}{b-a} \int_0^b x[(x - x_p)^2 + \left(\frac{c}{b-a}(x-a) - y_p\right)^2 + z_p^2]^{-1/2}\, dx$$
$$- y_p \int_0^a [(x - x_p)^2 + y_p^2 + z_p^2]^{-1/2}\, dx.$$

We introduce the following notation:

$$H_9 = \int_0^a [(x - x_p)^2 + y_p^2 + z_p^2]^{-1/2}\, dx.$$

Then it follows from this definition and others given earlier that

$$I_5 = y_p H_5 - \frac{c}{b} H_6 + [y_p + \frac{ac}{b-a}] H_7 - \frac{c}{b-a} H_8 - y_p H_9.$$

The only integral that has not been evaluated in this expression is H_9, which is

$$H_9 = \int_0^a [(x - x_p)^2 + y_p^2 + z_p^2]^{-1/2}\, dx$$

$$= \ln\left\{ \frac{(a - x_p) + [(a - x_p)^2 + y_p^2 + z_p^2]^{1/2}}{-x_p + [x_p^2 + y_p^2 + z_p^2]^{1/2}} \right\}$$

$$= \ln\left\{ \frac{(a - x_p) + r_3}{-x_p + r_1} \right\}$$

The evaluation of I_6:

$$I_6 = \frac{\partial}{\partial z_p} \iint_S \frac{y - y_p}{r} \, dxdy.$$

Following the same procedure used for I_5, one finds

$$I_6 = \frac{\partial}{\partial z_p} \int_0^b \int_0^{\frac{c}{b}x} \frac{y - y_p}{[(x - x_p)^2 + (y - y_p)^2 + z_p^2]^{1/2}} \, dydx$$

$$+ \frac{\partial}{\partial z_p} \int_b^a \int_0^{\frac{c}{(b-a)}(x-a)} \frac{y - y_p}{[(x - x_p)^2 + (y - y_p)^2 + z_p^2]^{1/2}} \, dydx$$

$$= \int_0^b \frac{\partial}{\partial z_p} [(x - x_p)^2 + (\frac{c}{b}x - y_p)^2 + z_p^2]^{1/2} \, dx$$

$$+ \int_b^a \frac{\partial}{\partial z_p} [(x - x_p)^2 + \left(\frac{c}{b-a}(x - a) - y_p\right)^2 + z_p^2]^{1/2} \, dx$$

$$- \int_0^a \frac{\partial}{\partial z_p} [(x - x_p)^2 + y_p^2 + z_p^2]^{1/2} \, dx$$

$$= z_p \int_0^b [(x - x_p)^2 + (\frac{c}{b}x - y_p)^2 + z_p^2]^{-1/2} \, dx$$

$$+ z_p \int_0^b [(x - x_p)^2 + \left(\frac{c}{b-a}(x - a) - y_p\right)^2 + z_p^2]^{-1/2} \, dx$$

$$- z_p \int_0^a [(x - x_p)^2 + y_p^2 + z_p^2]^{-1/2} \, dx.$$

Then it follows that

$$I_6 = z_p H_5 + z_p H_7 - z_p H_9.$$

The evaluation of I_7:

$$I_7 = \frac{\partial}{\partial x_p} \iint_S \frac{1}{r} \, dxdy.$$

Integrating in the x direction first, one finds

$$I_7 = \int_0^c \int_{\frac{b}{c}y}^{\frac{b-a}{c}y+a} \frac{\partial}{\partial x_p}\left[(x-x_p)^2+(y-y_p)^2+z_p^2\right]^{-1/2} dxdy$$

$$= -\int_0^c \left[\left(\frac{b-a}{c}y+a-x_p\right)^2+(y-y_p)^2+z_p^2\right]^{-1/2} dy$$
$$+\int_0^c \left[\left(\frac{b}{c}y-x_p\right)^2+(y-y_p)^2+z_p^2\right]^{-1/2} dy.$$

Therefore

$$I_7 = H_3 - H_1.$$

The evaluation of I_8:

$$I_8 = \frac{\partial}{\partial y_p}\iint_S \frac{1}{r} dxdy.$$

Integrating in the y direction first yields

$$I_8 = \int_0^b \int_0^{\frac{c}{b}x} \frac{\partial}{\partial y_p}\left[(x-x_p)^2+(y-y_p)^2+z_p^2\right]^{-1/2} dydx$$
$$+\int_b^a \int_0^{\frac{c}{(b-a)}(x-a)} \frac{\partial}{\partial y_p}\left[(x-x_p)^2+(y-y_p)^2+z_p^2\right]^{-1/2} dydx$$

$$= -\int_0^b \left[(x-x_p)^2+\left(\frac{c}{b}x-y_p\right)^2+z_p^2\right]^{-1/2} dy$$
$$+\int_0^b \left[(x-x_p)^2+(y-y_p)^2+z_p^2\right]^{-1/2} dy$$
$$-\int_b^a \left[(x-x_p)^2+\left(\frac{c}{b-a}(x-a)-y_p\right)^2+z_p^2\right]^{-1/2} dy$$
$$+\int_b^a \left[(x-x_p)^2+(y-y_p)^2+z_p^2\right]^{-1/2} dy$$

$$= \int_0^a \left[(x-x_p)^2 + (y-y_p)^2 + z_p^2\right]^{-1/2} dy$$
$$- \int_0^b \left[(x-x_p)^2 + (\frac{c}{b}x - y_p)^2 + z_p^2\right]^{-1/2} dy$$
$$- \int_b^a \left[(x-x_p)^2 + \left(\frac{c}{b-a}(x-a) - y_p\right)^2 + z_p^2\right]^{-1/2} dy$$

$$I_8 = H_9 - H_5 - H_7$$

The integral I_8 contains the integral I_{10}; therefore, we first evaluate I_{10} and then return to I_8. The evaluation of both these integral where arrived at with the help of a paper written by Smith and Hess [1962].

The evaluation of I_{10}:

$$I_{10} = \iint_S \frac{1}{r}\, dxdy.$$

We set up a new cylindrical coordinate system with the origin at the projection of point p on the local x-y plane, as shown in Figure 101. In this coordinate frame the integral over the area of the triangle can be written as the sum of three integrals. The strategy is to integrate from (0,0) to (*b*,*c*), then from (*b*,*c*) to (*a*,0), and finally from (*a*,0) to (0,0) The first produces the integral over the area of the triangle described by the vertices 1-2-4, the second produces the integral over the area of the triangle 2-3-4, and finally the third produces the integral over the area of the triangle 3-1-4.

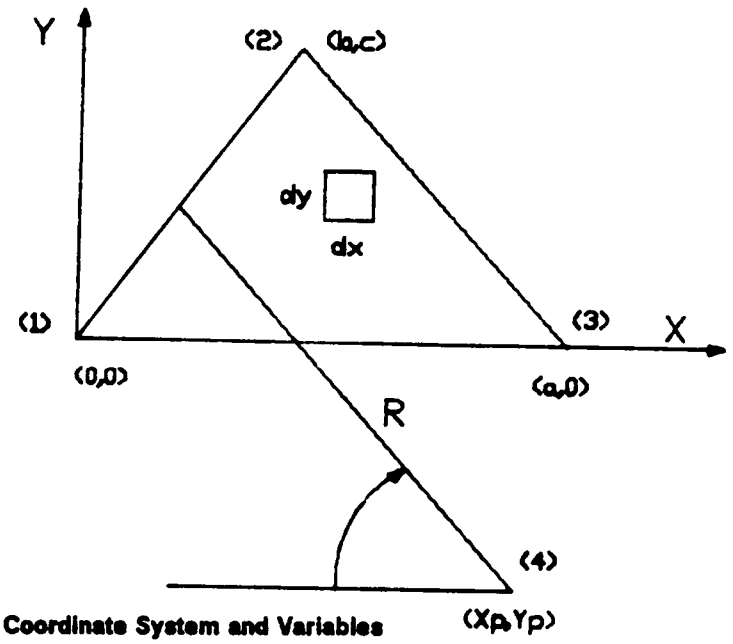

Figure 101. Cylindrical Coordinate System and Variables

As mentioned, the integral will be evaluated by using cylindrical coordinates with the origin at the projection of the point of interest on the triangular elements local x-y plane. The position vector can be written as the sum of the vertical component, z_p, and the position vector in the local x-y plane, $\vec{R}$ The magnitude of the position vector written in the elements local coordinate frame r is the quantity needed to evaluate I_{10} . This magnitude, written in terms of the components of the cylindrical coordinate frame, is

$$r^2 = R^2 + z_p^2$$

The differential area, in the cylindrical reference frame is

$$dxdy = R\ dRd\theta$$

where θ is measured from any convenient direction, in this case the negative local x axis. The integral I_{10} can be written as

$$\iint_S \frac{1}{r}\,dxdy = \oint \int \frac{R\ dRd\theta}{\sqrt{R^2 + z_p^2}}.$$

where R has the range of values from 0 to the value along the edge of the triangle. The integral can be simplified by using

$$dr = \frac{R\,dR}{\sqrt{R^2 + z_p^2}}.$$

The limits of integration are when

$$R = 0 \quad r = \sqrt{z_p^2} = |z_p|$$

and when

$$R = R \quad r = r.$$

The integral can then be written as

$$I_{10} = \oint \int_{|z_p|}^{r} dr d\theta$$

$$= \oint r(\theta) - |z_p|\, d\theta$$

$$= \oint r\, d\theta - |z_p| \Delta\theta.$$

where $\Delta\theta = 2\pi$ if the projection of the point p lies within the triangle and zero otherwise. Then, employing the strategy mentioned earlier, the integral can be written as

$$I_{10} = \int_{\theta_1}^{\theta_2} r\, d\theta + \int_{\theta_2}^{\theta_3} r\, d\theta + \int_{\theta_3}^{\theta_1} r\, d\theta - |z_p| \Delta\theta,$$

where θ_i is the angle measured from the negative x axis to the vertex as numbered in Figure 101. The first of the these three integrals is evaluated. New notation is introduced as follows:

$$R^2 = R_1^2 + s_1^2.$$

The new variables are defined in Figure 102. It follows that

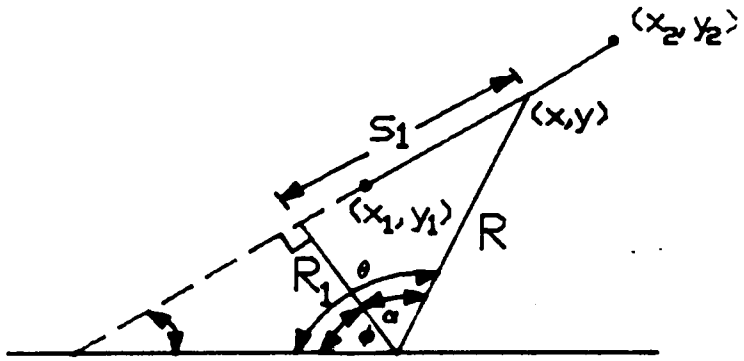

Figure 102. Variable Definitions

$$r = \sqrt{s_1^2 + R_1^2 + z_p^2},$$

where s_1 is a function only of θ and R_1 is constant. The variable r needs to be expressed in terms of θ . This relation is found by letting

$$\tan \alpha = \frac{s_1}{R_1}$$

Then

$$\frac{1}{\cos^2 \alpha} \, d\alpha = \frac{1}{R_1} \, ds_1.$$

From Figure 102

$$\alpha = \theta - \phi$$

where ϕ is a constant. Then it follows

$$d\alpha = d\theta$$

and

$$d\theta = \frac{\cos^2\alpha}{R_1}\, ds_1.$$

From Figure 102

$$\cos\alpha = \frac{R_1}{\sqrt{R_1^2 + s_1^2}}.$$

Therefore, whenever $\cos\alpha$ is negative R_1 is also negative. This situation occurs when ϕ is larger than θ . Thus, R_1 is negative only when the perpendicular projection is beyond the endpoint in the direction of increasing θ. The differential $d\theta$ is

$$d\theta = \frac{R_1^2}{R_1(R_1^2 + s_1^2)}\, ds_1$$

$$= \frac{R_1}{R_1^2 + s_1^2}\, ds_1.$$

The limits of the integral are changed to the new variable. The new variables are $s_1 = s_{11}$ when $\theta = \theta_1$, and $s_1 = s_{12}$ when $\theta = \theta_2$. Then the integral is

$$\int_{\theta_1}^{\theta_2} r\, d\theta = \int_{s_{11}}^{s_{12}} \sqrt{s_1^2 + R_1^2 + z_p^2}\, \frac{R_1}{R_1^2 + s_1^2}\, ds_1$$

$$= \int_{s_{11}}^{s_{12}} \frac{R_1(s_1^2 + R_1^2 + z_p^2)}{(R_1^2 + s_1^2)(s_1^2 + R_1^2 + z_p^2)^{1/2}}\, ds_1$$

$$= R_1 \int_{s_{11}}^{s_{12}} \frac{1}{(s_1^2 + R_1^2 + z_p^2)^{1/2}}\, ds_1$$

$$+ R_1 z_p^2 \int_{s_{11}}^{s_{12}} \frac{1}{(R_1^2 + s_1^2)(s_1^2 + R_1^2 + z_p^2)^{1/2}}\, ds_1.$$

The second integral is evaluated by substituting

$$t^2 = R_1^2 + z_p^2$$

and

$$s_1 = t \tan \psi.$$

The integral becomes

$$\int_{\theta_1}^{\theta_2} r\, d\theta = R_1 \int_{s_{11}}^{s_{12}} (s_1^2 + t^2)^{-1/2}\, ds_1 + R_1 z_p^2 \int_{\psi(s_{11})}^{\psi(s_{12})} \frac{t \sec^2 \psi\, d\psi}{(R_1^2 + t^2 \tan^2 \psi)(t^2 \tan^2 \psi + t^2)^{1/2}}$$

$$= R_1 \int_{s_{11}}^{s_{12}} (s_1^2 + t^2)^{-1/2}\, ds_1 + R_1 z_p^2 \int_{\psi(s_{11})}^{\psi(s_{12})} \frac{\sec \psi\, d\psi}{(R_1^2 + t^2 \tan^2 \psi)^{1/2}}.$$

Again changing variables, with

$$u = \sin \psi,$$

the integral is

$$\int_{\theta_1}^{\theta_2} r\, d\theta = R_1 \int_{s_{11}}^{s_{12}} (s_1^2 + t^2)^{-1/2}\, ds_1 + \frac{R_1 z_p^2}{z_p^2} \int_{u(s_{11})}^{u(s_{12})} \left[u^2 + \frac{R_1^2}{z_p^2} \right]^{-1} du$$

$$= R_1 \ln \left[s_1 + \sqrt{s_1^2 + t^2} \right] \Big|_{s_{11}}^{s_{12}} + R_1 \left(\frac{z_p^2}{R_1^2} \right)^{1/2} \tan^{-1} u \left(\frac{z_p^2}{R_1^2} \right)^{1/2} \Big|_{u(s_{11})}^{u(s_{12})}$$

$$= R_1 \ln\left\{ \frac{s_{12} + \left(s_{12}^2 + R_1^2 + z_p^2\right)^{1/2}}{s_{11} + \left(s_{11}^2 + R_1^2 + z_p^2\right)^{1/2}} \right\} + \frac{R_1}{|R_1|} |z_p| \tan^{-1}\left(\frac{|z_p|}{|R_1|} \sin\left(\tan^{-1} \frac{s_1}{t} \right) \right) \Bigg|_{s_{11}}^{s_{12}}$$

$$= R_1 \ln\left\{ \frac{s_{12} + \left(s_{12}^2 + R_1^2 + z_p^2\right)^{1/2}}{s_{11} + \left(s_{11}^2 + R_1^2 + z_p^2\right)^{1/2}} \right\}$$

$$+ \operatorname{sgn}(R_1) |z_p| \left[\tan^{-1}\left(\frac{|z_p|}{|R_1|} \frac{s_{12}}{\left(s_{12}^2 + R_1^2 + z_p^2\right)^{1/2}} \right) - \tan^{-1}\left(\frac{|z_p|}{|R_1|} \frac{s_{11}}{\left(s_{11}^2 + R_1^2 + z_p^2\right)^{1/2}} \right) \right].$$

From Figure 102

$$s_{12}^2 + R_1^2 + z_p^2 = (x_2 - x_p)^2 + (y_2 - y_p)^2 + z_p^2.$$

For the standard triangle

$$x_2 = b \qquad y_2 = c$$

and therefore

$$s_{12}^2 + R_1^2 + z_p^2 = (b - x_p)^2 + (c - y_p)^2 + z_p^2$$

which by definition reduces to

$$s_{12}^2 + R_1^2 + z_p^2 = r_2^2.$$

In a similar manner

$$s_{11}^2 + R_1^2 + z_p^2 = (x_1 - x_p)^2 + (y_1 - y_p)^2 + z_p^2$$

with

$$x_1 = 0 \qquad y_1 = 0$$

$$s_{11}^2 + R_1^2 + z_p^2 = x_p^2 + y_p^2 + z_p^2$$

$$s_{11}^2 + R_1^2 + z_p^2 = r_1^2.$$

Finally the first integral is

$$\int_{\theta_1}^{\theta_2} r\,d\theta = R_1 \ln\left\{\frac{s_{12}+r_2}{s_{11}+r_1}\right\} + \operatorname{sgn}(R_1)|z_p|\left[\tan^{-1}\left(\frac{|z_p|}{|R_1|}\frac{s_{12}}{r_2}\right) - \tan^{-1}\left(\frac{|z_p|}{|R_1|}\frac{s_{11}}{r_1}\right)\right].$$

Following the same procedure, one can show that

$$\int_{\theta_2}^{\theta_3} r\,d\theta = R_2 \ln\left\{\frac{s_{22}+r_3}{s_{21}+r_2}\right\} + \operatorname{sgn}(R_2)|z_p|\left[\tan^{-1}\left(\frac{|z_p|}{|R_2|}\frac{s_{22}}{r_3}\right) - \tan^{-1}\left(\frac{|z_p|}{|R_2|}\frac{s_{21}}{r_2}\right)\right],$$

and third integral can be written as

$$\int_{\theta_3}^{\theta_1} r\,d\theta = R_3 \ln\left\{\frac{s_{32}+r_1}{s_{31}+r_3}\right\} + \operatorname{sgn}(R_3)|z_p|\left[\tan^{-1}\left(\frac{|z_p|}{|R_3|}\frac{s_{32}}{r_1}\right) - \tan^{-1}\left(\frac{|z_p|}{|R_3|}\frac{s_{31}}{r_3}\right)\right].$$

The next step is to express the s_{ij} in terms of the coordinates of the vertices. To begin, we show that

$$\frac{s_{12}+r_2}{s_{11}+r_1} = \frac{r_1+r_2+d_1}{r_1+r_2-d_1}$$

where

$$d_1 = s_{12} - s_{11}.$$

This will be proved by showing the following is an identity

$$(s_{12}+r_2)(r_1+r_2-d_1) = (s_{11}+r_1)(r_1+r_2+d_1).$$

It follows that

$$s_{12}r_1 + s_{12}r_2 - s_{12}d_1 + r_1r_2 + r_2^2 - d_1r_2 = s_{11}r_1 + s_{11}r_2 + s_{11}d_1 + r_1^2 + r_1r_2 + d_1r_1.$$

By regrouping and canceling terms, one can obtain

$$r_2^2 - r_1^2 = r_1(s_{11} - s_{12}) + r_2(s_{11} - s_{12}) + r_1d_1 + r_2d_1 + d_1(s_{12} + s_{11}),$$

$$r_2^2 - r_1^2 = (s_{12} - s_{11})(s_{12} + s_{11}).$$

It follows from the definitions of r_1 and r_2 that

$$R_1^2 + s_{12}^2 + z_p^2 - R_1^2 - s_{11}^2 - z_p^2 = s_{12}^2 - s_{11}^2$$

which reduces to

$$s_{12}^2 - s_{11}^2 = s_{12}^2 - s_{11}^2,$$

thus completing the proof of

$$\frac{s_{12} + r_2}{s_{11} + r_1} = \frac{r_1 + r_2 + d_1}{r_1 + r_2 - d_1}.$$

In a similar manner it can easily be shown that

$$\frac{s_{22} + r_3}{s_{21} + r_2} = \frac{r_2 + r_3 + d_2}{r_2 + r_3 - d_2}$$

and

$$\frac{s_{32} + r_1}{s_{31} + r_3} = \frac{r_1 + r_3 + d_3}{r_1 + r_3 - d_3}.$$

Now to make the bookkeeping easier we let

$$Q_1 = \ln\left\{\frac{r_1 + r_2 + d_1}{r_1 + r_2 - d_1}\right\}$$

$$Q_2 = \ln\left\{ \frac{r_2 + r_3 + d_2}{r_2 + r_3 - d_2} \right\}$$

$$Q_3 = \ln\left\{ \frac{r_3 + r_1 + d_3}{r_3 + r_1 - d_3} \right\}$$

$$J_1 = \text{sgn}(R_1)\left[\tan^{-1}\left(\frac{|z_p|}{|R_1|}\frac{s_{12}}{r_2} \right) - \tan^{-1}\left(\frac{|z_p|}{|R_1|}\frac{s_{11}}{r_1} \right) \right]$$

$$J_2 = \text{sgn}(R_2)\left[\tan^{-1}\left(\frac{|z_p|}{|R_2|}\frac{s_{22}}{r_3} \right) - \tan^{-1}\left(\frac{|z_p|}{|R_2|}\frac{s_{21}}{r_2} \right) \right]$$

and

$$J_3 = \text{sgn}(R_3)\left[\tan^{-1}\left(\frac{|z_p|}{|R_3|}\frac{s_{32}}{r_1} \right) - \tan^{-1}\left(\frac{|z_p|}{|R_3|}\frac{s_{31}}{r_3} \right) \right]$$

then

$$\oint r\, d\theta = R_1Q_1 + R_2Q_2 + R_3Q_3 + |z_p|(J_1 + J_2 + J_3)$$

Finally the tenth integral is

$$I_{10} = R_1Q_1 + R_2Q_2 + R_3Q_3 + |z_p|(J_1 + J_2 + J_3 - \Delta\theta)$$

Now we return to the evaluation of I_9:

$$I_9 = \frac{\partial}{\partial z_p}\iint_S \frac{1}{r}\, dxdy.$$

The same steps are used as for I_{10}, the integral is then written as

$$I_9 = \oint \frac{z_p}{r}\, d\theta - \operatorname{sgn}(z_p)\Delta\theta$$

$$= \int_{s_{11}}^{s_{12}} \frac{z_p}{[s_1^2 + R_1^2 + z_p^2]^{1/2}} \frac{R_1}{R_1^2 + s_1^2}\, ds_1$$
$$+ \int_{s_{21}}^{s_{22}} \frac{z_p}{[s_2^2 + R_2^2 + z_p^2]^{1/2}} \frac{R_2}{R_2^2 + s_2^2}\, ds_2$$
$$+ \int_{s_{31}}^{s_{32}} \frac{z_p}{[s_3^2 + R_3^2 + z_p^2]^{1/2}} \frac{R_3}{R_3^2 + s_3^2}\, ds_3 - \operatorname{sgn}(z_p)\Delta\theta.$$

To evaluate the first integral we let

$$t^2 = R_1^2 + z_p^2$$

and

$$s_1 = t \tan \psi.$$

Then

$$\int_{s_{11}}^{s_{12}} \frac{z_p}{[s_1^2 + R_1^2 + z_p^2]^{1/2}} \frac{R_1}{R_1^2 + s_1^2}\, ds_1 = \int_{\psi(s_{11})}^{\psi(s_{12})} \frac{z_p R_1 t \sec^2 \psi}{(R_1^2 + t^2 \tan^2 \psi)[t^2 \tan^2 \psi + t^2]^{1/2}}\, d\psi$$

$$= \int_{\psi(s_{11})}^{\psi(s_{12})} \frac{z_p R_1 \sec \psi}{(R_1^2 + t^2 \tan^2 \psi)}\, d\psi.$$

This integral can be further reduced by multiplying top and bottom by $\cos^2\psi$

$$= z_p R_1 \int_{\psi(s_{11})}^{\psi(s_{12})} \frac{\cos \psi}{(R_1^2 \cos^2 \psi + t^2 \sin^2 \psi)}\, d\psi$$

$$= z_p R_1 \int_{\psi(s_{11})}^{\psi(s_{12})} \frac{\cos\psi}{(t^2 - R_1^2)\sin^2\psi + R_1^2}\, d\psi.$$

Because

$$t^2 - R_1^2 = z_p^2,$$

the integral is

$$= \frac{R_1}{z_p} \int_{\psi(s_{11})}^{\psi(s_{12})} \cos\psi \left[\sin^2\psi + \frac{R_1^2}{z_p^2} \right]^{-1} d\psi.$$

Again changing variables by letting

$$u = \sin\psi$$

one finds that the integral becomes

$$= \frac{R_1}{z_p} \int_{u(s_{11})}^{u(s_{12})} \left[u^2 + \left(\frac{R_1}{z_p} \right) \right]^{-1} du$$

$$= \frac{R_1}{z_p} \frac{|z_p|}{|R_1|} \left[\tan^{-1} \frac{|z_p|}{|R_1|} \sin\left(\tan^{-1} \frac{s_1}{t} \right) \right] \Bigg|_{s_{11}}^{s_{12}}$$

$$= \operatorname{sgn}(z_p)\operatorname{sgn}(R_1) \left[\tan^{-1} \left(\frac{|z_p|}{|R_1|} \frac{s_{12}}{(s_{12}^2 + R_1^2 + z_p^2)^{1/2}} \right) - \tan^{-1} \left(\frac{|z_p|}{|R_1|} \frac{s_{11}}{(s_{11}^2 + R_1^2 + z_p^2)^{1/2}} \right) \right]$$

$$= \operatorname{sgn}(z_p) J_1.$$

The same procedures can be followed to show

$$\int_{s_{21}}^{s_{22}} \frac{z_p}{[s_2^2 + R_2^2 + z_p^2]^{1/2}} \frac{R_2}{R_2^2 + s_2^2} \, ds_2 = \text{sgn}(z_p) J_2$$

and

$$\int_{s_{31}}^{s_{32}} \frac{z_p}{[s_3^2 + R_3^2 + z_p^2]^{1/2}} \frac{R_3}{R_3^2 + s_3^2} \, ds_3 = \text{sgn}(z_p) J_3.$$

Therefore, the ninth integral is

$$I_9 = \text{sgn}(z_p)[J_1 + J_2 + J_3 - \Delta\theta].$$

All the integrals have now been evaluated. Before recapping the results, we write the constants defined in integrals I_9 and I_{10} in terms of the coordinates of the general triangle. For this purpose, one side of the triangle is examined in detail. This side is shown in Figure 103.

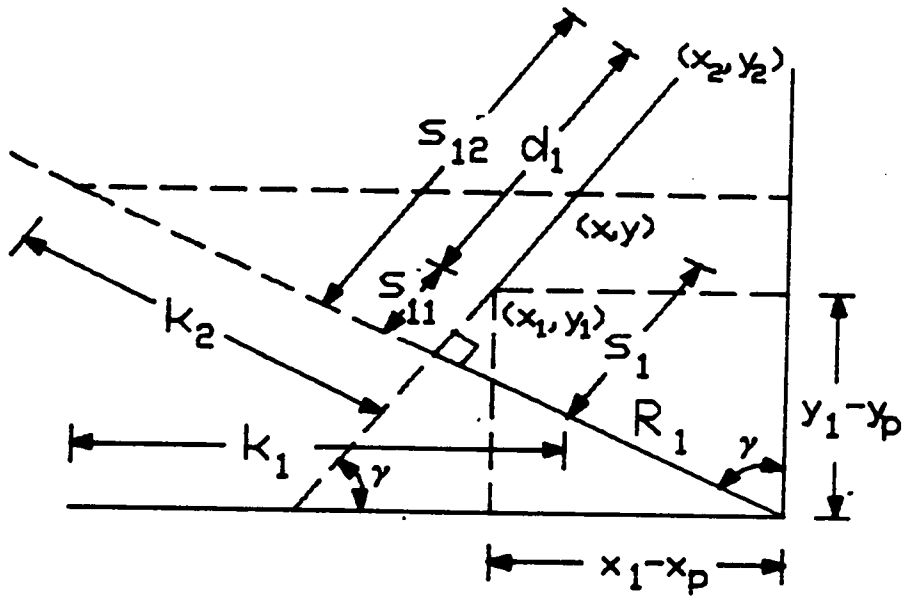

Figure 103. Side One of the Triangle

From Figure 103, it follows that

$$d_1 = [(x_2 - x_1)^2 + (y_2 - y_1)^2]^{1/2}$$

$$= [b^2 + c^2]^{1/2}.$$

Designating

$$C_1 = \cos\gamma = \frac{x_2 - x_1}{d_1} = \frac{b}{d_1}$$

$$S_1 = \sin\gamma = \frac{y_2 - y_1}{d_1} = \frac{c}{d_1}$$

one can in turn be used to define $s_{1/}$, again from Figure 103

$$C_1 = \frac{s_1}{k_1} \quad \text{or} \quad k_1 = \frac{s_1}{C_1}$$

and

$$\tan\gamma = \frac{(x_p - x) + k_1}{(y - y_p)},$$

then

$$\frac{S_1}{C_1} = \frac{(x_p - x) + \frac{s_1}{C_1}}{(y - y_p)}$$

or

$$S_1(y - y_p) - C_1(x_p - x) = s_1.$$

Therefore,

$$s_{12} = C_1(x_2 - x_p) + S_1(y_2 - y_p)$$

$$= C_1(b - x_p) + S_1(c - y_p)$$

and

$$s_{11} = C_1(x_1 - x_p) + S_1(y_1 - y_p)$$

$$= C_1(-x_p) + S_1(-y_p)$$

In a similar manner the remaining s_{ij} can be written as

$$d_2 = [(x_3 - x_2)^2 + (y_3 - y_2)]^{1/2} = [(a - b)^2 + c^2]^{1/2}$$

$$C_2 = \frac{x_3 - x_2}{d_2} = \frac{a - b}{d_2}$$

$$S_2 = \frac{y_3 - y_2}{d_2} = -\frac{c}{d_2}$$

$$s_{22} = C_2(a - x_p) + S_2(-y_p)$$

$$s_{21} = C_2(b - x_p) + S_2(c - y_p)$$

and

$$d_3 = [(x_1 - x_3)^2 + (y_1 - y_3)]^{1/2} = [a^2]^{1/2} = a$$

$$C_3 = \frac{x_1 - x_3}{d_3} = -1$$

$$S_3 = \frac{y_1 - y_3}{d_3} = 0$$

$$s_{32} = -1(-x_p) = x_p$$

$$s_{31} = -1(a - x_p) = x_p - a$$

Next we express R_1, R_2 and R_3 in terms of the coordinates of the vertices of the triangle. It follows from Figure 103 that

$$\cos\gamma = \frac{(y - y_p)}{R_1 + k_2}$$

$$k_2 = s_1 \tan\gamma$$

and also

$$R_1C_1 + S_1s_{11} = (y_1 - y_p),$$

then

$$R_1 = \frac{(y_1 - y_p)}{C_1} - \frac{S_1}{C_1} s_{11}$$

$$= \frac{(y_1 - y_p)}{C_1} - \frac{S_1}{C_1}[(x_1 - x_p)C_1 + (y_1 - y_p)S_1]$$

$$= (y_1 - y_p)[\frac{1 - S_1^2}{C_1}] - (x_1 - x_p)S_1$$

$$= (x_p - x_1)S_1 - (y_p - y_1)C_1$$

$$= x_pS_1 - y_pC_1.$$

The same approach can be used to show

$$R_2 = (x_p - x_2)S_2 - (y_p - y_2)C_2$$

$$= (x_p - b)S_2 - (y_p - c)C_2$$

and

$$R_3 = (x_p - x_3)S_3 - (y_p - y_3)C_3$$

$$= (x_p - a)S_3 - y_p C_3.$$

Next, one can relate Q_1, Q_2 and Q_3 to the H_i integrals by using the definitions stated earlier.

$$Q_1 = \ln\left\{\frac{s_{12} + r_2}{s_{11} + r_1}\right\}$$

$$= \ln\left\{\frac{\frac{b}{[b^2 + c^2]^{1/2}}(b - x_p) + \frac{c}{[b^2 + c^2]^{1/2}}(c - y_p) + r_2}{\frac{b}{[b^2 + c^2]^{1/2}}(-x_p) + \frac{c}{[b^2 + c^2]^{1/2}}(-y_p) + r_1}\right\}$$

$$= \ln\left\{\frac{\frac{b}{c}(b - x_p) + (c - y_p) + r_2\frac{[b^2 + c^2]^{1/2}}{c}}{-x_p\frac{b}{c} - y_p + r_1\frac{[b^2 + c^2]^{1/2}}{c}}\right\}$$

$$= \ln\left\{\frac{r_2\sqrt{\alpha_3} + \frac{b^2 + c^2}{c} - (\frac{b}{c}x_p + y_p)}{r_1\sqrt{\alpha_3} - (\frac{b}{c}x_p + y_p)}\right\}$$

$$= \ln\left\{\frac{r_2\sqrt{\alpha_3} + c\alpha_3 - \alpha_4}{r_1\sqrt{\alpha_3} - \alpha_4}\right\}.$$

Therefore,

$$Q_1 = \sqrt{\alpha_3}\, H_3.$$

$$Q_2 = \ln\left\{\frac{s_{22} + r_3}{s_{21} + r_2}\right\}$$

$$= \ln\left\{ \frac{r_3 + \dfrac{a-b}{[(a-b)^2+c^2]^{1/2}}(a-x_p) + \dfrac{c}{[(a-b)^2+c^2]^{1/2}} y_p}{r_2 + \dfrac{a-b}{[(a-b)^2+c^2]^{1/2}}(b-x_p) - \dfrac{c}{[(a-b)^2+c^2]^{1/2}}(c-y_p)} \right\}$$

$$= \ln\left\{ \frac{r_3 \dfrac{[(a-b)^2+c^2]^{1/2}}{c} + \dfrac{a-b}{c}(a-x_p) + y_p}{r_2 \dfrac{[(a-b)^2+c^2]^{1/2}}{c} + \dfrac{a-b}{c}(b-x_p) - (c-y_p)} \right\}$$

$$= \ln\left\{ \frac{r_3\sqrt{\alpha_1} - (\frac{b-a}{c}(a-x_p) - y_p)}{r_2\sqrt{\alpha_1} + b(\frac{a-b}{c}) - a(\frac{a-b}{c}) + a(\frac{a-b}{c}) + (\frac{b-a}{c})x_p - c + y_p} \right\}$$

$$= \ln\left\{ \frac{r_3\sqrt{\alpha_1} - \alpha_2}{r_2\sqrt{\alpha_1} + (x_p - a)(\frac{b-a}{c}) + y_p - \dfrac{(b-a)^2}{c} - c} \right\}$$

$$= \ln\left\{ \frac{r_3\sqrt{\alpha_1} - \alpha_2}{r_2\sqrt{\alpha_1} - \alpha_2 - c\alpha_1} \right\},$$

which previously was shown to be

$$\ln\left\{ \frac{r_3\sqrt{\alpha_1} - \alpha_2}{r_2\sqrt{\alpha_1} - \alpha_2 - c\alpha_1} \right\} = \ln\left\{ \frac{\sqrt{\alpha_1}\, r_2 + \alpha_2 + c\alpha_1}{\sqrt{\alpha_1}\, r_3 + \alpha_2} \right\}.$$

Therefore,

$$Q_2 = \sqrt{\alpha_1}\, H_1.$$

Finally,

$$Q_3 = \ln\left\{ \frac{s_{32} + r_1}{s_{31} + r_3} \right\}$$

$$= \ln\left\{ \frac{x_p + r_1}{x_p - a + r_3} \right\}.$$

Therefore,

$$Q_3 = H_9.$$

The last topic before recapping the results of this Appendix is to check some results that were presented by Smith and Hess. They assert that

$$I_7 = S_1Q_1 + S_2Q_2 + S_3Q_3.$$

Using the definitions of each variable, one finds that

$$S_1 = \frac{c}{[b^2 + c^2]^{1/2}} = \frac{1}{\sqrt{\alpha_3}},$$

$$S_2 = \frac{-c}{[(a-b)^2 + c^2]^{1/2}} = -\frac{1}{\sqrt{\alpha_1}},$$

$$S_3 = 0,$$

$$Q_1 = \sqrt{\alpha_3}\, H_3,$$

$$Q_2 = \sqrt{\alpha_1}\, H_1,$$

and

$$Q_3 = H_9,$$

one finds that the integral I_7 is

$$I_7 = = H_3 - H_1$$

which was obtained earlier. Also they state that

$$I_8 = -C_1Q_1 - C_2Q_2 - C_3Q_3.$$

Using the definitions

$$C_1 = \frac{b}{[b^2 + c^2]^{1/2}} = \frac{b}{c} \frac{1}{\sqrt{\alpha_3}},$$

$$C_2 = \frac{a-b}{[(a-b)^2 + c^2]^{1/2}} = \frac{a-b}{c} \frac{1}{\sqrt{\alpha_1}},$$

and

$$C_3 = -1$$

one can show the integral I_8 is

$$I_8 = = -\frac{a-b}{c} H_1 - \frac{b}{c} H_3 + H_9$$

which also checks with the results presented earlier.

Next we review the results obtained in this Appendix. The velocity components are

$$\begin{aligned} V_x = -\frac{1}{4\pi} [& \gamma_{y1}(a_1 I_3 + b_1 I_6 + a_1 x_p I_9 + b_1 y_p I_9 + I_9) \\ & + \gamma_{y2}(a_2 I_3 + b_2 I_6 + a_2 x_p I_9 + b_2 y_p I_9) \\ & + \gamma_{y3}(a_3 I_3 + b_3 I_6 + a_3 x_p I_9 + b_3 y_p I_9)] \end{aligned}$$

$$\begin{aligned} V_y = \frac{1}{4\pi} [& \gamma_{x1}(a_1 I_3 + b_1 I_6 + a_1 x_p I_9 + b_1 y_p I_9 + I_9) \\ & + \gamma_{x2}(a_2 I_3 + b_2 I_6 + a_2 x_p I_9 + b_2 y_p I_9) \\ & + \gamma_{x3}(a_3 I_3 + b_3 I_6 + a_3 x_p I_9 + b_3 y_p I_9)] \end{aligned}$$

and

$$\begin{aligned} V_z = \frac{1}{4\pi} [& \gamma_{y1}(a_1 I_1 + b_1 I_4 + a_1 x_p I_7 + b_1 y_p I_7 + I_7 + a_1 I_{10}) \\ & - \gamma_{x1}(a_1 I_2 + b_1 I_5 + a_1 x_p I_8 + b_1 y_p I_8 + I_8 + b_1 I_{10}) \\ & + \gamma_{y2}(a_2 I_1 + b_2 I_4 + a_2 x_p I_7 + b_2 y_p I_7 + a_2 I_{10}) \\ & - \gamma_{x2}(a_2 I_2 + b_2 I_5 + a_2 x_p I_8 + b_2 y_p I_8 + b_2 I_{10}) \\ & + \gamma_{y3}(a_3 I_1 + b_3 I_4 + a_3 x_p I_7 + b_3 y_p I_7 + a_3 I_{10}) \\ & - \gamma_{x3}(a_3 I_2 + b_3 I_5 + a_3 x_p I_8 + b_3 y_p I_8 + b_3 I_{10})], \end{aligned}$$

where

$$I_1 = (x_p - a)H_1 + (\frac{a-b}{c})H_2 - x_pH_3 + \frac{b}{c}H_4$$

$$I_2 = y_p(H_1 - H_3) + H_4 - H_2$$

$$I_3 = z_p(H_1 - H_3)$$

$$I_4 = x_pH_5 - H_6 + x_pH_7 - H_8 + r_3 - r_1$$

$$I_5 = y_pH_5 - \frac{c}{b}H_6 + [y_p + \frac{ac}{b-a}]H_7 - \frac{c}{b-a}H_8 - y_pH_9$$

$$I_6 = z_pH_5 + z_pH_7 - z_pH_9$$

$$I_7 = H_3 - H_1$$

$$I_8 = H_9 - H_5 - H_7$$

$$I_9 = \text{sgn}(z_p)[J_1 + J_2 + J_3 - \Delta\theta]$$

$$I_{10} = R_1Q_1 + R_2Q_2 + R_3Q_3 + |z_p|(J_1 + J_2 + J_3 - \Delta\theta)$$

$$H_1 = \frac{Q_2}{\sqrt{\alpha_1}}$$

$$H_2 = \frac{1}{\alpha_1}(r_2 - r_3) - \frac{\alpha_2}{\alpha_1}H_1$$

$$H_3 = \frac{Q_1}{\sqrt{\alpha_3}}$$

$$H_4 = \frac{1}{\alpha_3}[r_2 - r_1] + \frac{\alpha_4}{\alpha_3}H_3$$

$$H_5 = \frac{b}{c} H_3$$

$$H_6 = \frac{1}{\alpha_5}(r_2 - r_1) + \frac{\alpha_6}{\alpha_5} H_5$$

$$H_7 = \frac{a-b}{c} H_1$$

$$H_8 = \frac{1}{\alpha_7}[r_3 - r_2] + \frac{\alpha_8}{\alpha_7} H_7$$

$$H_9 = Q_3$$

$$\alpha_1 = (\frac{a-b}{c})^2 + 1$$

$$\alpha_2 = (\frac{b-a}{c})(a - x_p) - y_p$$

$$\alpha_3 = \frac{b^2 + c^2}{c^2}$$

$$\alpha_4 = \frac{b}{c} x_p + y_p$$

$$\alpha_5 = (\frac{c}{b})^2 + 1$$

$$\alpha_6 = x_p + \frac{c}{b} y_p$$

$$\alpha_7 = 1 + (\frac{c}{b-a})^2$$

$$\alpha_8 = x_p + a(\frac{c}{b-a})^2 + \frac{c}{b-a} y_p$$

$$r_1^2 = x_p^2 + y_p^2 + z_p^2$$

$$r_2^2 = (b - x_p)^2 + (c - y_p)^2 + z_p^2$$

$$r_3^2 = (a - x_p)^2 + y_p^2 + z_p^2$$

$$Q_1 = \ln\left\{ \frac{r_1 + r_2 + d_1}{r_1 + r_2 - d_1} \right\}$$

$$Q_2 = \ln\left\{ \frac{r_2 + r_3 + d_2}{r_2 + r_3 - d_2} \right\}$$

$$Q_3 = \ln\left\{ \frac{r_3 + r_1 + d_3}{r_3 + r_1 - d_3} \right\}$$

$$J_1 = \text{sgn}(R_1)\left[\tan^{-1}\left(\frac{|z_p|}{|R_1|} \frac{s_{12}}{r_2} \right) - \tan^{-1}\left(\frac{|z_p|}{|R_1|} \frac{s_{11}}{r_1} \right) \right]$$

$$J_2 = \text{sgn}(R_2)\left[\tan^{-1}\left(\frac{|z_p|}{|R_2|} \frac{s_{22}}{r_3} \right) - \tan^{-1}\left(\frac{|z_p|}{|R_2|} \frac{s_{21}}{r_2} \right) \right]$$

$$J_3 = \text{sgn}(R_3)\left[\tan^{-1}\left(\frac{|z_p|}{|R_3|} \frac{s_{32}}{r_1} \right) - \tan^{-1}\left(\frac{|z_p|}{|R_3|} \frac{s_{31}}{r_3} \right) \right]$$

$$d_1 = [b^2 + c^2]^{1/2}$$

$$d_2 = [(a - b)^2 + c^2]^{1/2}$$

$$d_3 = [a^2]^{1/2} = a$$

$$C_1 = \frac{b}{d_1}, \quad S_1 = \frac{c}{d_1}$$

$$C_2 = \frac{a - b}{d_2}, \quad S_2 = -\frac{c}{d_2}$$

$$C_3 = -1, \quad S_3 = 0$$

$$R_1 = x_p S_1 - y_p C_1$$

$$R_2 = (x_p - b)S_2 - (y_p - c)C_2$$

$$R_3 = (x_p - a)S_3 - y_p C_3$$

$$s_{12} = C_1(b - x_p) + S_1(c - y_p)$$

$$s_{11} = C_1(-x_p) + S_1(-y_p)$$

$$s_{22} = C_2(a - x_p) + S_2(-y_p)$$

$$s_{21} = C_2(b - x_p) + S_2(c - y_p)$$

$$s_{32} = C_3(-x_p) + S_3(-y_p)$$

$$s_{31} = C_3(a - x_p) + S_3(-y_p)$$

I.3 Numerical Singularities

The general triangular element, is always oriented with the longest side in the positive local x direction and the third vertex in the positive y direction. There are only three possible areas where numerical problems could arise. These are on the planes containing the edges of the triangles and perpendicular to the element, along the edges of the triangle, and on the surface of the triangle. Each of these areas is discussed in detail below.

First the planes containing the edge are examined. The reason there is a numerical problem on these planes is that the R_i are identically zero, and these appear in the denominators of the J_i. It follows from the definitions of the R_i that the conditions for them to be zero are:

1) For $R_1 = 0$ $\quad x_p = \frac{b}{c} y_p$

2) For $R_2 = 0$ $\quad x_p = -(y_p - c)\frac{(a-b)}{c} + b$

3) For $R_3 = 0$ $\quad y_p = 0$

These planes are shown in Figure 104.

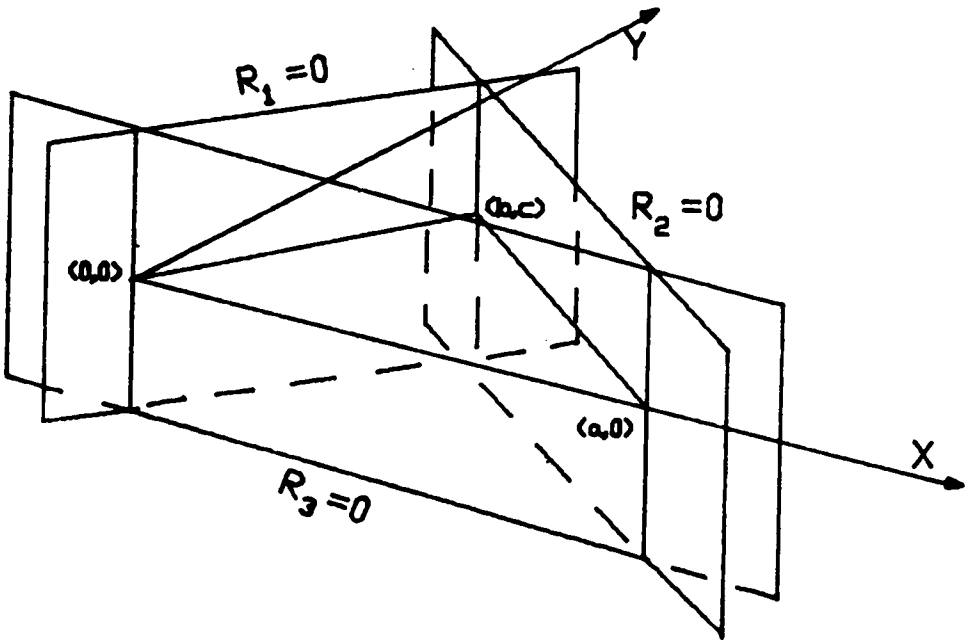

Figure 104. Planes of Numerical Singularities

Case 1, where $R_1 = 0$, is examined in detail below. The factor R_1 is zero on the plane described by

$$x_p = \frac{b}{c} y_p$$

The only term with R_1 in the denominator is J_1: therefore, this is the only term considered. The J_1 is determined by evaluating the limit as the plane is approached and setting J_1 at this limit on the plane. The limit is written as

$$\lim_{x_p \to \frac{b}{c} y_p} J_1 = \lim_{x_p \to \frac{b}{c} y_p} \operatorname{sgn}(R_1) \left[\tan^{-1}\left(\frac{|z_p|}{|R_1|} \frac{s_{12}}{r_2} \right) - \tan^{-1}\left(\frac{|z_p|}{|R_1|} \frac{s_{11}}{r_1} \right) \right]$$

$$= \lim_{x_p \to \frac{b}{c} y_p} \operatorname{sgn}(R_1) \lim_{x_p \to \frac{b}{c} y_p} \left[\tan^{-1}\left(\frac{|z_p|}{|R_1|} \frac{s_{12}}{r_2} \right) - \tan^{-1}\left(\frac{|z_p|}{|R_1|} \frac{s_{11}}{r_1} \right) \right].$$

The first factor is

$$\lim_{x_p \to \frac{b}{c} y_p} \operatorname{sgn}(R_1) = \begin{cases} 1 & x \to \frac{b}{c} y_p^+ \\ -1 & x \to \frac{b}{c} y_p^- \end{cases}.$$

The second factor is

$$\lim_{x_p \to \frac{b}{c} y_p} \left[\tan^{-1}\left(\frac{|z_p|}{|R_1|} \frac{s_{12}}{r_2} \right) - \tan^{-1}\left(\frac{|z_p|}{|R_1|} \frac{s_{11}}{r_1} \right) \right] =$$

$$\tan^{-1}\left[\lim_{x_p \to \frac{b}{c} y_p} \left(\frac{|z_p|}{|R_1|} \frac{s_{12}}{r_2} \right) \right] - \tan^{-1}\left[\lim_{x_p \to \frac{b}{c} y_p} \left(\frac{|z_p|}{|R_1|} \frac{s_{11}}{r_1} \right) \right].$$

Because

$$R_1 = \frac{c}{d_1} x_p - \frac{b}{d_1} y_p,$$

$$s_{12} = (b - x_p) \frac{b}{d_1} + (c - y_p) \frac{c}{d_1}$$

and

$$r_2 = [(b - x_p)^2 + (c - y_p)^2 + z_p^2]^{1/2},$$

the first limit can be expanded as

$$\lim_{x_p \to \frac{b}{c} y_p} \left(\frac{|z_p|}{|R_1|} \frac{s_{12}}{r_2} \right) = \lim_{x_p \to \frac{b}{c} y_p} \frac{|z_p|}{[(b - x_p)^2 + (c - y_p)^2 + z_p^2]^{1/2}} \lim_{x_p \to \frac{b}{c} y_p} \frac{s_{12}}{|R_1|},$$

the first of these limits is positive and finite except where $x_p = b$, $y_p = c$ and $z_p = 0$. This singularity will be examined later. The limit is written as

$$\lim_{x_p \to \frac{b}{c} y_p} \left(\frac{|z_p|}{|R_1|} \frac{s_{12}}{r_2} \right) = k_1 \lim_{x_p \to \frac{b}{c} y_p} \frac{s_{12}}{|R_1|}$$

where k_1 is positive. The definitions are used to write this limit as

$$\lim_{x_p \to \frac{b}{c} y_p} \frac{s_{12}}{|R_1|} = \lim_{x_p \to \frac{b}{c} y_p} \frac{(b - x_p)\frac{b}{d_1} + (c - y_p)\frac{c}{d_1}}{|\frac{c}{d_1} x_p - \frac{b}{d_1} y_p|}$$

$$= \lim_{x_p \to \frac{b}{c} y_p} \frac{(b - x_p)b + (c - y_p)c}{|cx_p - by_p|}$$

$$= \frac{\lim\limits_{x_p \to \frac{b}{c} y_p} (b - x_p)b + (c - y_p)c}{\lim\limits_{x_p \to \frac{b}{c} y_p} |cx_p - by_p|}.$$

The line $x_p = b$, $y_p = c$ and $z_p \neq 0$ will be discussed later. The denominator is always positive, the sign of the numerator is

$$\lim_{x_p \to \frac{b}{c} y_p} (b - x_p)b + (c - y_p)c = b^2 + c^2 - (\frac{b^2}{c} + c)y_p$$

$$= b^2 + c^2 - (b^2 + c^2)\frac{y_p}{c}$$

$$= \begin{cases} +k_2 & y_p < c \\ -k_2 & y_p > c \end{cases}$$

where k_2 is positive. Because the denominator tends to positive zero the first limit is

$$\lim_{x_p \to \frac{b}{c} y_p} \tan^{-1}\left(\frac{|z_p|}{|R_1|} \frac{s_{12}}{r_2} \right) = \begin{cases} \frac{\pi}{2} & y_p < c \\ -\frac{\pi}{2} & y_p > c \\ \text{undetermined} & y_p = c \end{cases}.$$

Because

$$R_1 = \frac{c}{d_1} x_p - \frac{b}{d_1} y_p,$$

$$s_{11} = -x_p \frac{b}{d_1} - y_p \frac{c}{d_1},$$

and

$$r_1 = [x_p^2 + y_p^2 + z_p^2]^{1/2},$$

the second limit is

$$\lim_{x_p \to \frac{b}{c} y_p} \left(\frac{|z_p|}{|R_1|} \frac{s_{11}}{r_1} \right) = \lim_{x_p \to \frac{b}{c} y_p} \frac{|z_p|}{[x_p^2 + y_p^2 + z_p^2]^{1/2}} \lim_{x_p \to \frac{b}{c} y_p} \frac{s_{11}}{|R_1|}.$$

The first of these limits is positive and finite except where $x_p = 0$, $y_p = 0$ and $z_p = 0$. This point is discussed later. The limit is written as

$$\lim_{x_p \to \frac{b}{c} y_p} \left(\frac{|z_p|}{|R_1|} \frac{s_{11}}{r_1} \right) = k_1 \lim_{x_p \to \frac{b}{c} y_p} \frac{s_{11}}{|R_1|}$$

where k_1 is positive. The previous definitions are used to write this limit as

$$\lim_{x_p \to \frac{b}{c} y_p} \frac{s_{11}}{|R_1|} = \lim_{x_p \to \frac{b}{c} y_p} \frac{-x_p \frac{b}{d_1} - y_p \frac{c}{d_1}}{\left| \frac{c}{d_1} x_p - \frac{b}{d_1} y_p \right|}$$

$$= \lim_{x_p \to \frac{b}{c} y_p} \frac{-x_p b - y_p c}{|c x_p - b y_p|}$$

$$= \frac{\lim\limits_{x_p \to \frac{b}{c} y_p} -x_p b - y_p c}{\lim\limits_{x_p \to \frac{b}{c} y_p} |c x_p - b y_p|}.$$

The line $x_p = 0$, $y_p = 0$ and $z_p \neq 0$ will be discussed later. The denominator is always positive, the sign of the numerator is

$$\lim_{x_p \to \frac{b}{c} y_p} -x_p b - y_p c = -\frac{b^2}{c} y_p - c y_p$$

$$= -(b^2 + c^2)\frac{y_p}{c}$$

$$= \begin{cases} +k_2 & y_p < 0 \\ -k_2 & y_p > 0 \end{cases}$$

where k_2 is positive. Because the denominator tends to positive zero, the second limit can be evaluated as

$$\lim_{x_p \to \frac{b}{c} y_p} \tan^{-1}\left(\frac{|z_p|}{|R_1|}\frac{s_{11}}{r_2}\right) = \begin{cases} \frac{\pi}{2} & y_p < 0 \\ -\frac{\pi}{2} & y_p > 0 \\ \text{undetermined} & y_p = 0 \end{cases}.$$

The total limit is determined by approaching the plane from both sides. The limits, as each side is approached are

$$\lim_{x_p \to \frac{b}{c} y_p^+} (J_1 - \Delta\theta) = \begin{cases} 1(-\frac{\pi}{2} - (-\frac{\pi}{2})) - 0 & y_p > c \\ 1(\frac{\pi}{2} - (-\frac{\pi}{2})) - 2\pi & 0 < y_p < c \\ 1(\frac{\pi}{2} - (\frac{\pi}{2})) - 0 & y_p < 0 \end{cases}$$

and

$$\lim_{x_p \to \frac{b}{c} y_p^-} (J_1 - \Delta\theta) = \begin{cases} -1(-\frac{\pi}{2} - (-\frac{\pi}{2})) - 0 & y_p > c \\ -1(\frac{\pi}{2} - (-\frac{\pi}{2})) - 0 & 0 < y_p < c \\ -1(\frac{\pi}{2} - (\frac{\pi}{2})) - 0 & y_p < 0 \end{cases}.$$

The limits are the same approaching from either direction. The quantity used in evaluating the velocity on this plane is chosen to be

$$(J_1 + J_2 + J_3 - \Delta\theta)\Big|_{x_p = \frac{b}{c} y_p} = \begin{cases} J_2 + J_3 & y_p > c \text{ or } y_p < 0 \\ J_2 + J_3 - \pi & 0 < y_p < c \\ \text{undetermined} & y_p = 0 \text{ or } y_p = c \end{cases}.$$

Case 2, where $R_2 = 0$ is determined in a similar manner. The singular component of the velocity calculations on the plane described by

$$x_p = \frac{(b-a)}{c} y_p + a$$

is

$$\lim_{x_p \to y'} (J_1 + J_2 + J_3 - \Delta\theta) = \begin{cases} J_1 + J_3 & y_p > c \text{ or } y_p < 0 \\ J_1 + J_3 - \pi & 0 < y_p < c \\ \text{undetermined} & y_p = 0 \text{ or } y_p = c \end{cases},$$

where

$$y' = \frac{(b-a)}{c} y_p + a.$$

Case 3, where $R_3 = 0$ is now determined. The singular component of the velocity calculations on the plane described by

$$y_p = 0$$

is

$$\lim_{y_p \to 0}(J_1 + J_2 + J_3 - \Delta\theta) = \begin{cases} J_1 + J_2 & x_p > a \text{ or } x_p < 0 \\ J_1 + J_2 - \pi & 0 < x_p < a \\ \text{undetermined} & x_p = 0 \text{ or } x_p = a \end{cases}.$$

The lines where the limits where classified as undetermined are now examined. These lines are described by

$$x_p = 0 \quad y_p = 0 \quad z_p \neq 0,$$

$$x_p = b \quad y_p = c \quad z_p \neq 0,$$

and

$$x_p = a \quad y_p = 0 \quad z_p \neq 0.$$

The first line segment has both J_1 and J_3 undetermined. The limit as this segment is approached is

$$\lim_{\substack{x_p \to 0 \\ y_p \to 0}}(J_1 + J_2 + J_3 - \Delta\theta) = \lim_{\substack{x_p \to 0 \\ y_p \to 0}}(J_1 + J_3 - \Delta\theta) + J_2$$

where

$$J_1 = \text{sgn}(R_1)\left[\tan^{-1}\left(\frac{|z_p|}{|R_1|}\frac{s_{12}}{r_2}\right) - \tan^{-1}\left(\frac{|z_p|}{|R_1|}\frac{s_{11}}{r_1}\right)\right]$$

and

$$J_3 = \text{sgn}(R_3)\left[\tan^{-1}\left(\frac{|z_p|}{|R_3|}\frac{s_{32}}{r_1}\right) - \tan^{-1}\left(\frac{|z_p|}{|R_3|}\frac{s_{31}}{r_3}\right)\right].$$

The above limit is evaluated by changing to cylindrical coordinates with the origin at (0,0,0). The point of interest is then written as

$$x_p = r\cos\theta$$

$$y_p = r\sin\theta.$$

and the factors needed to evaluate the limit are

$$R_1 = r\cos\theta\frac{c}{d_1} - r\sin\theta\frac{b}{d_1}$$

$$s_{12} = (b - r\cos\theta)\frac{b}{d_1} + (c - r\sin\theta)\frac{c}{d_1}$$

and

$$r_2 = [(b - r\cos\theta)^2 + (c - r\sin\theta)^2 + z_p^2]^{1/2}.$$

The limit

$$\lim_{r\to 0}\left(\frac{|z_p|}{|R_1|}\ \frac{s_{12}}{r_2}\right)$$

has no upper bound because $|z_p| > 0$, $|R_1| > 0$, $s_{12} > 0$ and $r_2 > 0$ in the limit and R_1 is the only quantity tending to zero; therefore,

$$\lim_{r\to 0}\tan^{-1}\left(\frac{|z_p|}{|R_1|}\ \frac{s_{12}}{r_2}\right) = \frac{\pi}{2}.$$

The same cylindrical coordinate frame is used to evaluate the velocity along the second line segment. The factors needed to evaluate the limit are

$$R_3 = r\sin\theta$$

$$s_{31} = r\cos\theta - a$$

$$r_3 = [(a - r\cos\theta)^2 + (r\sin\theta)^2 + z_p^2]^{1/2}.$$

The limit

$$\lim_{r\to 0}\left(\frac{|z_p|}{|R_3|}\ \frac{s_{31}}{r_3}\right)$$

has no lower bound because $|z_p|>0$, $|R_3|>0$, $s_{31}<0$ and $r_3>0$ in the limit and R_3 is the only quantity tending to zero, therefore

$$\lim_{r\to 0}\tan^{-1}\left(\frac{|z_p|}{|R_3|}\ \frac{s_{31}}{r_3}\right)=-\frac{\pi}{2}.$$

The remaining factors of J_1 and J_3 are

$$\lim_{r\to 0}\operatorname{sgn}(R_1)=\begin{cases} 1 & \tan^{-1}(\frac{c}{b})-\pi<\theta<\tan^{-1}(\frac{c}{b}) \\ -1 & \tan^{-1}(\frac{c}{b})<\theta<\tan^{-1}(\frac{c}{b})+\pi \\ \text{undetermined} & \theta=\tan^{-1}(\frac{c}{b})\text{ or }\theta=\tan^{-1}(\frac{c}{b})+\pi \end{cases}$$

which is

$$\lim_{r\to 0}\operatorname{sgn}(R_3)=\begin{cases} 1 & 0<\theta<\pi \\ -1 & -\pi<\theta<0 \\ \text{undetermined} & \theta=0\text{ or }\theta=\pi \end{cases},$$

$$\lim_{r\to 0}\left(\frac{|z_p|}{|R_1|}\ \frac{s_{11}}{r_1}\right)=|z_p|\lim_{r\to 0}\frac{1}{[r^2+z_p^2]^{1/2}}\lim_{r\to 0}\frac{s_{11}}{|R_1|}$$

$$=\frac{|z_p|}{|z_p|}\lim_{r\to 0}\frac{-rb\cos\theta-rc\sin\theta}{|rc\cos\theta-rb\sin\theta|}$$

$$=\begin{cases} \lim_{r\to 0}\dfrac{-rb\cos\theta-rc\sin\theta}{rc\cos\theta-rb\sin\theta} & \tan^{-1}(\frac{c}{b})-\pi<\theta<\tan^{-1}(\frac{c}{b}) \\ \lim_{r\to 0}\dfrac{-rb\cos\theta-rc\sin\theta}{rb\sin\theta-rc\cos\theta} & \tan^{-1}(\frac{c}{b})<\theta<\tan^{-1}(\frac{c}{b})+\pi \end{cases}$$

$$= \begin{cases} \dfrac{b\cos\theta + c\sin\theta}{b\sin\theta - c\cos\theta} & \tan^{-1}(\dfrac{c}{b}) - \pi < \theta < \tan^{-1}(\dfrac{c}{b}) \\ \dfrac{b\cos\theta - c\sin\theta}{c\cos\theta - b\sin\theta} & \tan^{-1}(\dfrac{c}{b}) < \theta < \tan^{-1}(\dfrac{c}{b}) + \pi \\ \text{undetermined} & \theta = \tan^{-1}(\dfrac{c}{b}) \text{ or } \theta = \tan^{-1}(\dfrac{c}{b}) + \pi \end{cases}$$

and

$$\lim_{r\to 0}\left(\frac{|z_p|}{|R_3|}\ \frac{s_{32}}{r_1}\right) = |z_p| \lim_{r\to 0}\frac{1}{[r^2 + z_p^2]^{1/2}} \lim_{r\to 0}\frac{r\cos\theta}{|r\sin\theta|}$$

$$= \frac{|z_p|}{|z_p|}\frac{\cos\theta}{|\sin\theta|}$$

$$= \begin{cases} \dfrac{\cos\theta}{\sin\theta} & 0 < \theta < \pi \\ -\dfrac{\cos\theta}{\sin\theta} & -\pi < \theta < 0 \\ \text{undetermined} & \theta = 0 \text{ or } \theta = \pi \end{cases}$$

The above limits are evaluated by examining five regions: 1) when

$$0 < \theta < \tan^{-1}(\frac{c}{b})$$

$$\lim_{r\to 0}(J_1 + J_3 - \Delta\theta) =$$

$$1\left[\frac{\pi}{2} - \tan^{-1}\left(\frac{b\cos\theta + c\sin\theta}{b\sin\theta - c\cos\theta}\right)\right] + 1\left[\tan^{-1}\left(\frac{\cos\theta}{\sin\theta}\right) - (-\frac{\pi}{2})\right] - 2\pi,$$

2) when

$$\tan^{-1}(\frac{c}{b}) < \theta < \pi$$

$$\lim_{r\to 0}(J_1 + J_3 - \Delta\theta) =$$

$$-1\left[\frac{\pi}{2}-\tan^{-1}\left(\frac{b\cos\theta+c\sin\theta}{c\cos\theta-b\sin\theta}\right)\right]+1\left[\tan^{-1}\left(\frac{\cos\theta}{\sin\theta}\right)-(-\frac{\pi}{2})\right],$$

3) when

$$\tan^{-1}(\frac{c}{b})-\pi<\theta<0$$

$$\lim_{r\to 0}(J_1+J_3-\Delta\theta)=$$

$$1\left[\frac{\pi}{2}-\tan^{-1}\left(\frac{b\cos\theta+c\sin\theta}{b\sin\theta-c\cos\theta}\right)\right]-1\left[\tan^{-1}\left(-\frac{\cos\theta}{\sin\theta}\right)-(-\frac{\pi}{2})\right],$$

4) when

$$-\pi<\theta<\tan^{-1}(\frac{c}{b})-\pi$$

$$\lim_{r\to 0}(J_1+J_3-\Delta\theta)=$$

$$1\left[\frac{\pi}{2}-\tan^{-1}\left(\frac{b\cos\theta+c\sin\theta}{c\cos\theta-b\sin\theta}\right)\right]-1\left[\tan^{-1}\left(-\frac{\cos\theta}{\sin\theta}\right)-(-\frac{\pi}{2})\right]$$

and 5) when

$$\theta=0\quad\theta=\pi\quad\theta=\tan^{-1}(\frac{c}{b})\quad\theta=\tan^{-1}(\frac{c}{b})+\pi.$$

$$\lim_{r\to 0}(J_1+J_3-\Delta\theta)$$

is undetermined. Because

$$\tan^{-1}x=\frac{\pi}{2}-\tan^{-1}\frac{1}{x}$$

$$\tan^{-1}\left(\frac{\cos\theta}{\sin\theta}\right)=\frac{\pi}{2}-\tan^{-1}\left(\frac{1}{\frac{\cos\theta}{\sin\theta}}\right)$$

$$\tan^{-1}\left(\frac{\cos\theta}{\sin\theta}\right)=\frac{\pi}{2}-\theta,$$

$$\tan^{-1}\left(-\frac{\cos\theta}{\sin\theta}\right)=\frac{\pi}{2}-\tan^{-1}(-\tan\theta)$$

$$\tan^{-1}\left(-\frac{\cos\theta}{\sin\theta}\right)=\frac{\pi}{2}+\theta,$$

and

$$\tan^{-1}x=-\tan^{-1}(-x)$$

these limits are numerically equivalent for all values of θ except where it is undetermined. This undetermined region is not a problem because for a continuous function the limit is independent of the path. Thus, any direction can be chosen to find the limit. The direction is chosen to be

$$\theta=\frac{\pi}{2},$$

then the limit is

$$\lim_{\substack{x_p\to 0\\ y_p\to 0}}(J_1+J_2+J_3-\Delta\theta)=J_2+\tan^{-1}(-\frac{c}{b})+\frac{\pi}{2}-\frac{\pi}{2}$$

or

$$\lim_{\substack{x_p\to 0\\ y_p\to 0}}(J_1+J_2+J_3-\Delta\theta)=J_2-\tan^{-1}(\frac{c}{b}).$$

The second line segment, describe by $x_p=b$, $y_p=c$ and $z_p\neq 0$, can be evaluated in a similar manner resulting in

$$\lim_{\substack{x_p \to a \\ y_p \to 0}} (J_1 + J_2 + J_3 - \Delta\theta) = J_1 - \tan^{-1}\left(\frac{c}{a-b}\right).$$

The third line segment, describe by $x_p = 0$, $y_p = 0$ and $z_p \neq 0$, can also be evaluated in a similar manner resulting in

$$\lim_{\substack{x_p \to b \\ y_p \to c}} (J_1 + J_2 + J_3 - \Delta\theta) = J_3 + \tan^{-1}\left(\frac{c}{b}\right) - \tan^{-1}\left(\frac{c}{b-a}\right) - \pi.$$

The induced velocity is now defined for the entire space except on the edges and on the surface of the element. The velocity is only needed at the vertices and on the interior of the element. The velocity is needed at the corner points to convect the wake away from the wing. Because the triangles are planar elements and the induced velocity is in a direction perpendicular to the plane the only nonzero component, of the induced velocity, is in the local z direction. The velocity in the z direction is

$$\begin{aligned} V_z = \frac{1}{4\pi} [& \gamma_{y1}(a_1 I_1 + b_1 I_4 + a_1 x_p I_7 + b_1 y_p I_7 + I_7 + a_1 I_{10}) \\ & - \gamma_{x1}(a_1 I_2 + b_1 I_5 + a_1 x_p I_8 + b_1 y_p I_8 + I_8 + b_1 I_{10}) \\ & + \gamma_{y2}(a_2 I_1 + b_2 I_4 + a_2 x_p I_7 + b_2 y_p I_7 + a_2 I_{10}) \\ & - \gamma_{x2}(a_2 I_2 + b_2 I_5 + a_2 x_p I_8 + b_2 y_p I_8 + b_2 I_{10}) \\ & + \gamma_{y3}(a_3 I_1 + b_3 I_4 + a_3 x_p I_7 + b_3 y_p I_7 + a_3 I_{10}) \\ & - \gamma_{x3}(a_3 I_2 + b_3 I_5 + a_3 x_p I_8 + b_3 y_p I_8 + b_3 I_{10})]. \end{aligned}$$

At the point $x_p = 0$, $y_p = 0$ and $z_p = 0$, the limits determined previously have remained undetermined because the Q_i are undetermined. The Q_i can be evaluated by changing to spherical coordinates with the origin at the point (0,0,0). First, by definition

$$\lim_{r \to 0} Q_1 = \lim_{r \to 0} \ln\left\{ \frac{r_1 + r_2 + d_1}{r_1 + r_2 - d_1} \right\}.$$

Because r_1 is always larger than d_1, as the corner is approached this limit tends to positive infinity at a logarithmic rate. Second,

$$\lim_{r\to 0} Q_2 = \lim_{r\to 0} \ln\left\{ \frac{r_2 + r_3 + d_2}{r_2 + r_3 - d_2} \right\}$$

which is

$$= \ln\left\{ \frac{(b^2 + c^2)^{1/2} + a + [(a-b)^2 + c^2]^{1/2}}{(b^2 + c^2)^{1/2} + a - [(a-b)^2 + c^2]^{1/2}} \right\}.$$

Third,

$$\lim_{r\to 0} Q_3 = \lim_{r\to 0} \ln\left\{ \frac{r_3 + r_1 + d_3}{r_3 + r_1 - d_3} \right\}.$$

Because r_3 is always larger than d_3, as the corner is approached this limit tends to positive infinity at a logarithmic rate.

The I_i are defined by neglecting all terms where Q_i is multiplied by x_p, y_p or z_p, because r goes to zero faster than Q_1 and Q_3 go to infinity. The integrals needed for the induced velocity are

$$I_1 = -aH_1 + \left(\frac{a-b}{c}\right)H_2 + \frac{b}{c}\left[\frac{1}{\alpha_3}(r_2 - r_1)\right]$$

$$I_2 = \frac{1}{\alpha_3}(r_2 - r_1) - \frac{1}{\alpha_1}(r_2 - r_3) - \frac{\alpha_2}{\alpha_1}H_1$$

$$I_4 = -\frac{1}{\alpha_5}(r_2 - r_1) - \frac{1}{\alpha_7}(r_3 - r_2) - \frac{\left(\frac{ac}{b-a}\right)}{\alpha_7}H_1 + r_3 - r_1$$

$$I_5 = -\frac{c}{b}\frac{1}{\alpha_5}(r_2 - r_1) - \frac{1}{\alpha_7}(r_3 - r_2) - aH_1 + \frac{\alpha_8}{\alpha_7}H_1$$

and

$$I_{10} = \lim_{r\to 0} R_2 Q_2.$$

$$= \frac{ac}{d_2} Q_2$$

This leaves the terms in which I_7 and I_8 appear in the velocity equation without being multiplied by x_p, y_p and z_p. These only appear in the terms involving γ_{y1} and γ_{x1}. These terms are truly singular, in that the induced velocity is infinite. These terms are neglected because the influence of elements that join at a node will cancel because they have the same vorticity at the shared node. The total induced velocity of an element on itself at the point (0,0,0) is defined as

$$V_x = 0$$

$$V_y = 0$$

and

$$\begin{aligned} V_z = \frac{1}{4\pi} [& \gamma_{y2}(a_2 I_1 + b_2 I_4 + a_2 I_{10}) \\ & - \gamma_{x2}(a_2 I_2 + b_2 I_5 + b_2 I_{10}) \\ & + \gamma_{y3}(a_3 I_1 + b_3 I_4 + a_3 I_{10}) \\ & - \gamma_{x3}(a_3 I_2 + b_3 I_5 + b_3 I_{10})]. \end{aligned}$$

In a similar manner, the velocity induced by an element on itself at the point (a,0,0) is defined as

$$V_x = 0$$

$$V_y = 0$$

and

$$V_z = \frac{1}{4\pi}[\gamma_{y1}(a_1 I_1 + b_1 I_4 + a_1 I_{10}) - \gamma_{x1}(a_1 I_2 + b_1 I_5 + b_1 I_{10}) + \gamma_{y3}(a_3 I_1 + b_3 I_4 + a_3 I_{10}) - \gamma_{x3}(a_3 I_2 + b_3 I_5 + b_3 I_{10})].$$

where

$$I_1 = \left(\frac{a-b}{c}\right) H_2 - aH_3 + \frac{b}{c} H_4$$

$$I_2 = H_4 - H_2$$

$$I_4 = r_3 - r_1 - \frac{1}{\alpha_7}(r_3 - r_2) + aH_5 - H_6$$

$$I_5 = -\frac{c}{b} H_6 - \frac{c}{b-a} \frac{1}{\alpha_7}(r_3 - r_2)$$

and

$$I_{10} = R_1 Q_1.$$

Finally, the velocity induced by an element on itself at the point (b,c,0) is defined as

$$V_x = 0$$

$$V_y = 0$$

and

$$V_z = \frac{1}{4\pi}[\gamma_{y1}(a_1 I_1 + b_1 I_4 + a_1 I_{10}) - \gamma_{x1}(a_1 I_2 + b_1 I_5 + b_1 I_{10}) + \gamma_{y2}(a_2 I_2 + b_2 I_4 + a_2 I_{10}) - \gamma_{x2}(a_3 I_2 + b_2 I_5 + b_2 I_{10})].$$

where

$$I_1 = \frac{a-b}{c}\frac{1}{\alpha_1}(r_2 - r_3) + \frac{b}{c}\frac{1}{\alpha_3}(r_2 - r_1)$$

$$I_2 = \frac{1}{\alpha_3}(r_2 - r_1) - \frac{1}{\alpha_1}(r_2 - r_3)$$

$$I_4 = -\frac{1}{\alpha_5}(r_2 - r_1) - \frac{1}{\alpha_7}(r_3 - r_2) + (r_3 - r_1)$$

$$I_5 = -\frac{c}{b}\frac{1}{\alpha_5}(r_2 - r_1) - \frac{c}{b-a}\frac{1}{\alpha_7}(r_3 - r_2) - cH_9$$

and

$$I_{10} = R_3 Q_3.$$

The final area needed to complete the evaluation is on the interior surface of the element. The induced velocity is needed in this area for the no-penetration conditions. The velocity on this plane must be perpendicular to the sheet; therefore,

$$V_x = 0$$

$$V_y = 0$$

and

$$\begin{aligned} V_z = \frac{1}{4\pi}[& \gamma_{y1}(a_1 I_1 + b_1 I_4 + a_1 x_p I_7 + b_1 y_p I_7 + I_7 + a_1 I_{10}) \\ & - \gamma_{x1}(a_1 I_2 + b_1 I_5 + a_1 x_p I_8 + b_1 y_p I_8 + I_8 + b_1 I_{10}) \\ & + \gamma_{y2}(a_2 I_1 + b_2 I_4 + a_2 x_p I_7 + b_2 y_p I_7 + a_2 I_{10}) \\ & - \gamma_{x2}(a_2 I_2 + b_2 I_5 + a_2 x_p I_8 + b_2 y_p I_8 + b_2 I_{10}) \\ & + \gamma_{y3}(a_3 I_1 + b_3 I_4 + a_3 x_p I_7 + b_3 y_p I_7 + a_3 I_{10}) \\ & - \gamma_{x3}(a_3 I_2 + b_3 I_5 + a_3 x_p I_8 + b_3 y_p I_8 + b_3 I_{10})]. \end{aligned}$$

Because V_z does not contain I_9, (the only integral not defined on the interior of the triangle when $z_p = 0$) the velocity is completely defined by the above equations.

The velocity induced at any point in the three dimensional space is known. The only exception is along the edge of the triangle. The velocity induced at the corners has been defined. The complete listing of the subroutine to find the induced velocity, including the limits developed in this section, is presented in the next section.

I.4 Subroutine VELE

```
CCCCCCCCCCCCCCCCCCCCCCCCCCCCCCCCCCCCCCCCCCCCCCCCCCCCCCCCCCCCCCCCCCCCCCCCCCCC
C                                                                             C
C                              ****************                               C
C                              *     VELE     *                               C
C                              ****************                               C
C                                                                             C
C       THIS SUBROUTINE FINDS THE VELOCITY INDUCED BY A VORTEX SHEET          C
C       AT THE POINT XP, YP, ZP.  THE VORTEX SHEET IS A TRIANGULAR            C
C       ELEMENT.  THE METHOD OF CALCULATING THE VELOCITY IS TO DEFINE         C
C       A LOCAL COORDINATE FRAME WHERE THE LOCAL X AXIS IS ALONG THE          C
C       LONGEST SIDE AND THE TRIANGLE AND THE Y AXIS IS SUCH THAT             C
C       THE OTHER VERTEX OF THE TRIANGLE HAS A POSITIVE COMPONENT.            C
C       THE TRIANGLE VERTICES ARE (0,0), (B,C) AND (A,0).  THIS               C
C       ASSURES A>0, B>0, C>0 AND A>B, ALSO THE TRIANGLE WILL BE IN           C
C       X-Y PLANE.  ONCE THE COORDINATE SYSTEM IS DEFINED THE VELOCITY        C
C       DUE TO SIX BASIS FUNCTIONS WILL BE CALCULATED IN THE LOCAL            C
C       FRAME FROM THE CLOSED FORM INTEGRALS.  THE SIX VELOCITY               C
C       VECTORS WILL THEN BE TRANSFORMED BACK TO THE ORIGINAL FRAME           C
C       BEFORE RETURNING TO THE CALLING ROUTINE.                              C
C                                                                             C
C       THE SIX CASES OF BASIS FUNCTIONS ARE:                                 C
C                                                                             C
C           CASE1 --- VORTICITY IN THE X, MAGNITUDE OF 1 AT (0,0)             C
C           CASE2 --- VORTICITY IN THE X, MAGNITUDE OF 1 AT (B,C)             C
C           CASE3 --- VORTICITY IN THE X, MAGNITUDE OF 1 AT (A,0)             C
C           CASE4 --- VORTICITY IN THE Y, MAGNITUDE OF 1 AT (0,0)             C
C           CASE5 --- VORTICITY IN THE Y, MAGNITUDE OF 1 AT (B,C)             C
C           CASE6 --- VORTICITY IN THE Y, MAGNITUDE OF 1 AT (A,0)             C
C                                                                             C
C       THE INPUT VARIABLES ARE:                                              C
C                                                                             C
C           XP    --- X POSITION OF THE POINT OF INTEREST                     C
C           YP    --- Y POSITION OF THE POINT OF INTEREST                     C
C           ZP    --- Z POSITION OF THE POINT OF INTEREST                     C
C           XNODE --- X POSITION IN THE BODY FRAME OF NODE(IDENTE,I)          C
C           YNODE --- Y POSITION IN THE BODY FRAME OF NODE(IDENTE,I)          C
C           ZNODE --- Z POSITION IN THE BODY FRAME OF NODE(IDENTE,I)          C
C           N(I,3)--- NODE NUMBER IDENTIFYING MATRIX OF ELEMENT IDENTE        C
C           IDENTE--- IDENTIFICATION NUMBER OF THE ELEMENT                    C
C           AELE(I)-- A OF TRIANGLE IDENTE                                    C
C           BELE(I)-- B OF TRIANGLE IDENTE                                    C
C           CELE(I)-- C OF TRIANGLE IDENTE                                    C
C           DIRCOS--- DIRECTION COSINE MATRIX OF ELEMENT IDENTE               C
C           ABASE --- THE BASIS OF THE ELEMENT 1-3 ARE A SUB I                C
C                     4-6 ARE B SUB I                                         C
C           FOURPI--- 4 X PI                                                  C
C                                                                             C
C       THE OUTPUT VARIABLES ARE:                                             C
C                                                                             C
C           VX(I) --- X VELOCITY FOR CASE I                                   C
C           VY(I) --- Y VELOCITY FOR CASE I                                   C
C           VZ(I) --- Z VELOCITY FOR CASE I                                   C
C                                                                             C
CCCCCCCCCCCCCCCCCCCCCCCCCCCCCCCCCCCCCCCCCCCCCCCCCCCCCCCCCCCCCCCCCCCCCCCCCCCC
      SUBROUTINE VELE
      IMPLICIT REAL*8(A-H,O-Z)
      PARAMETER (ME=366,MN=216)
      DIMENSION VP(6),VQ(6),VR(6)
      COMMON/VELINP/ XP,YP,ZP,IDENTE,NODE1,NODE2
      COMMON/CONSTS/ FOURPI,PI,CUTOFF,CUTWK
      COMMON/VELOUT/ VX(6),VY(6),VZ(6)
      COMMON/ELDATA/ NELE,NODE,N(ME,3),XNODE(MN),YNODE(MN),ZNODE(MN)
```

```
      COMMON/CORNER/ AELE(ME),BELE(ME),CELE(ME),DIRCOS(ME,3,3)
      COMMON/EBASIS/ ABASE(ME,6)
C
CC      COPING THE ORIGINAL VARIABLES
C
      XPDUM=XP
      YPDUM=YP
      ZPDUM=ZP
C
CC      PUTTING THE POINT OF INTEREST INTO LOCAL COORDINATES
C
      XNP=(XP-XNODE(N(IDENTE,1)))*DIRCOS(IDENTE,1,1)
     .   +(YP-YNODE(N(IDENTE,1)))*DIRCOS(IDENTE,1,2)
     .   +(ZP-ZNODE(N(IDENTE,1)))*DIRCOS(IDENTE,1,3)
      YNP=(XP-XNODE(N(IDENTE,1)))*DIRCOS(IDENTE,2,1)
     .   +(YP-YNODE(N(IDENTE,1)))*DIRCOS(IDENTE,2,2)
     .   +(ZP-ZNODE(N(IDENTE,1)))*DIRCOS(IDENTE,2,3)
      ZNP=(XP-XNODE(N(IDENTE,1)))*DIRCOS(IDENTE,3,1)
     .   +(YP-YNODE(N(IDENTE,1)))*DIRCOS(IDENTE,3,2)
     .   +(ZP-ZNODE(N(IDENTE,1)))*DIRCOS(IDENTE,3,3)
      XP=XNP
      YP=YNP
      ZP=ZNP
C
CC      COPING THE TRIANGLE LOCAL VERTICES INTO A,B,C
C
      A=AELE(IDENTE)
      B=BELE(IDENTE)
      C=CELE(IDENTE)
C
CC      THE INTEGRALS, FIRST THE PARAMETERS FOR I10
C
      D1=DSQRT(B*B+C*C)
      D2=DSQRT((A-B)*(A-B)+C*C)
      D3=A
      C1=B/D1
      C2=(A-B)/D2
      C3=-1.0D0
      S1=C/D1
      S2=-C/D2
      S3=0.0D0
      RR1= XP   *S1- YP   *C1
      RR2=(XP-B)*S2-(YP-C)*C2
      RR3=(XP-A)*S3- YP   *C3
      S11=  -XP *C1   -YP *S1
      S12=(B-XP)*C1+(C-YP)*S1
      S21=(B-XP)*C2+(C-YP)*S2
      S22=(A-XP)*C2   -YP *S2
      S31=(A-XP)*C3   -YP *S3
      S32=  -XP *C3   -YP *S3
      R1=DSQRT(XP*XP+YP*YP+ZP*ZP)
      R2=DSQRT((B-XP)*(B-XP)+(C-YP)*(C-YP)+ZP*ZP)
      R3=DSQRT((A-XP)*(A-XP)+YP*YP+ZP*ZP)
      DENOM1=R1+R2-D1
      DENOM2=R2+R3-D2
      DENOM3=R3+R1-D3
C
CC      SEEING IF THE VELOCITY IS TO BE CALCULATED AT A SINGULAR POINT
C
      IF(DABS(DENOM1).LT.CUTOFF.OR.
     .   DABS(DENOM2).LT.CUTOFF.OR.
     .   DABS(DENOM3).LT.CUTOFF)THEN
           DO 10 I=1,6
                VP(I)=0.0D0
                VQ(I)=0.0D0
                VR(I)=0.0D0
10         CONTINUE
           IF(DABS(XP).LT.CUTOFF.AND.
```

```
     .        DABS(YP).LT.CUTOFF.AND.
     .        DABS(ZP).LT.CUTOFF)THEN
C
CC      FOR THE CORNER XP=0, YP=0 AND ZP=0
C
           Q2=DLOG((R2+R3+D2)/DENOM2)
C
CC      DEFINING THE ALPHA PARAMETERS FOR THE H'S
C
           ALPHA1=((B-A)*(B-A)+C*C)/(C*C)
           ALPHA2=((B-A)/C)*A
           ALPHA3=(B*B+C*C)/(C*C)
           ALPHA4=0.0D0
           ALPHA5=(C*C+B*B)/(B*B)
           ALPHA6=0.0D0
           ALPHA7=((B-A)*(B-A)+C*C)/((B-A)*(B-A))
           ALPHA8=A*(C/(B-A))*(C/(B-A))
C
CC      NOW FOR THE H'S
C
           H1=Q2/DSQRT(ALPHA1)
           H2=(R2-R3)/ALPHA1-ALPHA2*H1/ALPHA1
           H4=(R2-R1)/ALPHA3
           H6=(R2-R1)/ALPHA5
           H7=(A-B)*H1/C
           H8=(R3-R2)/ALPHA7+ALPHA8*H7/ALPHA7
C
CC      FINDING I1 THROUGH I10
C
           AINT1=-A*H1+((A-B)/C)*H2+B*H4/C
           AINT2=-H2+H4
           AINT4=-H6-H8+R3-R1
           AINT5=-C*H6/B+(A*C)/(B-A)*H7-C*H8/(B-A)
           AINT10=RR2*Q2
C
CC      COPYING THE BASIS CONSTANTS INTO A1 THROUGH B3
C
           A1=ABASE(IDENTE,1)
           A2=ABASE(IDENTE,2)
           A3=ABASE(IDENTE,3)
           B1=ABASE(IDENTE,4)
           B2=ABASE(IDENTE,5)
           B3=ABASE(IDENTE,6)
C
CC      NOW THE VELOCITY COMPONENTS, FOR CASE1
C
           VP(1)=0.0D0
           VQ(1)=0.0D0
           VR(1)=0.0D0
C
CC      FOR CASE2
C
           VP(2)=0.0D0
           VQ(2)=0.0D0
           VR(2)=-A2*AINT2-B2*AINT5-B2*AINT10
C
CC      FOR CASE3
C
           VP(3)=0.0D0
           VQ(3)=0.0D0
           VR(3)=-A3*AINT2-B3*AINT5-B3*AINT10
C
CC      FOR CASE4
C
           VP(4)=0.0D0
           VQ(4)=0.0D0
           VR(4)=0.0D0
C
```

```
C       FOR CASE5
C
           VP(5)=0.0D0
           VQ(5)=0.0D0
           VR(5)=A2*AINT1+B2*AINT4+A2*AINT10
C
C       FOR CASE6
C
           VP(6)=0.0D0
           VQ(6)=0.0D0
           VR(6)=A3*AINT1+B3*AINT4+A3*AINT10
           END IF
           IF(DABS(XP-A).LT.CUTOFF.AND.
     .        DABS(YP).LT.CUTOFF.AND.
     .        DABS(ZP).LT.CUTOFF)THEN
C
C       FOR THE CORNER XP=A, YP=0 AND ZP=0
C
           Q1=DLOG((R1+R2+D1)/DENOM1)
C
C       DEFINING THE ALPHA PARAMETERS FOR THE H'S
C
           ALPHA1=((B-A)*(B-A)+C*C)/(C*C)
           ALPHA2=0.0D0
           ALPHA3=(B*B+C*C)/(C*C)
           ALPHA4=B/C*A
           ALPHA5=(C*C+B*B)/(B*B)
           ALPHA6=A
           ALPHA7=((B-A)*(B-A)+C*C)/((B-A)*(B-A))
           ALPHA8=A+A*(C/(B-A))*(C/(B-A))
C
C       NOW FOR THE H'S
C
           H2=(R2-R3)/ALPHA1
           H3=Q1/DSQRT(ALPHA3)
           H4=(R2-R1)/ALPHA3+ALPHA4*H3/ALPHA3
           H5=B*H3/C
           H6=(R2-R1)/ALPHA5+ALPHA6*H5/ALPHA5
           H8=(R3-R2)/ALPHA7
C
C       FINDING I1 THROUGH I10
C
           AINT1=((A-B)/C)*H2-A*H3+B*H4/C
           AINT2=-H2+H4
           AINT4=A*H5-H6-H8+R3-R1
           AINT5=-C*H6/B-C*H8/(B-A)
           AINT10=RR1*Q1
C
C       COPYING THE BASIS CONSTANTS INTO A1 THROUGH B3
C
           A1=ABASE(IDENTE,1)
           A2=ABASE(IDENTE,2)
           A3=ABASE(IDENTE,3)
           B1=ABASE(IDENTE,4)
           B2=ABASE(IDENTE,5)
           B3=ABASE(IDENTE,6)
C
C       NOW THE VELOCITY COMPONENTS, FOR CASE1
C
           VP(1)=0.0D0
           VQ(1)=0.0D0
           VR(1)=-A1*AINT2-B1*AINT5-B1*AINT10
C
C       FOR CASE2
C
           VP(2)=0.0D0
           VQ(2)=0.0D0
```

```
            VR(2)=0.0D0
C
CC        FOR CASE3
C
            VP(3)=0.0D0
            VQ(3)=0.0D0
            VR(3)=-A3*AINT2-B3*AINT5-B3*AINT10
C
CC        FOR CASE4
C
            VP(4)=0.0D0
            VQ(4)=0.0D0
            VR(4)=A1*AINT1+B1*AINT4+A1*AINT10
C
CC        FOR CASE5
C
            VP(5)=0.0D0
            VQ(5)=0.0D0
            VR(5)=0.0D0
C
CC        FOR CASE6
C
            VP(6)=0.0D0
            VQ(6)=0.0D0
            VR(6)=A3*AINT1+B3*AINT4+A3*AINT10
            END IF
            IF(DABS(XP-B).LT.CUTOFF.AND.
     .         DABS(YP-C).LT.CUTOFF.AND.
     .         DABS(ZP).LT.CUTOFF)THEN
C
CC        FOR THE CORNER XP=B, YP=C AND ZP=0
C
            Q3=DLOG((R3+R1+D3)/DENOM3)
C
CC        DEFINING THE ALPHA PARAMETERS FOR THE H'S
C
            ALPHA1=((B-A)*(B-A)+C*C)/(C*C)
            ALPHA2=((B-A)/C)*(A-B)-C
            ALPHA3=(B*B+C*C)/(C*C)
            ALPHA4=B/C*B+C
            ALPHA5=(C*C+B*B)/(B*B)
            ALPHA6=B+C/B*C
            ALPHA7=((B-A)*(B-A)+C*C)/((B-A)*(B-A))
            ALPHA8=B+A*(C/(B-A))*(C/(B-A))+C*(C/(B-A))
C
CC        NOW FOR THE H'S
C
            H2=(R2-R3)/ALPHA1
            H4=(R2-R1)/ALPHA3
            H6=(R2-R1)/ALPHA5
            H8=(R3-R2)/ALPHA7
            H9=Q3
C
CC        FINDING I1 THROUGH I10
C
            AINT1=((A-B)/C)*H2+B*H4/C
            AINT2=-H2+H4
            AINT4=-H6-H8+R3-R1
            AINT5=-C*H6/B-C*H8/(B-A)-C*H9
            AINT10=RR3*Q3
C
CC        COPYING THE BASIS CONSTANTS INTO A1 THROUGH B3
C
            A1=ABASE(IDENTE,1)
            A2=ABASE(IDENTE,2)
            A3=ABASE(IDENTE,3)
            B1=ABASE(IDENTE,4)
            B2=ABASE(IDENTE,5)
```

```
            B3=ABASE(IDENTE,6)
C
C       NOW THE VELOCITY COMPONENTS, FOR CASE1
C
            VP(1)=0.0D0
            VQ(1)=0.0D0
            VR(1)=-A1*AINT2-B1*AINT5-B1*AINT10
C
C       FOR CASE2
C
            VP(2)=0.0D0
            VQ(2)=0.0D0
            VR(2)=-A2*AINT2-B2*AINT5-B2*AINT10
C
C       FOR CASE3
C
            VP(3)=0.0D0
            VQ(3)=0.0D0
            VR(3)=0.0D0
C
C       FOR CASE4
C
            VP(4)=0.0D0
            VQ(4)=0.0D0
            VR(4)=A1*AINT1+B1*AINT4+A1*AINT10
C
C       FOR CASE5
C
            VP(5)=0.0D0
            VQ(5)=0.0D0
            VR(5)=A2*AINT1+B2*AINT4+A2*AINT10
C
C       FOR CASE6
C
            VP(6)=0.0D0
            VQ(6)=0.0D0
            VR(6)=0.0D0
            END IF
C
C       TRANSFORMING THE SIX VELOCITY VECTORS BACK TO GLOBAL
C
        ELSE
            Q1=DLOG((R1+R2+D1)/DENOM1)
            Q2=DLOG((R2+R3+D2)/DENOM2)
            Q3=DLOG((R3+R1+D3)/DENOM3)
C
C       SKIPPING THE LIMIT TESTS IF ALL THE RRS ARE NON ZERO
C
            IF(DABS(RR1).LT.CUTOFF.OR.
     .         DABS(RR2).LT.CUTOFF.OR.
     .         DABS(RR3).LT.CUTOFF)THEN
C
C       FIRST IF RR1=0 RR2 AND RR3 NONZERO
C
                IF(DABS(RR1).LT.CUTOFF.AND.
     .             DABS(RR2).GE.CUTOFF.AND.
     .             DABS(RR3).GE.CUTOFF)THEN
                  P2=DABS(RR2)/RR2*(DATAN(DABS(ZP/RR2)*S22/R3)
     .                             -DATAN(DABS(ZP/RR2)*S21/R2))
                  P3=DABS(RR3)/RR3*(DATAN(DABS(ZP/RR3)*S32/R1)
     .                             -DATAN(DABS(ZP/RR3)*S31/R3))
                  IF(YP.GT.C.OR.YP.LT.0.0D0)THEN
                       SUMP=P2+P3
                  ELSE
                       SUMP=P2+P3-PI
                  END IF
                END IF
C
```

```
C       SECOND IF RR2=0 RR1 AND RR3 NONZERO
C
                IF(DABS(RR1).GE.CUTOFF.AND.
     .             DABS(RR2).LT.CUTOFF.AND.
     .             DABS(RR3).GE.CUTOFF)THEN
                  P1=DABS(RR1)/RR1*(DATAN(DABS(ZP/RR1)*S12/R2)
     .                             -DATAN(DABS(ZP/RR1)*S11/R1))
                  P3=DABS(RR3)/RR3*(DATAN(DABS(ZP/RR3)*S32/R1)
     .                             -DATAN(DABS(ZP/RR3)*S31/R3))
                  IF(YP.GT.C.OR.YP.LT.0.0D0)THEN
                       SUMP=P1+P3
                  ELSE
                       SUMP=P1+P3-PI
                  END IF
                END IF
C
C       THIRD IF RR3=0 RR1 AND RR2 NONZERO
C
                IF(DABS(RR1).GE.CUTOFF.AND.
     .             DABS(RR2).GE.CUTOFF.AND.
     .             DABS(RR3).LT.CUTOFF)THEN
                  P1=DABS(RR1)/RR1*(DATAN(DABS(ZP/RR1)*S12/R2)
     .                             -DATAN(DABS(ZP/RR1)*S11/R1))
                  P2=DABS(RR2)/RR2*(DATAN(DABS(ZP/RR2)*S22/R3)
     .                             -DATAN(DABS(ZP/RR2)*S21/R2))
                  IF(XP.GT.A.OR.XP.LT.0.0D0)THEN
                       SUMP=P1+P2
                  ELSE
                       SUMP=P1+P2-PI
                  END IF
                END IF
C
C       IF BOTH RR1 AND RR3 ARE ZERO
C
                IF(DABS(RR1).LT.CUTOFF.AND.DABS(RR3).LT.CUTOFF)THEN
                     P2=DABS(RR2)/RR2*(DATAN(DABS(ZP/RR2)*S22/R3)
     .                                -DATAN(DABS(ZP/RR2)*S21/R2))
                     SUMP=P2+DATAN(-C/B)
                END IF
C
C       IF BOTH RR1 AND RR2 ARE ZERO
C
                IF(DABS(RR1).LT.CUTOFF.AND.DABS(RR2).LT.CUTOFF)THEN
                     P3=DABS(RR3)/RR3*(DATAN(DABS(ZP/RR3)*S32/R1)
     .                                -DATAN(DABS(ZP/RR3)*S31/R3))
                     SUMP=P3+DATAN(C/B)-DATAN(C/(B-A))-PI
                END IF
C
C       IF BOTH RR2 AND RR3 ARE ZERO
C
                IF(DABS(RR2).LT.CUTOFF.AND.DABS(RR3).LT.CUTOFF)THEN
                     P1=DABS(RR1)/RR1*(DATAN(DABS(ZP/RR1)*S12/R2)
     .                                -DATAN(DABS(ZP/RR1)*S11/R1))
                     SUMP=P1+DATAN(C/(B-A))
                END IF
             ELSE
                P1=DABS(RR1)/RR1*(DATAN(DABS(ZP/RR1)*S12/R2)
     .                           -DATAN(DABS(ZP/RR1)*S11/R1))
                P2=DABS(RR2)/RR2*(DATAN(DABS(ZP/RR2)*S22/R3)
     .                           -DATAN(DABS(ZP/RR2)*S21/R2))
                P3=DABS(RR3)/RR3*(DATAN(DABS(ZP/RR3)*S32/R1)
     .                           -DATAN(DABS(ZP/RR3)*S31/R3))
                DTHETA=0.0D0
                IF(RR1.GT.0.0D0.AND.RR2.GT.0.0D0.AND.RR3.GT.0.0D0)THEN
                     DTHETA=2.0D0*PI
                END IF
                SUMP=P1+P2+P3-DTHETA
```

```
            END IF
C
CC      PUTTING TOGETHER I10 AND I9 FIRST THE LIMIT IF ZP=0
C
            IF(RR1.GT.0.0D0.AND.RR2.GT.0.0D0.AND.RR3.GT.0.0D0.AND.
     .         DABS(ZP).LT.CUTOFF)THEN
                AINT9=0.0D0
            ELSE
                IF(DABS(ZP).LT.CUTOFF)THEN
                    AINT9=0.0D0
                ELSE
                    AINT9=DABS(ZP)/ZP*SUMP
                END IF
            END IF
            AINT10=RR1*Q1+RR2*Q2+RR3*Q3+DABS(ZP)*SUMP
C
CC      DEFINING THE ALPHA PARAMETERS FOR THE H'S
C
            ALPHA1=((B-A)*(B-A)+C*C)/(C*C)
            ALPHA2=((B-A)/C)*(A-XP)-YP
            ALPHA3=(B*B+C*C)/(C*C)
            ALPHA4=B/C*XP+YP
            ALPHA5=(C*C+B*B)/(B*B)
            ALPHA6=XP+C/B*YP
            ALPHA7=((B-A)*(B-A)+C*C)/((B-A)*(B-A))
            ALPHA8=XP+A*(C/(B-A))*(C/(B-A))+YP*(C/(B-A))
C
CC      NOW FOR THE H'S
C
            H1=Q2/DSQRT(ALPHA1)
            H2=(R2-R3)/ALPHA1-ALPHA2*H1/ALPHA1
            H3=Q1/DSQRT(ALPHA3)
            H4=(R2-R1)/ALPHA3+ALPHA4*H3/ALPHA3
            H5=B*H3/C
            H6=(R2-R1)/ALPHA5+ALPHA6*H5/ALPHA5
            H7=(A-B)*H1/C
            H8=(R3-R2)/ALPHA7+ALPHA8*H7/ALPHA7
            H9=Q3
C
CC      FINDING I1 THROUGH I8
C
            AINT1=(XP-A)*H1+((A-B)/C)*H2-XP*H3+B*H4/C
            AINT2=YP*H1-H2-YP*H3+H4
            AINT3=ZP*H1-ZP*H3
            AINT4=XP*H5-H6+XP*H7-H8+R3-R1
            AINT5=YP*H5-C*H6/B+(YP+(A*C)/(B-A))*H7-C*H8/(B-A)-YP*H9
            AINT6=ZP*H5+ZP*H7-ZP*H9
            AINT7=H3-H1
            AINT8=-H5-H7+H9
C
CC      COPYING THE BASIS CONSTANTS INTO A1 THROUGH B3
C
            A1=ABASE(IDENTE,1)
            A2=ABASE(IDENTE,2)
            A3=ABASE(IDENTE,3)
            B1=ABASE(IDENTE,4)
            B2=ABASE(IDENTE,5)
            B3=ABASE(IDENTE,6)
C
CC      NOW THE VELOCITY COMPONENTS, FOR CASE1
C
            VP(1)=0.0D0
            VQ(1)=A1*AINT3+B1*AINT6+A1*XP*AINT9+B1*YP*AINT9+AINT9
            VR(1)=-A1*AINT2-B1*AINT5-A1*XP*AINT8-B1*YP*AINT8-AINT8
     .            -B1*AINT10
C
CC      FOR CASE2
C
```

```
            VP(2)=0.0D0
            VQ(2)=A2*AINT3+B2*AINT6+A2*XP*AINT9+B2*YP*AINT9
            VR(2)=-A2*AINT2-B2*AINT5-A2*XP*AINT8-B2*YP*AINT8-B2*AINT10
C
CC        FOR CASE3
C
            VP(3)=0.0D0
            VQ(3)=A3*AINT3+B3*AINT6+A3*XP*AINT9+B3*YP*AINT9
            VR(3)=-A3*AINT2-B3*AINT5-A3*XP*AINT8-B3*YP*AINT8-B3*AINT10
C
CC        FOR CASE4
C
            VP(4)=-A1*AINT3-B1*AINT6-A1*XP*AINT9-B1*YP*AINT9-AINT9
            VQ(4)=0.0D0
            VR(4)=A1*AINT1+B1*AINT4+A1*XP*AINT7+B1*YP*AINT7+AINT7
     .           +A1*AINT10
C
CC        FOR CASE5
C
            VP(5)=-A2*AINT3-B2*AINT6-A2*XP*AINT9-B2*YP*AINT9
            VQ(5)=0.0D0
            VR(5)=A2*AINT1+B2*AINT4+A2*XP*AINT7+B2*YP*AINT7+A2*AINT10
C
CC        FOR CASE6
C
            VP(6)=-A3*AINT3-B3*AINT6-A3*XP*AINT9-B3*YP*AINT9
            VQ(6)=0.0D0
            VR(6)=A3*AINT1+B3*AINT4+A3*XP*AINT7+B3*YP*AINT7+A3*AINT10
         END IF
C
CC        TRANSFORMING THE SIX VELOCITY VECTORS BACK TO GLOBAL
C
         DO 20 I=1,6
            VX(I)=VP(I)*DIRCOS(IDENTE,1,1)
     .           +VQ(I)*DIRCOS(IDENTE,2,1)
     .           +VR(I)*DIRCOS(IDENTE,3,1)
            VX(I)=VX(I)/FOURPI
            VY(I)=VP(I)*DIRCOS(IDENTE,1,2)
     .           +VQ(I)*DIRCOS(IDENTE,2,2)
     .           +VR(I)*DIRCOS(IDENTE,3,2)
            VY(I)=VY(I)/FOURPI
            VZ(I)=VP(I)*DIRCOS(IDENTE,1,3)
     .           +VQ(I)*DIRCOS(IDENTE,2,3)
     .           +VR(I)*DIRCOS(IDENTE,3,3)
            VZ(I)=VZ(I)/FOURPI
   20    CONTINUE
C
CC        RESTORING THE ORIGINAL VARIABLES
C
         XP=XPDUM
         YP=YPDUM
         ZP=ZPDUM
         RETURN
         END
```

Appendix II

Velocity Induced by a Variable Vortex Filament

II.1 Integral Equations

The velocity induced by a general vortex filament is

$$\vec{V}_c = V_x\vec{i} + V_y\vec{j} + V_z\vec{k}$$

where $\vec{V}_c$ is the induced velocity and $\vec{i}, \vec{j}$ and $\vec{k}$ are the unit vectors of the local coordinate frame of the filament. The circulation on the filament, in the filament's local coordinate frame the x-axis always runs along the filament, has the form

$$\Gamma(x) = G_1\frac{x^2}{2} + G_2x + G_3.$$

The velocity induced by a vortex filament can be written as

$$\vec{V}_c = \frac{1}{4\pi}\int\Gamma(x)\frac{d\vec{l}\times(\vec{r}-\vec{s})}{|\vec{r}-\vec{s}|^3}.$$

A vortex filament is shown in Figure 105.

From Figure 105

$$d\vec{l} = dx\vec{i}.$$

and

$$\vec{p} = \vec{r} - \vec{s}.$$

The cross product can then be expanded so that the velocity is

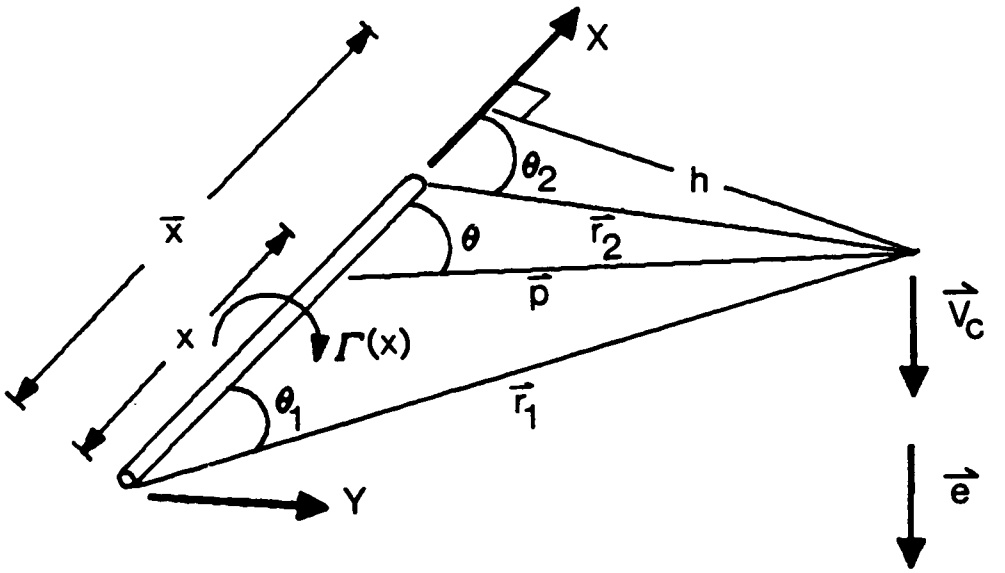

Figure 105. Coordinate Frame of a Vortex Core

$$\vec{V}_c = \frac{1}{4\pi}\int \Gamma(x)\,\frac{dx|\vec{p}|\sin\theta}{|\vec{p}|^3}\,\frac{\vec{i}\times\vec{r}}{|\vec{i}\times\vec{r}|}.$$

With the definitions

$$p = |\vec{p}|$$

and

$$\vec{e} = \frac{\vec{i}\times\vec{r}}{|\vec{i}\times\vec{r}|},$$

the induced velocity is

$$\vec{V}_c = \frac{1}{4\pi}\int \Gamma(x)\,\frac{\sin\theta}{p^2}\,dx\vec{e}.$$

The following variable substitution can be used to further expand the integral,

$$\sin\theta = \frac{h}{p}$$

where h is the perpendicular distance from the local x axis to the point of interest, and because

$$x = \bar{x} - h\cot\theta$$

Then the integral becomes

$$\vec{V}_c = \frac{1}{4\pi}\int_{\theta_1}^{\theta_2}\Gamma(x)\frac{\sin\theta}{\left(\frac{h}{\sin\theta}\right)^2}h\,\mathrm{cosec}^2\theta\,d\theta\vec{e},$$

which can be reduced to

$$\vec{V}_c = \frac{1}{4\pi}\int_{\theta_1}^{\theta_2}\Gamma(x)\frac{\sin\theta}{h}\,d\theta\vec{e}.$$

where $\bar{x}$ is the distance from the origin of the coordinate frame to the point where the perpendicular is measured, the velocity is

$$\vec{V}_c = \frac{G_1}{8\pi}\int_{\theta_1}^{\theta_2}(\bar{x}^2 - 2h\bar{x}\cot\theta + h^2\cot^2\theta)\sin\theta\,d\theta\vec{e} + \frac{G_2}{4\pi}\int_{\theta_1}^{\theta_2}(\bar{x} - h\cot\theta)\sin\theta\,d\theta\vec{e} + \frac{G_3}{4\pi}\int_{\theta_1}^{\theta_2}\sin\theta\,d\theta\vec{e}$$

or

$$\vec{V}_c = \frac{G_1}{4\pi h}\vec{e}\left[\frac{h^2}{2}\left[\cos\theta + \ln\left(\tan\frac{\theta}{2}\right)\right] - h\bar{x}\sin\theta - \frac{\bar{x}^2}{2}\cos\theta\right]\Bigg|_{\theta_1}^{\theta_2}$$
$$+ \frac{G_2}{4\pi h}\vec{e}\left[-\bar{x}\cos\theta - h\sin\theta\right]\Bigg|_{\theta_1}^{\theta_2}$$
$$- \frac{G_3}{4\pi h}\vec{e}\left[\cos\theta\right]\Bigg|_{\theta_1}^{\theta_2}.$$

The definitions of h and $\bar{x}$ lead to the following expressions in terms of r and θ

$$h^2 - \bar{x}^2 = r_1^2\sin^2\theta_1 - r_1^2\cos^2\theta_1$$

$$= r_1^2\left[\frac{1}{2}(1 - \cos 2\theta_1) - \frac{1}{2}(1 + \cos 2\theta_1)\right]$$

$$= -r_1^2\cos 2\theta_1,$$

$$h\bar{x} = r_1^2\sin\theta_1\cos\theta_1$$

$$= r_1^2\sin 2\theta_1$$

and

$$-h(\sin\theta_2 - \sin\theta_1) - \bar{x}(\cos\theta_2 - \cos\theta_1) =$$
$$-r_1(\sin\theta_1\sin\theta_2 - \sin^2\theta_1) - r_1(\cos\theta_1\cos\theta_2 - \cos^2\theta_1)$$

$$= -r_1(\sin\theta_1\sin\theta_2 + \cos\theta_1\cos\theta_2) + r_1(\sin^2\theta_1 + \cos^2\theta_1)$$

$$= r_1[1 - \cos(\theta_1 - \theta_2)].$$

The above definitions and the substitution

$$\tan\left(\frac{\theta}{2}\right) = \frac{1 - \cos\theta}{\sin\theta}$$

can be used to show that the induced velocity is

$$\vec{V}_c = \frac{G_1}{4\pi h}\vec{e}\left[\frac{1}{2}r_1^2 \sin^2\theta_1 \ln\left\{\frac{(1-\cos\theta_2)\sin\theta_1}{(1-\cos\theta_1)\sin\theta_2}\right\}\right.$$
$$\left.+\frac{1}{2}r_1^2\cos 2\theta_1(\cos\theta_1-\cos\theta_2)+r_1^2\sin 2\theta_1(\sin\theta_1-\sin\theta_2)\right]$$
$$+\frac{G_2}{4\pi h}\vec{e}[r_1(1-\cos(\theta_1-\theta_2))]$$
$$+\frac{G_3}{4\pi h}\vec{e}[\cos\theta_1-\cos\theta_2]$$

The last term of this equation is the well known Biot-Savart law.

II.2 Vortex Core Singularities

The only possible numerical problems, occur when h goes to zero; *h* is zero along the x axis. Three distinct areas exist where h goes to zero. Two areas are outside the filament; the other is on the filament. The three regions are defined in Figure 106.

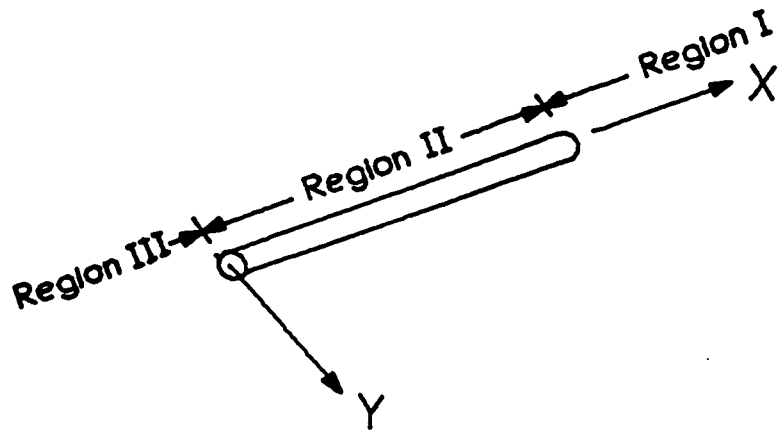

Figure 106. Regions of Numerical Difficulties

The variable substitutions

$$d_1 = [(l+x)^2 + h^2]^{1/2}$$

and

$$d_2 = [x^2 + h^2]^{1/2}$$

lead to the sine and cosine terms being

$$\sin\theta_1 = \frac{h}{d_1}, \qquad \sin\theta_1 = \frac{h}{d_2},$$

$$\cos\theta_1 = \frac{l+x}{d_1} \text{ and } \cos\theta_1 = \frac{x}{d_2}$$

where l and x are shown in Figure 107.

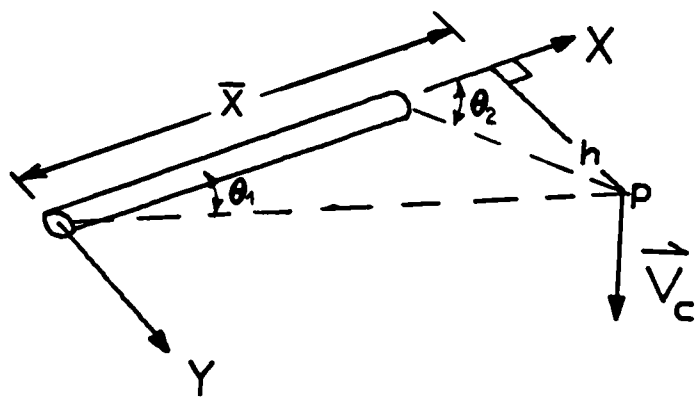

Figure 107. Definitions of New Variables

All three regions will be investigated by using a Taylor-series expansion of the sine and cosine for small h. To second order, the expansions are

$$\sin\theta_1 = \frac{h}{(\bar{x}^2 + h^2)^{1/2}} = \frac{h}{|\bar{x}|}\frac{1}{\left(1 + \frac{h^2}{\bar{x}^2}\right)^{1/2}} \qquad \text{if } \bar{x} \neq 0$$

$$= \frac{h}{|\bar{x}|}\left(1 - \frac{h^2}{2\bar{x}^2} + \ldots\right) \qquad \text{if } \left|\frac{h}{\bar{x}}\right| < 1$$

$$= \frac{h}{|\bar{x}|} + O\left(\frac{h^2}{\bar{x}^2}\right) \quad \text{for } |\frac{h}{\bar{x}}| << 1,$$

$$\sin\theta_2 = \frac{h}{\left[(l-\bar{x})^2 + h^2\right]^{1/2}}$$

$$= \frac{h}{|l-\bar{x}|} \frac{1}{\left[1 + \frac{h^2}{(l-\bar{x})^2}\right]^{1/2}} \quad \text{if } (l-\bar{x}) \neq 0$$

$$= \frac{h}{|l-\bar{x}|}\left[1 - \frac{h^2}{2(l-\bar{x})^2} + \ldots\right] \quad \text{if } |\frac{h}{l-\bar{x}}| < 1$$

$$= \frac{h}{|l-\bar{x}|} + O\left(\frac{h^3}{(l-\bar{x})^3}\right) \quad \text{for } |\frac{h}{l-\bar{x}}| << 1,$$

$$\cos\theta_1 = \frac{\bar{x}}{(\bar{x}^2 + h^2)^{1/2}} = \text{sgn}(\bar{x}) \frac{1}{\left(1 + \frac{h^2}{\bar{x}^2}\right)^{1/2}} \quad \text{if } \bar{x} \neq 0$$

$$= \text{sgn}(\bar{x})\left(1 - \frac{h^2}{2\bar{x}^2} + \ldots\right) \quad \text{if } |\frac{h}{\bar{x}}| < 1$$

$$= \text{sgn}(\bar{x})\left(1 - \frac{h^2}{2\bar{x}^2}\right) + O\left(\frac{h^4}{\bar{x}^4}\right) \quad \text{for } |\frac{h}{\bar{x}}| << 1,$$

and

$$\cos\theta_2 = \frac{l-\bar{x}}{\left[(l-\bar{x})^2 + h^2\right]^{1/2}} = \text{sgn}(l-\bar{x}) \frac{1}{\left[1 + \frac{h^2}{(l-\bar{x})^2}\right]^{1/2}} \quad \text{if } (l-\bar{x}) \neq 0$$

$$= \text{sgn}(l-\bar{x})\left[1 - \frac{h^2}{2(l-\bar{x})^2} + \ldots\right] \quad \text{if } |\frac{h}{l-\bar{x}}| < 1$$

$$= \operatorname{sgn}(l-\bar{x})\left[1-\frac{h^2}{2(l-\bar{x})^2}\right]+O\left(\frac{h^4}{(l-\bar{x})^4}\right) \quad \text{for } \left|\frac{h}{l-\bar{x}}\right| << 1.$$

Now consider

$$\lim_{h\to 0}\frac{r_1^2\sin^2\theta_1}{h}\ln\left\{\frac{(1-\cos\theta_2)\sin\theta_1}{(1-\cos\theta_1)\sin\theta_2}\right\}$$

$$= \lim_{h\to 0}\frac{\bar{x}^2+h^2}{h}\frac{h^2}{\bar{x}^2}\ln\left\{\frac{\dfrac{h^2}{2(l+\bar{x})^2}\dfrac{h}{\bar{x}}}{\dfrac{h^2}{2\bar{x}^2}\dfrac{h}{(l+\bar{x})}}\right\} \quad \text{if } \bar{x}\neq 0 \text{ or } \bar{x}-l\neq 0.$$

It follows that, for $\bar{x}\neq 0$ or $\bar{x}-l\neq 0$,

$$\lim_{h\to 0}\frac{r_1^2\sin^2\theta_1}{h}\ln\left\{\frac{(1-\cos\theta_2)\sin\theta_1}{(1-\cos\theta_1)\sin\theta_2}\right\}=0.$$

Now consider

$$\lim_{h\to 0}\frac{r_1^2}{h}\cos 2\theta_1(\cos\theta_1-\cos\theta_2)$$

$$= \lim_{h\to 0}\frac{\bar{x}^2+h^2}{h}(\cos^2\theta_1-\sin^2\theta_1)(\cos\theta_1-\cos\theta_2)$$

$$= \lim_{h\to 0}\frac{\bar{x}^2+h^2}{h}\left(1-\frac{h^2}{\bar{x}^2}-\frac{h^2}{\bar{x}^2}\right)\left[\operatorname{sgn}(\bar{x})\left(1-\frac{h^2}{2\bar{x}^2}\right)-\operatorname{sgn}(\bar{x}-l)\left(1-\frac{h^2}{2(\bar{x}-l)^2}\right)\right]$$

$$\text{if } \bar{x}\neq 0 \text{ or } \bar{x}-l\neq 0,$$

$$= \lim_{h\to 0}\frac{\bar{x}^2+h^2}{h}(1-\begin{cases}O(h^2) \text{ if } \operatorname{sgn}(\bar{x})=\operatorname{sgn}(\bar{x}-l)\\ O(1) \text{ if } \operatorname{sgn}(\bar{x})=-\operatorname{sgn}(\bar{x}-l)\end{cases} \quad \text{if } \bar{x}\neq 0 \text{ or } \bar{x}-l\neq 0.$$

Therefore,

$$\lim_{h\to 0}\frac{r_1^2}{h}\cos 2\theta_1(\cos\theta_1-\cos\theta_2)=\begin{cases}0 \text{ if } \operatorname{sgn}(\bar{x})=\operatorname{sgn}(\bar{x}-l)\\ \infty \text{ if } \operatorname{sgn}(\bar{x})=-\operatorname{sgn}(\bar{x}-l)\end{cases}\quad \text{if } \bar{x}\neq 0 \text{ or } \bar{x}-l\neq 0.$$

Now consider

$$\lim_{h\to 0}\frac{r_1^2}{h}\sin 2\theta_1(\sin\theta_1-\sin\theta_2)$$

$$\lim_{h\to 0}\frac{\bar{x}^2+l^2}{h}2\cos\theta_1\sin\theta_1(\sin\theta_1-\sin\theta_2)$$

$$=2\lim_{h\to 0}\frac{\bar{x}^2+l^2}{h}\operatorname{sgn}(\bar{x})\left(1-\frac{h^2}{2\bar{x}^2}\right)\frac{h}{|\bar{x}|}\left(\frac{h}{|\bar{x}|}-\frac{h}{|\bar{x}-l|}\right)$$

$$=0 \quad \text{if } \bar{x}\neq 0 \text{ or } \bar{x}-l\neq 0.$$

Now consider

$$\lim_{h\to 0}\frac{r_1}{h}(1-\cos(\theta_1-\theta_2))$$

$$=\lim_{h\to 0}\frac{\bar{x}^2+h^2}{h}(1-\cos\theta_1\cos\theta_2-\sin\theta_1\sin\theta_2)$$

$$=\lim_{h\to 0}\frac{\bar{x}^2+h^2}{h}\left[1-\operatorname{sgn}(\bar{x})\operatorname{sgn}(\bar{x}-l)\left(1-\frac{h^2}{2\bar{x}^2}-\frac{h^2}{2(\bar{x}-l)^2}\right)-\frac{h}{|\bar{x}|}\frac{h}{|\bar{x}-l|}\right]$$

$$=\begin{cases}0 \text{ if } \operatorname{sgn}(\bar{x})=\operatorname{sgn}(\bar{x}-l)\\ \infty \text{ if } \operatorname{sgn}(\bar{x})=-\operatorname{sgn}(\bar{x}-l)\end{cases}\quad \text{if } \bar{x}\neq 0 \text{ or } \bar{x}-l\neq 0.$$

Suppose $\bar{x}=0$

$$\sin\theta_1=1\,,\qquad \cos\theta_1=0$$

$$\sin\theta_2=\frac{h}{(l^2+h^2)^{1/2}}\,,\qquad \cos\theta_2=-\frac{l}{(l^2+h^2)^{1/2}}$$

$$r_1 = h$$

$$\lim_{h\to 0} \frac{r_1^2 \sin^2\theta_1}{h} \ln\left\{ \frac{(1-\cos\theta_2)\sin\theta_1}{(1-\cos\theta_1)\sin\theta_2} \right\}$$

$$= \lim_{h\to 0} h(1) \ln\left\{ \frac{\left((l^2+h^2)^{1/2}+l\right)(1)}{h} \right\} = 0$$

$$\lim_{h\to 0} \frac{r_1^2}{h} [\cos 2\theta_1(\cos\theta_1 - \cos\theta_2) + \sin 2\theta_1(\sin\theta_1 - \sin\theta_2)] = 0$$

$$\lim_{h\to 0} \frac{r_1}{h} (1 - \cos\theta_1\cos\theta_2 - \sin\theta_1\sin\theta_2) = 1$$

and

$$\lim_{h\to 0} \frac{1}{h} (\cos\theta_1 - \cos\theta_2) = \infty.$$

The same results are obtained when $\bar{x} = l$.

The results of this investigation show that all numerical difficulties encountered when trying to evaluate the velocity due to a vortex core can be removed by establishing a cylinder of radius cutoff along the x axis of the core inside of which the induced velocity is set to zero.

Section II.3 presents the subroutine used to determine the velocity induced by a variable strength vortex core using the above equations. The following section has a shortened version of subroutine VELVF that only calculates the induced velocity due to a constant strength filament, such as those in the wake mesh.

II.3 Subroutine VELVF

```
CCCCCCCCCCCCCCCCCCCCCCCCCCCCCCCCCCCCCCCCCCCCCCCCCCCCCCCCCCCCCCCCCCCCCCCCCC
C                                                                      C
C                            **********                                C
C                            *  VELVF  *                                C
C                            **********                                C
C                                                                      C
C       THIS SUBROUTINE CALCULATES THE VELOCITY INDUCED AT A POINT     C
C       BY A VARIABLE STRENGTH VORTEX FILAMENT.  THIS FILAMENT         C
C       IS ALONG ONE SIDE OF A TRIANGULAR ELEMENT.  THE VORTEX         C
C       STRENGTH IS GIVEN BY G(X)=1/2 G1 X**2 + G2 X + G3.             C
C                                                                      C
C       THE THREE CASES OF THE BASIS ARE:                              C
C                                                                      C
C           CASE1 --- INFLUENCE WITH G1=1 G2=G3=0                      C
C           CASE2 --- INFLUENCE WITH G2=1 G1=G3=0                      C
C           CASE3 --- INFLUENCE WITH G3=1 G1=G2=0                      C
C                                                                      C
C       THE INPUT VARIABLES ARE:                                       C
C                                                                      C
C           XP    --- X POSITION OF THE POINT OF INTEREST              C
C           YP    --- Y POSITION OF THE POINT OF INTEREST              C
C           ZP    --- Z POSITION OF THE POINT OF INTEREST              C
C           XNODE --- X POSITION IN THE BODY FRAME OF NODE             C
C           YNODE --- Y POSITION IN THE BODY FRAME OF NODE             C
C           ZNODE --- Z POSITION IN THE BODY FRAME OF NODE             C
C           NODE1 --- FIRST NODE OF THE CORE                           C
C           NODE2 --- SECOND NODE OF THE CORE                          C
C           FOURPI -- FOUR TIMES PI                                    C
C           CUTWK  -- CUTOFF DISTANCE INSIDE WHICH THE VEL=0           C
C                                                                      C
C       THE OUTPUT VARIABLES ARE:                                      C
C                                                                      C
C           VXVF(I) - X VELOCITY FOR CASE I                            C
C           VYVF(I) - Y VELOCITY FOR CASE I                            C
C           VZVF(I) - Z VELOCITY FOR CASE I                            C
C                                                                      C
CCCCCCCCCCCCCCCCCCCCCCCCCCCCCCCCCCCCCCCCCCCCCCCCCCCCCCCCCCCCCCCCCCCCCCCCCC
      SUBROUTINE VELVF
      IMPLICIT REAL*8 (A-H,O-Z)
      PARAMETER (ME=366,MN=216)
      COMMON/CONSTS/ FOURPI,PI,CUTOFF,CUTWK
      COMMON/VELINP/ XP,YP,ZP,IDENTE,NODE1,NODE2
      COMMON/VELVFO/ VXVF(3),VYVF(3),VZVF(3)
      COMMON/ELDATA/ NELE,NODE,N(ME,3),XNODE(MN),YNODE(MN),ZNODE(MN)
      DIMENSION F(3)
C
C       FINDING THE POSITION OF THE FILAMENT
C
      X1=XNODE(NODE1)
      Y1=YNODE(NODE1)
      Z1=ZNODE(NODE1)
      X2=XNODE(NODE2)
      Y2=YNODE(NODE2)
      Z2=ZNODE(NODE2)
C
C       CREATING THE R1 VECTOR
C
      R1X=XP-X1
      R1Y=YP-Y1
      R1Z=ZP-Z1
      R1MAG=DSQRT(R1X*R1X+R1Y*R1Y+R1Z*R1Z)
C
```

```
C       CREATING THE R2 VECTOR
C
      R2X=XP-X2
      R2Y=YP-Y2
      R2Z=ZP-Z2
      R2MAG=DSQRT(R2X*R2X+R2Y*R2Y+R2Z*R2Z)
C
C       CREATING A VECTOR IN THE DIRECTION OF THE FILAMENT
C
      OMX=X2-X1
      OMY=Y2-Y1
      OMZ=Z2-Z1
      OMMAG=DSQRT(OMX*OMX+OMY*OMY+OMZ*OMZ)
C
C       USING THE CROSS PRODUCT FOR VECTOR IN DIRECTION OF VELOCITY
C
      EX=OMY*R1Z-OMZ*R1Y
      EY=OMZ*R1X-OMX*R1Z
      EZ=OMX*R1Y-OMY*R1X
      EMAG=DSQRT(EX*EX+EY*EY+EZ*EZ)
C
C       CHECKING IF THE POINT IS INSIDE THE CUTOFF LIMIT
C
      IF((EMAG/OMMAG/OMMAG).LT.CUTWK) THEN
           DO 10 I=1,3
                VXVF(I)=0.0D0
                VYVF(I)=0.0D0
                VZVF(I)=0.0D0
10         CONTINUE
      ELSE
C
C       MAKING THE E VECTOR A UNIT VECTOR
C
           EX=EX/EMAG
           EY=EY/EMAG
           EZ=EZ/EMAG
C
C       FINDING THETA 1 AND THETA 2 BY USING THE DOT PRODUCT
C
           COST1=(R1X*OMX+R1Y*OMY+R1Z*OMZ)/(R1MAG*OMMAG)
           THETA1=DACOS(COST1)
           SINT1=DSIN(THETA1)
           COST2=(R2X*OMX+R2Y*OMY+R2Z*OMZ)/(R2MAG*OMMAG)
           THETA2=DACOS(COST2)
           SINT2=DSIN(THETA2)
C
C       THE CONSTANT MULTIPLIED BY ALL FACTORS
C
           FACT=1.0D0/(R1MAG*SINT1*FOURPI)
C
C       THE INFLUENCE OF G1
C
           F(1)=FACT*R1MAG*R1MAG*0.5D0*(
     .          SINT1*SINT1*DLOG(((1.0D0-COST2)*SINT1)
     .                          /((1.0D0-COST1)*SINT2))
     .          +DCOS(2.0D0*THETA1)*(COST1-COST2)
     .          +DSIN(2.0D0*THETA1)*(SINT1-SINT2))
C
C       THE INFLUENCE OF G2
C
           F(2)=FACT*R1MAG*(1.0D0-DCOS(THETA1-THETA2))
C
C       THE INFLUENCE OF G3
C
           F(3)=FACT*(COST1-COST2)
C
C       PUTTING TOGETHER THE VELOCITY
C
```

```
          DO 20 I=1,3
               VXVF(I)=EX*F(I)
               VYVF(I)=EY*F(I)
               VZVF(I)=EZ*F(I)
20        CONTINUE
     END IF
     RETURN
     END
```

II.4 Subroutine VELCF

```
CCCCCCCCCCCCCCCCCCCCCCCCCCCCCCCCCCCCCCCCCCCCCCCCCCCCCCCCCCCCCCCCCCCCCCCCC
C                                                                      C
C                        ************                                  C
C                        *   VELCF   *                                  C
C                        ************                                  C
C                                                                      C
C       THIS SUBROUTINE CALCULATES THE VELOCITY FOR A CONSTANT         C
C       STRENGTH VORTEX FILAMENT USING THE BIOT-SAVART LAW.            C
C                                                                      C
C       THE INPUT VARIABLES ARE:                                       C
C                                                                      C
C           XP     --- X POSITION OF THE POINT OF INTEREST             C
C           YP     --- Y POSITION OF THE POINT OF INTEREST             C
C           ZP     --- Z POSITION OF THE POINT OF INTEREST             C
C           X1     --- X POSITION IN THE BODY FRAME OF FIRST NODE      C
C           Y1     --- Y POSITION IN THE BODY FRAME OF FIRST NODE      C
C           Z1     --- Z POSITION IN THE BODY FRAME OF FIRST NODE      C
C           X2     --- X POSITION IN THE BODY FRAME OF SECOND NODE     C
C           Y2     --- Y POSITION IN THE BODY FRAME OF SECOND NODE     C
C           Z2     --- Z POSITION IN THE BODY FRAME OF SECOND NODE     C
C           FOURPI -- FOUR TIMES PI                                    C
C           CUTWK  -- CUTOFF DISTANCE INSIDE WHICH THE VEL=0           C
C                                                                      C
C       THE OUTPUT VARIABLES ARE:                                      C
C                                                                      C
C           VXCF   --- X VELOCITY                                      C
C           VYCF   --- Y VELOCITY                                      C
C           VZCF   --- Z VELOCITY                                      C
C                                                                      C
CCCCCCCCCCCCCCCCCCCCCCCCCCCCCCCCCCCCCCCCCCCCCCCCCCCCCCCCCCCCCCCCCCCCCCCCC
      SUBROUTINE VELCF
      IMPLICIT REAL*8(A-H,O-Z)
      COMMON/VCFINP/ X1,Y1,Z1,X2,Y2,Z2,VXCF,VYCF,VZCF
      COMMON/VELINP/ XP,YP,ZP,IDENTE,NODE1,NODE2
      COMMON/CONSTS/ FOURPI,PI,CUTOFF,CUTWK
C
C       CREATING THE OMEGA VECTOR
C
      OMX=X2-X1
      OMY=Y2-Y1
      OMZ=Z2-Z1
      OM2=OMX*OMX+OMY*OMY+OMZ*OMZ
C
C       CREATING THE R1 VECTOR
C
      R1X=XP-X1
      R1Y=YP-Y1
      R1Z=ZP-Z1
C
C       CREATING THE R2 VECTOR
C
      R2X=XP-X2
      R2Y=YP-Y2
      R2Z=ZP-Z2
C
C       CREATING THE F VECTOR WHICH IS OMEGA X R1
C
      FX=OMY*R1Z-OMZ*R1Y
      FY=OMZ*R1X-OMX*R1Z
      FZ=OMX*R1Y-OMY*R1X
C
C       FINDING THE MAGNITUDE OF THE F VECTOR AND SEEING IF IT IS LT
```

```
C       THE CUTOFF LENGTH
C
      FMAG2=FX*FX+FY*FY+FZ*FZ
      IF((FMAG2/OM2/OM2).LE.(CUTWK*CUTWK))THEN
C
C       RETURNING THE VALUE OF ZERO IF INSIDE THE CUTOFF
C
      VXCF=0.0D0
      VYCF=0.0D0
      VZCF=0.0D0
      ELSE
C
C       FINDING THE FACTOR TO BE MULTIPLIED BY GAMMA FOR THE VELOCITY
C
      R12=R1X*R1X+R1Y*R1Y+R1Z*R1Z
      R22=R2X*R2X+R2Y*R2Y+R2Z*R2Z
      R1MAG=DSQRT(R12)
      R2MAG=DSQRT(R22)
C
C       FINDING G1 = (OMEGA . R1)/ /R1/ AND G2 = (OMEGA . R2)/ /R2/
C
      G1=(OMX*R1X+OMY*R1Y+OMZ*R1Z)/R1MAG
      G2=(OMX*R2X+OMY*R2Y+OMZ*R2Z)/R2MAG
      FACTOR=(G1-G2)/(FOURPI*FMAG2)
C
C       FINDING THE VELOCITY AT THE POINT OUTSIDE THE CUTOFF
C
      VXCF=FACTOR*FX
      VYCF=FACTOR*FY
      VZCF=FACTOR*FZ
      END IF
      RETURN
      END
```

Appendix III

Total Velocity at a Point in the Flow Field

III.1 Total Velocity Equation

The velocity at a point in the flow field is the sum of the induced velocity of the disturbance and the free stream. The disturbance velocity is the sum of the velocity induced by the bound surface (the wing), and the free surface (the wake). The total velocity at a point is

$$\vec{V} = \vec{V}_{bnd} + \vec{V}_{wk} - \vec{V}_{ls}$$

where $\vec{V}_{bnd}$ is the velocity due to the bound surface, $\vec{V}_{wk}$ is the velocity due to the wake and $\vec{V}_{ls}$ is the velocity of the lifting-surface, the apparent free stream. This formulation results in the velocity, as calculated in Equation III-1, being the absolute velocity at the point in terms of the base vectors of the body reference frame. The subroutines used to calculate the total velocity are presented in the following sections. Section III.2 is the bound velocity routine, Section III.3 is the wake velocity routine, and Section III.4 is the lifting-surface velocity routine.

III.2 Subroutine VELBND

```
CCCCCCCCCCCCCCCCCCCCCCCCCCCCCCCCCCCCCCCCCCCCCCCCCCCCCCCCCCCCCCCCCCCCCCCCCC
C                                                                      C
C                      **************                                  C
C                      *    VELBND  *                                  C
C                      **************                                  C
C                                                                      C
C       THIS ROUTINE CALCULATES THE VELOCITY INDUCED AT A POINT        C
C       BY THE BOUND VORTEX.  THE METHOD USE'S THE GLOBAL              C
C       VOTICITY AT A NODE, TRANSFORM IT INTO LOCAL COORDINATES        C
C       AND MULTIPLIES IT BY THE APPROAPRIATE VELE OUTPUT.             C
C       THE VELOCITY DUE TO THE EDGE CORES IS THEN CALCULATED.         C
C       THESE TWO VELOCITIES ARE THEN ADDED TO FORM THE TOTAL          C
C       BOUND VELOCITY.                                                C
C                                                                      C
C       THE INPUT VARIABLES ARE:                                       C
C                                                                      C
C           ANORX --- NODAL NORMAL IN THE BODY X DIRECTION             C
C           ANORY --- NODAL NORMAL IN THE BODY Y DIRECTION             C
C           ANORZ --- NODAL NORMAL IN THE BODY Z DIRECTION             C
C           CFACT --- FACTOR C AT EACH NODE OF ELEMENT IDENTE          C
C           DIRCOS--- DIRECTION COSINE MATRIX OF ELEMENT I             C
C           G1    --- QUADRADIC CIRCULATION STRENGTH OF EDGE I         C
C           G2    --- LINEAR CIRCULATION STRENGTH OF EDGE I            C
C           G3    --- CONSTANT CIRCULATION STRENGTH OF EDGE I          C
C           N(I,J)--- NODAL MATRIX FOR ELEMENT I NODE J                C
C           NCIRC --- NUMBER OF EDGES IN EACH CIRCUIT                  C
C           NELE  --- NUMBER OF ELEMENTS                               C
C           NTOTCR--- NUMBER OF EGDE CIRCUITS                          C
C           OMEX  --- NODAL VORTICITY IN THE BODY X DIRECTION          C
C           OMEY  --- NODAL VORTICITY IN THE BODY Y DIRECTION          C
C           OMEZ  --- NODAL VORTICITY IN THE BODY Z DIRECTION          C
C           VX    --- OUTPUT VELOCITY FROM VELE IN X DIRECTION         C
C           VY    --- OUTPUT VELOCITY FROM VELE IN Y DIRECTION         C
C           VZ    --- OUTPUT VELOCITY FROM VELE IN Z DIRECTION         C
C           VXVF  --- OUTPUT VELOCITY FROM VELVF IN X DIRECTION        C
C           VYVF  --- OUTPUT VELOCITY FROM VELVF IN Y DIRECTION        C
C           VZVF  --- OUTPUT VELOCITY FROM VELVF IN Z DIRECTION        C
C                                                                      C
C       THE OUTPUT VARIABLES ARE:                                      C
C                                                                      C
C           IDENTE--- INPUT TO VELE ROUTINE ELEMENT IDENTIFIER         C
C           NODE1 --- INPUT TO VELVF ROUTINE FIRST NODE NUMBER         C
C           NODE2 --- INPUT TO VELVF ROUTINE SECOND NODE NUMBER        C
C           VBX   --- X BOUND VELOCITY                                 C
C           VBX   --- Y BOUND VELOCITY                                 C
C           VBZ   --- Z BOUND VELOCITY                                 C
C                                                                      C
C                                                                      C
CCCCCCCCCCCCCCCCCCCCCCCCCCCCCCCCCCCCCCCCCCCCCCCCCCCCCCCCCCCCCCCCCCCCCCCCCC
      SUBROUTINE VELBND
      IMPLICIT REAL*8(A-H,O-Z)
      PARAMETER (ME=366,MN=216,MW=80,MC=3,MCI=80)
      COMMON/ELDATA/ NELE,NODE,N(ME,3),XNODE(MN),YNODE(MN),ZNODE(MN)
      COMMON/EDGEDA/ NOPEN,NCLOSE,NTOTCR,NEDG(MC,MCI,2),NCIRC(MC)
      COMMON/CORNER/ AELE(ME),BELE(ME),CELE(ME),DIRCOS(ME,3,3)
      COMMON/VELINP/ XP,YP,ZP,IDENTE,NODE1,NODE2
      COMMON/VELVFO/ VXVF(3),VYVF(3),VZVF(3)
      COMMON/GNUMBE/ G1(MC,MCI),G2(MC,MCI),G3(MC,MCI)
      COMMON/VELOUT/ VX(6),VY(6),VZ(6)
      COMMON/OMEGAL/ OMLOCX(3),OMLOCY(3)
      COMMON/GNORMS/ ANORX(MN),ANORY(MN),ANORZ(MN),CFACT(ME,3)
      COMMON/GOMEGB/ OMEX(MN),OMEY(MN),OMEZ(MN)
```

```
      COMMON/VBOUND/ VBX,VBY,VBZ
C
CC       INITIALIZING THE VELOCITIES
C
      VBX=0.0D0
      VBY=0.0D0
      VBZ=0.0D0
C
CC       LOOPING THROUGH THE ELEMENTS FOR EACH ONE'S CONTRIBUTION
C
      DO 10 I=1,NELE
           IDENTE=I
C
CC       FINDING THE LOCAL VORTICITY AT EACH NODE OF ELEMENT I
C
           DO 20 J=1,3
                ANX=ANORX(N(I,J))*DIRCOS(I,1,1)
     .             +ANORY(N(I,J))*DIRCOS(I,1,2)
     .             +ANORZ(N(I,J))*DIRCOS(I,1,3)
                ANY=ANORX(N(I,J))*DIRCOS(I,2,1)
     .             +ANORY(N(I,J))*DIRCOS(I,2,2)
     .             +ANORZ(N(I,J))*DIRCOS(I,2,3)
                ANZ=ANORX(N(I,J))*DIRCOS(I,3,1)
     .             +ANORY(N(I,J))*DIRCOS(I,3,2)
     .             +ANORZ(N(I,J))*DIRCOS(I,3,3)
                A11=CFACT(I,J)*(ANX*ANX+ANZ*ANZ)/(ANZ*ANZ)
                A12=CFACT(I,J)*ANX*ANY/(ANZ*ANZ)
                A22=CFACT(I,J)*(ANY*ANY+ANZ*ANZ)/(ANZ*ANZ)
                WOMEGX=OMEX(N(I,J))*DIRCOS(I,1,1)
     .                +OMEY(N(I,J))*DIRCOS(I,1,2)
     .                +OMEZ(N(I,J))*DIRCOS(I,1,3)
                WOMEGY=OMEX(N(I,J))*DIRCOS(I,2,1)
     .                +OMEY(N(I,J))*DIRCOS(I,2,2)
     .                +OMEZ(N(I,J))*DIRCOS(I,2,3)
                OMLOCX(J)=A11*WOMEGX+A12*WOMEGY
                OMLOCY(J)=A12*WOMEGX+A22*WOMEGY
   20      CONTINUE
C
CC       CALLING THE VELOCITY FOR ELEMENT I
C
           CALL VELE
C
CC       ADDING TO THE OTHER ELEMENTS
C
           DO 30 J=1,3
                VBX=VBX+VX(J)*OMLOCX(J)
     .                 +VX(J+3)*OMLOCY(J)
                VBY=VBY+VY(J)*OMLOCX(J)
     .                 +VY(J+3)*OMLOCY(J)
                VBZ=VBZ+VZ(J)*OMLOCX(J)
     .                 +VZ(J+3)*OMLOCY(J)
   30      CONTINUE
   10 CONTINUE
C
CC       ADDING THE INFLUENCE OF THE CORES ALONG THE EDGE
C
      DO 40 I=1,NTOTCR
           DO 50 J=1,NCIRC(I)
                NODE1=NEDG(I,J,1)
                NODE2=NEDG(I,J,2)
                     CALL VELVF
                     VBX=VBX+G1(I,J)*VXVF(1)
     .                      +G2(I,J)*VXVF(2)
     .                      +G3(I,J)*VXVF(3)
                     VBY=VBY+G1(I,J)*VYVF(1)
     .                      +G2(I,J)*VYVF(2)
     .                      +G3(I,J)*VYVF(3)
                     VBZ=VBZ+G1(I,J)*VZVF(1)
```

```
     .                    +G2(I,J)*VZVF(2)
     .                    +G3(I,J)*VZVF(3)
50        CONTINUE
40   CONTINUE
     RETURN
     END
```

III.3 Subroutine VELWK

```
CCCCCCCCCCCCCCCCCCCCCCCCCCCCCCCCCCCCCCCCCCCCCCCCCCCCCCCCCCCCCCCCCCCCCCC
C                                                                      C
C                        **************                                C
C                        *    VELWK   *                                C
C                        **************                                C
C                                                                      C
C       THIS SUBROUTINE FINDS THE VELOCITY INDUCED AT A POINT IN       C
C       SPACE CAUSED BY THE WAKE I.E. THE FREE VORTEX SHEET.           C
C       THIS IS DONE BY SUMMING THE CONTRIBUTION FROM ALL THE          C
C       WAKE FILAMENTS.                                                C
C                                                                      C
C        THE INPUT VARIABLES ARE:                                      C
C                                                                      C
C            GWAKE --- CIRCULATION AROUND WAKE RING                    C
C            NWPTS --- NUMBER OF COLUMNS IN THE WAKE MESH              C
C            NCOVCR--- NUMBER OF CONVECTING CIRCUITS                   C
C            NRWAKE--- NUMBER OF ROWS IN THE WAKE MESH                 C
C            VXCF  --- X VELOCITY OF A CORE FROM VELCF                 C
C            VYCF  --- Y VELOCITY OF A CORE FROM VELCF                 C
C            VZCF  --- Z VELOCITY OF A CORE FROM VELCF                 C
C                                                                      C
C        THE OUTPUT VARIABLES ARE:                                     C
C                                                                      C
C            X1    --- INPUT TO VELCF FIRST X POSITION OF CORE        C
C            Y1    --- INPUT TO VELCF FIRST Y POSITION OF CORE        C
C            Z1    --- INPUT TO VELCF FIRST Z POSITION OF CORE        C
C            X2    --- INPUT TO VELCF SECOND X POSITION OF CORE       C
C            Y2    --- INPUT TO VELCF SECOND Y POSITION OF CORE       C
C            Z2    --- INPUT TO VELCF SECOND Z POSITION OF CORE       C
C            VWKX  --- X WAKE VELOCITY                                 C
C            VWKY  --- Y WAKE VELOCITY                                 C
C            VWKZ  --- Z WAKE VELOCITY                                 C
C                                                                      C
C                                                                      C
CCCCCCCCCCCCCCCCCCCCCCCCCCCCCCCCCCCCCCCCCCCCCCCCCCCCCCCCCCCCCCCCCCCCCCC
      SUBROUTINE VELWK
      IMPLICIT REAL*8(A-H,O-Z)
      PARAMETER (ME=366,MN=216,MW=80,MC=3,MCI=80)
      COMMON/VCFINP/ X1,Y1,Z1,X2,Y2,Z2,VXCF,VYCF,VZCF
      COMMON/VEWAKE/ VWKX,VWKY,VWKZ
      COMMON/P01WAK/ X1WAK(MC,MCI,MW),Y1WAK(MC,MCI,MW),Z1WAK(MC,MCI,MW)
      COMMON/P02WAK/ X2WAK(MC,MCI,MW),Y2WAK(MC,MCI,MW),Z2WAK(MC,MCI,MW)
      COMMON/TIMESD/ TIME,DTIME,NMOTIO,NCURTM,NTIME,NSTIME,NWPTS,MAXWK
      COMMON/STRWAK/ GAVE(MC,MCI),GWAKE(MC,MCI,MW),NRWAKE(MC,MW)
      COMMON/CONVEC/ NCOVCR,NCONCR(MCI),NCON(MC,MCI,2),NCONPO(MCI)
C
C       SETTING THE INITIAL VALUE IN THE SUM
C
      VWKX=0.0D0
      VWKY=0.0D0
      VWKZ=0.0D0
C
C       LOOPING THROUGH ALL THE WAKE
C
      DO 10 I=1,NWPTS
           IP1=I+1
C
C       LOOPING THROUGH ALL THE CIRCUTS
C
           DO 20 J=1,NCOVCR
C
```

```
C       LOOPING THROUGH EACH ELEMENT IN A CIRCUT
C
                DO 30 K=1,NRWAKE(J,I)-1
                   KP1=K+1
C
C       EACH WAKE ELEMENT LOOKS LIKE
C                       2(J,K,I)          1(J,K,I)
C                          +<---------------+
C                          |        2       |
C                          |      -----     |
C                        3 |     |  G  |    1|   |
C                          |     |     |     |   | GAVE
C                          |      ----->    |   V
C                          V        4       |
C                          +--------------->+
C                       2(J,KP1,I)        1(J,KP1,I)
C
                X1=X1WAK(J,KP1,I)
                Y1=Y1WAK(J,KP1,I)
                Z1=Z1WAK(J,KP1,I)
                X2=X1WAK(J,K,I)
                Y2=Y1WAK(J,K,I)
                Z2=Z1WAK(J,K,I)
                CALL VELCF
                VX1=VXCF
                VY1=VYCF
                VZ1=VZCF
C
C       THE SECOND SEGMENT
C
                X1=X1WAK(J,K,I)
                Y1=Y1WAK(J,K,I)
                Z1=Z1WAK(J,K,I)
                X2=X2WAK(J,K,I)
                Y2=Y2WAK(J,K,I)
                Z2=Z2WAK(J,K,I)
                CALL VELCF
                VX2=VXCF
                VY2=VYCF
                VZ2=VZCF
C
C       THE THIRD SEGMENT
C
                X1=X2WAK(J,K,I)
                Y1=Y2WAK(J,K,I)
                Z1=Z2WAK(J,K,I)
                X2=X2WAK(J,KP1,I)
                Y2=Y2WAK(J,KP1,I)
                Z2=Z2WAK(J,KP1,I)
                CALL VELCF
                VX3=VXCF
                VY3=VYCF
                VZ3=VZCF
C
C       THE FOURTH SEGMENT
C
                X1=X2WAK(J,KP1,I)
                Y1=Y2WAK(J,KP1,I)
                Z1=Z2WAK(J,KP1,I)
                X2=X1WAK(J,KP1,I)
                Y2=Y1WAK(J,KP1,I)
                Z2=Z1WAK(J,KP1,I)
                CALL VELCF
                VX4=VXCF
                VY4=VYCF
                VZ4=VZCF
C
```

```
C       ADDING THE CONTRIBUTION OF THE ONE ONTO THE REST
C
                VWKX=VWKX+GWAKE(J,K,I)*(VX1+VX2+VX3+VX4)
                VWKY=VWKY+GWAKE(J,K,I)*(VY1+VY2+VY3+VY4)
                VWKZ=VWKZ+GWAKE(J,K,I)*(VZ1+VZ2+VZ3+VZ4)
   30       CONTINUE
   20       CONTINUE
   10 CONTINUE
      RETURN
      END
```

III.4 Subroutine VELLS

```
CCCCCCCCCCCCCCCCCCCCCCCCCCCCCCCCCCCCCCCCCCCCCCCCCCCCCCCCCCCCCCCCCCCCCCC
C                                                                      C
C                        **************                                C
C                        *    VELLS   *                                C
C                        **************                                C
C                                                                      C
C       THIS SUBROUTINE FINDS THE VELOCITY AT A POINT IN SPACE         C
C       CAUSED BY MOVING THE LOCAL COORDINATE FRAME.                   C
C                                                                      C
C                                                                      C
C        THE INPUT VARIABLES ARE:                                      C
C                                                                      C
C            CBTOIN--- DIRECTION COSINE MATRIX OF BODY TO INERTIAL     C
C            PMOMX --- X POSITION OF ROTATION POINT                    C
C            PMOMY --- Y POSITION OF ROTATION POINT                    C
C            PMOMZ --- Z POSITION OF ROTATION POINT                    C
C            WBNX  --- X COMPONENT OF ANGULAR VELOCITY VECTOR          C
C            WBNY  --- Y COMPONENT OF ANGULAR VELOCITY VECTOR          C
C            WBNZ  --- Z COMPONENT OF ANGULAR VELOCITY VECTOR          C
C            XP    --- X POSITION WHERE VELOCITY IS TO BE FOUND        C
C            YP    --- Y POSITION WHERE VELOCITY IS TO BE FOUND        C
C            ZP    --- Z POSITION WHERE VELOCITY IS TO BE FOUND        C
C                                                                      C
C        THE OUTPUT VARIABLES ARE:                                     C
C                                                                      C
C            VLSX  --- X VELCOITY DUE TO MOVING BODY FRAME             C
C            VLSY  --- Y VELCOITY DUE TO MOVING BODY FRAME             C
C            VLSZ  --- Z VELCOITY DUE TO MOVING BODY FRAME             C
C                                                                      C
CCCCCCCCCCCCCCCCCCCCCCCCCCCCCCCCCCCCCCCCCCCCCCCCCCCCCCCCCCCCCCCCCCCCCCC
      SUBROUTINE VELLS
      IMPLICIT REAL*8(A-H,O-Z)
      COMMON/VLSURF/ VLSX,VLSY,VLSZ
      COMMON/VELINP/ XP,YP,ZP,IDENTE,NODE1,NODE2
      COMMON/RATED1/ WBNX,WBNY,WBNZ
      COMMON/MODATA/ PMOMX,PMOMY,PMOMZ,SPAN,CHORD
      COMMON/CMTRIX/ CBTOIN(3,3)
C
C       FINDING THE R VECTOR FROM THE CENTER OF ROTATION
C
      RX=XP-PMOMX
      RY=YP-PMOMY
      RZ=ZP-PMOMZ
C
C       FINDING THE VELOCITY DUE TO THE ROTATION RATE
C
      VX=WBNY*RZ-WBNZ*RY
      VY=WBNZ*RX-WBNX*RZ
      VZ=WBNX*RY-WBNY*RX
C
C       ADDING THE VELOCITY DUE TO THE ANGLE OF ATTACK
C
      VLSX=CBTOIN(1,1)+VX
      VLSY=CBTOIN(1,2)+VY
      VLSZ=CBTOIN(1,3)+VZ
      RETURN
      END
```

Bibliography

Atta, E.H. "Unsteady Flow Over Arbitrary Wing-Planforms Including Tip Separation", M.S. Thesis, Engineering Science and Mechanics, VPI&SU, Blacksburg, VA, 1976

Asfar, K.R., D.T. Mook and A.H. Nayfeh "Application of the Vortex-Lattice Technique to Arbitrary Bodies" AIAA Paper No. 78-1205, 1978

Belotserkovskii, S.M. "Calculation of the Flow Around Wings of Arbitrary Planform in a Wide Range of Angles of Attack", NASA TT F-12 291, 1969

Belotserkovskii, S.M. and M.I. Nisht "Nonstationary Nonlinear Theory of a Thin Wing of Arbitrary Planform" ***Fluid Dynamics vol 9*** , 1974

Earnshaw, P.B. and J.A. Lawford "Low-Speed Wind-Tunnel Experiments on a Series of Sharp-Edged Delta Wings" R&M 3424, British Aeronautical Research Council, 1964

Elzebda, J.M., D.T. Mook and A.H. Nayfeh "Unsteady Aerodynamic Interference for Lifting Surfaces" AIAA Paper No. 85-1801, 1985

Elzebda, J.M. "Two-Degree-of-Freedom Subsonic Wing Rock and Nonlinear Aerodynamic Interference", Ph.D Dissertation, Engineering Science and Mechanics, VPI&SU, Blacksburg, VA, 1986

Fink, P.T. and J. Taylor "Some Low-Speed Experiments with 20 deg Delta Wings" R&M 3489, British Aeronautical Research Council, 1955

Garnahan, B., H.A. Luther and J.O. Wilkes ***Applied Numerical Methods*** John Wiley & Sons, Inc., New York, New York, 1969

Harvey, J.K. "Some Measurements on a Yawed Slender Delta Wing with Leading-Edge separation" R&M 3160, British Aeronautical Research Council, 1958

Hermes, H. and J.P. LaSalle ***Functional Analysis and Time Optimal Control***, Academic Press, New York and London, 1969

Hess, J.L. and A.M.O. Smith "Calculation of Nonlinear Potential Flow about Arbitrary Three Dimensional Bodies" Douglas Rept. E.S. 40622, 1962

Hoeijmakes, H.W.M. "Computational Vortex Flow Aerodynamics" AGARD Cp-342, 1984

Hummel, D. "On The Vortex Formation Over Slender Wing at Large Angles of Incidence" AGARD CP-247, 1979

Kandil, O.A. "Prediction of the Steady Aerodynamic Loads on Lifting Surfaces Having Sharp-Edge Separation", Ph.D Dissertation, Engineering Science and Mechanics, VPI&SU, Blacksburg, VA, 1974

Kandil, O.A., D.T. Mook and A.H. Nayfeh "Nonlinear Prediction of the Aerodynamic Loads on Lifting Surfaces" AIAA Paper No. 74-503, 1974

Kandil, O.A., L-C. Chu and E.C. Yates "A Hybrid Vortex Method for Lifting Surfaces with Free-Vortex Flow" AIAA Paper No. 80-70, 1980

Kandil, O.A., L-C. Chu and T. Tureaud "Steady and Unsteady Nonlinear Hybrid Vortex Method for Lifting Surfaces at Large Angles of Attack", AIAA Journal, Vol. 22, No. 3, pp.329-336, 1984

Karamcheti, K. ***Principles of Ideal-Fluid Aerodynamics*** Robert E Krieger Publishing Co., 1980

Kim, M.J. "Application of Panel Methods For Subsonic Aerodynamics", Ph.D Dissertation, Engineering Science and Mechanics, VPI&SU, Blacksburg, VA, 1985

Kim, M.J., and D.T. Mook "Application of Continuous Vorticity Panels to General Unsteady Incompressible Two-Dimensional Flow", Journal of Aircraft, 23, pp.464-471, 1986

Konstadinopoulos, P. "A Vortex-Lattice Method for General Unsteady Subsonic Aerodynamics", M.S. Thesis, Engineering Science and Mechanics, VPI&SU, Blacksburg, VA, 1981

Konstadinopoulos, P., D.T. Mook and A.H. Nayfeh "A Numerical Method for General Unsteady Aerodynamics" AIAA Paper 81-1877, 1981

Lamar, J.E. "Extension of Leading Edge Suction Analogy To Wings with Separated Flow Around the Side Edges at Subsonic Speeds" NASA TR R-428, 1974

Levin, D. and J. Katz "Dynamic Load Measurements with Delta Wings Undergoing Self-Induced Roll-Oscillations" AIAA Paper No. 82-1320, 1982

McKinney, O.M. and H.M. Drake "Flight Characteristics at Low Speed of Delta-Wing Models" NACA RM L7R07, 1948

Maddox, S.A. "An Extension of a Vortex-Lattice Method to Include the Effects of Leading Edge Separation" M.S. Thesis, Engineering Science and Mechanics, VPI&SU, Blacksburg, VA, 1973

Mook, D.T. and S.A. Maddox "An Extension of a Vortex-Lattice Method to Include the Effects of Leading Edge Separation", Journal of Aircraft, 11, pp.127-128, 1974

Mook, D.T., S. Roy, G. Choksi and D.M. Alexander "On the Numerical Simulation of the Unsteady Wake Behind an Airfoil" AIAA Paper 87-0190, 1987

Nakamura Y., A. Leonard, and P.R. Spalart "Numerical Simulation of Vortex Breakdown by the Vortex-Filament Method" AGARD CP-342, 1984

Nguyen, L.T., L. Yip and J.R. Chambers "Self-Induced Wing Rock of Slender Delta Wings" AIAA Paper No. 81-1883, 1981

Orlik-Ruckemann, K.J. "Effects of High Angles of Attack on Dynamic Stability Parameters" AGARD CP-247, 1979

Peckham, D.H. "Low-Speed Wind-Tunnel Tests on a Series of Uncambered Slender Pointed Wings with Sharp Edges" R&M 3186, British Aeronautical Research Council, 1958

Schlottmann, F. "Investigations on Rolling Damping of Slender Wings" Arbitrary Planform in a Wide Range of Angles of Attack", NASA TT F-15 729, 1971

Shanks, R.E. "Low-Subsonic Measurements of Static and Dynamic Stability Derivatives of Six Flat-Plate Wings Having Leading Edge-Sweep of 70 to 84 degrees" NASA TN D-1822, 1963

Thrasher, D.F., D.T. Mook, O.A. Kandil and A.H. Nayfeh "Application of the Vortex-Lattice Concept to General Unsteady Lifting Surface Problem" AIAA Paper No. 77-1157, 1977

Thrasher, D.F. "Nonlinear Unsteady Aerodynamics with Application to Dynamic-Aerodynamic Interaction" M.S. Thesis, Engineering Science and Mechanics, VPI&SU, Blacksburg, VA, 1979

Totsi, L.P. "Low-Speed Static Stability and Damping-In-Roll Characteristics of Some Swept and Unswept Low-Aspect-Ratio Wings" NACA TN 1468, 1947

Wentz, W.H. and D.L. Kohlman "Vortex Breakdown on Slender Sharp Edged Wings" Journal of Aircraft, Vol 8, No 3, 1968

Woodgate L. and P.G. Pugh "Measurements of the Pitching-Moment Derivatives on a Sharp-Edged Delta Wing in Incompressible Flow" R&M 3186, British Aeronautical Research Council, 1963

Woodgate L. "Measurements of the Pitching-Moment Derivatives on a Sharp-Edged Delta Wing in Incompressible Flow" NPL Aero Report No. 1274, 1968

Yen, A. "A Continuous Vorticity Panel Method for Prediction of Steady Aerodynamic Loads on Lifting Surfaces", Ph.D Dissertation, Engineering Science and Mechanics, VPI&SU, Blacksburg, VA, 1982

Young, Fluid Dynamics Panel, Symposium on Aerodynamics of Vortical Type Flows in Three Dimensions, AGARD CP-342, 1984

The vita has been removed from the scanned document